NM1-62

Permit Application

Volume 3
Part 3 of 3

APPLICATION FOR PERMIT
SUNDANCE WEST

VOLUME III: LANDFILL ENGINEERING CALCULATIONS
SECTION 7: TENSILE STRESS ANALYSIS

ATTACHMENT III.7.A

KOERNER, ROBERT M. 2005.

DESIGNING WITH GEOSYNTHETICS, 5th EDITION

NEW JERSEY: PEARSON PRENTICE HALL.

DESIGNING WITH GEOSYNTHETICS

FIFTH EDITION

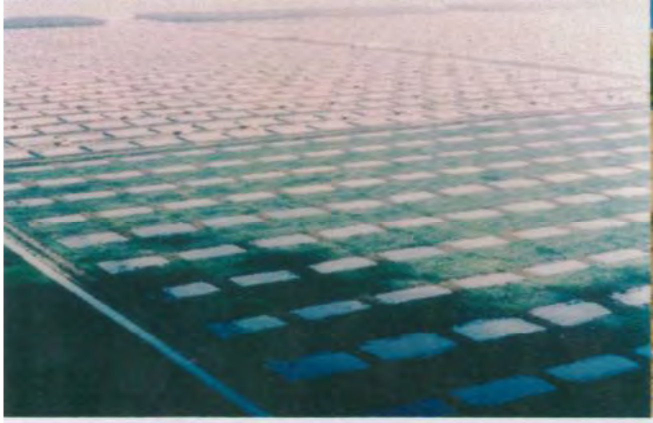

ROBERT M. KOERNER

b = width of stone void, and
y = deformation into stone void.

Example 2.9

Given a truck with 700 kPa tire inflation pressure on a stone base course consisting of 50 mm maximum-sized stone with a geotextile beneath it, calculate (**a**) the required grab tensile stress on the geotextile, and (**b**) the factor of safety for a geotextile whose maximum grab strength is 500 N with cumulative reduction factors of 2.5. Use a value of $f(\epsilon) = 0.52$.

Solution: (a) Using an empirical relationship that $d_v = 0.33\ d_a$ and the value of $f(\epsilon) = 0.52$, the required grab tensile strength is as follows:

$$\begin{aligned} T_{\text{reqd}} &= p'(d_v)^2(0.52) \\ &= p'(0.33\ d_a)^2(0.52) \\ &= 0.057p'd_a^2 \\ &= 0.057(700)(1000)(0.050)^2 \\ T_{\text{reqd}} &= 100\ N \end{aligned}$$

(b) The factor of safety on a 500 N maximum grab tensile geotextile with reduction factors of 2.5, is as follows:

$$\begin{aligned} \text{FS} &= \frac{T_{\text{allow}}}{T_{\text{reqd}}} \\ &= \frac{500/2.5}{100} \\ \text{FS} &= 2.0, \text{ which is acceptable.} \end{aligned}$$

2.5.4 Puncture Resistance

The geotextile must always survive the installation process. This is not just related to the roadway separation function; indeed, fabric survivability is critical in all types of applications; without it the best of designs are futile (recall Figure 2.20). In this regard, sharp stones, tree stumps, roots, miscellaneous debris, and other items, either on the ground surface beneath the geotextile or placed above it, could puncture through the geotextile during backfilling and when traffic loads are imposed. The design method suggested for this situation is shown schematically in Figure 2.32. For these conditions, the vertical force exerted on the geotextile (which is gradually tightening around the protruding object) is as follows:

$$\boxed{F_{\text{reqd}} = p'd_a^2S_1S_2S_3} \tag{2.30}$$

where

F_{reqd} = required vertical puncturing force to be resisted,
d_a = average diameter of the puncturing aggregate or sharp object,

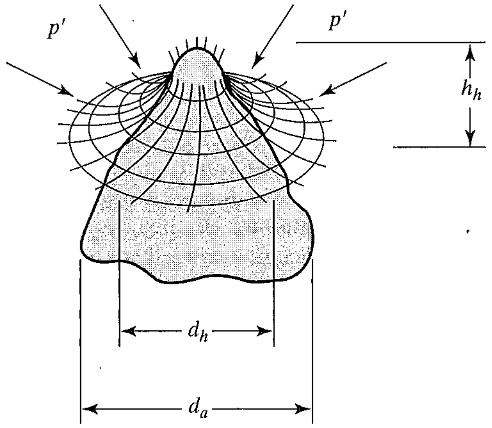

Figure 2.32 Visualization of a stone puncturing a geotextile as pressure is applied from above.

p' = pressure exerted on the geotextile (approximately 100% of tire inflation pressure at the ground surface for thin covering thicknesses),
S_1 = protrusion factor of the puncturing object (see Table 2.13),
S_2 = scale factor to adjust the ASTM D4833 puncture test value that uses a 8.0 mm diameter puncture probe to the actual puncturing object (see Table 2.13), and
S_3 = shape factor to adjust the ASTM D4833 flat puncture probe to the actual shape of the puncturing object (see Table 2.13).

Example 2.10

What is the factor of safety against puncture of a geotextile from a subrounded 25 mm diameter stone on the ground surface mobilized by a loaded truck with tire inflation pressure of 550 kPa traveling on the surface of the base course? The geotextile has an ultimate puncture strength of 300 N according to ASTM D4833.

TABLE 2.13 RECOMMENDED VALUES FOR FACTORS USED IN PUNCTURE ANALYSIS (DIMENSIONLESS)

Puncturing Object	S_1	S_2	S_3
Angular and relatively large	0.9	0.8	0.9
Angular and relatively small	0.6	0.6	0.7
Subrounded and relatively large	0.7	0.6	0.6
Subrounded and relatively small	0.4	0.4	0.5
Rounded and relatively large	0.5	0.4	0.4
Rounded and relatively small	0.2	0.2	0.3

S_1 = protrusion factor
S_2 = scale factor
S_3 = shape factor
see equation (2.30)

Solution: Using the full stress on the geotextile of 550 kPa and factors from Table 2.13 of 0.55, 0.50, and 0.55 for S_1, S_2, and S_3 respectively, we see that

$$F_{\text{reqd}} = p' d_a^2 S_1 S_2 S_3$$
$$= (550)(1000)(25 \times 0.001)^2(0.55)(0.50)(0.55)$$
$$F_{\text{reqd}} = 52 \text{ N}$$

Assuming that the cumulative reduction factors are 2.0, the factor of safety is as follows:

$$\text{FS} = \frac{F_{\text{allow}}}{F_{\text{reqd}}}$$
$$= \frac{300/2.0}{52}$$
$$\text{FS} = 2.9, \text{ which is acceptable}$$

2.5.5 Impact (Tear) Resistance

As with the puncture requirement just described, the resistance of a geotextile to impact is as much a survivability criterion as it is a separation function. Yet in many instances of separation the geotextile must resist the impact of various objects. The most obvious one is that of a rock falling on it, but there are also situations in which construction equipment and materials can cause or contribute to impact damage on geotextiles.

The problem addresses the energy mobilized by a free-falling object of known weight and height of drop. Rarely will an object be intentionally impelled onto an exposed geotextile with additional force, so only gravitational energy will be assumed.

To develop a design procedure, we assume a free-falling rock of specific gravity of 2.60, varying in diameter from 25 to 600 mm and falling from heights of 0.5 to 5 m. Using this data, the design curves in Figure 2.33 are developed. The relationship used is as follows:

$$E = mgh$$
$$= (V \times \rho)gh$$
$$= [V \times (\rho_w G_s)]gh$$
$$= \left(\frac{\pi(d_a/1000)^3}{6}\right)\left(\frac{1000\ kg}{m^3}\right)(2.6)(9.81)h$$
$$E = 13.35 \times 10^{-6}\, d_a{}^3 h \tag{2.31}$$

where

E = energy developed (Joules),
m = mass of the falling object (kg),
g = acceleration due to gravity (m/sec^2),

is the basis of design in the procedure to follow. It should be noted, however, that a number of generic techniques are available, and that Hausmann [69] has assessed and compared them to one another.

Analytic Method. Giroud and Noiray [70] use the geometric model shown in Figure 2.36 for a tire wheel load of pressure p_{ec} on a $B \times L$ area, which dissipates through h_o thickness of stone base without geotextile and h thickness of stone base with a geotextile. The geometry indicated results in a stress on the soil subgrade of p_o (without geotextile) and p (with geotextile) as follows:

$$p_o = \frac{P}{2(\mathrm{B} + 2h_o \tan \alpha_o)(\mathrm{L} + 2h_o \tan \alpha_o)} + \gamma h_o \tag{2.32}$$

$$\boxed{p = \frac{P}{2(\mathrm{B} + 2h \tan \alpha)(L + 2h \tan \alpha)} + \gamma h} \tag{2.33}$$

where

P = axle load, and

γ = unit weight of the stone aggregate.

Since the pressure exerted by the axle load through the aggregate and into the soil subgrade is known, the shallow-foundation theory of geotechnical engineering can now be utilized. We have assumed throughout the analysis that the soil is functioning in its undrained condition and thus that its shear strength is represented completely by the cohesion (i.e., $\tau = c$). The tacit assumption is that the soil subgrade consists of saturated fine-grained silt and clay soils. Critical in this design method are the assumptions that without the geotextile the maximum pressure that can be maintained corresponds to the elastic limit of the soil, that is,

$$p_o = \pi c + \gamma h_o \tag{2.34}$$

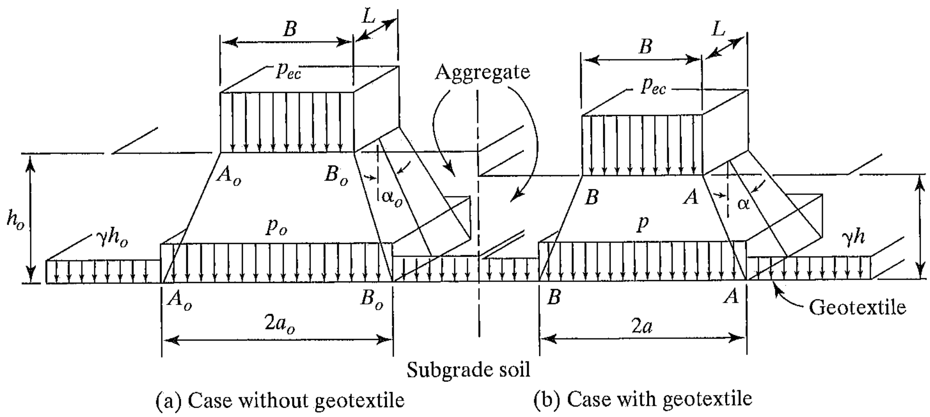

(a) Case without geotextile (b) Case with geotextile

Figure 2.36 Load distribution by aggregate layer. (After Giroud and Noiray [70])

TABLE 5.7 PEAK FRICTION VALUES AND EFFICIENCIES OF VARIOUS GEOSYNTHETIC INTERFACES*

(a) Soil-to-Geomembrane Friction Angles

	Soil type					
Geomembrane	Concrete Sand ($\phi = 30^\circ$)		Ottawa Sand ($\phi = 28^\circ$)		Mica Schist Sand ($\phi = 26^\circ$)	
HDPE						
Textured	30°	(100%)	26°	(92%)	22°	(83%)
Smooth	18°	(56%)	18°	(61%)	17°	(63%)
PVC						
Rough	27°	(88%)	—	—	25°	(96%)
Smooth	25°	(81%)	—	—	21°	(79%)
CSPE-R	25°	(81%)	21°	(72%)	23°	(87%)

(b) Geomembrane-to-Geotextile Friction Angles

	Geomembrane				
	HDPE		PVC		CSPE-R
Geotextile	Textured	Smooth	Rough	Smooth	Undulating
Nonwoven needle-punched	32°	8°	23°	21°	15°
Nonwoven heat-bonded	28°	11°	20°	18°	21°
Woven monofilament	19°	6°	11°	10°	9°
Woven slit-film	32°	10°	28°	24°	13°

(c) Soil-to-Geotextile Friction Angles

	Soil type					
Geotextile	Concrete Sand ($\phi = 30^\circ$)		Ottawa Sand ($\phi = 28^\circ$)		Mica Schist Sand ($\phi = 26^\circ$)	
Nonwoven needle-punched	30°	(100%)	26°	(92%)	25°	(96%)
Nonwoven heat-bonded	26°	(84%)	—	—	—	—
Woven monofilament	26°	(84%)	—	—	—	—
Woven slit-film	24°	(77%)	24°	(84%)	23°	(87%)

*Efficiency percentages (in parentheses) are based on Equations (5.8) at (5.9).

Source: Extended from Martin et al. [18].

harder geomembranes being the lowest. A much more extensive and recent paper is by Narejo and Koerner [19].

The frictional behavior of geomembranes placed on clay soils is of considerable importance for composite liners containing solid or liquid wastes. The current requirements are for the clay to have a hydraulic conductivity equal to or less than 1×10^{-7} cm/s and for the geomembrane to be placed directly upon the clay. While an indication of the shear strength parameters has been investigated (e.g., Narejo and Koerner [19] and Koerner et al. [20]), the data are so sensitive to the variables discussed

APPLICATION FOR PERMIT
SUNDANCE WEST

VOLUME III: LANDFILL ENGINEERING CALCULATIONS
SECTION 7: TENSILE STRESS ANALYSIS

ATTACHMENT III.7.B

SHARMA, HARI D. AND LEWIS, SANGEETA, P. 1994.

WASTE CONTAINMENT SYSTEMS, WASTE STABILIZATION,

AND LANDFILLS: DESIGN AND EVALUATION.

NEW YORK: JOHN WILEY AND SONS.

WASTE CONTAINMENT SYSTEMS, WASTE STABILIZATION, AND LANDFILLS: DESIGN AND EVALUATION

HARI D. SHARMA, Ph.D, P.E.
Chief Engieer and Director
EMCON Associates
San Jose, California

SANGETTA P. LEWIS, P.E.
Project Manager
CH$_2$M Hill
Oakland, California

A Wiley-Interscience Publication
JOHN WILEY & SONS, INC.
New York / Chichester / Toronto / Brisbane / Singapore

stress cracking may occur. The recommended elongation for shear test acceptance is greater than 50 percent (Rollin et al., 1991; Giroud and Peggs, 1990; Carlson et al., 1993).

Destructive testing procedures other than shear and peel tests are available to evaluate geomembrane seams, although their use has not yet been widely accepted. Several researchers (Peggs and Charron, 1989; Rollin et al., 1989, 1991; Halse et al., 1991b; Carlson et al., 1993) have suggested the use of microtomes (microscopic evaluation of thin geomembrane sections) to evaluate possible initiation of stress cracking in seams. Another reported method is impact testing (Rollin et al., 1993).

Geomembrane seams may also be tested using nondestructive test methods. These test methods do not measure the seam strength, but rather, detect whether holes exist in the seams. The most commonly used methods are the vacuum test, pressure test, and copper wire spark test. The vacuum test procedure involves placing a soapy solution over a seam approximately 1 to 2 feet in length. A vacuum box with a clear viewing window is placed over the seam length and a vacuum pressure of approximately 5 psi is applied. If a stream of soap bubbles is detected through the viewing window, a leak exists and must be repaired.

Pressure tests can be performed only on double-wedge weld seams. These tests are performed by sealing both ends of an unobstructed double-wedge weld length and then applying approximately 30 psi of air pressure in the channel between the welds through a fine needle. A pressure gage is attached to the needle, and the pressure is monitored for approximately 5 minutes. A reduction in pressure greater than 2 psi during the 5-minute period usually indicates that air is escaping through a leak in the seam. This leak must be located and repaired. In the copper wire spark test, a copper wire is welded into the seam. A current is passed through the copper wire, and any sparks indicate that a hole is present.

3.2 GEOTEXTILES

3.2.1 Types and Functions

Geotextiles are synthetic fabrics used in geotechnical engineering for various applications. The majority of geotextiles are composed of polypropylene or polyester fibers; a small percentage are composed of polyamide or polyethylene. Among the geosynthetics, geotextiles appear to have the most associated terminology and the widest ranging properties. This is due in part to the numerous types of fibers and geotextile manufacturing processes.

The types of fibers used in the manufacture of geotextiles include monofilament, staple, and slit[20] film. If fibers are twisted or spun together, they are known as a yarn. Monofilament fibers are created by extruding molten polymer through an apparatus containing several small-diameter holes, known as a spinnaret. The extruded polymer strings are then cooled and stretched to align the polymers and give

---

[20] Slit-film fibers are also known as split-film fibers.

the fiber increased strength. Staple fibers are also manufactured by extruding polymer through a spinnaret; however, the extruded strings are twisted together and cut into 1- to 4-inch lengths. The staple fibers are then spun into longer fibers known as staple yarns. Finally, slit-film fibers are manufactured by extruding a continuous sheet of polymer and cutting it into fibers by knives or lanced air jets. Slit-film fibers are rectangular in cross section rather than the circular cross sections of the monofilament and staple fibers.

The fibers or yarns are formed into geotextiles using either woven or nonwoven (spunbonded) methods. Woven geotextiles are formed using traditional weaving methods and a variety of weave types. Common terminology associated with woven geotextiles include machine direction, cross machine direction, selvage, warp, and weft. The machine direction refers to the direction in the plane of fabric parallel to the direction of manufacture, and conversely, the cross machine direction refers to the direction in the plane of fabric perpendicular to the direction of manufacture. The machine direction is also known as the warp, since warp yarns are those yarns placed lengthwise on the weaving loom; and the cross machine direction is known as the weft, since weft yarns are woven between and perpendicular to the warp yarns. The selvage is the finished area on both sides of the geotextile width that prevents the yarns from unraveling.

To create nonwoven geotextiles, the manufactured fibers are placed and oriented on a moving conveyor belt. The fibers are bonded by needle punching, melt bonding, or resin bonding. The needle-punching process consists of pushing numerous barbed needles through the fiber web. The fibers are thus mechanically interlocked into a stable configuration. As the name implies, the melt bonding process consists of melting and pressurizing fibers together at their crossover points. In resin bonding, an acrylic resin is applied to the fiber web to form the geotextile.

In waste containment facilities, geotextiles are most commonly used for filtration, separation, reinforcement, cushioning, and drainage. A relatively new application for geotextiles is an alternative daily cover over refuse. Typically, nonwoven geotextiles are used in waste containment facilities for filtration, separation, cushioning, and drainage. Woven geotextiles are usually used for reinforcement. Both woven and nonwoven geotextiles may be used for alternative daily cover.

3.2.2 Material Properties

As with geomembranes, there are numerous tests that may be performed on geotextiles. However, geotextiles have numerous different applications where geomembranes are used almost exclusively as a barrier material. In developing geotextile specifications, it is important that the designer understand the material tests and specify material properties important for the geotextiles' intended use. The following sections therefore indicate the geotextile application for which the material test is significant. Index or quality control tests are also discussed.

The material properties generally specified for waste containment system applications are thickness, mass per unit area, uniaxial tensile strength, multiaxial tensile strength, puncture resistance, trapezoid tear strength, apparent opening size, permittivity, transmissivity, and ultraviolet resistance. In specifying geotextile material properties, the designer should be aware that many reported material properties and test methods were borrowed from the textile industry. Many tests are therefore more applicable to evaluating fabric for clothing rather than for engineering fabrics. Most geotextile properties reported by manufacturers are index or quality control tests and are not intended for engineering design. Hopefully, as further research on geotextiles is performed, material tests to evaluate engineering properties will be developed.

Thickness (ASTM D 177,[21] D 5199). The average thickness of a geotextile is measured using a thickness gage under a gradually applied, specified pressure. The pressure to be applied depends on the material type. For geotextiles, a pressure of approximately 0.3 psi is typically used. The thickness of a geotextile alone is generally not critical for design. It is, however, related to other material properties, such as mass per unit area, tensile strength, puncture resistance, and tear resistance. Thickness is also important if the geotextile is used for cushioning and in calculating permeability coefficients.

Mass per Unit Area (ASTM D 5261[22]). The mass per unit area of a geotextile is determined by weighing several test specimens of known area, taken from various locations of the fabric sample. The calculated values are averaged to obtain the mean mass per unit area of the sample. Geotextiles, especially nonwoven geotextiles, are commonly referred to by an abbreviated form of their mass per unit area. For example, a nonwoven geotextile that is 8 ounces per square yard is commonly referred to as an 8-ounce geotextile. Although this is obviously incorrect, the problem is not as much in the terminology as it is in specifying the mass per unit area as a design value. Many specifiers attribute a certain mass per unit area to a certain set of mechanical and hydraulic properties, such as puncture resistance, tear resistance, apparent opening size, and tensile strength. While the mass per unit area is related to these properties, there is not a direct correlation. Therefore, geotextiles with a mass per unit area of 8 oz/yd^2 can have widely varying mechanical and hydraulic properties. A certain mass per unit area may be required, however, if the geotextile is to be used as a cushion.

Uniaxial Tensile Strength (ASTM D 4632,[23] D 4595[24]). The uniaxial tensile strength of geotextiles is measured in a tensile testing machine by applying a continually increasing load along the longitudinal length of a specimen. The specimen is grasped within clamps, specially designed to prevent slippage (Figure 3.33). The distance between clamps (called the gage dimension) and the specimen dimensions

---

[21] ASTM D 1777: Standard Method for Measuring Thickness of Textile Materials.

[22] ASTM D 5261: Standard Test Method for Measuring Mass per Unit Area of Geotextiles.

[23] ASTM D 4632: Standard Test Method for Breaking Load and Elongation of Geotextiles (Grab Method).

[24] ASTM D 4595: Standard Test Method for Tensile Properties by the Wide-Width Strip Method.

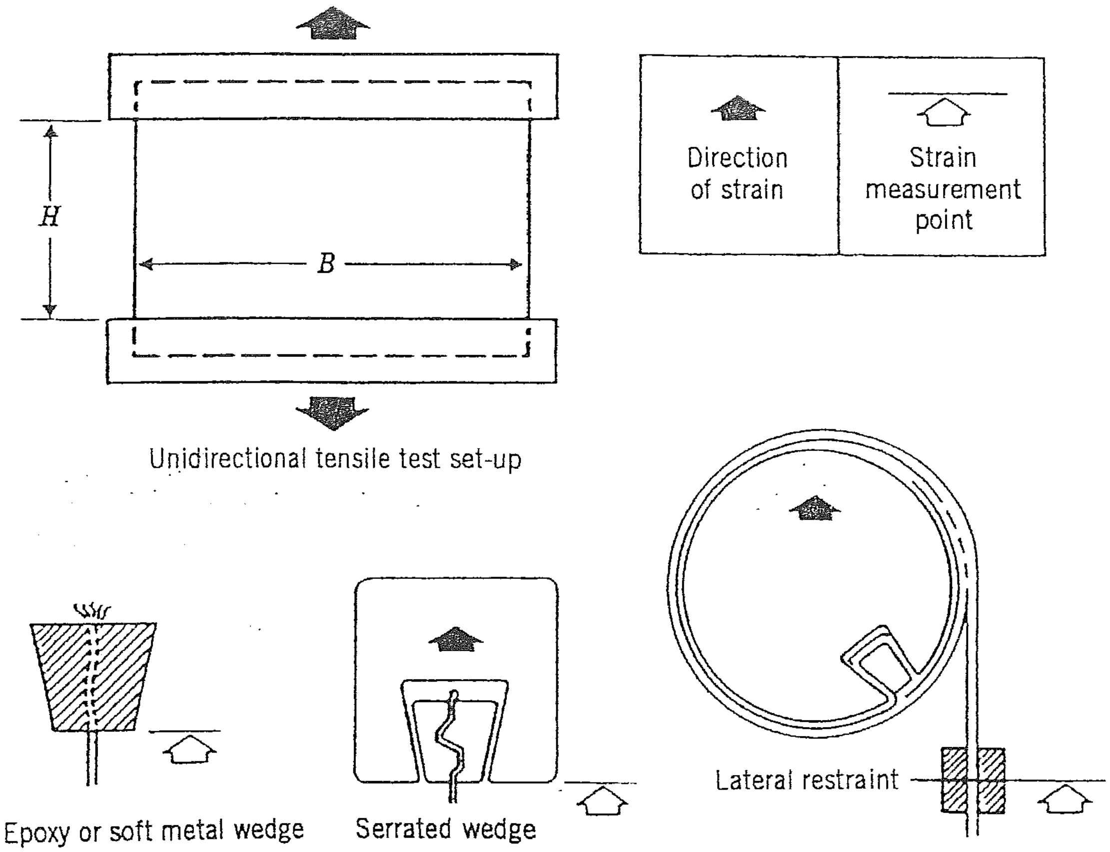

Figure 3.33 Clamping systems for uniaxial tension test. (From Myles, 1987.)

are standardized. While the test values typically reported are the breaking load (reported in pounds) and apparent elongation (reported as a percentage increase in length), a load elongation curve or a stress-strain curve can also be produced (Figure 3.34). The stress-strain curve is generated by dividing the load by the width and thickness of the geotextile specimen. Since the thickness of the geotextile typically decreases as tensile load is applied and is also variable throughout the specimen, the "stress" is often reported as the load divided by the specimen width (in lb/in.). This curve is important in assessing geotextile strength, particularly for strain compatibility in soil reinforcement applications.

Researchers throughout the world have studied the factors affecting the uniaxial tensile strength of geotextiles (Shrestha and Bell, 1982; Moritz and Murray, 1982; Richards and Scott, 1986; Rowe and Ho, 1986; Cazzuffi et al., 1986; Myles, 1987; deGroot et al., 1990; Anjiang et al., 1990; Wayne et al., 1993). These factors include specimen size, aspect ratio (width-to-length ratio), stain rates, gage length, clamping conditions, fabric type and construction, and anisotropic conditions. This research has led to the standardization of uniaxial tension testing procedures and the following general trends:

- The breaking force per unit width measured in a uniaxial tensile test is not affected significantly by the sample width (Moritz and Murray, 1982; Shrestha and Bell, 1982; Richards and Scott, 1986; Rowe and Ho, 1986; Cazzuffi et

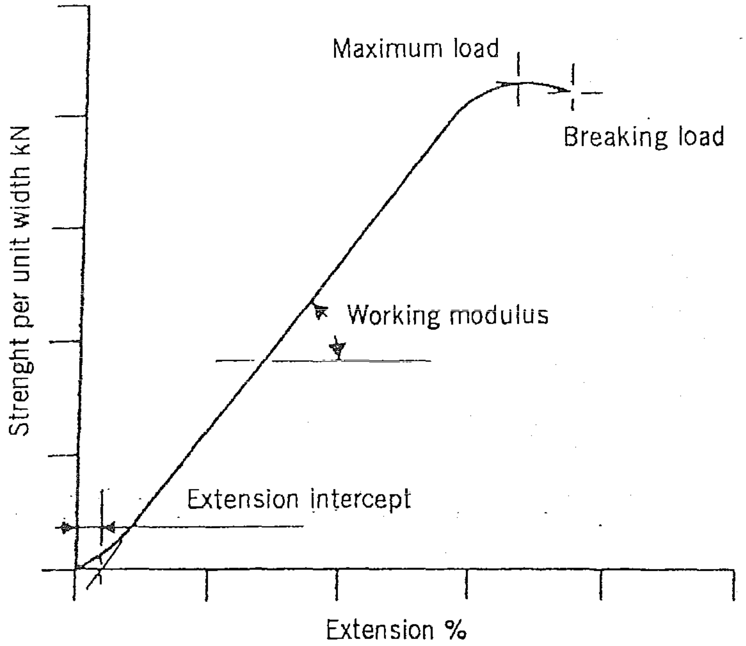

Figure 3.34 Strength per unit width versus extension curve for uniaxial tension test. (From Myles, 1987.)

al., 1986; Wayne et al., 1993) but may be influenced by the gage length[25] (Shrestha and Bell, 1982; Richards and Scott, 1986; Montalvo and Sickler, 1993).

- Depending on the type of geotextile, the modulus and elongation properties may vary with specimen width and gage length (Shrestha and Bell, 1982; Rowe and Ho, 1986; Richards and Scott, 1986; Wayne et al., 1993).
- Both woven and nonwoven geotextiles show anisotropic behavior. The anisotropic behavior in woven geotextile is expected due to the machine and cross directions. For nonwoven geotextiles, anisotropy is due to potential fluctuations and irregularity in the manufacturing process (Novais-Ferreira and Quaresma, 1982; Richards and Scott, 1986; Cazzuffi et al., 1986).
- Fabric structure has a significant influence on the stress-stain behavior. Woven and heat-bonded geotextiles show high strength and modulus and low elongation; needle-punched geotextiles have low strength and modulus and high elongation (Moritz and Murray, 1982; Shrestha and Bell, 1982; Richards and Scott, 1986).

Standard test methods have been developed for uniaxial geotextile tensile testing. The two commonly used standards include the grab (ASTM D 4632) and wide-width (ASTM D 4595) methods. The strip test is also often used and reported in the literature. Figure 3.35 shows various tensile test specimen sizes.

The strip and grab tensile tests utilize procedures originally established for the

[25] The gage length is defined as the length of the specimen between clamps.

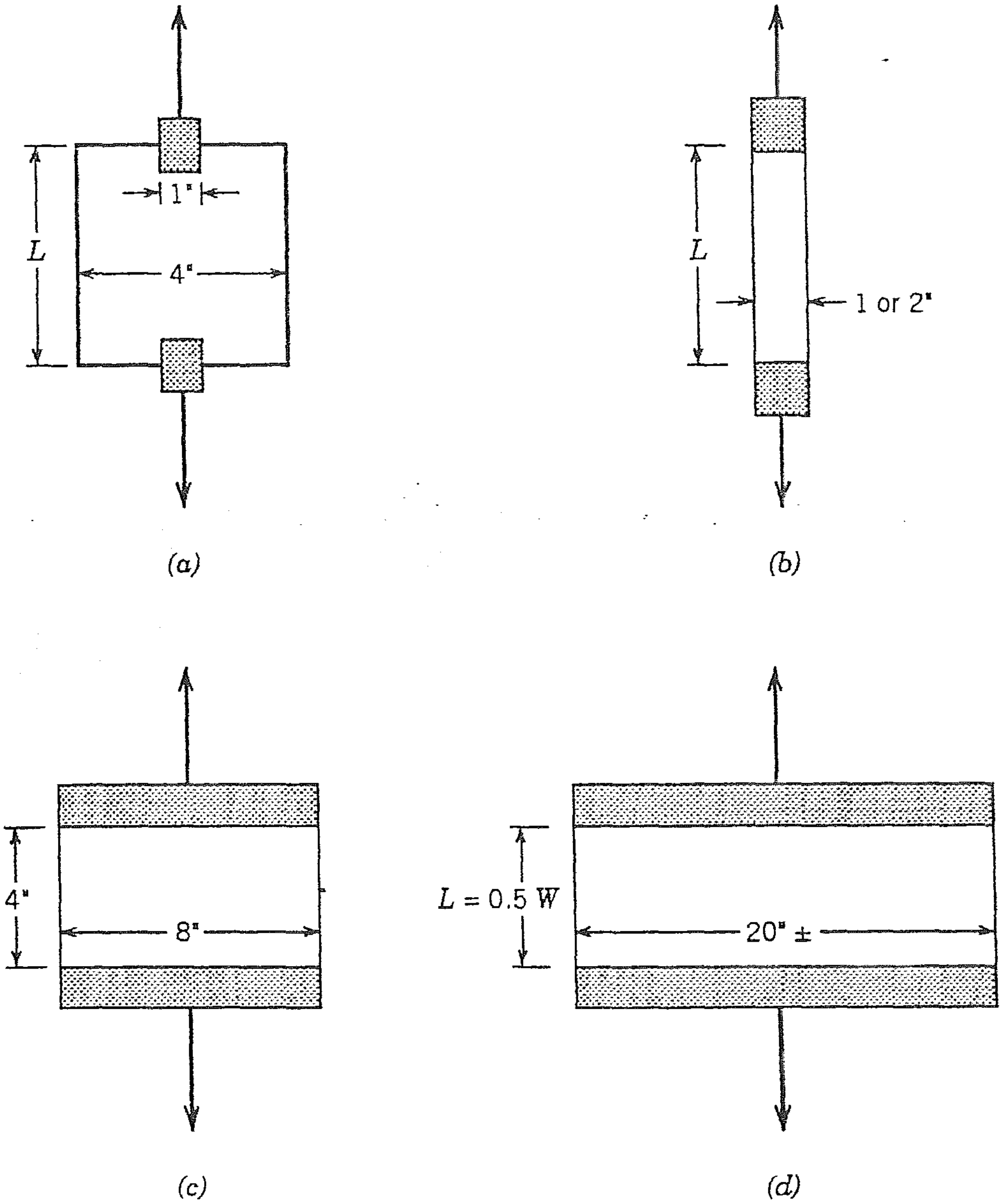

Figure 3.35 Various tensile test specimen sizes: *(a)* ASTM D4632 grab; *(b)* "narrow" strip; *(c)* ASTM D4595 wide width; *(d)* very wide width. (From Koerner, 1990.)

textile industry. The *strip tensile test* is typically performed on a 1- to 2-inch-wide specimen. As the tensile load is applied to this specimen, the specimen necks in its central region. These edge effects have significant influence on the tensile strength. In the *grab tensile test,* as shown in Figure 3.35, the clamps holding the specimen do not hold the entire width of the specimen. The grab method measures the "effective strength" of the geotextile, that is, the strength of the material in a specific width, together with the additional strength contributed by adjacent material. Both the grab and strip tests are useful as quality control or acceptance tests but have limited usefulness for design. Table 3.9 presents a range of typical grab tensile strength values for some nonwoven geotextiles.

The recommended tensile test for design is the *wide-width tensile test,* ASTM D 4595. This test was developed specifically for geotextiles and uses an 8-inch-wide

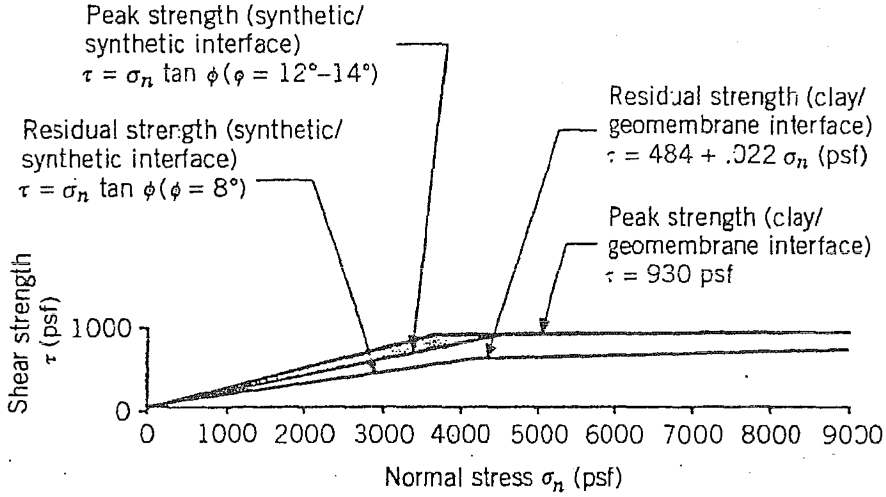

Figure 3.61 Liner strength relations. (From Byrne et al., 1992. Reproduced by permission of ASCE.)

1987; Soil and Material Engineers, 1987; Leach et al., 1987; Koutsourais et al., 1990; Swan et al., 1990; O'Rourke et al., 1990; Mitchell et al., 1990; Ojeshina, 1990; Druschel and O'Rourke, 1991; Somasundaram and Khilnani, 1991; Sharma and Hullings, 1993). The results are highly variable due to the large range of soil types and testing conditions. Both peak and residual values are included within the reported range. Table 3.14 also includes recommended soil geomembrane interface strengths.

As shown in Figure 3.61, the interface strength of clay–geomembrane exhibits a linear shear strength (τ) and normal stress (σ_n) relationship at lower normal stresses. The interface friction angles (δ) reported in Table 3.14 represent this behavior. At higher normal loads, the interface friction angle becomes very low and for all practical purposes τ tends to become independent of σ_n. The authors' experience on various low-plasticity (CL) and high-plasticity (CH) clays tested against both smooth and textured HDPE geomembrane confirms this τ–σ_n behavior. Recommended values presented in Table 3.14 should be used only as a guide in feasibility studies. Tests on site-specific materials and selected geomembranes should be conducted for final design purposes.

3.6.3 Geosynthetic-to-Geosynthetic Shear Strength

Several researchers have tested various geosynthetic-to-geosynthetic interfaces (Martin et al., 1984; Williams and Houlihan, 1986; Koutsourais et al., 1990; Mitchell et al., 1990; Lydick and Zagorski, 1990; Ojeshina, 1990; Somasundaram and Khilnani, 1991). The results of these studies are summarized in Table 3.15. The primary components of interface friction between multiple layers of geosynthetics are sliding between layers and dilation at the geosynthetic surface (Williams and Houlihan, 1986).

TABLE 3.15 Typical Range of Reported Geosynthetic to Geosynthetic Friction Angles (Degrees)

	PVC	HDPE Smooth	HDPE Textured	Geonet
Woven Geotextile	10–28	7–11	9–17	9–18
Nonwoven, needle-punched Geotextile	16–26	8–12	15–33	10–27
Nonwoven, resin/heat-bonded Geotextile	18–21	9–11	15–16	17–21
Geonet	11–24	5–19	7–25	—

The testing conditions may also have a significant effect on results. Mitchell et al. (1990) noted that polishing of geomembrane surfaces by geotextiles reduced interface friction. Also, the orientation of geonet strands can affect the interface strength between geonets and geomembranes (Geotek, 1987; Mitchell et al., 1990). Site-specific tests should therefore be performed using the actual materials and anticipated shear conditions.

3.6.4 Geosynthetic Clay Liner Shear Strength

Limited information is currently available on the internal shear strength of GCLs, due primarily to their relatively short history. The tests that have been performed are also difficult to compare, due to the numerous variations in test conditions. Many of these variations, such as strain rate, normal load, sample size, and consolidation conditions, are similar to the variations experienced when comparing shear strength testing of other geosynthetics. An additional variation of GCLs, however, is the hydrating conditions, including the hydrating liquid. Hydration can occur under free swell, constrained swell, or partially constrained swell, or the sample may be tested unhydrated. Even if hydrated under free-swell conditions, it may be difficult to assess whether full hydration has occurred since the bentonite may be restricted from free swell by the bonded geotextiles. Also, due to the large water absorption of bentonite, most shear strength test results will incorporate some immeasurable pore pressure effects unless the test is performed at extremely low displacement rates.

Table 3.16 presents the results of direct shear testing performed under various hydration conditions. The tests were performed at a strain rate of 9 mm/min and at normal stresses up to 60 kPa. Although these test results provide some information on the internal shear strength of GCLs, it is highly recommended that project specific testing be performed.

since creases in the geomembrane caused by sharp corners may lead to environmental stress cracking.

8.3.3.6 *Placement of Soils over Geomembranes.* As discussed in Section 8.3.3.2, soil should be "floated" over geomembranes such that a minimum 12 inches of this material exists between the construction equipment and the geomembrane at all times. This minimizes the possibility of geomembrane puncture and impact damage since the effective stress exerted by the construction equipment is reduced and the soil is not dumped on top of the geomembrane.

Soil placement over polyethylene geomembranes should occur in the early morning when there is adequate lighting and the geomembrane is contracted. By midday, wrinkles often develop in polyethylene geomembranes, making soil placement difficult. On days where the temperature exceeds 100°F, the wrinkles can be as large as 1 to 2 feet high. Even in the morning, 6-inch-high wrinkles can easily develop. If it cannot be avoided, soils may be placed over geomembrane wrinkles by placing the soil directly on top of the wrinkle such that it forms two smaller wrinkles. By continuously placing soil directly above the wrinkle, the wrinkle will eventually work itself out. Therefore, if possible, the geomembrane should not be permanently anchored until the soil overlying the geomembrane has been placed. In no situation should the geomembrane wrinkle be allowed to fold over under the weight of the overlying soil. These folds will crease the geomembrane and provide a preferential location for stress cracking and eventual leakage.

Placement of soils over geomembranes on slopes should occur from the bottom of slope upward. This will minimize the stresses on the geomembrane from construction equipment. Soils should be placed over geomembranes as soon as possible following geomembrane installation. This prevents UV degradation of the geomembrane and damage from ongoing construction activities, and also provides for good contact between the geomembrane and underlying material.

8.3.4 Structural Details

8.3.4.1 *Anchorage.* Anchor trenches are used at the top of side-slope liners to hold installed geosynthetics in place against applied loads and to prevent potential tears caused by wind intrusion beneath the geosynthetics. As shown in Figure 8.19, anchor trenches can generally be classified as flat, rectangular, or V-shaped. Selection of the appropriate anchor trench configuration for any particular site depends on the required holding capacity, access considerations, dimensional constraints, and available construction equipment. Often, a contractor may request that the anchor trench configuration be modified based on the equipment available. All such modifications should be checked and approved by the designer.

The holding capacity of anchor trenches is developed by the applied normal load of the soil placed above the geosynthetics, which creates frictional resistance between the geosynthetics and the underlying soil; there is minimal friction resistance developed between the upper soil and the geosynthetic since the soil above the

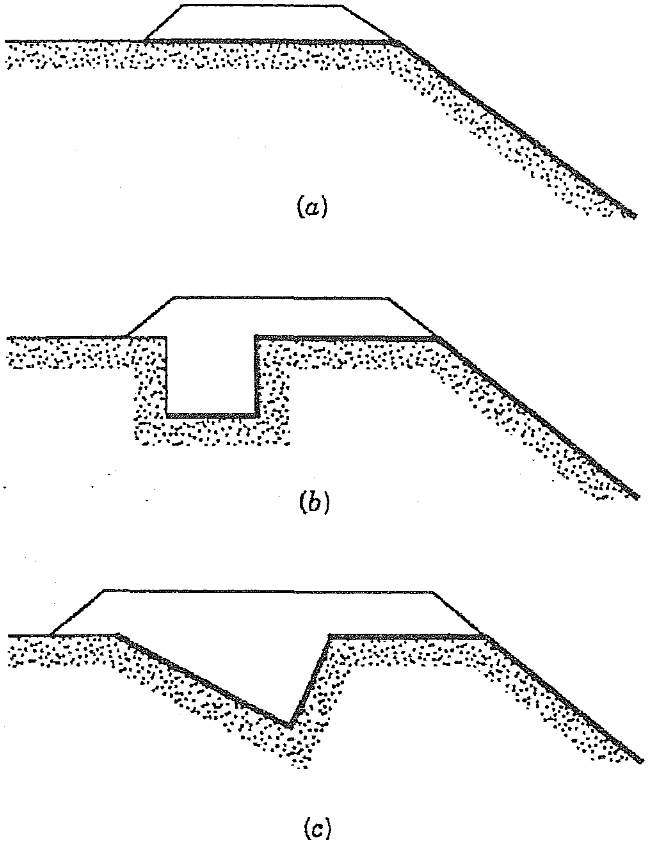

Figure 8.19 Typical anchor trench configurations: *(a)* flat anchor; and *(b)* rectangular anchor; and *(c)* V-shaped anchor.

geosynthetic is likely to move with the geosynthetic. The soil depth, type of soil or other material underlying the geosynthetics, and geosynthetic anchorage length are therefore the key factors in developing the required anchor trench holding capacity.

The easiest anchor trench configuration to analyze is the flat anchor. The free-body diagram for the flat anchor and the development of equation (8.14) for anchorage length is shown in Figure 8.20.

$$L = \frac{T \cos \beta - T \sin \beta \tan \delta_L}{\gamma d \tan \delta_L} \tag{8.14}$$

There is no ideal solution for rectangular or V trenches. Koerner (1990) recommends that the problem be solved using imaginary, frictionless pulleys, as shown in Figure 8.21.

The anchor trench should be designed to resist pullout loads (T) caused by the self-weight of the geosynthetics. For geomembranes that may be exposed to severe temperature and wind loading conditions, stresses caused by these forces should also be evaluated. Ideally, the anchor trench should be designed to allow the geosynthetics to pull out slightly rather than cause tearing of the geosynthetics. The reasoning for this is that even if complete pullout occurred, it would usually be easier to replace pulled-out materials than to repair torn geosynthetics. The maxi-

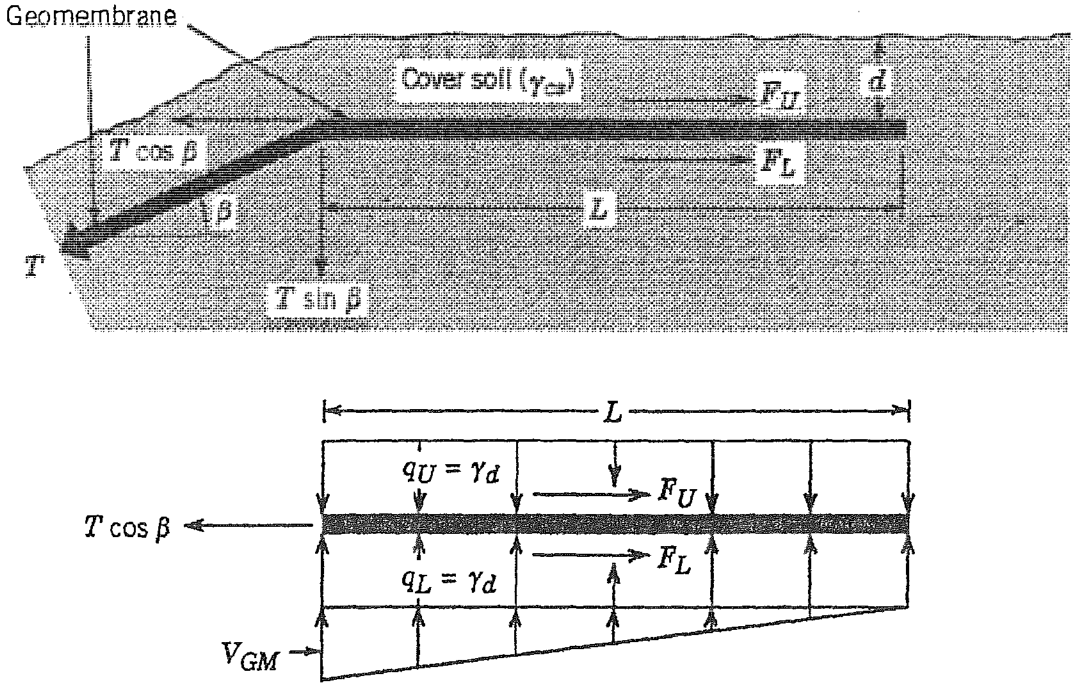

$F_U = q_U \tan \delta_U (L)$ [neglected since cover soil moves with geomembrane]

$$F_L = q_L + 0.5\, v_{GM} \tan \delta_L (L)$$

$$= \left[q_U + 0.5 \left(\frac{2\, T \sin \beta}{L} \right) \right] \tan \delta_L (L)$$

$$T \cos \beta = q_L \tan \delta_L (L) + T \sin \beta \tan \delta_L$$

$$L = \frac{T \cos \beta - T \sin \beta \tan \delta_L}{\gamma_d \tan \delta_L}$$

Where: V_{GM} = vertical force due to geomembrane
F_U = friction force above geomembrane
F_L = friction force below geomembrane
q_U = stress above geomembrane due to cover soil weight
q_L = stress below geomembrane due to cover soil weight
T = tensile force in geomembrane
β = slope angle
d =
= unit weight of cover soil
δ = interface fraction angle

Figure 8.20 Design of a flat anchor. (From Koerner, 1990.)

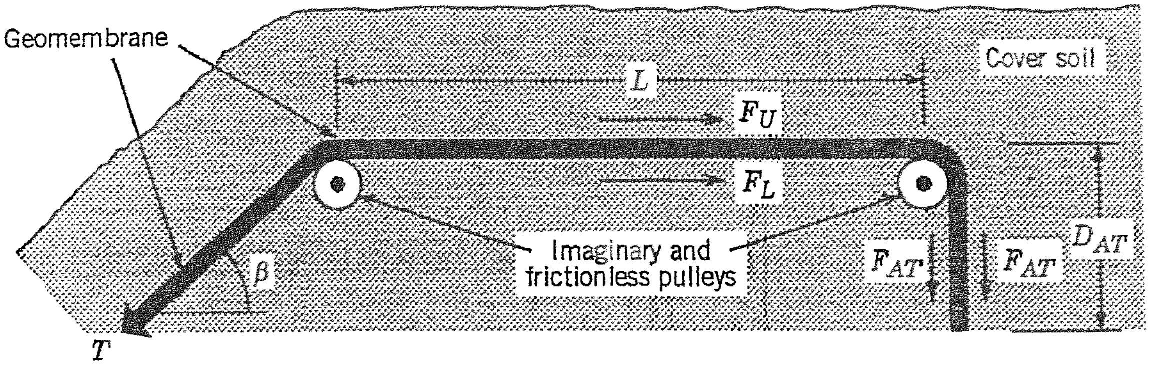

$T = F_U + F_L + 2F_{AT}$

Where: T = tensile stress in geomembrane

F_U = friction force above geomembrane (assumed to be negligible since cover soil likely moves with geomembrane)

$F_L = q \tan \delta(L)$

q = surcharge pressure = γd

d = depth of cover soil

γ = unit weight of cover soil

δ = interface friction angle

L = runout length

$F_{AT} = (\sigma_h \text{ ave}) \tan \delta (d_{AT})$

σ_h = average horizontal stress in anchor trench

$= k_o \sigma_V$

$\sigma_V = \gamma$ Have

Have = average depth of anchor trench (requires an estimate)

$k_o = 1 - \sin \phi$

ϕ = angle of shearing resistance of backfill soil

D_{AT} = depth of anchor trench (unknown)

Figure 8.21 Design of a rectangular and V anchor trenches. (From Koerner, 1990.)

mum holding capacity of the anchor trench should therefore be slightly less than the ultimate tensile strength of the geosynthetic to be anchored, irrespective of the applied loads. If the applied loads are greater than the tensile strength of the geosynthetics, measures should be taken to reduce the applied loads or higher-strength geosynthetics should be used.

If soil materials are placed above side-slope geosynthetics, the load caused by soil, seepage forces, and construction equipment should be assessed. Often, a high-strength reinforcing geotextile or geogrid is required to hold the soil on the slopes. Druschel and Underwood (1993) used a force equilibrium method to assess the required anchorage force for these high-strength materials. The free-body and force vector diagram for this method are illustrated in Figures 8.22 and 8.23, respectively. As shown, the items[4] to be evaluated include the toe buttress resistance, soil

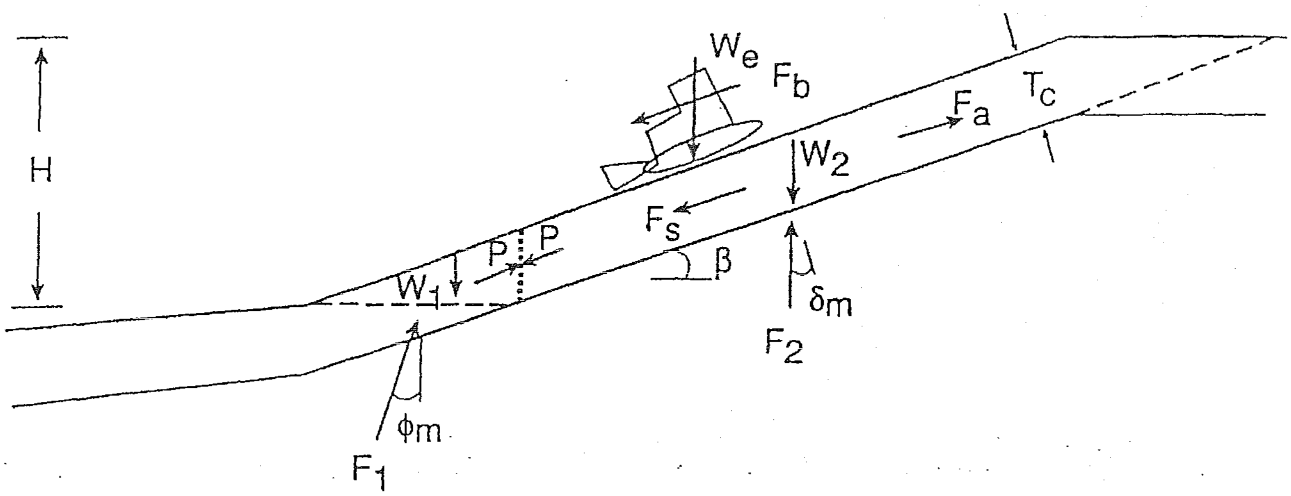

Note: P, F_s, F_a, and F_b, are assumed to be parallel to β

Figure 8.22 Free-body diagram of side-slope forces. (From Druschel and Underwood, 1993.)

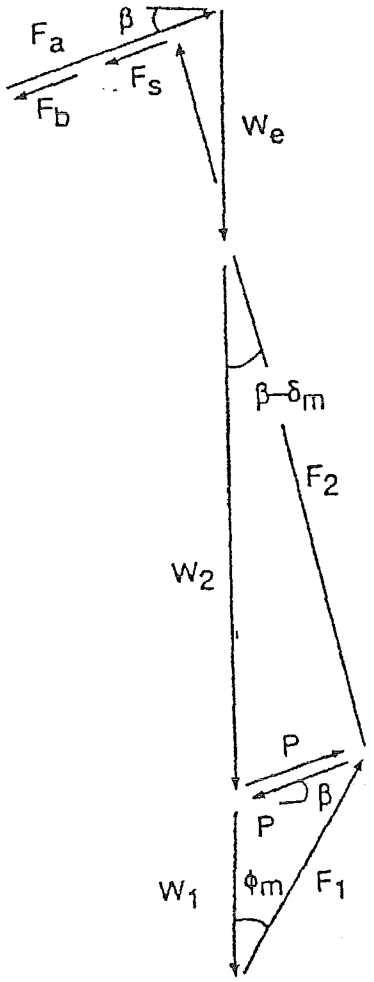

Figure 8.23 Force vector diagram. (From Druschel and Underwood, 1993.)

cover, equipment load, and seepage forces. The equation for the required anchorage force is

$$F_a=\frac{\gamma_w T_w^2}{2\tan\beta}\left(\frac{\tan\phi_m}{\cos^2\beta}+\frac{2H\tan\delta_m}{\cos\beta}-\frac{\tan\delta_m}{\cos\beta}\right)+W_e\left[0.3+\frac{\sin(\beta-\delta_m)}{\cos\delta_m}\right]-\frac{\gamma_c T_c^2\sin(\beta-\delta_m)}{2\sin\beta\cos\beta\cos\delta_m}\left[\frac{\sin\phi_m\cos\delta_m}{\cos(\beta+\phi_m)\sin(\beta-\delta_m)}+1-\frac{2H\cos\beta}{T_c}\right] \tag{8.15}$$

where H = side-slope height
T_c = cover soil thickness
β = side-slope angle
γ_w = unit weight of water
γ_c = unit weight of cover soil
δ = interface friction angle
δ_m = interface friction angle (mobilized)
ϕ = soil shear strength angle
ϕ_m = soil shear strength angle (mobilized)
W_2 = weight of side slope soil
W_1 = weight of toe buttress soil
W_e = weight of equipment on the sideslope (equipment weight divided by equipment width)
F_b = equipment braking force (approximately 30 percent of equipment's weight acting downslope and parallel to interface)
T_w = thickness of seepage
W_{w1} = weight of seepage water in toe buttress
W_{w2} = weight of seepage water in side-slope soil
F_a = geosynthetic anchorage force
F_s = seepage force
F_1 = toe buttress reaction force
F_2 = side-slope reaction force
P = side slope/toe buttress reaction force

Although this equation may seem complex, it is relatively straightforward and easily adaptable to a computer spreadsheet. Figures 8.24 and 8.25 present the variation in anchorage force with slope height assuming an interface friction angle of 9 and 12°, respectively. The reinforcing geotextile or geogrid selected should have a yield strength greater than the required anchorage force and should be able to attain the required anchorage force at a strain level of approximately 2 percent.

---

[4] Further discussion of these forces is provided in Chapter 10.

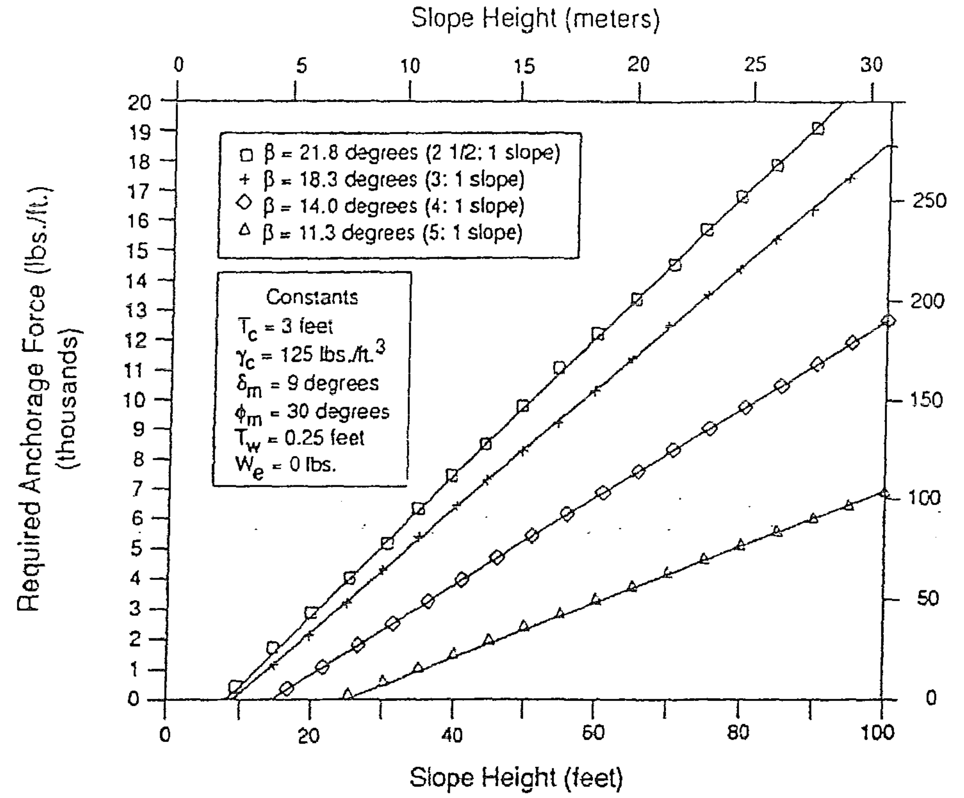

Figure 8.24 Anchorage force required for slope with 9° interface friction angle. (From Druschel and Underwood, 1993.)

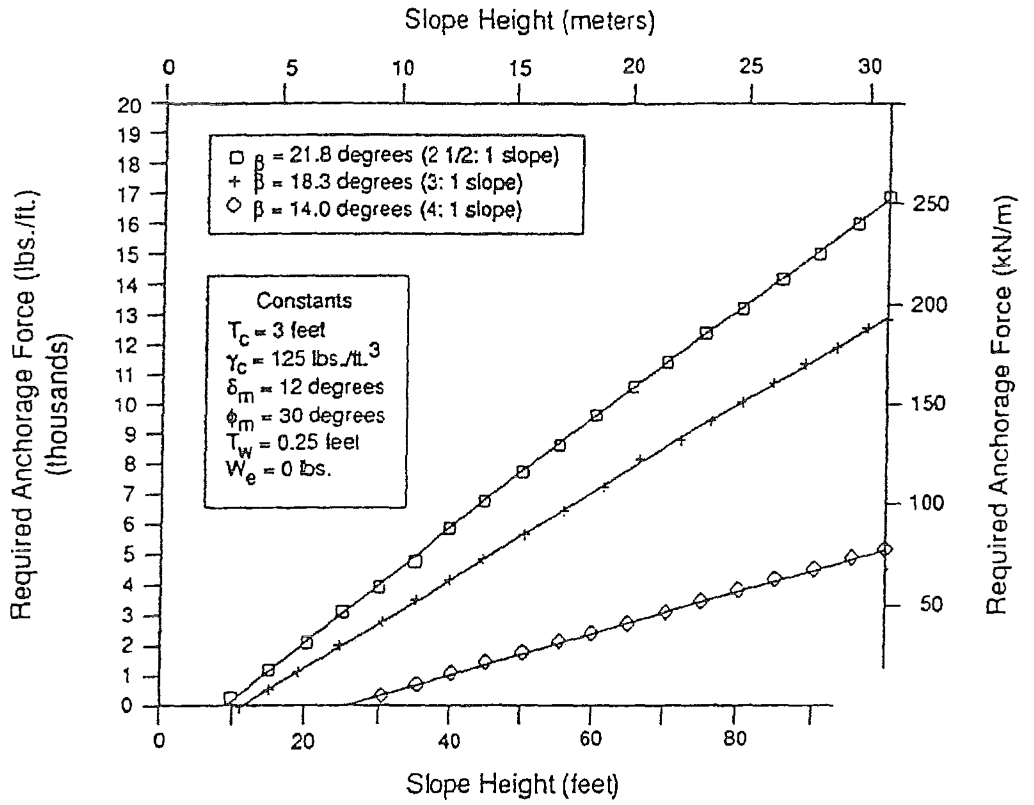

Figure 8.25 Anchorage force required for slope with 12° interface friction angle. (From Druschel and Underwood, 1993.)

Example 8.4. A 50-foot-high 3H:1V side slope is lined with 60-mil single sided textured HDPE (textured side down against underlying clay and smooth side facing up). Calculate various stresses in the liner and determine the anchor trench capacity assuming that it is 3 feet deep and 2 feet wide. At the base, a 3-foot thickness of soil, consisting of a 1-foot drainage layer and a 2-foot-thick operations layer, is already in place.

SOLUTION

A. *Forces on Geomembrane.* The forces on the geomembrane include those due to self-weight, temperature, and wind.

1. *Force (F_w) per foot width due to self-weight (W).*

$$F_w = W \sin \beta - F$$

where

$$W = L\, t\, \gamma = \frac{H}{\sin \beta}\, t\, \gamma$$

and where

$F = W \cos\beta \tan \beta$

$H =$ exposed height of geomembrane $= 50 - 3 = 47$ ft

$\sin \beta = \sin [\tan^{-1}(1/3)] = \sin 18.3° = 0.314$

$\cos\beta = 18.3° = 0.95$

$t =$ geomembrane thickness $= \dfrac{60}{1000 \times 12} = 0.005$ ft

$\gamma =$ unit weight of geomembrane $= \mathrm{SG} \cdot \gamma_w = (0.94)(62.4 \text{ lb/ft}^3) = 59 \text{ lb/ft}^3$

Therefore,

$$W = \frac{47}{0.314}\,(0.005)(59) = 44.1 \text{ lb/ft width}$$

and assuming that $\delta = 15°$ yields

$$F = (44.1)(0.95)(\tan 15°) = 11.23 \text{ lb/ft width}$$

and

$$\begin{aligned} F_w &= 44.1(0.314) - 11.23 \\ &= 2.62 \text{ lb/ft width} \end{aligned}$$

2. *Thermal forces (F_t) per foot width due to temperature change (ΔT).* Assume that the coefficient of thermal expansion $\mu = 1 \times 10^{-4}$/°F and the temperature fluctuations of the geomembrane during the day and the night are 120°F and 60°F, respectively. From equation (8.12),

$$\Delta L = \mu \, L \, \Delta T$$

which in terms of thermal strain may be written as

$$\epsilon_t = \mu \, \Delta T$$

Therefore,

$$\epsilon_t = 1 \times 10^{-4} \times (120 - 60) = 6 \times 10^{-3}$$

From the geomembrane stress-strain curve (test data sheet), σ corresponding to $\epsilon_t = 6 \times 10^{-3}$ is ~ 300 psi.

$$F_t = \sigma A = 300 \times 144 \times \frac{0.06}{12} = 216 \text{ lb/ft}$$

3. *Forces (F_{wind}) per foot width due to wind loading.* From equation (8.13)

$$q = 0.002556 V^2$$

Assuming that $V = 50$ miles/h, we have

$$q = 0.002556(50)^2 = 6.39 \text{ lb/ft}^2$$

Assuming that half of this force is supported by the drainage and operations layer and the other half is supported by the anchor trench gives us

$$F_{\text{wind}} = \tfrac{1}{2} q L = (6.39)(\tfrac{1}{2})(149.7) = 478 \text{ lb/ft width}$$

4. *Total design forces (F_d)*

$$\begin{aligned} F_d &= F_w + F_t + F_{\text{wind}} \\ &= 3 + 216 + 478 = 697 \text{ lb/ft width} \end{aligned}$$

B. *Anchor Trench Capacity.* From Figure 8.21.

$$\begin{aligned} T &= F_U + F_L + 2F_{\text{AT}} \\ &= 0 + \gamma d \tan \delta L + 2\sigma_{\text{have}} \tan \delta (d_{\text{AT}}) \end{aligned}$$

Assuming that $d = 3$ ft, $\delta = 15°$, $L = 3$ ft, $\phi = 30°$, $d_{\text{AT}} = 3$ ft yields

$$\sigma_{\text{have}} = k_0\left(\frac{\gamma h}{2}\right) = (1 - \sin \phi)\left(\frac{125 \times 3}{2}\right) = 94$$

$T = 125(2) \tan 15(3) + 2(94) \tan 15(3) = 352$ lb/ft width
additional resistance due to backfill soil = $(3+3) \times 2 \times 125$ $(\tan 20° + \tan 15°) = 948$ lb/ft
total $T = 352 + 948 = 1300$ lb/ft

C. *Allowable Stress*

Minimum allowable stress at yield = 2000 psi:

$$F_{\text{all}} = \sigma t$$
$$= 2000(0.06) = 120 \text{ lb/in.} = 1440 \text{ lb/ft}$$

D. *Comparison of Various Forces*

F_d = design force = 697 lb/ft width
T = anchor trench capacity = 1300 lb/ft width
F_{all} = allowable force = 1440 lb/ft width

The anchor trench should be designed to:

- Resist the design force = 697 lb/ft
- Allow the geomembrane to slip out before the allowable stress is reached

Therefore,

$$F_d < T < F_{\text{all}}$$
$$697 < 1300 < 1440 \text{ lb/ft width} \qquad \text{OK}$$
$$\text{FS against pullout} = \frac{T}{F_d} = \frac{1300}{697} = 1.87$$
$$\text{FS against geomembrane failure} = \frac{F_{\text{all}}}{F_d} = \frac{1440}{697} = 2.07$$

8.3.4.2 Connection/Termination. As discussed in Section 8.3.1, most landfill liners are constructed in phases. Adequate liner connection and termination details are therefore critical in maintaining liner continuity between phases. To provide satisfactory connection/termination details, the designer must first envision how the connection will be constructed, the required construction equipment access, and how much overlap is necessary between the lining systems. Typically a 4- to 5-foot overlap is sufficient for the clay liner and 2 to 3 feet for the geosynthetics. To avoid a preferential leachate flow path, the connection between clay liners should not be vertical but rather, stair-stepped at an angle (Figure 8.26). This requires some reworking of the existing clay liners but will lead to a continuous bond between the existing and future clay liners. For future connection of geomembrane liners, the edge of the existing geomembrane liner should be kept as clean as possible for proper seaming. This is often achieved by wrapping the final leading edge of the geomembrane with a nonwoven geotextile prior to placing any cover materials over the geomembrane.

Connection/termination details parallel to landfill sideslopes should also be considered, especially for geomembranes. Often the edge of a geomembrane is left

APPLICATION FOR PERMIT
SUNDANCE WEST

VOLUME III: LANDFILL ENGINEERING CALCULATIONS
SECTION 7: TENSILE STRESS ANALYSIS

ATTACHMENT III.7.C

QIAN, XUEDE; KOERNER, ROBERT M.; AND GRAY, DONALD H. 2002.

GEOTECHNICAL ASPECTS OF LANDFILL DESIGN AND CONSTRUCTION.

NEW YORK: PRETENCE HALL.

GEOTECHNICAL ASPECTS OF LANDFILL DESIGN AND CONSTRUCTION

Xuede Qian
Geotechnical Engineering Specialist
Michigan Department of Environmental Quality

Robert M. Koerner
H. L. Bowman Professor of Civil Engineering, Drexel University
Director, Geosynthetic Research Institute

Donald H. Gray
Professor of Civil and Environmental Engineering
The University of Michigan

PRENTICE HALL
Upper Saddle River, New Jersey 07458

Solution:

Assume the runout resistance force is equal to the geomembrane allowable tensile force. From the design equations just presented,

$$T\cdot(\cos\beta) = 350(144)(0.030/12)\cos 18.4^\circ$$
$$= 120 \text{ lb/ft } (1.75 \text{ kN/m})$$
$$T\cdot(\sin\beta) = 39.8 \text{ lb/ft } (0.58 \text{ kN/m})$$
$$q_B = \gamma_s\cdot d_{CS} = (100)(1.0) = 100 \text{ lb/ft } (1.46 \text{ kN/m})$$

which, when substituted into Equation 4.11, gives

$$T\cdot(\cos\beta) = q_B\cdot\tan\delta_C(L_{RO}) + T\cdot\sin\beta\cdot\tan\delta_C$$
$$120 = 100(\tan 20^\circ)(L_{RO}) + 39.8(\tan 20^\circ) \qquad (4.11)$$
$$120 = 36.4\cdot L_{RO} + 14.5$$

from which it follows that

$$L_{RO} = 2.9 \text{ ft } (0.88 \text{ m}); \text{ use } 3.0 \text{ ft (use 1 m)}$$

Note that the runout lengt\h is strongly dependent on the value of allowable stress used in the analysis. To mobilize the full strength of the geomembrane would require a longer runout length or an anchor trench. However, this might not be desirable. Pullout, without geomembrane failure, might be preferable to tensile rupture and separation of the geomembrane. Thus, the design runout or anchor resistance capacity should fall between the ultimate strength and allowable strength of a geosynthetic liner (Qian, 1995). That is,

$$\text{Ultimate Strength} > \text{Runout and/or Anchor Resistance Capacity} > \text{Allowable Strength}$$
$$\text{Runout and/or Anchor Resistance Capacity} = T/t$$
$$\sigma_{\text{allow}} = \sigma_{\text{ult}}/FS, \text{ and } T_{\text{allow}} = \sigma_{\text{allow}}\cdot t,$$

where T = geomembrane tensile force (i.e., runout or anchor resistance force) per unit width;
t = geomembrane thickness;
σ_{ult} = ultimate geomembrane stress (e.g., yield or break);
FS = factor of safety based on geomembrane strength;
σ_{allow} = allowable geomembrane stress; and
T_{allow} = allowable geomembrane force per unit width.

4.7.2 Design of Rectangular Anchor Trench

The situation with a rectangular anchor trench in place at the end of the runout section is illustrated in Figure 4.9. The configuration requires some important assumptions regarding the state of stress within the anchor trench and its resistance mechanism. In order to establish static equilibrium, an imaginary and frictionless pulley is assumed at

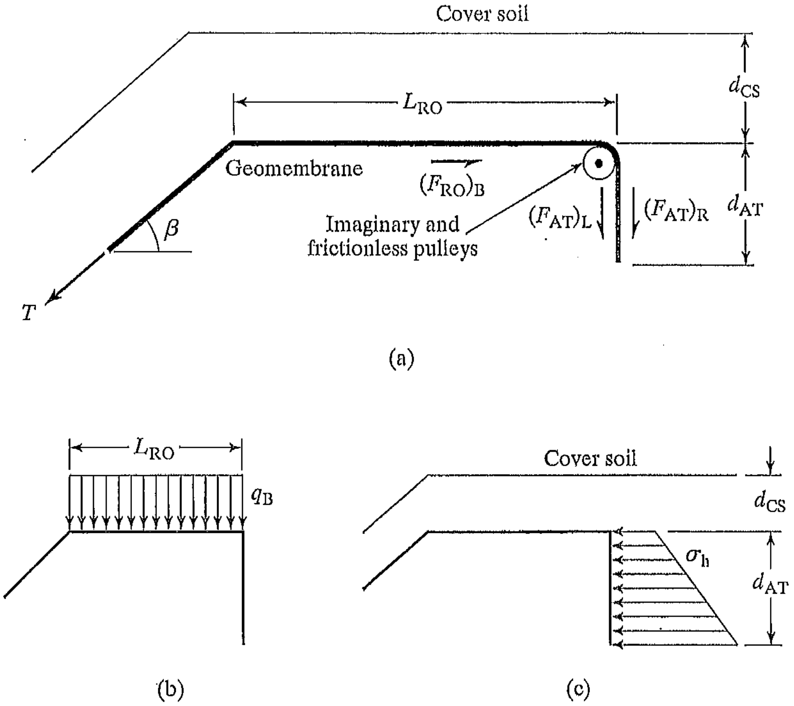

FIGURE 4.9 Cross Section of Geomembrane Runout Section with a Rectangular Anchor Trench and Related Stresses and Forces Involved

the top edge of the anchor trench, as shown in Figure 4.9 (Qian, 1995), which allows the geomembrane to be considered as a continuous member along its entire length.

From Figure 4.9, the following force summations lead to the appropriate design equations:

From $\Sigma F_V = 0$,

$$T\cdot(\sin\beta) = 0.5\cdot V_{GM}L_{RO}$$

The cover soil pressure on the runout length is

$$q_B = \gamma_s\cdot d_{CS}$$

The lateral earth force acting on both sides of the geomembrane buried in the anchor trench is

$$P_L = P_R = K_o\cdot\gamma_s\cdot(d_{CS} + 0.5\cdot d_{AT})\cdot d_{AT}$$

The vertical force due to the geomembrane force is

$$V_{GM} = \frac{2\cdot T\cdot\sin\beta}{L_{RO}}$$

The friction force above the runout geomembrane is always neglected in the anchor trench design, since the cover soil probably moves along with the geomembrane as it deforms.

From $\Sigma F_H = 0$,

$$T\cdot(\cos\beta) = (F_{RO})_B + (F_{AT})_L + (F_{AT})_R \tag{4.13}$$

and

$$\begin{aligned}(F_{RO})_B &= q_B\cdot L_{RO}\cdot\tan\delta_C + 0.5\cdot V_{GM}\cdot L_{RO}\cdot\tan\delta_C\\ &= q_B\cdot L_{RO}\cdot\tan\delta_C + 0.5\cdot(2\cdot T\cdot\sin\beta/L_{RO})\cdot L_{RO}\cdot\tan\delta_C\end{aligned}$$

or

$$(F_{RO})_B = q_B\cdot L_{RO}\cdot\tan\delta_C + T\cdot\sin\beta\cdot\tan\delta_C \tag{4.14}$$

Because $q_B = \gamma_s \cdot d_{CS}$, the friction force beneath the runout geomembrane is

$$(F_{RO})_B = \gamma_s\cdot d_{CS}\cdot L_{RO}\cdot\tan\delta_C + T\cdot\sin\beta\cdot\tan\delta_C \tag{4.15}$$

The friction force between the left side of the geomembrane and the side wall of the anchor trench is

$$(F_{AT})_L = (\sigma_h)_{ave}\cdot d_{AT}\cdot\tan\delta_C$$

The friction force between the right side of the geomembrane and the side wall of the anchor trench is

$$(F_{AT})_R = (\sigma_h)_{ave}\cdot d_{AT}\cdot\tan\delta_F$$

where $(\sigma_h)_{ave} = K_o\cdot(\sigma_v)_{ave}$

Because $K_o = 1 - \sin\phi$ and $(\sigma_v)_{ave} = \gamma_s\cdot(d_{CS} + 0.5\cdot d_{AT})$

$$(\sigma_h)_{ave} = (1 - \sin\phi)\cdot\gamma_s\cdot(d_{CS} + 0.5d_{AT}) \tag{4.16}$$

So

$$(F_{AT})_L = (1 - \sin\phi)\cdot\gamma_s\cdot(d_{CS} + 0.5\cdot d_{AT})\cdot d_{AT}\cdot\tan\delta_C \tag{4.17}$$

and

$$(F_{AT})_R = (1 - \sin\phi)\cdot\gamma_s\cdot(d_{CS} + 0.5\cdot d_{AT})\cdot d_{AT}\cdot\tan\delta_F \tag{4.18}$$

Substituting Equations 4.15, 4.17, and 4.18 into Equation 4.13 gives

$$\begin{aligned}T\cdot(\cos\beta - \sin\beta\cdot\tan\delta_L) = {}&\gamma_s\cdot d_{CS}\cdot L_{RO}\cdot\tan\delta_C +\\ &(1 - \sin\phi)\cdot\gamma_s\cdot(d_{CS} + 0.5\cdot d_{AT})\cdot d_{AT}\cdot(\tan\delta_C + \tan\delta_F)\end{aligned}$$

which leads to

$$T = \frac{\gamma_s\cdot d_{CS}\cdot L_{RO}\cdot\tan\delta_C + (1 - \sin\phi)\cdot\gamma_s\cdot(d_{CS} + 0.5\cdot d_{AT}\cdot(\tan\delta_C + \tan\delta_F}{\cos\beta - \sin\beta\cdot\tan\delta_C} \tag{4.19}$$

or

$$T = \frac{q_B\cdot L_{RO}\cdot\tan\delta_C + K_o\cdot(\sigma_v)_{ave}\cdot d_{AT}\cdot(\tan\delta_C + \tan\delta_F)}{\cos\beta - \sin\beta\cdot\tan\delta_C} \tag{4.20}$$

When $\delta_C = \delta_F = \delta$, Equation 4.19 becomes

$$T = \frac{\gamma_s\cdot d_{CS}\cdot L_{RO}\cdot\tan\delta + 2\cdot(1 - \sin\phi)\cdot\gamma_s + 0.5\cdot d_{AT}\cdot\tan\delta}{\cos\beta - \sin\beta\cdot\tan\delta} \tag{4.21}$$

and Equation 4.20 becomes

$$T = \frac{q_B \cdot L_{RO} \cdot \tan\delta + 2 \cdot K_o \cdot (\sigma_v)_{ave} \cdot d_{AT} \cdot \tan\delta}{\cos\beta - \sin\beta \cdot \tan\delta} \tag{4.22}$$

where T = geomembrane tensile force (i.e., anchor trench resistance force) per unit width;
$(F_{RO})_B$ = friction force beneath runout geomembrane;
$(F_{AT})_L$ = friction force between the left side of the geomembrane and the side wall of the anchor trench;
$(F_{AT})_R$ = friction force between the right side of the geomembrane and the side wall of the anchor trench;
$(\sigma_h)_{ave}$ = average horizontal stress in anchor trench;
$(\sigma_v)_{ave}$ = average vertical stress in anchor trench;
H_{ave} = average depth of anchor trench;
K_o = coefficient of at-rest earth pressure;
L_{RO} = runout length;
d_{CS} = depth of cover soil;
d_{AT} = anchor trench depth;
γ_s = unit weight of cover and backfill soil;
ϕ = friction angle of backfill soil in anchor trench;
δ_C = friction angle between geomembrane and underlying soil;
δ_F = friction angle between geomembrane and backfill soil;
δ = friction angle between geomembrane and soil; and
β = sideslope angle, measured from horizontal.

Note that because this situation results in one equation with two unknowns, thus a choice of L_{RO} or d_{AT} is necessary to calculate the other.

EXAMPLE 4.4

A 60-mil (1.5-mm) HDPE geomembrane of allowable stress 840 lb/in^2 (5,800 kN/m^2) is placed on a 3(H) to 1(V) sideslope. There is a cover soil of 12 inches (0.3 m) placed over the geomembrane. The unit weight of cover soil and backfill soil in the anchor trench is 110 lb/ft^3 (17.3 kN/m^3). The friction angle between the geomembrane and the underlying soil is 18 degrees, and the friction angle between the geomembrane and the backfill soil in the anchor trench is 22 degrees. The friction of the backfill soil is 30 degrees. Determine the required runout length for a 24-inch-deep (0.6-meter-deep) anchor trench.

Solution:

Assume the anchor resistance force is equal to the geomembrane allowable tensile force. Using the previously developed design equation from Figure 4.9,

$$T \cdot (\cos\beta) = (F_{RO})_B + (F_{AT})_L + (F_{AT})_R \tag{4.13}$$

where $T = T_{allow} = \sigma_{allow} \cdot t$

From Equation 4.19, we have

$$T = \frac{\gamma_s \cdot d_{CS} \cdot L_{RO} \cdot \tan\delta_C + (1 - \sin\phi) \cdot \gamma_s \cdot (d_{CS} + 0.5 \cdot d_{AT}) \cdot d_{AT} \cdot (\tan\delta_C + \tan\delta_F)}{\cos\beta - \sin\beta \cdot \tan\delta_C} \tag{4.19}$$

and

$$\sigma_{\text{allow}} \cdot t \cdot (\cos\beta - \sin\beta \cdot \tan\delta_C) = \gamma_s \cdot d_{CS} \cdot L_{RO} \cdot \tan\delta_C + (1 - \sin\phi) \cdot \gamma_s \cdot (d_{CS} + 0.5 \cdot d_{AT}) \cdot d_{AT} \cdot (\tan\delta_C + \tan\delta_F)$$

so that

$$\sigma_{\text{allow}} \cdot t = (840)(144)(0.060)/12 = 605 \text{ lb/ft } (8.83 \text{ kN/m}) \text{ and } (605)[(\cos 18.4°) - (\sin 18.4°)(\tan 18°)] = (110)(1)(\tan 18°)(L_{RO}) + (0.5)(110)(2)(2)(\tan 18° + \tan 22°)$$

or

$$(605)(0.846) = (35.74) \cdot L_{RO} + (220)(0.729) \text{ which yields } 512.83 = (35.74) \cdot L_{RO} + 160.38 \text{ or } L_{RO} = 9.86 \text{ ft } (2.96 \text{ m})$$

Thus, use the runout length $L_{RO} = 10$ ft (3 m).

The geomembrane can also be extended along the trench bottom to increase resistance force, which is called an L-shaped rectangular anchor trench. A typical layout in an L-shaped rectangular anchor trench, which is widely used in landfill projects, is shown in Figure 4.10. In order to establish the static equilibrium equation, two imaginary and frictionless pulleys are assumed at the top edge and the bottom corner of the anchor trench, as shown in Figure 4.10 (Qian, 1995). This assumption again allows the geomembrane to be considered as a continuous member.

The friction force above a runout geomembrane is always neglected in the anchor trench design, since the cover soil probably moves together with the geomembrane as it deforms.

From $\Sigma F_H = 0$

$$T \cdot (\cos\beta) = (F_{RO})_B + (F_{AT})_L + (F_{AT})_R + (F_{AB})_B + (F_{AB})_U \tag{4.23}$$

The friction force between the geomembrane and the underlying soil at the bottom of the anchor trench is

$$(F_{AB})_B = \sigma_{vB} \cdot L_{AT} \cdot \tan\delta_C \tag{4.24}$$

The friction force between the geomembrane and the overlying soil at the bottom of the anchor trench is

$$(F_{AB})_U = \sigma_{vB} \cdot L_{AT} \cdot \tan\delta_F \tag{4.25}$$

Because $\sigma_{vB} = \gamma_s \cdot (d_{CS} + d_{AT})$,

$$(F_{AB})_B = \gamma_s \cdot (d_{CS} + d_{AT}) \cdot L_{AT} \cdot \tan\delta_C \tag{4.26}$$

and

$$(F_{AB})_U = \gamma_s \cdot (d_{CS} + d_{AT}) \cdot L_{AT} \cdot \tan\delta_F \tag{4.27}$$

Substituting Equations 4.15, 4.17, 4.18, 4.26, and 4.27 into Equation 4.23 gives

$$T \cdot (\cos\beta - \sin\beta \cdot \tan\delta_L) = \gamma_s \cdot d_{CS} \cdot L_{RO} \cdot \tan\delta_C + \gamma_s \cdot (\tan\delta_C + \tan\delta_F) [(1 - \sin\phi) \cdot \gamma_s \cdot (d_{CS} + 0.5 \cdot d_{AT}) \cdot d_{AT} + (d_{CS} + d_{AT}) \cdot L_{AT}]$$

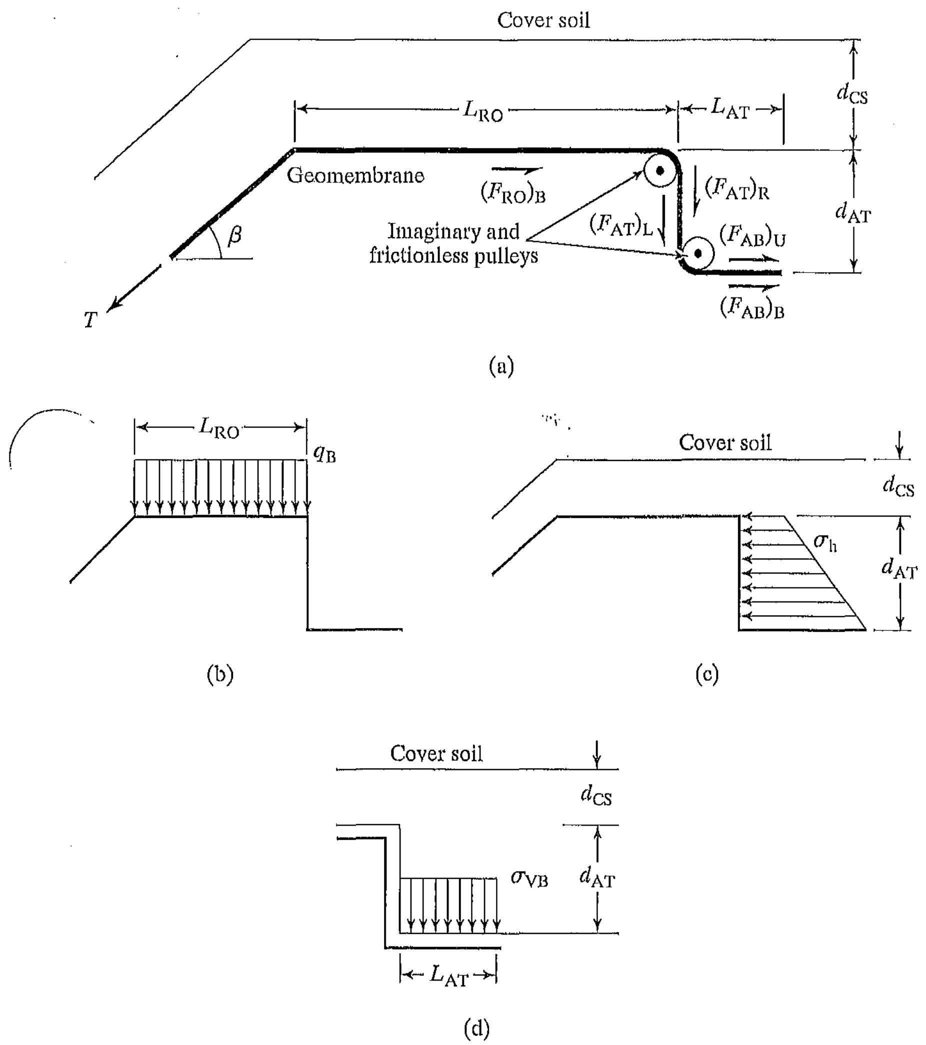

FIGURE 4.10 Cross Section of Geomembrane Runout Section with an L-Shaped Rectangular Anchor Trench and Related Stresses and Forces Involved

~~which leads to~~

$$\frac{{}_s\cdot d_{CS}\cdot L_{RO}\cdot\tan\delta_C + \gamma_s\cdot[(1-\sin\phi)\cdot\gamma_s\cdot(d_{CS}+0.5\cdot d_{AT})\cdot d_{AT} + (d_{CS}+d_{AT})\cdot L_{AT}](\tan\delta_C+\tan\delta_F)}{\cos\beta+\sin\beta\cdot\tan\delta_C} \qquad (4.28)$$

or

$$T = \frac{q_B\cdot L_{RO}\cdot\tan\delta_C + [K_o\cdot(\sigma_v)_{ave}\cdot d_{AT} + \sigma_{vB}\cdot L_{AT}](\tan\delta_C+\tan\delta_F)}{\cos\beta-\sin\beta\cdot\tan\delta_C} \qquad (4.29)$$

When $\delta_C = \delta_F = \delta$, Equation 4.28 becomes

$$T = \frac{\gamma_s \cdot d_{CS} \cdot L_{RO} \cdot \tan\delta + 2 \cdot \gamma_s \cdot [(1 - \sin\phi) \cdot \gamma_s \cdot (d_{CS} + 0.5 \cdot d_{AT}) \cdot d_{AT} + (d_{CS} + d_{AT}) \cdot L_{AT}] \cdot \tan\delta}{\cos\beta - \sin\beta \cdot \tan\delta} \tag{4.30}$$

and Equation 4.29 becomes

$$T = \frac{q_B \cdot L_{RO} \cdot \tan\delta + 2 \cdot [K_o \cdot (\sigma_v)_{ave} \cdot d_{AT} + \sigma_{vB} \cdot L_{AT}] \cdot \tan\delta}{\cos\beta - \sin\beta \cdot \tan\delta} \tag{4.31}$$

where T = geomembrane tensile force (i.e., anchor trench resistance force) per unit width;
$(F_{RO})_B$ = friction force beneath runout geomembrane;
$(F_{AT})_L$ = friction force between the left side of the geomembrane and the side wall of the anchor trench;
$(F_{AT})_R$ = friction force between the right side of the geomembrane and the side wall of the anchor trench;
$(F_{AB})_B$ = friction force between the geomembrane and the underlying soil at the bottom of the anchor trench;
$(F_{AB})_U$ = friction force between the geomembrane and the overlying soil at the bottom of the anchor trench;
$(\sigma_v)_{ave}$ = average vertical stress in anchor trench;
K_o = coefficient of at-rest earth pressure;
L_{RO} = runout length;
d_{CS} = depth of cover soil;
d_{AT} = anchor trench depth;
γ_s = unit weight of cover and backfill soil;
ϕ = friction angle of backfill soil in anchor trench;
δ_C = friction angle between the geomembrane and the underlying soil;
δ_F = friction angle between the geomembrane and the backfill soil;
δ = friction angle between the geomembrane and the soil; and
β = sideslope angle, measured from horizontal.

The design of an anchor trench is considered to be adequate if mobilized stress lies between the yield stress and allowable stress of the geosynthetic components. It should be mentioned that many manufacturers specify 1.5-feet- (0.45-m)-deep anchor trenches and a 3.0-feet- (0.90-m)-long runout section.

EXAMPLE 4.5

Calculate the resistant capacity of a given geomembrane in a L-shaped rectangular anchor trench of known dimensions. The geomembrane is 60-mil (1.5-mm) HDPE with an ultimate strength (at yield) 2,100 lb/in^2 (14,500 kN/m^2) and an allowable strength 840 lb/in^2(5,800 kN/m^2).

The runout length is 3 feet (0.9 m). The cover soil is 1 foot (0.3 m). The anchor trench is 2 feet (0.6 m) wide and 2 feet (0.6 m) deep. The side slope angle is 18.4 degrees [3(H) : 1(V)]. The unit weight of soil is 110 lb/ft^3 (17.3 kN/m^3). The soil friction angle is 30 degrees. The friction angle between the soil and the geomembrane is 20 degrees.

Solution:

The resistance capacity of the geomembrane in the anchor can be calculated from Equation 4.31 as

$$T = \frac{q_B \cdot L_{RO} \cdot \tan\delta + 2\cdot[K_o \cdot (\sigma_v)_{ave} \cdot d_{AT} + \sigma_{vB} \cdot L_{AT}] \cdot \tan\delta}{\cos\beta - \sin\beta \cdot \tan\delta}$$

where

$$\begin{aligned} q_B &= \gamma_s \cdot d_{CS} = 110 \times 1 = 110 \text{ lb/ft}^2 \text{ (5.27 kN/m}^2\text{)} \\ K_o &= 1 - \sin\phi = 1 - 0.5 = 0.5 \\ (\sigma_v)_{ave} &= \gamma_s \cdot (d_{cs} + 0.5 \cdot d_{AT}) \\ &= 110 \times (1 + 0.5 \times 2) = 110 \times 2 = 220 \text{ lb/ft}^2 \text{ (10.53 kN/m}^2\text{)} \\ \sigma_{vB} &= \gamma_s \cdot (d_{cs} + d_{AT}) = 110 \times (1 + 2) = 330 \text{ lb/ft}^2 \text{ (15.80 kN/m}^2\text{)} \end{aligned}$$

Substituting these calculated values into Equation 4.31 yields

$$\begin{aligned} T &= \frac{q_B \cdot L_{RO} \cdot \tan\delta + 2\cdot[K_o \cdot (\sigma_v)_{ave} \cdot d_{AT} + \sigma_{vB} \cdot L_{AT}] \cdot \tan\delta}{\cos\beta - \sin\beta \cdot \tan\delta} \\ &= \frac{(110)(2)(\tan 20^\circ) + 2[(0.5)(220)(2) + (330)(2)](\tan 20^\circ)}{\cos 18.4^\circ - (\sin 18.4^\circ)(\tan 20^\circ)} \\ &= \frac{(110)(2)(0.364) + 2(220 + 660)(0.364)}{0.949 - (0.316)(0.364)} \\ &= \frac{80.08 + 640.64}{0.834} \\ &= \frac{720.72}{0.834} \\ &= 864 \text{ lb/ft (12.61 kN/m)} \end{aligned}$$

So,

Anchor Resistance Capacity = 864 lb/ft = 72 lb/in ÷ 0.06 in = 1,200 lb/in^2 (8,270 kN/m^2), which leads to the following inequalities:

Ultimate Strength	>	Anchor Resistance Capacity	>	Allowable Strength
2,100 lb/in^2	>	1,200 lb/in^2	>	840 lb/in^2
(14,500 kN/m^2	>	8,270 kN/m^2	>	5,800 kN/m^2)

The results of the calculation indicate the design anchor resistance capacity falls between the yield stress and allowable stress of a geosynthetic membrane liner. Therefore, the anchor trench dimensions are acceptable.

By using a model as presented here, any set of conditions can be used to analyze and arrive at an acceptable design solution. Even situations in which geotextiles and geonets or geocomposites are used in conjunction with a geomembrane can be analyzed in a similar manner.

be normally consolidated under the surcharge of about 4 m of fill. The soft clay layer, however, was underconsolidated below the fill layer. The excess pore pressures caused by the placement of the fill in the 1970s and 1980s had experienced very little dissipation—particularly between elevations of −10 and −20 m—at the time waste placement started. In the middle zone of the soft clay layer, the difference between the actual undrained strength and the one used in the stability analyses was of the order of 10 kN/m^2. The original short-term stability analysis did not consider the possibility of failure surfaces extending to the river (like the one that actually happened), where there was no fill layer over the soft clay, and, hence, the soft clay did not have the undrained strength assumed in the stability calculations.

As noted, this case history had a geosynthetic lining system that failed along with the rotational movement. However, the lining system could not (and was not) a contributing issue to the failure. The little reinforcement benefit that may have been provided by the geosynthetic layer is negligible in the context of this large of a waste mass. This, as with the previous two case histories, was completely a geotechnical-related failure of the classical rotational failure mode except now a portion of the failure surface passes through waste materials.

13.5.3 General Remarks

It should be obvious from these three case histories that proper site characterization during the design stage and well before waste placement is critical. Irrespective of the high shear strength of waste materials, if the soil foundation fails, it will eventually propagate through the waste mass and cause the entire system to fail. Once a crack is observed on the surface of the waste mass, the entire failure surface beneath it has been mobilized. Failure of the mass is then imminent.

The situation is obviously important when dealing with soft, fine-grained soils. Typically, but certainly not always, such soils are near rivers, harbors, and estuaries. Best available geotechnical practice must be followed (recall Section 13.3.3). Even beyond site investigation, laboratory testing, and design which lead to site-specific plans and specifications, one should consider field instrumentation. Piezometers placed in the subsoil and inclinometers placed at the toe of the waste slope (and beyond) could be most valuable in providing an instantaneous assessment of the landfill as waste is being placed. Unfortunately, such instrumentation is rarely provided, even for sensitive site situations.

13.6 WASTE MASS FAILURES

The relatively low interface shear strengths of components within liner systems can lead to translational failures of the type shown in Figure 13.1(f). However, failure can only occur if the toe of the waste mass is unsupported by an opposing slope or large soil berm. Unfortunately, unsupported toe conditions are often the case. Canyon landfills are very common in areas of mountainous or rolling topography. Even when an excavation is dug for a landfill, the waste mass during filling is generally left unsupported at its toe. This section deals with the instability of such situations.

13.6.1 Translational Failure Analysis

While the approach to translational failures is generally similar to that described in Section 13.5.1, the failure surface is not circular, but usually piecewise linear. Thus, the simplified Bishop method is not applicable. A translational (or two-wedge) failure analysis is used to calculate the factor of safety for the landfill against possible mass movement of the type of "translational (or wedge) failure along liner" [Figure 13.1(f)] in the interim filling condition.

The waste mass shown in Figure 13.24(a) can be divided into two discrete parts, one active wedge lying on the side slope and tending to cause failure, and another passive wedge lying on the cell bottom floor and tending to resist failure. The forces acting on the active and passive wedges are shown in Figure 13.24(a). The individual forces, friction angles, and slope angles involved in the analysis are listed as follows:

W_P = weight of the passive wedge;

N_P = normal force acting on the bottom of the passive wedge;

F_P = frictional force acting on the bottom of the passive wedge (parallel to the bottom of the passive wedge);

E_{HP} = normal force from the active wedge acting on the passive wedge (unknown in magnitude, but with the direction perpendicular to the interface of the active and passive wedges);

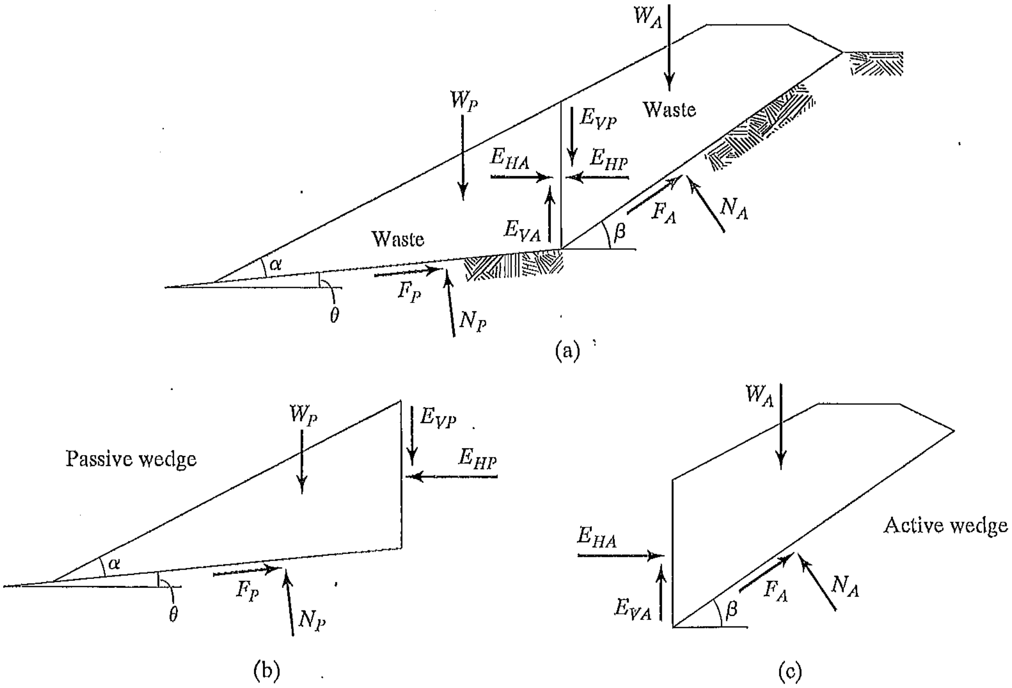

FIGURE 13.24 Forces Acting on Two adjacent Wedges for Solid Waste Filled in Landfill

E_{VP} = frictional force acting on the side of the passive wedge (unknown in magnitude, but with the direction parallel to the interface of the active and passive wedges);

FS_P = factor of safety for the passive wedge;

δ_P = minimum interface friction angle of multi-layer liner components beneath the passive wedge;

ϕ_s = friction angle of the solid waste;

α = angle of the solid waste slope, measured from horizontal, degrees;

θ = angle of the landfill cell subgrade, measured from horizontal, degrees;

W_A = weight of the active wedge;

W_T = total weight of the active and passive wedges;

N_A = normal force acting on the bottom of the active wedge;

F_A = frictional force acting on the bottom of the active wedge (parallel to the bottom of the active wedge);

E_{HA} = normal force from passive wedge acting on the active wedge (unknown in magnitude, but with the direction perpendicular to the interface of the active and passive wedges), $E_{HA} = E_{HP}$;

E_{VA} = frictional force acting on the side of the active wedge (unknown in magnitude, but with the direction parallel to the interface of the active and passive wedges), $E_{VA} = E_{VP}$;

FS_A = factor of safety for the active wedge;

δ_A = minimum interface friction angle of multi-layer liner components beneath the active wedge;

β = angle of the side slope, measured from horizontal, degrees;

FS = factor of safety for the entire solid waste mass.

Considering the force equilibrium of the passive wedge [Figure 13.24(b)], the forces acting on it are

$\Sigma F_Y = 0$:

$$W_P + E_{VP} = N_P \cdot \cos\theta + F_P \cdot \sin\theta \tag{13.47}$$

$$F_P = N_P \cdot \tan\delta_P / FS_P \tag{13.48}$$

$$E_{VP} = E_{HP} \cdot \tan\phi_s / FS_P \tag{13.49}$$

Substituting Equations 13.48 and 13.49 into Equation 13.47 gives

$$W_P + E_{HP} \cdot \tan\phi_s / FS_P = N_P \cdot (\cos\theta + \sin\theta \cdot \tan\delta_P / FS_P), \text{ and} \tag{13.50}$$

when $\Sigma F_X = 0$,

$$F_P \cdot \cos\theta = E_{HP} + N_P \cdot \sin\theta \tag{13.51}$$

Substituting Equation (13.48) into Equation (13.51) gives

$$N_P \cdot \cos\theta \cdot \tan\delta_P / FS_P = E_{HP} + N_P \cdot \sin\theta$$

$$N_P \cdot (\cos\theta \cdot \tan\delta_P / FS_P - \sin\theta) = E_{HP}$$

$$N_P = \frac{E_{HP}}{\cos\theta \cdot \tan\delta_P/FS_P - \sin\theta} \tag{13.52}$$

Substituting Equation 13.52 into Equation 13.50 gives

$$W_P + E_{HP} \cdot \tan\phi_s/FS_P = \frac{E_{HP} \cdot (\cos\theta + \sin\theta \cdot \tan\delta_P/FS_P)}{\cos\theta \cdot \tan\delta_P/FS_P - \sin\theta}$$

$$\begin{aligned} E_{HP} \cdot (\cos\theta + \sin\theta \cdot \tan\delta_P/FS_P) &= W_P \cdot (\cos\theta \cdot \tan\delta_P/FS_P - \sin\theta) \\ &\quad + E_{HP} \cdot (\cos\theta \cdot \tan\delta_P/FS_P - \sin\theta) \cdot \tan\phi_s/FS_P \end{aligned}$$

$$\begin{aligned} E_{HP} \cdot (\cos\theta + \sin\theta \cdot \tan\delta_P/FS_P - \cos\theta \cdot \tan\delta_P \cdot \tan\phi_s/FS_P^2 + \sin\theta \cdot \tan\phi_s/FS_P) \\ = W_P \cdot (\cos\theta \cdot \tan\delta_P/FS_P - \sin\theta) \end{aligned}$$

$$E_{HP} = \frac{W_P \cdot (\cos\theta \cdot \tan\delta_P/FS_P - \sin\theta)}{\cos\theta + (\tan\delta_P + \tan\phi_s) \cdot \sin\theta/FS_P - \cos\theta \cdot \tan\delta_P \cdot \tan\phi_s/FS_P^2} \tag{13.53}$$

Considering the force equilibrium of the active wedge [Figure 13.12(c)] yields

$\Sigma F_Y = 0$:

$$W_A = F_A \cdot \sin\beta + N_A \cdot \cos\beta + E_{VA} \tag{13.54}$$

$$F_A = N_A \cdot \tan\delta_A/FS_A \tag{13.55}$$

$$E_{VA} = E_{HA} \cdot \tan\phi_s/FS_A \tag{13.56}$$

Substituting Equations 13.55 and 13.56 into Equation 13.54 gives

$$W_A = N_A \cdot (\cos\beta + \sin\beta \cdot \tan\delta_A/FS_A) + E_{HA} \cdot \tan\phi_s/FS_A \tag{13.57}$$

$\Sigma F_X = 0$:

$$F_A \cdot \cos\beta + E_{HA} = N_A \cdot \sin\beta \tag{13.58}$$

Substituting Equation 13.55 into Equation 13.58 gives

$$E_{HA} = N_A \cdot (\sin\beta - \cos\beta \cdot \tan\delta_A/FS_A)$$

$$N_A = \frac{E_{HA}}{\sin\beta - \cos\beta \cdot \tan\delta_A/FS_A} \tag{13.59}$$

Substituting Equation 13.59 into Equation 13.57 gives

$$W_A = E_{HA} \cdot \frac{\cos\beta + \sin\beta \cdot \tan\delta_A/FS_A}{\sin\beta - \cos\beta \cdot \tan\delta_A/FS_A} + E_{HA} \cdot \tan\phi_S/FS_A$$

$$E_{HA} \cdot \frac{\cos\beta + \sin\beta \cdot \tan\delta_A/FS_A + \sin\beta \cdot \tan\phi_s/FS_A - \cos\beta \cdot \tan\delta_A \cdot \tan\phi_s/FS_A^2}{\sin\beta - \cos\beta \cdot \tan\delta_A/FS_A} = W_A$$

$$E_{HA} = \frac{W_A \cdot (\sin\beta - \cos\beta \cdot \tan\delta_A/FS_A)}{\cos\beta + (\tan\delta_A + \tan\phi_s) \cdot \sin\beta/FS_A - \cos\beta \cdot \tan\delta_A \cdot \tan\phi_s/FS_A^2} \tag{13.60}$$

Because $E_{\mathrm{HA}} = E_{\mathrm{HP}}$ and $FS_{\mathrm{A}} = FS_{\mathrm{P}} = FS$, Equation 13.60 must equal Equation 13.53, giving

$$\begin{aligned}&\frac{W_{\mathrm{A}}\cdot(\sin\beta - \cos\beta\cdot\tan\delta_{\mathrm{A}}/FS)}{\cos\beta + (\tan\delta_{\mathrm{A}} + \tan\phi_{\mathrm{s}})\cdot\sin\beta/FS - \cos\beta\cdot\tan\delta_{\mathrm{A}}\cdot\tan\phi_{\mathrm{s}}/FS^2}\\ &= \frac{W_{\mathrm{P}}\cdot(\cos\theta\cdot\tan\delta_{\mathrm{P}}/FS - \sin\theta)}{\cos\theta + (\tan\delta_{\mathrm{P}} + \tan\phi_{\mathrm{s}})\cdot\sin\theta/FS - \cos\theta\cdot\tan\delta_{\mathrm{P}}\cdot\tan\phi_{\mathrm{s}}/FS^2}\end{aligned}$$

$$\begin{aligned}&W_{\mathrm{A}}\cdot(\sin\beta - \cos\beta\cdot\tan\delta_{\mathrm{A}}/FS)[\cos\theta + (\tan\delta_{\mathrm{P}} + \tan\phi_{\mathrm{s}})\cdot\sin\theta/FS - \cos\theta\cdot\tan\delta_{\mathrm{P}}\cdot\tan\phi_{\mathrm{s}}/FS^2]\\ &= W_{\mathrm{P}}\cdot(\cos\theta\cdot\tan\delta_{\mathrm{P}}/FS - \sin\theta)[\cos\beta + (\tan\delta_{\mathrm{A}} + \tan\phi_{\mathrm{s}})\cdot\sin\beta/FS - \cos\beta\cdot\tan\delta_{\mathrm{A}}\cdot\tan\phi_{\mathrm{s}}/FS^2]\end{aligned}$$

$$\begin{aligned}&(W_{\mathrm{A}}\cdot\sin\beta - W_{\mathrm{A}}\cdot\cos\beta\cdot\tan\delta_{\mathrm{A}}/FS)[\cos\theta + (\tan\delta_{\mathrm{P}} + \tan\phi_{\mathrm{s}})\cdot\sin\theta/FS - \cos\theta\cdot\tan\delta_{\mathrm{P}}\cdot\tan\phi_{\mathrm{s}}/FS^2]\\ &= (W_{\mathrm{P}}\cdot\cos\theta\cdot\tan\delta_{\mathrm{P}}/FS - W_{\mathrm{P}}\cdot\sin\theta)[\cos\beta + (\tan\delta_{\mathrm{A}} + \tan\phi_{\mathrm{s}})\cdot\sin\beta/FS - \cos\beta\cdot\tan\delta_{\mathrm{A}}\cdot\tan\phi_{\mathrm{s}}/FS^2]\end{aligned}$$

$$\begin{aligned}&W_{\mathrm{A}}\cdot\sin\beta\cdot\cos\theta + W_{\mathrm{A}}\cdot(\tan\delta_{\mathrm{P}} + \tan\phi_{\mathrm{s}})\cdot\sin\beta\cdot\sin\theta/FS - W_{\mathrm{A}}\cdot\sin\beta\cdot\cos\theta\cdot\tan\delta_{\mathrm{P}}\cdot\tan\phi_{\mathrm{s}}/FS^2\\ &- W_{\mathrm{A}}\cdot\cos\beta\cdot\cos\theta\cdot\tan\delta_{\mathrm{A}}/FS - W_{\mathrm{A}}\cdot(\tan\delta_{\mathrm{P}} + \tan\phi_{\mathrm{s}})\cdot\cos\beta\cdot\sin\theta\cdot\tan\delta_{\mathrm{A}}/FS^2\\ &+ W_{\mathrm{A}}\cdot\cos\beta\cdot\cos\theta\cdot\tan\delta_{\mathrm{A}}\cdot\tan\delta_{\mathrm{P}}\cdot\tan\phi_{\mathrm{s}}/FS^3 = W_{\mathrm{P}}\cdot\cos\beta\cdot\cos\theta\cdot\tan\delta_{\mathrm{P}}/FS\\ &+ W_{\mathrm{P}}\cdot(\tan\delta_{\mathrm{A}} + \tan\phi_{\mathrm{s}})\cdot\sin\beta\cdot\cos\theta\cdot\tan\delta_{\mathrm{P}}/FS^2 - W_{\mathrm{P}}\cdot\cos\beta\cdot\cos\theta\cdot\tan\delta_{\mathrm{A}}\cdot\tan\delta_{\mathrm{P}}\cdot\tan\phi_{\mathrm{s}}/FS^3\\ &- W_{\mathrm{P}}\cdot\cos\beta\cdot\sin\theta - W_{\mathrm{P}}\cdot(\tan\delta_{\mathrm{A}} + \tan\phi_{\mathrm{s}})\cdot\sin\beta\cdot\sin\theta/FS + W_{\mathrm{P}}\cdot\cos\beta\cdot\sin\theta\cdot\tan\delta_{\mathrm{A}}\cdot\tan\phi_{\mathrm{s}}/FS^2\end{aligned}$$

$$\begin{aligned}&(W_{\mathrm{A}}\cdot\sin\beta\cdot\cos\theta + W_{\mathrm{P}}\cdot\cos\beta\cdot\sin\theta)\cdot FS^3 + [W_{\mathrm{A}}\cdot(\tan\delta_{\mathrm{P}} + \tan\phi_{\mathrm{s}})\cdot\sin\beta\cdot\sin\theta\\ &+ W_{\mathrm{P}}\cdot(\tan\delta_{\mathrm{P}} + \tan\phi_{\mathrm{s}})\cdot\sin\beta\cdot\sin\theta - W_{\mathrm{A}}\cdot\cos\beta\cdot\cos\theta\cdot\tan\delta_{\mathrm{A}} - W_{\mathrm{P}}\cdot\cos\beta\cdot\cos\theta\cdot\tan\delta_{\mathrm{P}}]\cdot FS^2\\ &- [W_{\mathrm{A}}\cdot(\tan\delta_{\mathrm{P}} + \tan\phi_{\mathrm{s}})\cdot\cos\beta\cdot\sin\theta\cdot\tan\delta_{\mathrm{A}} + W_{\mathrm{P}}\cdot(\tan\delta_{\mathrm{A}} + \tan\phi_{\mathrm{s}})\cdot\sin\beta\cdot\cos\theta\cdot\tan\delta_{\mathrm{P}}\\ &+ W_{\mathrm{A}}\cdot\sin\beta\cdot\cos\theta\cdot\tan\delta_{\mathrm{P}}\cdot\tan\phi_{\mathrm{S}} + W_{\mathrm{P}}\cdot\cos\beta\cdot\sin\theta\cdot\tan\delta_{\mathrm{A}}\cdot\tan\phi_{\mathrm{s}}]\cdot FS\\ &+ (W_{\mathrm{A}}\cdot\cos\beta\cdot\cos\theta\cdot\tan\delta_{\mathrm{A}}\cdot\tan\delta_{\mathrm{P}}\cdot\tan\phi_{\mathrm{s}} + W_{\mathrm{P}}\cdot\cos\beta\cdot\cos\theta\cdot\tan\delta_{\mathrm{A}}\cdot\tan\delta_{\mathrm{P}}\cdot\tan\phi_{\mathrm{s}}) = 0\end{aligned}$$

$$\begin{aligned}&(W_{\mathrm{A}}\cdot\sin\beta\cdot\cos\theta + W_{\mathrm{P}}\cdot\cos\beta\cdot\sin\theta)\cdot FS^3 + [(W_{\mathrm{A}}\cdot\tan\delta_{\mathrm{P}} + W_{\mathrm{P}}\cdot\tan\delta_{\mathrm{A}} + W_{\mathrm{T}}\cdot\tan\phi_{\mathrm{s}})\cdot\sin\beta\cdot\sin\theta\\ &- (W_{\mathrm{A}}\cdot\tan\delta_{\mathrm{A}} + W_{\mathrm{P}}\cdot\tan\delta_{\mathrm{P}})\cdot\cos\beta\cdot\cos\theta]\cdot FS^2 - [W_{\mathrm{T}}\cdot\tan\phi_{\mathrm{s}}\cdot(\sin\beta\cdot\cos\theta\cdot\tan\delta_{\mathrm{P}}\\ &+ \cos\beta\cdot\sin\theta\cdot\tan\delta_{\mathrm{A}}) + (W_{\mathrm{A}}\cdot\cos\beta\cdot\sin\theta + W_{\mathrm{P}}\cdot\sin\beta\cdot\cos\theta)\cdot\tan\delta_{\mathrm{A}}\cdot\tan\delta_{\mathrm{P}}]\cdot FS\\ &+ W_{\mathrm{T}}\cdot\cos\beta\cdot\cos\theta\cdot\tan\delta_{\mathrm{A}}\cdot\tan\delta_{\mathrm{P}}\cdot\tan\phi_{\mathrm{s}} = 0 \qquad (13.61)\end{aligned}$$

Equation 13.61 is now solved as follows:

$$a\cdot FS^3 + b\cdot FS^2 + c\cdot FS + d = 0 \qquad (13.62)$$

$$\begin{aligned}a &= W_{\mathrm{A}}\cdot\sin\beta\cdot\cos\theta + W_{\mathrm{P}}\cdot\cos\beta\cdot\sin\theta\\ b &= (W_{\mathrm{A}}\cdot\tan\delta_{\mathrm{P}} + \mathrm{W}_{\mathrm{P}}\cdot\tan\delta_{\mathrm{A}} + W_{\mathrm{T}}\cdot\tan\phi_{\mathrm{s}})\cdot\sin\beta\cdot\sin\theta\\ &\qquad - (W_{\mathrm{A}}\cdot\tan\delta_{\mathrm{A}} + W_{\mathrm{P}}\cdot\tan\delta_{\mathrm{P}})\cdot\cos\beta\cdot\cos\theta\\ c &= -[W_{\mathrm{T}}\cdot\tan\phi_{\mathrm{s}}\cdot(\sin\beta\cdot\cos\theta\cdot\tan\delta_{\mathrm{P}} + \cos\beta\cdot\sin\theta\cdot\tan\delta_{\mathrm{A}})\\ &\qquad + (W_{\mathrm{A}}\cdot\cos\beta\cdot\sin\theta + W_{\mathrm{P}}\cdot\sin\beta\cdot\cos\theta)\cdot\tan\delta_{\mathrm{A}}\cdot\tan\delta_{\mathrm{P}}]\\ d &= W_{\mathrm{T}}\cdot\cos\beta\cdot\cos\theta\cdot\tan\delta_{\mathrm{A}}\cdot\tan\delta_{\mathrm{P}}\cdot\tan\phi_{\mathrm{s}}\end{aligned}$$

When the cell subgrade is very small (i.e., $\theta \approx 0$), $\sin\theta \approx 0$, and $\cos\theta \approx 1$, Equation 13.62 then becomes

$$a\cdot FS^3 + b\cdot FS^2 + c\cdot FS + d = 0 \qquad (13.63)$$

where $a = W_{\mathrm{A}}\cdot\sin\beta$
$b = -(W_{\mathrm{A}}\cdot\tan\delta_{\mathrm{A}} + W_{\mathrm{P}}\cdot\tan\delta_{\mathrm{P}})\cdot\cos\beta$

$$c = -(W_T \cdot \tan\phi_s + W_P \cdot \tan\delta_A) \cdot \sin\beta \cdot \tan\delta_P$$
$$d = W_T \cdot \cos\beta \cdot \tan\delta_A \cdot \tan\delta_P \cdot \tan\phi_s$$

In the conventional translational (or two-wedge) failure analysis method, the direction of the resultant force E_P of E_{HP} and E_{VP} (or the resultant force E_A of E_{HA} and E_{VA}), which acts on the interface between the passive wedge and active wedge, is usually assumed to be parallel to waste filling slope. The effect of the waste property of the interface between the active and passive wedges (i.e., shear strength of the waste) on the stability is not considered for this assumption. Actually, the real direction of the resultant force E_A of E_{HA} and E_{VA} (or the direction of the interwedge force) should be calculated as

$$\begin{aligned} \tan\omega &= E_{VP}/E_{HP} \\ &= (E_{HP} \cdot \tan\phi_s/FS)/E_{HP} \\ &= \tan\phi_s/FS \\ \omega &= \tan^{-1}(\tan\phi_s/FS) \end{aligned} \tag{13.64}$$

where ω = inclination angle of the interwedge force (i.e., the resultant force of E_{HP} and E_{VP}), measured from horizontal, degrees;
ϕ_s = friction angle of solid waste;
FS = factor of safety for the entire solid waste mass.

Municipal solid waste usually settles a considerable amount during the filling operation. Review of field settlements from several landfills indicates that municipal solid waste landfills usually settle approximately 15 to 30% of the initial height because of placement and decomposition. The large settlement of the waste fill induces shear stresses in the liner system on the side slope, all of which tends to displace the liner downslope. The large settlement of the waste fill also causes the large deformation of the landfill cover to induce shear stresses in the final cover system. These shear stresses induce shear displacements along specific interfaces in the liner and cover systems that may lead to the mobilization of a residual interface strength. In addition, thermal expansion and contraction of the side slope liner and cover systems during construction and filling may also contribute to the accumulation of shear displacements and the mobilization of a residual interface shear strength in the liner system (Qian, 1994; Stark and Poeppel, 1994).

Earthquake loading can provide permanent displacements along landfill liner interfaces, resulting in a permanent reduction in their available shear resistance following the completion of the dynamic loading. Post-earthquake static stability must therefore be evaluated using shear strengths that are compatible with the shear displacements predicted to be experienced during the earthquake. In areas of high seismicity, this probably implies that the static stability of the final configuration of the landfill should be assured assuming the mobilization of full residual strength conditions (Byrne, 1994).

Landfill stability should be considered not only during construction and operation periods, but also for the duration of the closure period. Land development of closed landfills should be also considered in the future. Thus, the shear strengths (e.g., δ_P, δ_A, and ϕ_s) used in stability analysis must be carefully selected based on actual site-specific conditions.

EXAMPLE 13.8

Calculate the factor of safety for a landfill filling shown in Figure 13.25. Use a translational failure analysis and the following information:

Minimum interface friction angle of bottom liner system, $\delta_P = 20°$;
Minimum interface residual friction angle of side slope liner system, $\delta_A = 14°$;
Friction angle of solid waste, $\phi_s = 33°$;
Waste unit weight $= 10.2\ \mathrm{kN/m^3}$;
Landfill subgrade is 2% [50(H) : 1(V)];
Waste filling slope is 25% [4(H) : 1(V)];
Side slope angle, $\beta = 18.4°$;
Height of side slope is 30 m;
Distance between the top edge of waste and the top edge of side slope is 20 m.

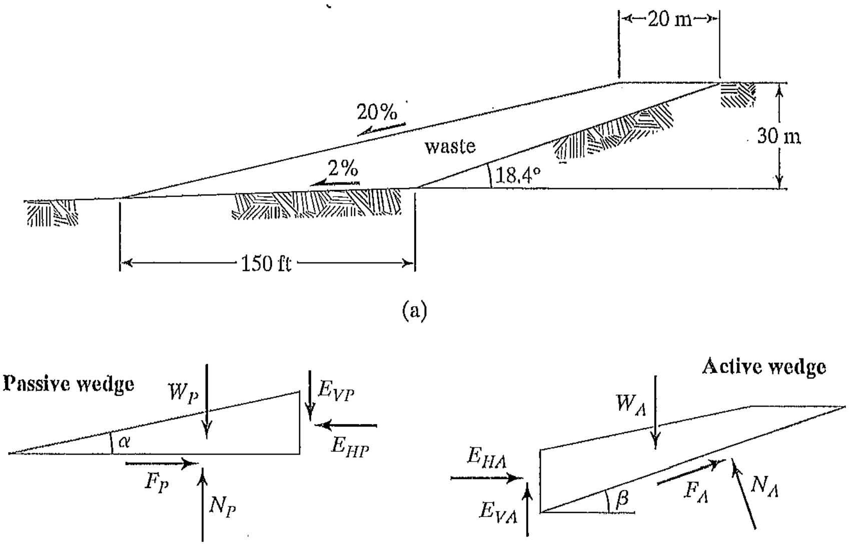

(a)

(b) (c)

FIGURE 13.25 Cross Section of a Solid Waste Landfill during Filling Condition

Solution The forces acting on the solid waste mass are shown in Figure 13.25. The side slope angle is at 18.4° and the slope angle of cell subgrade is 1.15° according to a 2% slope; hence,

$$\sin\beta = \sin(18.4°) = 0.3162, \cos\beta = \cos(18.4°) = 0.9487,$$
$$\sin\theta = \sin(1.15°) = 0.0200, \cos\theta = \cos(1.15°) = 0.9998$$
$$\tan\delta_A = \tan(14°) = 0.2493, \tan\delta_P = \tan(20°) = 0.3640,$$
$$\tan\phi_s = \tan(33°) = 0.6494.$$

The total weight of solid waste mass is

$$W_T = 10{,}987 \text{ kN/m}$$

The weight of the passive wedge is

$$W_P = 3{,}465 \text{ kN/m}$$

The weight of the active wedge is

$$W_A = W_T - W_P = 10{,}987 - 3{,}465 = 7{,}522 \text{ kN/m}$$

Use Equation 13.62 to calculate FS.

Calculate the coefficients of a, b, c, and d in Equation 13.62:

$$\begin{aligned}
a &= W_A \cdot \sin\beta \cdot \cos\theta + W_P \cdot \cos\beta \cdot \sin\theta \\
&= 7{,}522 \times 0.3162 \times 0.9998 + 3{,}465 \times 0.9487 \times 0.0200 \\
&= 2{,}444 \text{ kN/m} \\
b &= (W_A \cdot \tan\delta_P + W_P \cdot \tan\delta_A + W_T \cdot \tan\phi_s) \cdot \sin\phi \cdot \sin\theta - (W_A \cdot \tan\delta_A + W_P \cdot \tan\delta_P) \cdot \cos\beta \cdot \cos\theta \\
&= (7{,}522 \times 0.3640 + 3.465 \times 0.2493 + 10{,}987 \times 0.6494) \times 0.3162 \times 0.0200 - \\
&\quad (7{,}522 \times 0.2493 + 3{,}465 \times 0.3640 \times 0.9487 \times 0.9998 \\
&= -2{,}907 \text{ kN/m} \\
c &= -[W_T \cdot \tan\phi_s \cdot (\sin\beta \cdot \cos\theta \cdot \tan\delta_P + \cos\beta \cdot \sin\theta \cdot \tan\delta_A) + \\
&\quad (W_A \cdot \cos\beta \cdot \sin\theta \cdot W_P \cdot \sin\beta \cdot \cos\theta) \cdot \tan\delta_A \cdot \tan\delta_P] \\
&= -[10{,}987 \times 0.6494 \times (0.3162 \times 0.9998 \times 0.3640 + 0.9487 \times 0.0200 \times 0.2493) + \\
&\quad (7{,}522 \times 0.9487 \times 0.0200 + 3{,}465 \times 0.3162 \times 0.9998) \times 0.2493 \times 0.3640] \\
&= -967 \text{ kN/m} \\
d &= W_T \cdot \cos\beta \cdot \cos\theta \cdot \tan\delta_A \cdot \tan\delta_P \cdot \tan\phi_s \\
&= 10{,}987 \times 0.9487 \times 0.9998 \times 0.2493 \times 0.3640 \times 0.6494 \\
&= 614 \text{ kN/m}
\end{aligned}$$

$$a \cdot FS^3 + b \cdot FS^2 + c \cdot FS + d = 0 \qquad (13.62)$$
$$2{,}444 \cdot FS^3 - 2{,}907 \cdot FS^2 - 967 \cdot FS + 614 = 0$$
$$FS^3 - 1.189 \cdot FS^2 - 0.396 \cdot FS + 0.251 = 0$$
$$FS^3 + 0.251 = 1.189 \cdot FS^2 + 0.396 \cdot FS$$

which is solved by trial and error as in the following table:

Assumed FS	$FS^3 + 0.251$	$1.189 \cdot FS^2 + 0.396 \cdot FS$	Closure
(1)	(2)	(3)	(2) − (3)
1.5	3.626	3.269	0.357
1.4	2.995	2.885	0.110
1.3	2.448	2.524	−0.076
1.35	2.711	2.702	0.009
1.34	2.657	2.666	−0.009
1.345	2.684	2.684	0

Thus, $FS = 1.345$.
The direction of the resultant force of E_{HP} and E_{VP} (i.e., direction of the interwedge force) can be calculated from Equation 13.34 as

$$\begin{aligned} \tan\omega &= \tan\phi_s/FS \qquad (13.64) \\ &= \tan(33°)/1.345 \\ &= 0.649/1.345 \\ &= 0.483 \\ \omega &= 25.8° \end{aligned}$$

Recall that the inclination of waste filling slope is 20%, which is only 11.3°. Thus, the direction of the resultant force of E_{HP} and E_{VP} is definitely not parallel to the waste filling slope as is often assumed in these types of calculations (Corps of Engineers, 1960).

13.6.2 Case Histories

Alternatively, for the analysis of the case histories that follow, which failed in a translational manner, the simplified Janbu method was used. (See Koerner and Soong, 2000.) This derivation is also readily available in the literature and leads to a similar equation for the FS-value, but it is now modified with an f_o-value. The resulting equation is

$$FS = (f_o) \cdot \frac{\sum_{i=1}^{n} [c \cdot \Delta b_i + (W_i - u_i \cdot \Delta b_i) \cdot \tan\phi]/m_i}{\sum_{i=1}^{n} W_i \cdot \sin\theta_i} \qquad (13.65)$$

where m_i is defined in Equation 13.31, and f_o is a function of the curvature ratio of the failure surface and the type of soil. Since these surfaces are linear, however, the depth-to-length ratio is zero and the value of $f_o = 1.0$. The analysis becomes quite straightforward. (See Schuster and Krizek, 1978.)

To illustrate the seriousness of translational failures (they have represented the largest waste mass failures to date), three case histories are presented next.

APPLICATION FOR PERMIT
SUNDANCE WEST

VOLUME III: LANDFILL ENGINEERING CALCULATIONS
SECTION 7: TENSILE STRESS ANALYSIS

ATTACHMENT III.7.D

CETCO® LINING TECHNOLOGIES, 2009.

BENTOMAT® GCL DIRECT SHEAR DATABASE (TR-114BM)

LINING TECHNOLOGIES
Laboratory Data Reports

BENTOMAT® DIRECT SHEAR TESTING SUMMARY

The following table summarizes the direct shear testing on Bentomat that has been performed by CETCO and other laboratories on a project-specific basis for the past several years. This data will give the designer some general information about the shear strength of commonly used GCL interfaces and should be the first step in evaluating a proposed liner system where slope stability is a concern.

The variables in any direct shear test are numerous, including specimen preparation; hydration pressures, liquids, and sequencing, and rate of shear, and others. Test results will vary accordingly, which is partially accountable for the wide range of data reported even for similar interfaces.

This data is for informational purposes only and is not intended to replace project-specific interface testing, which CETCO emphatically recommends. CETCO makes no warranty as to the usefulness of the data. Individual test reports for most of the summarized data can be provided upon request.

BENTOMAT GCL DIRECT SHEAR DATABASE

TR-114BM

Lab[1]	Report Date	GCL Tested	Interface Tested[2]		Testing Conditions					Mohr-Coulomb Failure Envelopes[6]				Comments[8]
										Peak		Large Displacement[7]		
			GCL	Other	Normal Stresses (psi)	Hydration.[3] psf	hrs	Consol.[4]	SDR[5] (in/min)	Angle (deg)	adhesion (psf)	Angle (deg)	adhesion (psf)	
Internal Shear Results														
SGI	Oct-08	200R	Internal		75	200	24	48 hrs @ load	0.04	23 °	0	7 °	0	
SGI	Apr-09	ST	Internal		1.4	200	24	48 hrs @ load	0.004	73 °	0	--	--	sliding at gripping surface
PGL	Feb-08	ST	Internal		1.4	48 hrs @ load			0.004	77 °	0	--	--	sliding at gripping surface
SGI	Jun-06	ST	Internal		34.7	200	24	24 hrs	0.04	27 °	0	7 °	0	
SGI	Jun-06	ST	Internal		34.7	200	24	24 hrs	0.04	31 °	0	8 °	0	
SGI	Jun-06	ST	Internal		34.7	200	24	24 hrs	0.04	38 °	0	9 °	0	
SGI	Jun-06	ST	Internal		34.7	200	24	24 hrs	0.04	31 °	0	7 °	0	
SGI	Jun-06	ST	Internal		34.7	200	24	24 hrs	0.04	42 °	0	9 °	0	
SGI	Jun-06	ST	Internal		34.7	200	24	24 hrs	0.04	34 °	0	7 °	0	
SGI	Jun-06	ST	Internal		34.7	200	24	24 hrs	0.04	26 °	0	7 °	0	
SGI	Oct-06	ST	Internal		34.7	200	24	24 hrs	0.04	37 °	0	8 °	0	
PGL	Feb-03	ST	Internal		5 20 45	432	7 days	48 hrs @ load	0.004	22.7 °	1146	19.3 °	676	
SGI	Aug-01	ST	Internal		10 30 50	24 hrs @ load			0.001	32 °	1645	13 °	160	
SGI	Aug-01	ST	Internal		10 30 50	24 hrs @ load			0.001	39 °	1050	15 °	220	
SGI	Aug-01	ST	Internal		10 30 50	24 hrs @ load			0.001	38 °	1105	17 °	190	
SGI	Apr-09	ST	Internal		75	200	24	48 hrs @ load	0.004	32 °	0	8 °	0	

BENTOMAT GCL DIRECT SHEAR DATABASE
TR-114BM

Lab[1]	Report	GCL	Interface Tested[2]		Testing Conditions					Mohr-Coulomb Failure Envelopes[6]				Comments[8]
										Peak		Large Displacement[7]		
					Normal Stresses	Hydration.[3]		Consol.[4]	SDR[5]	Angle	adhesion	Angle	adhesion	
	Date	Tested	GCL	Other	(psi)	psf	hrs		(in/min)	(deg)	(psf)	(deg)	(psf)	
SGI	Jan-09	ST	Internal		75	200	24	48 hrs @ load	0.04	32 °	0	7 °	0	
SGI	Feb-08	ST	Internal		75	200	24	48 hrs @ load	0.04	38 °	0	8 °	0	
SGI	Jan-07	ST	Internal		75	200	24	48 hrs @ load	0.004	33 °	0	11 °	0	
SGI	Oct-98	ST	Internal		36 75 145	167	6 days	step-load	0.00006	22 °	1545	6 °	731	
SGI	Jan-09	ST	Internal		150	200	24	48 hrs @ load	0.04	24 °	0	6 °	0	
SGI	Feb-01	ST	Internal		50 100 150	48 hrs @ load			0.04	15 °	1195	8 °	-310	
SGI	Feb-01	ST	Internal		150 250 400	48 hrs @ load			0.04	11 °	2875	5 °	1080	
SGI	Feb-01	ST	Internal		50 to 400 psi	48 hrs @ load			0.04	12 °	2095	6 °	275	
SGI	Apr-09	DN	Internal		1.4	200	24	48 hrs @ load	0.004	75 °	0	--	--	sliding at gripping surface
SGI	Feb-08	DN	Internal		1.4	24 hrs @ load			0.004	77 °	0	--	--	sliding at gripping surface
TRI	Apr-03	DN	Internal		0.7 1.7 3.5	24 hrs @ load			0.04	47.3 °	2813	26.6 °	392	
SGI	Jun-01	DN	Internal		1.0 2.6 6.5	72	120	step-load	0.004	46 °	215	42 °	120	
PGL	Jul-06	DN	Internal		7 21	200	48	24 hrs @ load	0.04	14.5 °	2326	0.5 °	1436	
SGI	Sep-08	DN	Internal		5 25 50	200	24	24 hrs	0.04	34 °	1155	7 °	425	
SGI	Sep-08	DN	Internal		5 25 50	200	24	24 hrs	0.04	33 °	1260	8 °	425	
SGI	Sep-08	DN	Internal		5 25 50	200	24	24 hrs	0.04	35 °	990	8 °	430	

BENTOMAT GCL DIRECT SHEAR DATABASE

TR-114BM

Lab[1]	Report Date	GCL Tested	Interface Tested[2]		Testing Conditions					Mohr-Coulomb Failure Envelopes[6]				Comments[8]
										Peak		Large Displacement[7]		
					Normal Stresses (psi)	Hydration.[3]		Consol.[4]	SDR[5] (in/min)	Angle (deg)	adhesion (psf)	Angle (deg)	adhesion (psf)	
			GCL	Other		psf	hrs							
SGI	Sep-08	DN	Internal		5 25 50	200	24	24 hrs	0.04	32 °	1185	8 °	380	
SGI	Sep-08	DN	Internal		5 25 50	200	24	24 hrs	0.04	35 °	1120	7 °	385	
SGI	Sep-08	DN	Internal		5 25 50	200	24	24 hrs	0.04	33 °	1190	8 °	380	
SGI	Sep-08	DN	Internal		5 25 50	200	24	24 hrs	0.04	34 °	1150	7 °	410	
SGI	Sep-00	DN	Internal		10 25 50	24 hrs @ load			0.001	31 °	1000	12 °	770	GCL peel = 45 lbs
SGI	Sep-00	DN	Internal		10 25 50	24 hrs @ load			0.001	30 °	1155	10 °	170	GCL peel = 27 lbs
SGI	Mar-01	DN	Internal		15 30 60	48 hrs @ load			0.04	24 °	1655	7 °	180	
SGI	Apr-09	DN	Internal		75	200	24	48 hrs @ load	0.004	33 °	0	8 °	0	
SGI	Feb-08	DN	Internal		75	200	24	48 hrs @ load	0.04	40 °	0	8 °	0	
SGI	Jan-07	DN	Internal		75	200	24	48 hrs @ load	0.004	36 °	0	12 °	0	
SGI	Jun-08	DN	Internal		150	200	24	48 hrs @ load	0.04	28 °	0	7 °	0	
SGI	Sep-02	DN	Internal		34.7 150	As-received (21.6%)			0.04	23 °	1715	13 °	1100	
SGI	Apr-09	SDN	Internal		1.4	200	24	48 hrs @ load	0.004	76 °	0	--	--	sliding at gripping surface
GT	Nov-08	SDN	Internal		1.4	200	24	48 hrs @ load	0.004	74 °	0	--	--	
SGI	Aug-09	SDN	Internal		10 30 70	144	48	24 hrs @ load	0.004	34 °	1248	6 °	1020	
SGI	Apr-09	SDN	Internal		75	200	24	48 hrs @ load	0.004	37 °	0	8 °	0	

BENTOMAT GCL DIRECT SHEAR DATABASE

TR-114BM

Lab[1]	Report Date	GCL Tested	Interface Tested[2]		Testing Conditions					Mohr-Coulomb Failure Envelopes[6]				Comments[8]
										Peak		Large Displacement[7]		
			GCL	Other	Normal Stresses (psi)	Hydration.[3] psf	Hydration.[3] hrs	Consol.[4]	SDR[5] (in/min)	Angle (deg)	adhesion (psf)	Angle (deg)	adhesion (psf)	
SGI	Feb-08	SDN	Internal		75	200	24	48 hrs @ load	0.04	34 °	0	7 °	0	
SGI	Jan-07	SDN	Internal		75	200	24	48 hrs @ load	0.004	36 °	0	12 °	0	
TRI	Apr-08	SDN	Internal		90	24 hrs @ load			0.04	39.1 °	0	15.5 °	0	
SGI	Oct-06	SDN	Internal		5 20 90	115	24	step-load	0.004	22 °	755	5 °	435	
TRI	Oct-07	SDN	Internal		41.7 83.3 125	200	24	step-load	0.04	27.2 °	680	17.1 °	0	
SGI	Jun-03	SDN	Internal		150 250 400	48 hrs @ load			0.04	12 °	1390	5 °	1715	
SGI	Aug-08	STM	Internal		1.4	48 hrs @ load			0.004	73 °	0	--	--	sliding at gripping surface
SGI	Feb-01	CL	Internal		139	144	21 days	168 hrs @ load	0.04	25 °	0	7 °	0	
Interface Shear Results (with geomembranes)														
TRI	May-09	200R		40-mil smooth LLDPE	1 2 4	24 hrs @ load			0.04	11.2 °	4	10 °	4	
SGI	Mar-05	ST	W	60-mil text. HDPE	0.7	48 hrs @ load			0.04	34 °	0	25 °	0	co-extruded textured geomembrane
PGL	Feb-01	ST	white NW	40-mil text. LLDPE	0.35 0.69 1.39	50	24	24 hrs @ load	0.04	29 °	196	16 °	176	co-extruded textured geomembrane
SGI	Dec-08	ST	W	60-mil text. HDPE	2.8	200	24	48 hrs @ load	0.04	40 °	0	26 °	0	co-extruded textured geomembrane
SGI	Apr-07	ST	W	30-mil PVC	1 2 3	100	24	24 hrs @ load	0.04	16 °	5	15 °	5	smooth side
SGI	Apr-07	ST	NW	30-mil PVC	1 2 3	100	24	24 hrs @ load	0.04	14 °	0	14 °	0	smooth side
SGI	Jan-06	ST	W	30-mil PVC	1 2 3	200	48	--	0.04	15 °	5	15 °	0	faille side
SGI	Jan-96	ST	W	30-mil PVC	2 4 6	24 hrs @ load			0.04	17 °	24	17 °	24	

BENTOMAT GCL DIRECT SHEAR DATABASE

TR-114BM

Lab[1]	Report Date	GCL Tested	Interface Tested[2]		Testing Conditions							Mohr-Coulomb Failure Envelopes[6]				Comments[8]
					Normal Stresses (psi)			Hydration.[3]		Consol.[4]	SDR[5] (in/min)	Peak		Large Displacement[7]		
			GCL	Other				psf	hrs			Angle (deg)	adhesion (psf)	Angle (deg)	adhesion (psf)	
PGL	Jun-01	ST	NW	40-mil text. LLDPE	1.3	2.6	6.3	72	72	step-load	0.001	24.8 °	230	18.9 °	203	embossed textured geomembrane
TRI	Apr-08	ST		60-mil text. HDPE	0.7	3.5	6.9	100	24	step-load	0.04	23.9 °	107	16.4 °	62	co-extruded textured geomembrane
TRI	Feb-06	ST	NW	60-mil text. HDPE	1.7	3.5	6.9	200	48	24 hrs @ load	0.04	26.7 °	0	23.9 °	0	co-extruded textured geomembrane
TRI	Sep-05	ST	NW	60-mil text. HDPE	2	5	10	24 hrs @ load			0.04	33.8 °	223	20.2 °	181	embossed textured geomembrane
TRI	Aug-06	ST	W	60-mil text. HDPE	3.5	6.9	13.9	48 hrs @ load			0.04	28 °	50	23.6 °	9	embossed textured geomembrane
TRI	Aug-09	ST	W	60-mil text. HDPE	6.9	13.9	20.8	24 hrs @ load			0.04	21.5 °	291	15.1 °	129	embossed textured geomembrane
PGL	Feb-03	ST	W	80-mil text. HDPE	5	20	45	432	7 days	48 hrs @ load	0.004	22.5 °	83	13.6 °	130	embossed textured geomembrane
PGL	Mar-06	ST	W	80-mil text. HDPE	5	20	45	432	7 days	48 hrs @ load	0.004	20 °	379	13.3 °	413	embossed textured geomembrane
PGL	Mar-07	ST	NW	60-mil text. HDPE	13.9	27.8	55.6	500	6 days	24 hrs @ load	0.04	18.1 °	70.5	12.2 °	222.5	
EMCON	Jun-05	ST	NW	60-mil text. HDPE	13.9	34.7	69.4	300	48	24 hrs @ load	0.04	20.6 °	426	8.1 °	738	embossed textured geomembrane
SGI	Jun-09	ST	W	60-mil text. HDPE	75			200	24	48 hrs @ load	0.04	24 °	0	10 °	0	co-extruded textured geomembrane
SGI	Jun-09	ST	W	60-mil text. HDPE	75			200	24	48 hrs @ load	0.04	23 °	0	11 °	0	co-extruded textured geomembrane
SGI	Dec-08	ST	W	60-mil text. HDPE	75			200	24	48 hrs @ load	0.04	22 °	0	11 °	0	co-extruded textured geomembrane
EMCON	Jul-05	ST	NW	60-mil text. HDPE	13.9	55.6	83.3	300	48	24 hrs @ load	0.04	17.8 °	404.9	6.4 °	463.6	
JLT	Oct-04	ST		60-mil text. HDPE	20	45	90	108	3 days	step-load	0.001	24.3 °	323	15.3 °	243	co-extruded textured geomembrane
TRI	Apr-08	ST		60-mil text. HDPE	6.9	69.4	139	100	24	step-load	0.04	18.9 °	0	7.6 °	192	co-extruded textured geomembrane

BENTOMAT GCL DIRECT SHEAR DATABASE

TR-114BM

Lab[1]	Report Date	GCL Tested	Interface Tested[2]		Testing Conditions					Mohr-Coulomb Failure Envelopes[6]				Comments[8]
										Peak		Large Displacement[7]		
			GCL	Other	Normal Stresses (psi)	Hydration.[3]		Consol.[4]	SDR[5] (in/min)	Angle (deg)	adhesion (psf)	Angle (deg)	adhesion (psf)	
						psf	hrs							
SGI	2003	ST	W	60-mil text. HDPE	139	Hydrated			0.04	14.5 °	0	10.1 °	0	Encapsulated design
SGI	Sep-09	ST	NW	60-mil text. HDPE	13.9 139	200	24	step-load	0.04	21 °	550	8 °	590	co-extruded textured geomembrane
SGI	Sep-09	ST	W	60-mil text. HDPE	13.9 139	200	24	step-load	0.04	18 °	575	8 °	385	co-extruded textured geomembrane
VE	Jun-09	ST		60-mil text. LLDPE	39 78 156	96 hrs @ load			0.04	18 °	990	4 °	1600	embossed textured geomembrane
SGI	2003	ST	W	60-mil text. HDPE	208	Hydrated			0.04	13.7 °	0	9.8 °	0	Encapsulated design
GA	Oct-08	ST		60-mil smooth LLDPE	75 150 300	24 hrs @ load			0.04	15 °	662	4.2 °	3355	GCL internal failure @ 300 psi
SGI	Mar-09	DN	white NW	60-mil text. HDPE	1 2 3	240	48	24 hrs @ load	0.04	33 °	65	27 °	30	embossed textured geomembrane
SGI	Mar-09	DN	white NW	60-mil text. HDPE	1 2 3	240	48	24 hrs @ load	0.04	36 °	50	26 °	45	embossed textured geomembrane
SGI	Mar-09	DN	white NW	60-mil text. HDPE	1 2 3	240	48	24 hrs @ load	0.04	35 °	60	27 °	40	embossed textured geomembrane
SGI	Jan-06	DN	black NW	30-mil PVC	1 2 3	200	48	--	0.04	15 °	0	15 °	0	faille side
PGL	Jun-01	DN	black NW	Textured HDPE	1.3 2.6 6.3	216	72	step-load	0.001	21.4 °	225	18.5 °	184	2-inch displacement
PGL	Jun-01	DN	black NW	Textured HDPE	1.3 2.6 6.3	72	72	step-load	0.001	24.8 °	230	18.9 °	203	2-inch displacement
SGI	May-01	DN	black NW	40-mil text. LLDPE	1 2.6 6.5	72	120	step-load	0.004	32 °	5	28 °	5	embossed textured geomembrane
PGL	Mar-08	DN	white NW	60-mil text. HDPE	5 7 9	24 hrs @ load			0.04	22.5 °	309	22.5 °	305	
EMCON	May-03	DN		Textured HDPE	13.9	Partially hydrated b/w 2 GMs with 0.3" holes			0.04	18.8 °	0	14.3 °	0	Encapsulated b/w GMs with 0.3" holes
GT	Aug-07	DN	black NW	60-mil text. HDPE	18	Hydrated			0.04	26.6 °	0	18.5 °	0	embossed textured geomembrane

BENTOMAT GCL DIRECT SHEAR DATABASE

TR-114BM

Lab[1]	Report Date	GCL Tested	Interface Tested[2]		Testing Conditions							Mohr-Coulomb Failure Envelopes[6]				Comments[8]
					Normal Stresses (psi)			Hydration.[3]		Consol.[4]	SDR[5]	Peak		Large Displacement[7]		
			GCL	Other				psf	hrs		(in/min)	Angle (deg)	adhesion (psf)	Angle (deg)	adhesion (psf)	
SGI	Feb-00	DN	black NW	60-mil text. HDPE	7	14	35	72	72	step-load	0.0016	29 °	370	18 °	375	
PGL	Jul-05	DN		60-mil text. HDPE	13.9	27.8	41.7	48 hrs @ load			0.04	17.2 °	359	15.4 °	275	
SGI	Jul-03	DN	black NW	60-mil text. HDPE	10.4	20.8	41.7	48 hrs @ load			0.04	27 °	60	18 °	25	co-extruded textured geomembrane
SGI	Feb-08	DN	black NW	60-mil text. HDPE	15	30	50	1440	48	24 hrs @ load	0.04	27 °	530	16 °	390	co-extruded textured geomembrane
PGL	Jan-05	DN	white NW	80-mil text. HDPE	15	30	50	1440	48	24 hrs @ load	1	17.2 °	151	8.5 °	303	
PGL	Feb-07	DN		60-mil text. HDPE	10	30	60	24 hrs @ load			0.02	24 °	254	22.6 °	65	
PGL	Dec-06	DN		60-mil text. HDPE	10	30	60	24 hrs @ load			0.02	19.2 °	155	15.5 °	147	
PGL	Dec-06	DN		60-mil text. HDPE	10	30	60	24 hrs @ load			0.02	18.5 °	342	18.6 °	108	
SGI	Jul-02	DN	white NW	60-mil text. HDPE	6.9	34.7	69.4	125	24	48 hrs @ load	0.04	23 °	520	12 °	380	co-extruded textured geomembrane
SGI	Jun-03	DN		40- and 60-mil textured HDPE	69.4			Partially hydrated b/w 2 GMs with 0.25" holes			0.04	29 °	0	21 °	0	Encapsulated b/w GMs with 0.25" holes
EMCON	Jun-03	DN		Textured HDPE	69.4			Partially hydrated b/w 2 GMs with 0.3" holes			0.04	19.6 °	0	6.5 °	0	Encapsulated b/w GMs with 0.3" holes
SGI	Feb-08	DN	white NW	60-mil text. HDPE	25	50	75	1440	48	24 hrs @ load	0.04	23 °	570	10 °	420	co-extruded textured geomembrane
SGI	Feb-08	DN	white NW	60-mil text. HDPE	25	50	75	1440	48	24 hrs @ load	0.04	28 °	345	13 °	415	co-extruded textured geomembrane
PGL	Mar-08	DN	black NW	60-mil text. HDPE	25	50	75	24 hrs @ load			0.04	23.6 °	0	22.2 °	0	
SGI	Apr-09	DN	black NW	60-mil text. HDPE	75			200	24	step-load	0.04	30 °	0	14 °	0	embossed textured geomembrane
TRI	Oct-07	DN	black NW	60-mil textured HDPE	25	50	75	24 hrs @ load			0.04	22.7 °	52	11.9 °	409	co-extruded textured geomembrane

BENTOMAT GCL DIRECT SHEAR DATABASE

TR-114BM

Lab[1]	Report Date	GCL Tested	Interface Tested[2]		Testing Conditions					Mohr-Coulomb Failure Envelopes[6]				Comments[8]
					Normal Stresses (psi)	Hydration.[3]		Consol.[4]	SDR[5] (in/min)	Peak		Large Displacement[7]		
			GCL	Other		psf	hrs			Angle (deg)	adhesion (psf)	Angle (deg)	adhesion (psf)	
TRI	Oct-07	DN	black NW	60-mil textured HDPE	25 50 75	24 hrs @ load			0.04	10.8 °	1516	5.4 °	1194	co-extruded textured geomembrane
TRI	Oct-07	DN	black NW	60-mil textured HDPE	25 50 75	24 hrs @ load			0.04	20.4 °	455	9.6 °	644	co-extruded textured geomembrane
PGL	Mar-07	DN	white NW	60-mil text. LLDPE	25 50 75	24 hrs @ load			0.04	23 °	0	22 °	0	embossed textured geomembrane
PGL	Mar-06	DN	white NW	60-mil text. LLDPE	25 50 75	24 hrs @ load			0.04	20 °	334	8.6 °	1216	embossed textured geomembrane
GA	Mar-02	DN	black NW	80-mil text. LLDPE	20.8 41.7 83.3	288	24	10 minutes	0.04	21.7 °	789	11.7 °	559	co-extruded textured geomembrane
GA	Mar-02	DN	black NW	60-mil text. LLDPE	20.8 41.7 83.3	288	24	10 minutes	0.04	21.5 °	361	6.7 °	880.5	embossed textured geomembrane
PGL	Apr-07	DN		60-mil text. HDPE	20.8 41.7 83.3	48 hrs @ load			0.04	20.9 °	0	12.3 °	545	
JLT	May-07	DN	black NW	60-mil text. HDPE	20 45 90	115	4 days	step-load	0.005	22.1 °	77	13 °	239	co-extruded textured geomembrane
SGI	May-08	DN	black NW	60-mil text. HDPE	1.4 100	200	24	48 hrs @ load	0.04	24 °	130	12 °	80	co-extruded textured geomembrane
TRI	Jul-08	DN		60-mil text. HDPE	139	144	24	step-load	0.04	22 °	0	10.2 °	0	co-extruded textured geomembrane
VE	May-03	DN		40- and 60-mil text. HDPE	13.9 27.8 55.6 111	250	48	16 hrs @ load	0.04	24 °	260	10 °	650	Encapsulated design
SGI	Jul-09	DN	black NW	60-mil text. HDPE	13.9 27.8 55.6 111	144	24	24 hrs @ load	0.04	22 °	560	11 °	585	co-extruded textured geomembrane
VE	May-03	DN		40- and 60-mil text. HDPE	27.8 111	As-received (25% moisture)			0.04	26 °	0	16 °	140	Encapsulated design
EMCON	Nov-02	DN		60-mil text. HDPE	27.8 55.6 111	48 hrs @ load			0.04	26 °	0	16.8 °	0	co-extruded textured geomembrane
SGI	2003	DN		40- and 80-mil HDPE	5 20 80 120	wetted conditions (not fully hydrated)			0.04	27 °	150	19 °	95	Encapsulated design (slip b/w 80-mil + GCL)
SGI	2003	DN		40- and 80-mil HDPE	5 20 80 120	wetted conditions (not fully hydrated)			0.04	29 °	270	19 °	120	Encapsulated design (slip b/w 80-mil + GCL)

BENTOMAT GCL DIRECT SHEAR DATABASE

TR-114BM

Lab[1]	Report Date	GCL Tested	Interface Tested[2]		Testing Conditions								Mohr-Coulomb Failure Envelopes[6]				Comments[8]
					Normal Stresses (psi)				Hydration.[3]		Consol.[4]	SDR[5] (in/min)	Peak		Large Displacement[7]		
			GCL	Other					psf	hrs			Angle (deg)	adhesion (psf)	Angle (deg)	adhesion (psf)	
SGI	2003	DN		40- and 80-mil HDPE	5	20	80	120	wetted conditions (not fully hydrated)			0.04	28 °	140	20 °	20	Encapsulated design (slip b/w 80-mil + GCL)
SGI	2003	DN		40- and 80-mil HDPE	5	20	80	120	wetted conditions (not fully hydrated)			0.04	29 °	145	19 °	50	Encapsulated design (slip b/w 80-mil + GCL)
SGI	2003	DN		40- and 80-mil HDPE	5	20	80	120	wetted conditions (not fully hydrated)			0.04	27 °	580	20 °	70	Encapsulated design (slip b/w 80-mil + GCL)
SGI	2003	DN		40- and 80-mil HDPE	5	20	80	120	wetted conditions (not fully hydrated)			0.04	27 °	235	19 °	95	Encapsulated design (slip b/w 80-mil + GCL)
SGI	Jun-08	DN	black NW	60-mil text. HDPE	41.7	83.3	125		24 hrs @ load			0.04	26 °	105	15 °	620	2-inch displacement
SGI	Jun-08	DN	black NW	60-mil text. HDPE	41.7	83.3	125		24 hrs @ load			0.04	25 °	165	13 °	870	2-inch displacement
SGI	Jun-08	DN	black NW	60-mil text. HDPE	41.7	83.3	125		24 hrs @ load			0.04	26 °	110	16 °	485	2-inch displacement
SGI	Jun-08	DN	black NW	60-mil text. HDPE	41.7	83.3	125		24 hrs @ load		24 hrs @ load	0.04	26 °	20	16 °	350	2-inch displacement
SGI	Jun-08	DN	black NW	60-mil text. HDPE	41.7	83.3	125		24 hrs @ load			0.04	26 °	50	15 °	165	2-inch displacement
SGI	Jul-08	DN	black NW	60-mil text. HDPE	125				24 hrs @ load		24 hrs @ load	0.04	25.1 °	0	16.4 °	0	2-inch displacement
SGI	Aug-03	DN	white NW	60-mil text. HDPE	41.7	83.3	125		0	24	48 hrs @ load	0.04	22 °	835	15 °	40	2-inch displacement
SGI	Aug-03	DN	white NW	60-mil text. HDPE	41.7	83.3	125		0	24	48 hrs @ load	0.04	25 °	315	16 °	255	2-inch displacement
TRI	Jun-09	DN		60-mil text. HDPE	20.8	55.6	104	139	125	20	24 hrs @ load	0.04	24.9 °	0	8.7 °	617	embossed textured geomembrane
GTX	Apr-07	DN		HDPE	34.7	69.4	104	139	48 hrs @ load			0.04	26 °	588	12 °	398	
SGI	Feb-00	DN	black NW	60-mil text. HDPE	7 to 150 psi				72	72	step-load	0.0016	22 °	760	11 °	710	
SGI	Oct-02	DN		80-mil text. HDPE	15	25	100	150	1440	48	24 hrs @ load	0.04	23 °	120	14 °	330	co-extruded textured geomembrane

BENTOMAT GCL DIRECT SHEAR DATABASE

TR-114BM

Lab[1]	Report Date	GCL Tested	Interface Tested[2]		Testing Conditions								Mohr-Coulomb Failure Envelopes[6]				Comments[8]
					Normal Stresses (psi)				Hydration.[3]		Consol.[4]	SDR[5] (in/min)	Peak		Large Displacement[7]		
			GCL	Other					psf	hrs			Angle (deg)	adhesion (psf)	Angle (deg)	adhesion (psf)	
SGI	Nov-02	DN		80-mil text. HDPE	25	100	150		As-received (25% moisture)			0.04	24 °	335	18 °	120	co-extruded textured geomembrane
SGI	Feb-00	DN	black NW	60-mil text. HDPE	35	100	150		72	72	step-load	0.0016	21 °	1305	9 °	1105	
GTX	Jul-05	DN	white NW	60-mil text. HDPE	69.4	111	167		24 hrs @ load			0.04	16 °	102	5 °	707	
SGI	Apr-09	DN	black NW	60-mil text. HDPE	75	150	250	400	200	24	step-load	0.04	18 °	2450	5 °	2220	embossed textured geomembrane
SGI	Jul-09	DN	black NW	60-mil text. HDPE	150	250	400		200	24	step-load	0.04	17 °	3705	4 °	3435	GCL internal failure @ 400 psi
TRI	Mar-07	SDN	black NW	40-mil text. LLDPE	0.7	2.8	4.9		100	24	24 hrs @ load	0.04	32.6 °	148	22.5 °	83	embossed textured geomembrane
TRI	Mar-07	SDN	black NW	60-mil text. HDPE	0.7	2.8	4.9		24 hrs @ load			0.04	39.3 °	31	26.7 °	44	embossed textured geomembrane
TRI	Mar-07	SDN	black NW	50-mil text. LLDPE	0.7	2.8	4.9		24 hrs @ load			0.04	44.3 °	97	44.5 °	0	structured GM/Drainage Liner
TRI	Mar-07	SDN	black NW	40-mil text. LLDPE	0.7	2.8	4.9		100	24	24 hrs @ load	0.04	32.6 °	148	22.5 °	83	embossed textured geomembrane
SGI	May-03	SDN	black NW	40-mil text. HDPE	0.7	3.5	6.9		100	24	24 hrs @ load	0.04	30 °	25	19 °	20	co-extruded textured geomembrane
TRI	Jul-08	SDN	Black NW	60-mil text. HDPE	3.5	13.9	31.3	62.5	200	24	step-load	0.04	15.8 °	243	6.5 °	303	co-extruded textured geomembrane
TRI	May-07	SDN		60-mil text. HDPE	6.9	41.7	83.3		250	24	step-load	0.04	23.8 °	467	10.6 °	365	embossed textured geomembrane
SGI	Oct-06	SDN	white NW	60-mil text. HDPE	5	20	90		115	24	step-load	0.04	23 °	695	8 °	425	co-extruded textured geomembrane
PGL	Apr-04	SDN		60-mil text. HDPE	25	60	100		24 hrs @ load			0.04	24.7 °	308	14.1 °	155	
PGL	Sep-04	SDN		60-mil text. HDPE	25	60	100		24 hrs @ load			0.04	22.6 °	0	14.5 °	203	
PGL	Sep-04	SDN		60-mil text. HDPE	25	60	100		24 hrs @ load			0.04	18.9 °	387	15.2 °	333	

BENTOMAT GCL DIRECT SHEAR DATABASE

TR-114BM

Lab[1]	Report Date	GCL Tested	Interface Tested[2]		Testing Conditions					Mohr-Coulomb Failure Envelopes[6]				Comments[8]
										Peak		Large Displacement[7]		
			GCL	Other	Normal Stresses (psi)	Hydration.[3] psf	Hydration.[3] hrs	Consol.[4]	SDR[5] (in/min)	Angle (deg)	adhesion (psf)	Angle (deg)	adhesion (psf)	
PGL	Sep-04	SDN		60-mil text. HDPE	25 60 100	24 hrs @ load			0.04	26.4 °	0	24.1 °	0	
PGL	Sep-04	SDN		60-mil text. HDPE	25 60 100	24 hrs @ load			0.04	22.6 °	0	14.5 °	203	
PGL	Sep-04	SDN		60-mil text. HDPE	25 60 100	24 hrs @ load			0.04	18.9 °	387	15.2 °	333	
PGL	Sep-04	SDN		60-mil text. HDPE	25 60 100	24 hrs @ load			0.04	26.4 °	0	24.1 °	0	
EMCON	Dec-02	SDN	white NW	60-mil text. HDPE	27.8 55.6 111	220	24	24 hrs @ load	0.04	21.2 °	0	11.4 °	0	co-extruded textured geomembrane
TRI	Oct-07	SDN	black NW	60-mil text. HDPE	41.7 83.3 125	200	24	step-load	0.04	22.7 °	0	10.5 °	0	embossed textured geomembrane
GA	Oct-08	SDN		60-mil smooth LLDPE	75 150 300	24 hrs @ load			0.04	18.3 °	662	12.4 °	2246	
SGI	Jun-03	SDN		80-mil text. LLDPE	150 250 400	48 hrs @ load			0.04	11 °	540	7 °	325	co-extruded textured geomembrane
TRI	Jun-07	STM	white NW	60-mil text. LLDPE	100	200	24	step-load	0.04	20.1 °	0	11.5 °	0	co-extruded textured geomembrane
SGI	May-07	STM	white NW	40-mil text. LLDPE	100	200	24	48 hrs @ load	0.04	24 °	0	10 °	0	co-extruded textured geomembrane
SGI	Aug-09	STM	white NW	60-mil text. LLDPE	39 78 156	96 hrs @ load			0.04	21 °	720	9 °	1185	embossed textured geomembrane
Interface Shear Results (with soil)														
ARD	Aug-01	ST	W	SOIL	2.3 3 3.75	24 hrs @ load			0.04	38.7 °	0	38.7 °	0	CIDCO Pit sand
ARD	Aug-01	ST	NW	SOIL	2.3 3 3.75	24 hrs @ load			0.04	36.5 °	0	36.5 °	0	CIDCO Pit sand
ARD	Aug-01	ST	W	SOIL	2.3 3 3.75	24 hrs @ load			0.04	38.1 °	0	38.1 °	0	Michigan Pit sand
ARD	Aug-01	ST	NW	SOIL	2.3 3 3.75	24 hrs @ load			0.04	36.7 °	0	35.6 °	0	Michigan Pit sand
STS	Jan-00	ST	W	SOIL	1 2 4	48 hrs @ load			0.04	28.6 °	293	28 °	241	Topsoil: 62 pcf, 15%

BENTOMAT GCL DIRECT SHEAR DATABASE

TR-114BM

Lab[1]	Report Date	GCL Tested	Interface Tested[2]		Testing Conditions								Mohr-Coulomb Failure Envelopes[6]				Comments[8]
					Normal Stresses (psi)				Hydration.[3]		Consol.[4]	SDR[5] (in/min)	Peak		Large Displacement[7]		
			GCL	Other					psf	hrs			Angle (deg)	adhesion (psf)	Angle (deg)	adhesion (psf)	
TRI	Nov-03	ST	NW	SOIL	1.4	3.6	7.1		24 hrs @ load			0.04	17.7 °	139	18.2 °	135	Soil: 99 pcf, 17%
TRI	Oct-05	ST	W	SOIL	2	5	10		24 hrs @ load			0.04	23.2 °	134	19.9 °	117	Soil: 114 pcf, 14%
TRI	Aug-09	ST	NW	SOIL	7.4	15.4	23.5		24 hrs @ load			0.04	28.1 °	5	25.9 °	0	
PGL	Mar-07	ST	W	SOIL	13.9	27.8	55.6		500	6 days	24 hrs @ load	0.04	21.4 °	279	8.7 °	926	Soil: 110 pcf, 15.2%
TRI	Jul-08	ST	NW	SOIL	3.5	13.9	55.6		24 hrs @ load			0.04	28.7 °	176	16.1 °	474	Soil: 94 pcf, 14.2%
TRI	Nov-06	ST	NW	SOIL	8.1	27.8	55.7		24 hrs @ load			0.04	21.6 °	0	21.6 °	0	Soil: 110 pcf, 12.4%
SGI	Jul-04	ST	W	SOIL	1	20	40	60	24 hrs @ load			0.04	23 °	145	22 °	120	
SGI	Aug-08	ST	NW	SOIL	10	35	60		100	24	24 hrs @ load	0.04	7 °	475	7 °	360	
SGI	Feb-04	ST	W	SOIL	20.8	52.1	79.9		72	7 days	step-load	0.0016	9.9 °	930	6.7 °	500	Clay
SGI	Feb-04	ST	W	SOIL	20.8	52.1	79.9		72	7 days	step-load	0.0016	10 °	1025	7 °	590	Clay
EMCON	Jul-05	ST	W	SOIL	13.9	55.6	83.3		300	48	24 hrs @ load	0.04	15.6 °	561.1	15.6 °	435.8	
NTH	2005	ST	NW	SOIL	25	50	100		144	24	--	0.04	11.9 °	0	7.9 °	0	Clay: 95 pcf, 8%
SGI	Apr-06	ST	W	SOIL	20.8	79.9	139		72	7 days	step-load	0.004	12 °	905	--	--	Clay; GCL internal failure at 139 psi load
JLT	Jan-03	DN		SOIL	0.3	0.7	1.4		24 hrs @ load			0.04	36.3 °	2	29 °	1	Angular gravel
CETCO	Mar-00	DN	black NW	SOIL	0.7	1.4	2.1		24 hrs @ load			0.04	25.2 °	315	--	--	SP, 108 pcf, 11%
GTX	Jul-05	DN	black NW	SOIL	0.7	1.4	2.8		24 hrs @ load		24 hrs @ load	0.04	31 °	60	18 °	27	

BENTOMAT GCL DIRECT SHEAR DATABASE

TR-114BM

Lab[1]	Report Date	GCL Tested	Interface Tested[2]		Testing Conditions					Mohr-Coulomb Failure Envelopes[6]				Comments[8]
										Peak		Large Displacement[7]		
					Normal Stresses (psi)	Hydration.[3]		Consol.[4]	SDR[5] (in/min)	Angle (deg)	adhesion (psf)	Angle (deg)	adhesion (psf)	
			GCL	Other		psf	hrs							
TRI	Nov-08	DN	white NW	SOIL	0.8 1.6 2.9	24 hrs @ load			0.04	41.1 °	0	28.4 °	29	Soil: 105 pcf, 13.5%
SGI	Nov-08	DN	black NW	SOIL	1 2 3	240	48	24 hrs @ load	0.04	32 °	25	31 °	5	
SGI	Nov-08	DN	black NW	SOIL	1 2 3	240	48	24 hrs @ load	0.04	31 °	25	31 °	5	
TRI	Nov-08	DN	black NW	SOIL	0.7 1.5 3	24 hrs @ load			0.04	18.9 °	70	10.9 °	82	Soil: 105 pcf, 14.1%
PGL	Jun-01	DN	white NW	SOIL	1.3 2.6 6.3	72	72	step-load	0.001	21.2 °	207	21.6 °	184	2-inch displacement; soil: 103 pcf, 17%
PGL	Jun-01	DN	white NW	SOIL	1.3 2.6 6.3	216	72	step-load	0.001	23.2 °	206	20.8 °	194	2-inch displacement; soil: 103 pcf, 17%
SGI	Jun-01	DN	white NW	SOIL	1.0 2.6 6.5	72	120	step-load	0.004	35 °	65	34 °	40	
PGL	Mar-08	DN	black NW	SOIL	5 7 9	24 hrs @ load			0.04	33.6 °	342	33.6 °	337	Soil: 107 pcf, 13.4%
ARD	Oct-05	DN	white NW	SOIL	2 5 9.9	48 hrs @ load			0.04	28.2 °	64	28.4 °	47	Medium to fine silty sand: 117 pcf, 9.5%
ARD	Oct-05	DN	black NW	SOIL	2 5 9.9	48 hrs @ load			0.04	29.3 °	42	29.4 °	38	Medium to fine silty sand: 117 pcf, 9.5%
SGI	Apr-01	DN	black NW	SOIL	1 5 10	48 hrs @ load			0.04	36 °	35	35 °	10	Soil: 124 pcf, 9 %
GT	Aug-07	DN	white NW	SOIL	3 5 10 18	Hydrated			0.04	25.8 °	81	24.3 °	92	Soil: 100 pcf, 19.4%
GT	Aug-07	DN	white NW	SOIL	3 5 10 18	Hydrated			0.04	25.1 °	96	16.1 °	135	Soil: 93 pcf, 20.9%
SGI	Jul-03	DN	white NW	SOIL	10.4 20.8 41.7	48 hrs @ load			0.04	28 °	40	26 °	10	
SGI	Mar-01	DN	white NW	SOIL	55.6	1000	24	24 hrs @ load	0.04	26 °	0	23 °	0	
PGL	Dec-06	DN		SOIL	10 30 60	24 hrs @ load			0.02	32.5 °	491	7.5 °	1319	Soil: 92 pcf, 17.5%

BENTOMAT GCL DIRECT SHEAR DATABASE

TR-114BM

Lab[1]	Report Date	GCL Tested	Interface Tested[2]		Testing Conditions					Mohr-Coulomb Failure Envelopes[6]				Comments[8]
										Peak		Large Displacement[7]		
					Normal Stresses	Hydration.[3]		Consol.[4]	SDR[5]	Angle	adhesion	Angle	adhesion	
			GCL	Other	(psi)	psf	hrs		(in/min)	(deg)	(psf)	(deg)	(psf)	
PGL	Dec-06	DN		SOIL	10 30 60	24 hrs @ load			0.02	36.9 °	305	23.2 °	751	
PGL	Aug-04	DN	white NW	SOIL	6.9 41.7 69.4	125	20	16 hrs @ load	0.04	28.6 °	312	15.6 °	854	Soil: 120 pcf, 12%
PGL	Aug-04	DN	white NW	SOIL	6.9 34.7 69.4	125	20	16 hrs @ load	0.04	20.8 °	177	17.3 °	190	Soil: 114 pcf, 14.9%
PGL	Aug-04	DN	white NW	SOIL	6.9 41.7 69.4	125	20	16 hrs @ load	0.04	28.6 °	312	15.6 °	854	Soil: 120 pcf, 12%
PGL	Aug-04	DN	white NW	SOIL	6.9 34.7 69.4	125	20	16 hrs @ load	0.04	20.8 °	177	17.3 °	190	Soil: 114 pcf, 14.9%
PGL	Mar-06	DN	black NW	SOIL	25 50 75	24 hrs @ load			0.04	32 °	61	32 °	0	Soil: 109 pcf, 14.9%
PGL	Apr-07	DN		SOIL	20.8 41.7 83.3	48 hrs @ load			0.04	32.2 °	0	31.9 °	0	
PGL	Jul-03	DN		SOIL	3.5 20.8 41.7 83.3	125	24	16 hrs @ load	0.04	22.3 °	320	19 °	322	Soil: 91 pcf, 22%; GCL internal failure at 83 psi
GTX	Apr-07	DN		SOIL	34.7 69.4 104 139	48 hrs @ load			0.04	20 °	1940	-3 °	3247	Brown silty gravel
GTX	Jul-05	DN	black NW	SOIL	69.4 111 167	24 hrs @ load			0.04	11 °	1833	4 °	975	Brown clay with silt: 69 pcf, 45%
OSU	Jan-05	SDN	white NW	SOIL	0.8	Dry			0.04	40.5 °	0	33.2 °	0	Topsoil: 93 pcf, 18%
OSU	Jan-05	SDN	white NW	SOIL	0.8	2 days @ load			0.04	36.1 °	0	25.5 °	0	Topsoil: 93 pcf, 37.8%
OSU	Jan-05	SDN	black NW	FGD	0.8	Dry			0.04	44.8 °	0	41.5 °	0	FGD: 93 pcf, 68.4%
OSU	Jan-05	SDN	black NW	FGD	0.8	2 days @ load			0.04	38.3 °	0	35.3 °	0	FGD: 93 pcf, 68.4%
OSU	Jan-05	SDN	white NW	SOIL	0.8	2 days @ load			0.04	36.3 °	0	14.3 °	0	Topsoil: 93 pcf, 38.2%
JLT	Feb-07	SDN		SOIL	0.7 2.1	12 hrs @ load			0.04	27 °	44	17 °	41	Soil: 116 pcf, 16.4%

BENTOMAT GCL DIRECT SHEAR DATABASE

TR-114BM

Lab^1	Report Date	GCL Tested	Interface Tested^2		Testing Conditions								Mohr-Coulomb Failure Envelopes^6				Comments^8
					Normal Stresses (psi)				Hydration.^{3}		Consol.^{4}	SDR^5 (in/min)	Peak		Large Displacement^7		
			GCL	Other					psf	hrs			Angle (deg)	adhesion (psf)	Angle (deg)	adhesion (psf)	
SGI	2/205	SDN	black NW	COAL REFUSE		0.7	2.8		144	24	24 hrs @ load	0.04	32 °	40	31 °	40	Coal Refuse
SGI	Jul-06	SDN	black NW	SOIL	0.7	1.4	2.8		24 hrs @ load			0.04	34 °	5	33 °	0	Gravel (34R)
SGI	Jul-06	SDN	white NW	SOIL	0.7	1.4	2.8		24 hrs @ load			0.04	32 °	30	31 °	10	Fine brown sand
TRI	Apr-07	SDN	white NW	SOIL	0.9	3.0	5.2		100	24	24 hrs @ load	0.04	25.3 °	108	23.6 °	117	Soil: 103 pcf, 19.6%
ARD	Jul-03	SDN	white NW	SOIL	2	3.8	5.9		24 hrs @ load			0.04	28.5 °	72	27.7 °	79	Fine brown sand with silt
ARD	Jul-03	SDN	black NW	SOIL	2	3.8	5.9		24 hrs @ load			0.04	33.5 °	43	33.5 °	43	Fine brown sand with silt
TRI	Jul-08	SDN	Black NW	SOIL	3.5	13.9	31.3	62.5	100	24	step-load	0.04	19.3 °	587	19.1 °	561	Soil: 112 pcf, 17%
SGI	2/205	SDN	white NW	SOIL	83				144	24	24 hrs @ load	0.04	27 °	0	22 °	0	Compacted Subgrade
SGI	2/205	SDN	white NW	SOIL	13.9	34.7	55.6	83.3	144	24	24 hrs @ load	0.04	23 °	365	18 °	485	Compacted Subgrade
SGI	Oct-06	SDN	black NW	SOIL	5	20	90		115	24	step-load	0.04	17 °	245	9 °	140	Compacted clay
TRI	May-07	SDN		SOIL	9.3	52.3	91.6		250	24	step-load	0.04	21.6 °	317	6.6 °	1270	Soil: 102 pcf, 12.9%
EMCON	Dec-02	SDN	white NW	SOIL	27.8	55.6	111		220	24	24 hrs @ load	0.04	26.8 °	1320	2.7 °	3140	Sand
TRI	Oct-07	SDN	white NW	SOIL	41.7	83.3	125		200	24	step-load	0.04	28.8 °	0	5.8 °	2935	Soil: 100 pcf, 12.9%
SGI	Feb-02	CL	smooth plastic	SOIL	0.7	1.4	2.8		24 hrs @ load			0.04	20 °	50	20 °	40	Graded Aggregate Base
SGI	Feb-02	CL	smooth plastic	SOIL	0.7	1.4	2.8		24 hrs @ load			0.04	18 °	40	16 °	40	Silty sand
SGI	Feb-02	CL	smooth plastic	SOIL	0.7	1.4	2.8		24 hrs @ load			0.04	19 °	70	18 °	70	Clay

BENTOMAT GCL DIRECT SHEAR DATABASE

TR-114BM

Lab[1]	Report Date	GCL Tested	Interface Tested[2]		Testing Conditions					Mohr-Coulomb Failure Envelopes[6]				Comments[8]
					Normal Stresses	Hydration.[3]		Consol.[4]	SDR[5]	Peak		Large Displacement[7]		
			GCL	Other	(psi)	psf	hrs		(in/min)	Angle (deg)	adhesion (psf)	Angle (deg)	adhesion (psf)	
PGL	Dec-05	CL	smooth plastic	SOIL	0.7 1.4 2.8	Interface sprayed with water			0.04	29.6 °	67	24.4 °	54	Clayey sand: 113 pcf, 14%
PGL	Dec-05	CL	smooth plastic	SOIL	0.7 1.4 2.8	Interface sprayed with water			0.04	37 °	14	33 °	8	Silty sand: 115 pcf, 11.5%
PGL	Dec-05	CL	smooth plastic	SOIL	0.7 1.4 2.8	Interface sprayed with water			0.04	25 °	66	18.5 °	71	CL: 102 pcf, 17.5%
PGL	Dec-05	CL	smooth plastic	SOIL	0.7 1.4 2.8	Interface sprayed with water			0.04	22.9 °	78	21.8 °	49	CH: 92.8 pcf, 22.6%
PGL	Dec-05	CL	smooth plastic	SOIL	0.7 1.4 2.8	Interface sprayed with water			0.04	22.9 °	57	22.5 °	58	SP: 106.5 pcf, 5%
SGI	May-00	CL	W	SOIL	0.5 1.0 2.1	24 hrs @ load			0.04	36 °	10	36 °	10	
CETCO	Mar-00	CLT	W	SOIL	0.7 1.4 2.1	24 hrs @ load			0.04	24.9 °	278	--	--	SP, 108 pcf, 11%
CETCO	Feb-00	CLT	20-mil text. HDPE	SOIL	0.7 1.4 2.1	24 hrs @ load			0.04	41.7 °	108	--	--	SP, 108 pcf, 11%
SGI	Mar-01	CLT	20-mil text. HDPE	SOIL	55.6	1000	24	24 hrs @ load	0.04	24 °	0	21 °	0	
Interface Shear Results (with drainage geocomposites, geonets, and geotextiles)														
GT	Dec-00	ST	W	drainage geocomposite	1.4 2.8 4.2	100	24	--	0.04	25 °	0	20.7 °	1	
EMCON	Jul-05	ST	W	drainage geocomposite	13.9 55.6 83.3	300	48	24 hrs @ load	0.04	19.7 °	0	8.3 °	331	
PGL	Sep-03	ST	NW	drainage geocomposite	5 19.4 60 83.3	144	48	24 hrs @ load	0.04	19.8 °	129	13.6 °	164	
PGL	Jul-06	ST	W	geonet	1.5 3 6	24 hrs @ load			0.04	23.5 °	33.5	23.6 °	29	
GT	Dec-00	DN	black NW	drainage geocomposite	1.4 2.8 4.2	100	24	--	0.04	28 °	0	21.9 °	0	
TRI	Sep-06	DN		drainage geocomposite	1.4 2.8 5.6	24 hrs @ load			0.04	30.1 °	14	27.2 °	0	
PGL	Sep-09	DN	white NW	drainage geocomposite	0.35 2.78 6.94	24 hrs @ load			0.04	21.7 °	96	13.8 °	68	

BENTOMAT GCL DIRECT SHEAR DATABASE

TR-114BM

Lab[1]	Report Date	GCL Tested	Interface Tested[2]		Testing Conditions							Mohr-Coulomb Failure Envelopes[6]				Comments[8]
					Normal Stresses (psi)			Hydration.[3]		Consol.[4]	SDR[5]	Peak		Large Displacement[7]		
			GCL	Other				psf	hrs		(in/min)	Angle (deg)	adhesion (psf)	Angle (deg)	adhesion (psf)	
GTX	Oct-00	DN	black NW	drainage geocomposite	10	30	70	144	72	24 hrs @ load	0.04	22 °	144	18 °	0	
GT	Aug-08	DN	white NW	drainage geocomposite	20.8	41.7	83.3	200	24	48 hrs @ load	0.04	28.7 °	152	16.5 °	515	
PGL	Dec-06	DN		Nonwoven geotextile	2	3.5	5	24 hrs @ load			0.04	20.7 °	160	6.3 °	167	
GT	Dec-04	SDN	black NW	drainage geocomposite	0.7	1.4	2.8	Hydrated			0.04	21.6 °	9	17.2 °	10	
TRI	Jun-07	SDN		drainage geocomposite	6.9	41.7	83.3	250	24	step-load	0.04	21.4 °	0	9.5 °	278	
TRI	Oct-07	SDN	white NW	drainage geocomposite	41.7	83.3	125	200	24	step-load	0.04	27.5 °	0	21.6 °	0	
SGI	Jul-06	SDN	white NW	Nonwoven geotextile	0.7	1.4	2.8	24 hrs @ load			0.04	27 °	35	20 °	20	
TRI	Jun-07	CL	smooth plastic	drainage geocomposite	0.7	1.4	2.8	200	24	24 hrs @ load	0.04	19.2 °	33	10.8 °	46	
ATT	Dec-98	CL	smooth plastic	drainage geocomposite	1	2	3	72	48	--	0.04	14 °	72	11.6 °	72	
SGI	Mar-01	CLT	20-mil text. HDPE	drainage geocomposite	55.6			1000	48	24 hrs @ load	0.04	23 °	0	19 °	0	

BENTOMAT GCL DIRECT SHEAR DATABASE

TR-114BM

Notes:

(1) Laboratories:
ARD = Ardaman and Associates, Orlando FL
ATT = Advanced Terra Testing, inc. Lakewood, CO
CETCO = CETCO, Hoffman Estates, IL
EMCON = Emcon Assoc. (now Shaw Group), Mahwah, NJ
GA = Golder Associates, Atlanta, Georgia
GT = Geotechnics, East Pittsburgh, PA
GTX = Geotesting Express, Boxborough, MA
JLT = J&L Testing, Canonsburg, PA
OSU = Ohio State University, Columbus, OH
PGL= Precision Laboratory, Orange, CA
SGI = SGI Testing Services LLC, Atlanta, GA (formerly GeoSyntec)
STS = STS Consultants, Ltd., Vernon Hills, IL
TRI = TRI Laboratory, Austin, TX
VE = Vector Engineering, Grass Valley, CA

(2) Internal = Failure forced within the GCL (between the geotextiles).
NW = Non-woven geotextile of Bentomat.
W = Woven geotextile of Bentomat.

(3) Hydrated = specimen was soaked under the specified load for the specified duration prior to testing. Hydration methods may vary
Dry = specimen was tested in the as-received moisture (typically 25-30 percent).
Wetted = specimen was partially hydrated.

(4) Consolidation. If the hydration load does not equal the ultimate normal load for shearing, the normal load is increased in steps.

(5) SDR = Shear Displacement Rate.

(6) Mohr-Coulomb failure envelope, $\tau = c_a + \sigma \tan \phi$, determined by a least-squares, “best-fit” straight line through the shear strength-normal stress test results. Two shear strength components are shown: c_a = adhesion and ϕ = friction angle. Caution should be exercised in using these strength parameters for applications involving normal stresses outside the range of the stresses covered. Refer to TR-264 for discussion of cohesion (or adhesion) and friction angle in direct shear tests.

(7) Measured at 3" displacement, unless otherwise noted.

(8) Including information on: geomembrane type; soil type, density, and moisture content; observed GCL internal failure during interface shearing; and any other unique testing conditions.

APPLICATION FOR PERMIT
SUNDANCE WEST

VOLUME III: LANDFILL ENGINEERING CALCULATIONS
SECTION 7: TENSILE STRESS ANALYSIS

ATTACHMENT III.7.E

KOERNER, ROBERT M. AND KOERNER, GEORGE R. 2007.

INTERPETATION(S) OF LABORATORY GENERATED INTERFACE SHEAR STREGTH DATA FOR GEOSYNTHETIC MATERIALS WITH EMPHISIS ON THE ADHESION VALUE.

GRI WHITE PAPER #11. GEOSYNTHETICS INSTITUTE

Geosynthetic Institute
475 Kedron Avenue
Folsom, PA 19033-1208 USA
TEL (610) 522-8440
FAX (610) 522-8441

GRI White Paper #11

Interpretation(s) of Laboratory Generated Interface Shear Strength Data for Geosynthetic Materials With Emphasis on the Adhesion Value

by

Robert M. Koerner and George R. Koerner
Geosynthetic Institute
475 Kedron Avenue
Folsom, PA 19033 USA

Phone (610) 522-8440
Fax (610) 522-8441

E-mail:
robert.koerner@coe.drexel.edu
gkoerner@dca.net

September 11, 2007

Interpretation(s) of Laboratory Generated Interface Shear Strength Data for Geosynthetic Materials With Emphasis on the Adhesion Value

The beginning point of this White Paper is based on the assumption that a designer has a credible set of laboratory generated shear stress versus shear displacement curves on the desired geosynthetic-to-geosynthetic or geosynthetic-to-soil interface tested per ISO 12957 or ASTM D5321, or ASTM D6243 if geosynthetic clay liners are involved. In this regard we are considering having such data as shown in Figure 1. It is clearly seen that many behavioral trends are possible.

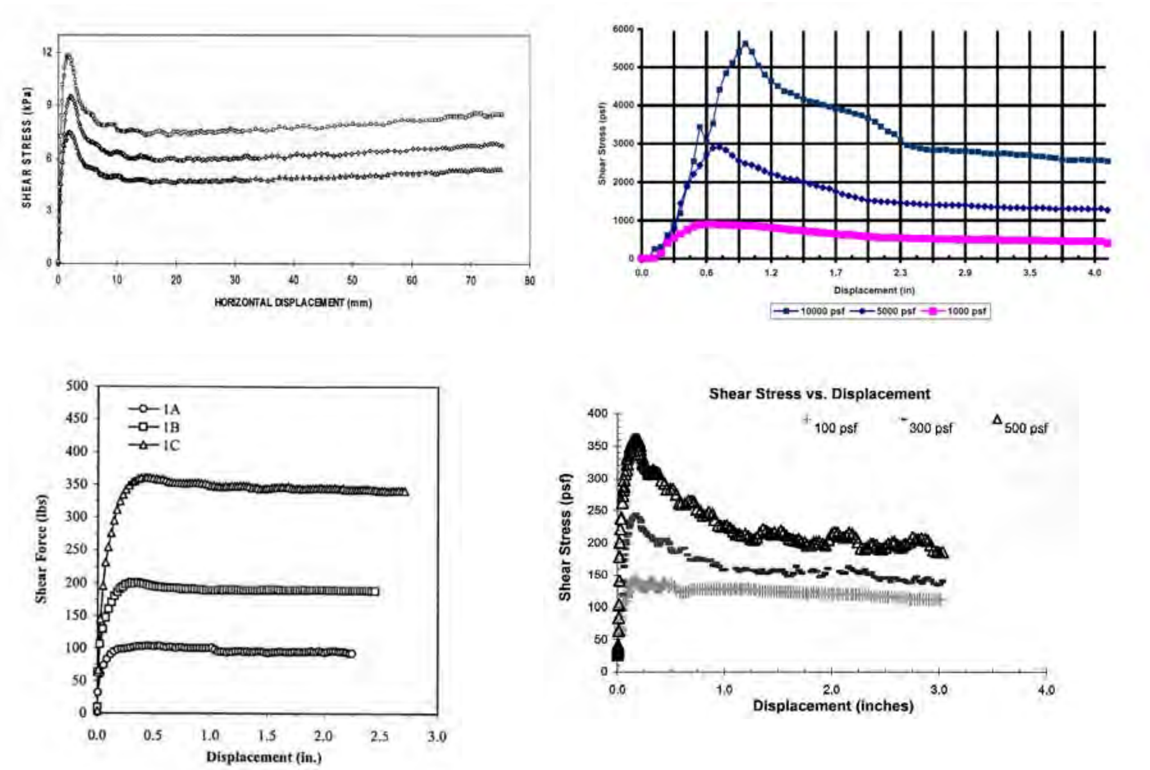

Figure 1 – Various stress versus displacement curves for different geosynthetic materials. (Data compliments of TRI, Golder, Precision and SGI Laboratories)

Either the designer or the testing laboratory will have to generate the Mohr-Coulomb failure envelope from these curves by selecting one point on each normal stress curve and plotting the results on a normal stress versus shear stress curve as shown in Figure 2a. A least squares fit of the data point produces the failure envelope. Even further, one might have more than one such failure envelopes; peak, large displacement and/or residual. Please note, however, that this White Paper is <u>not</u> about the selection of peak, large displacement or residual values and the technical literature is abundant on that subject.

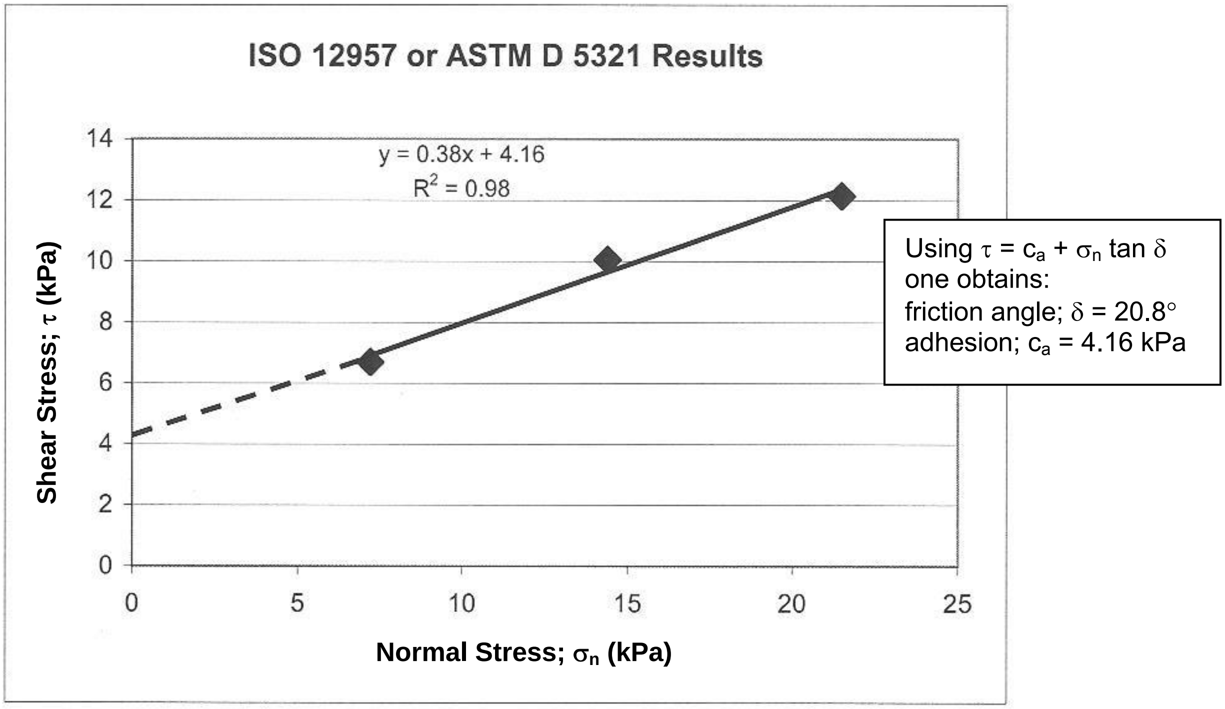

Using $\tau = c_a + \sigma_n \tan \delta$ one obtains:
friction angle; $\delta = 20.8°$
adhesion; $c_a = 4.16$ kPa

Figure 2a – Three point laboratory data leading to the drawing of a failure envelope and subsequent measurement of friction angle and shear strength intercept (or adhesion) values.

At any rate, to begin the present discussion on the interpretation of the selected failure envelope, the designer is confronted with something like that shown Figure 2a. Here the data points are clearly identified and the failure envelope is usually generated by a least squares fitting procedure. The dashed extension to the y-axis is often the general assumption particularly for low normal stresses as indicated. Note that there are indeed exceptions to this situation such as curved failure envelopes within the normal stress range tested, or zero normal stress tests. They are special cases and will be discussed later.

Interpretation #1 – Use of full “c_a” and full “δ” values

Assuming that the previous failure envelope is based on credible laboratory procedures, properly simulated insofar as representative samples, normal stress selection, moisture conditions, strain rate, etc., our recommended approach is to use the shear strength parameters directly in your slope stability analysis and, if found to be adequate, for your materials specification criteria as well. For landfill cover veneer stability problems all GSI Members and Associate Members should have our spread sheet calculation program which is extremely easy to use. For others, there are many computer codes available. For a hypothetical veneer slope stability example using the two shear strength parameters (c_a and δ) from Figure 2a, the input information is as follows:

- cover soil thickness h = 0.3 m
- slope angle β = 18.4° (3-to-1)
- length of slope L = 30.0 m
- unit weight of cover soil γ = 18.0 kN/m^3
- friction angle of cover soil ϕ = 30.0 deg
- cohesion of cover soil c = 0.0 kN/m^2
- friction angle of interface δ = 20.8 deg
- adhesion of interface c_a = 4.16 kPa (= 87 psf)

By using the program just mentioned or similar procedure, the resulting slope factor-of-safety value is; FS = 3.62. This is a relatively high value and would generally be considered quite conservative. One point worth mentioning, however, is the strong influence of the adhesion value on factor-of-safety. To illustrate this, we now vary the c_a-value between zero and ten while holding everything else the same. This procedure results in the following table; clearly illustrating the sensitivity of the FS-value to this particular parameter.

Adhesion; "c_a"		Resulting FS-value
kPa	lb/ft^2	
0	0	1.18
2	42	2.35
4	84	3.53
6	125	4.70
8	167	5.80
10	209	7.05

Presented now is the heart of this White Paper concerning the *issue of how reliable is this laboratory generated c_a-value?* The ultimate decision is yours as the designer, but our opinions on different geosynthetic materials and related interfaces are as follows:

(a) For textured geomembranes against geotextiles or soil, the asperities (be they manufactured as structured, blown film, or impinged) are on the material giving rise to the high adhesion values, so we recommend using the adhesion value accordingly. Only by continuously rubbing the surfaces against one another can asperity reorientation occur and we feel this is an artifact of aggressive laboratory testing as has been done (and reported) using the ring shear testing device in particular. Alternatively, concern has been expressed when testing at very high normal stresses. The thought in both instances is that if you eliminate adhesion from textured geomembranes you are essentially assuming smooth geomembrane sheet. This is a designer's prerogative, but be prepared to have very gentle slopes in so doing.

(b) For smooth geomembranes against other geosynthetics or soil, a small adhesion is often observed. This is particularly the case for LLDPE, fPP, EPDM, and PVC. Each of these geomembranes are less hard than HDPE, and thus an indentation can be visualized (particularly dealing with soil) which is clearly a function of the applied normal stress. Assuming that the appropriate normal stresses were used in the direct shear test, we feel that one is generally justified in its use.

(c) For geotextiles thermally bonded to geonets or other types of drainage cores, we feel that the full value of adhesion should be used. Most of these geocomposites can barely be "delaminated" in the conducting of the test and we have never heard of a field delamination problem from a properly manufactured geocomposite interface in this regard.

(d) For the internal shear strength of reinforced GCLs, the fibers would have to pull-out or break (or both) for a loss of adhesion. While you can force this to happen in the lab, we have no evidence of this occurring in the field. Test results invariably show high adhesion values. Furthermore, longevity (durability) of the fibers in a hydrated bentonite atmosphere promises 100-year lifetime, or longer. We have a creep-related paper in this regard. Thus, we see no reason not to use the laboratory generated value of adhesion for reinforced GCLs manufactured by either needlepunching or stitching. Of course, the upper and lower interfaces of the GCLs must be independently evaluated.

(e) For certain geosynthetic-to-soil interfaces, the interface shear behavior may force the failure plane into the soil. This results in the identification of the soil's shear strength and if there is a shear strength intercept it is a cohesion value and can be used accordingly.

Thus, if adhesion from short-term testing is indicated by the failure envelope and the long-term permanence of the physical or mechanical mechanism giving rise to this adhesion is logical to anticipate, its use in a stability analysis and subsequent material's specification is felt to be generally justified.

Interpretation #2 – Use of zero "c_a" and full "δ" value

For the situation where an adhesion is indicated by the failure envelope and you as the designer feel that its long-term existence is not justified, the most conservative approach you can take is to simply translate the entire failure envelope in a parallel manner down by the amount of adhesion indicated on the original data-generated graph; see Figure 2b.

The effect of this very conservative approach on the FS-value of the slope is substantial. The shear strength is now represented by a friction angle alone and the site-specific result will be very flat slopes. For example, the 3-to-1 slope in the hypothetical example given previously with an adhesion of zero, now has a FS = 1.18 using this approach. For the interfaces mentioned previously, we do not recommend this approach.

Alternatively, one could also decrease the adhesion slightly, but not entirely. That said, we really don't know how to comment on this type of "compromise" situation?

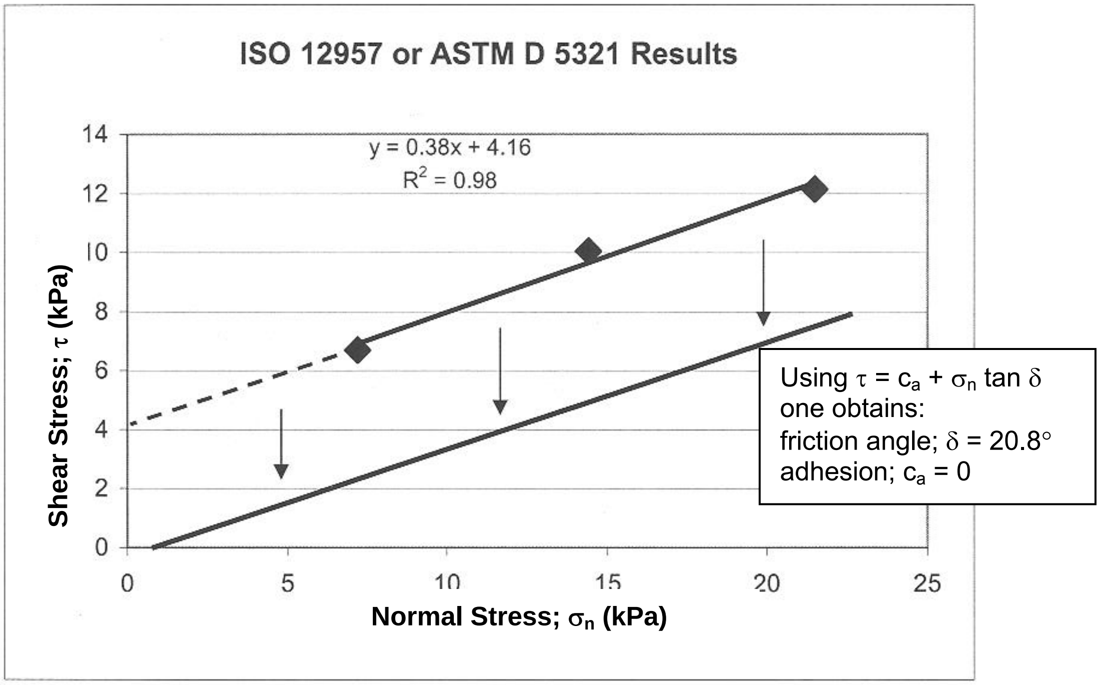

Figure 2b – Parallel translation downward of the entire laboratory generated failure envelope by an amount equal to the y-axis intercept, i.e., the adhesion.

Interpretation #3 – Use of zero "c_a" at zero normal stress only

A hybrid interpretation somewhere between the interpretations just presented is sometimes suggested, but its logic is somewhat difficult to fathom. In essence, the adhesion is lost only at zero normal stress but not at higher normal stresses. Thus, the failure envelope is forced through the origin but thereafter it is based on a least squares fit of the laboratory tested points as they were generated. Figure 3 illustrates the situation where the resulting friction angle is seen to be 32.2°. For our hypothetical example, this results in FS = 1.93. Alternatively, and equally difficult to fathom, is when only one laboratory point is generated and the failure envelope is forced through it and the origin. Both approaches are the least conservative of those mentioned in this White Paper giving rise to a rotation of the failure envelope and the highest friction angle possible. The angle resulting from this practice has been variously called "secant friction angle", "secant angle", or "modulus angle". Of the group, secant angle is probably the best description for this interpretation since it shouldn't be confused with the Mohr-Coulomb friction angle, and modulus brings with it completely other test procedures like tension testing.

We generally do not recommend such approaches for the reason that adhesion should be an intrinsic property of the interface involved and not be arbitrarily eliminated or used on the basis of a particular normal stress, or stresses. (That stated, if the interface is tested at zero normal stress and found to have zero adhesion, the origin is a valid point and should then be used accordingly).

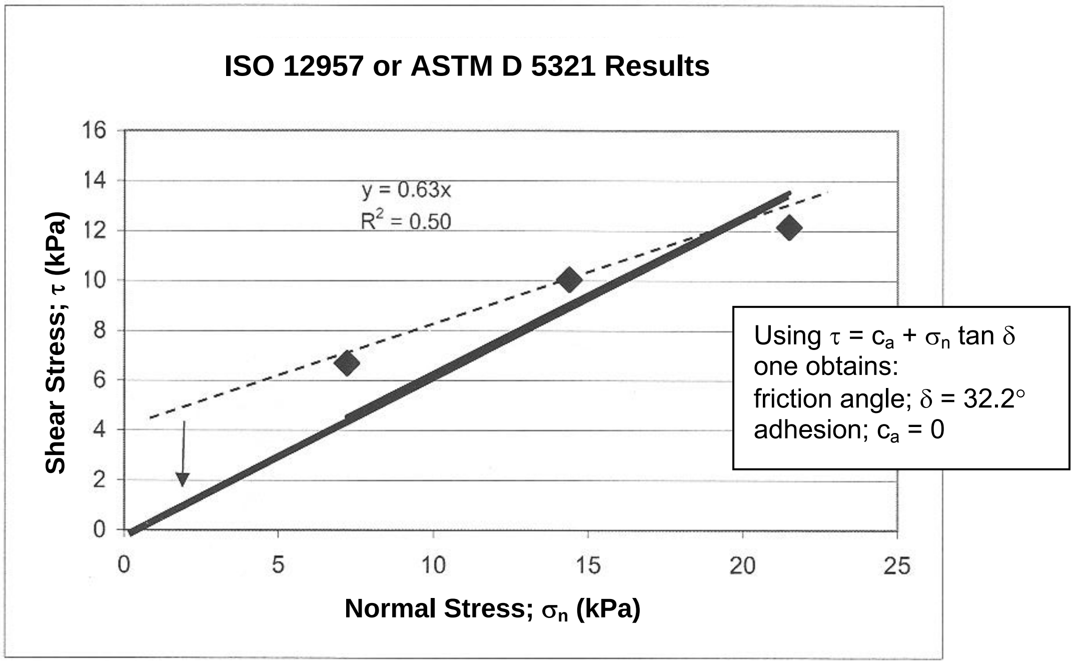

Using $\tau = c_a + \sigma_n \tan \delta$
one obtains:
friction angle; $\delta = 32.2°$
adhesion; $c_a = 0$

Figure 3 – Elimination of adhesion at zero normal stress but not at any of the three laboratory measured data points.

Interpretation #4 – Use of the total shear strength at a particular normal stress

A very straightforward approach to a specification value is to require a certain shear strength value at a particular normal stress. This is particularly the case if the failure envelope is curved as mentioned previously. In so doing, a specifier is requiring a single point to be taken from the failure envelope which is targeted at the expected field normal stress. Figure 4 suggests that if the field normal stress is 17.2 kPa it results in a required shear strength of 10.7 kPa, or greater. The shear strength value is thereby reflective of both a frictional component and adhesion, neither of which are specifically identified.

In so doing one avoids specifying individual “c_a” and “δ” values and much of the previous discussion is altogether avoided. The method can be extended to give two, or more, values of shear strength (or even the equation of the failure envelope) at different normal stresses in the form of a “required” table.

This approach has been used by a select few designers but is far from common practice. There is nothing of a fundamental nature which says it cannot be done and it would avoid some of the other complications inherent with different approaches.

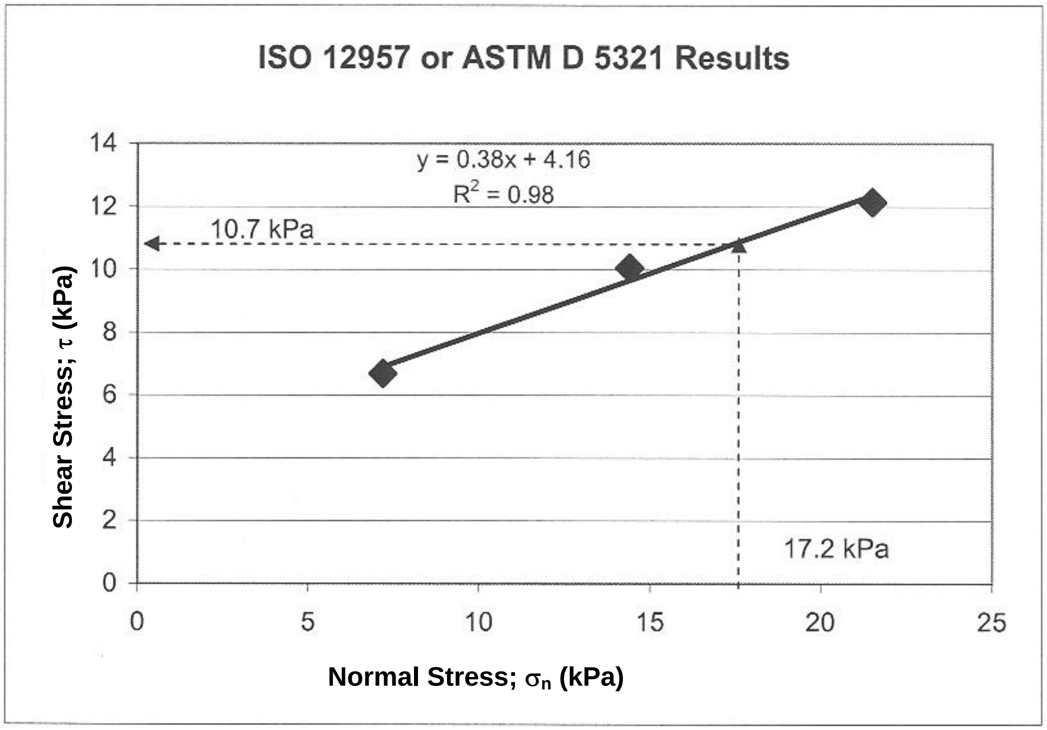

Figure 4 – Use of a laboratory generated failure envelope by specifying a site-specific normal stress and requiring a minimum value of shear strength taken directly off of the y-axis.

In summary, there are probably other or intermediate interpretations of an interface shear strength failure envelope for use in design and then a subsequent specification, but those presented here are felt to be the most common.

APPLICATION FOR PERMIT
SUNDANCE WEST

VOLUME III: LANDFILL ENGINEERING CALCULATIONS
SECTION 7: TENSILE STRESS ANALYSIS

ATTACHMENT III.7.F

THIEL, RICHARD. *A TECHNCIAL NOTE REGARDING INTERPRETATION OF COHESION (OR ADHESION) AND FRICTION ANGLE IN DIRECT SHEAR TESTS.* GEOSYNTHETICS, APRIL MAY 2009 VOLUME 27: PAGES 10-19.

A technical note regarding interpretation of cohesion (or adhesion) and friction angle in direct shear tests

By Richard Thiel

Introduction

Direct shear testing with geosynthetics is generally performed in accordance with ASTM D5321, *Standard Test Method for Determining the Coefficient of Soil to Geosynthetic or Geosynthetic to Geosynthetic Friction by the Direct Shear Method.* There is also a related standard, D6243, *Standard Test Method for Determining the Internal and Interface Shear Resistance of Geosynthetic Clay Liner by the Direct Shear Method.* This technical note applies to both equally.

Interpreting lab results

There is often confusion expressed in the industry regarding how laboratory results should be interpreted, specifically: whether one should use both the friction angle and cohesion (or adhesion) parameters; whether cohesion should be ignored; whether secant friction angles are more appropriate; what to do if the data are nonlinear; and how the data should be interpolated or extrapolated.

The goal of this technical note is to provide some guidance to take the mystery out of these questions. In the end, all data should be evaluated by an experienced practitioner qualified to use the test results properly.

What this note will not do is go into the subtleties of requesting, setting up, calibrating, and performing a direct shear test. That would be the subject of additional articles.

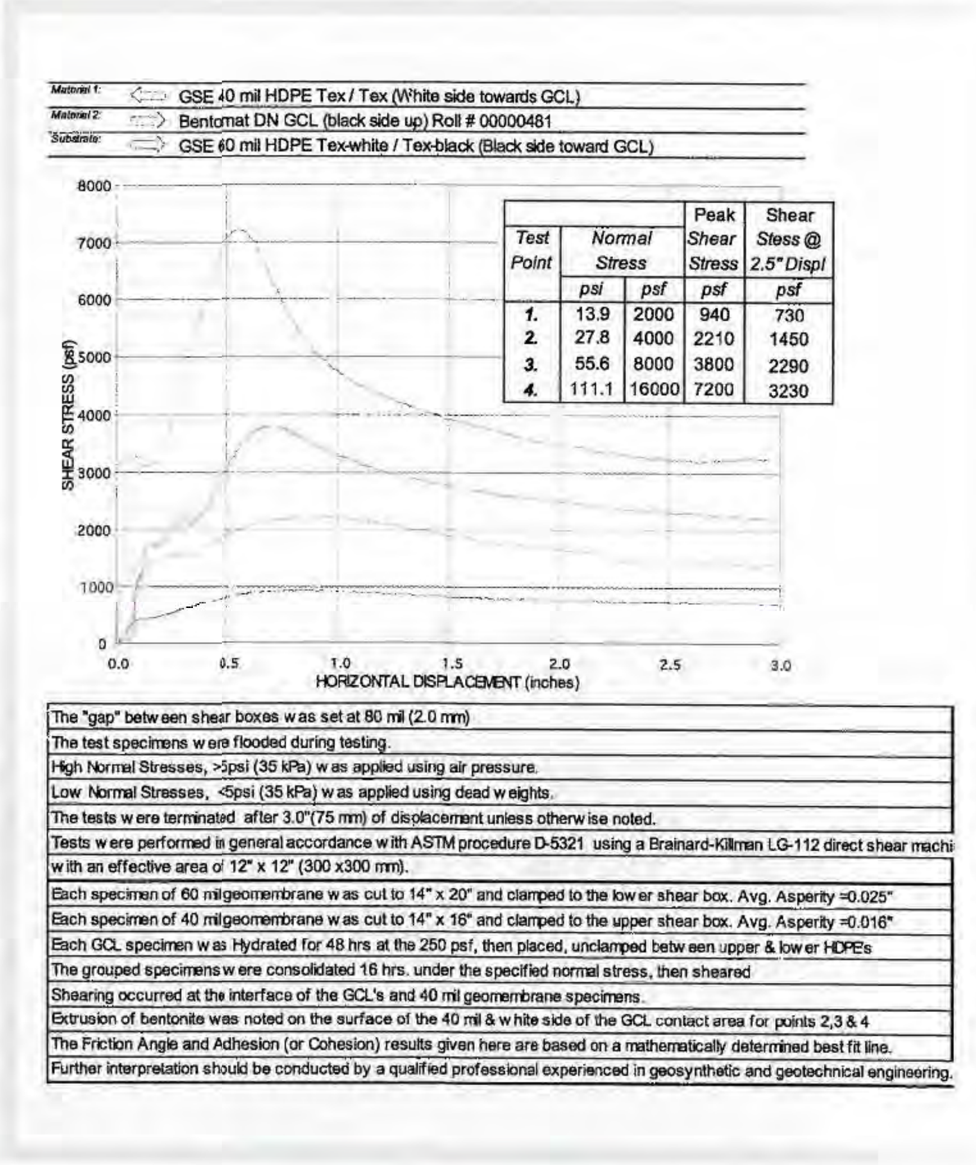

GSE 40 mil HDPE Tex / Tex (White side towards GCL)
Bentomat DN GCL (black side up) Roll # 00000481
GSE 60 mil HDPE Tex-white / Tex-black (Black side toward GCL)

Test Point	Normal Stress		Peak Shear Stress	Shear Stess @ 2.5" Displ
	psi	psf	psf	psf
1.	13.9	2000	940	730
2.	27.8	4000	2210	1450
3.	55.6	8000	3800	2290
4.	111.1	16000	7200	3230

The "gap" between shear boxes was set at 80 mil (2.0 mm)
The test specimens were flooded during testing.
High Normal Stresses, >5psi (35 kPa) was applied using air pressure.
Low Normal Stresses, <5psi (35 kPa) was applied using dead weights.
The tests were terminated after 3.0"(75 mm) of displacement unless otherwise noted.
Tests were performed in general accordance with ASTM procedure D-5321 using a Brainard-Killman LG-112 direct shear machi
with an effective area of 12" x 12" (300 x300 mm).
Each specimen of 60 mil geomembrane was cut to 14" x 20" and clamped to the lower shear box. Avg. Asperity =0.025"
Each specimen of 40 mil geomembrane was cut to 14" x 16" and clamped to the upper shear box. Avg. Asperity =0.016"
Each GCL specimen was Hydrated for 48 hrs at the 250 psf, then placed, unclamped between upper & lower HDPE's
The grouped specimens were consolidated 16 hrs. under the specified normal stress, then sheared
Shearing occurred at the interface of the GCL's and 40 mil geomembrane specimens.
Extrusion of bentonite was noted on the surface of the 40 mil & white side of the GCL contact area for points 2,3 & 4
The Friction Angle and Adhesion (or Cohesion) results given here are based on a mathematically determined best fit line.
Further interpretation should be conducted by a qualified professional experienced in geosynthetic and geotechnical engineering.

This article will also not definitively describe how direct shear test data should be interpreted. That is the responsibility of a professional with specific expertise, and one article could never presume to cover all of the considerations that might apply to any unique design problem that might arise. That is why professionals are trained and mentored in basic geotechnical principles: so they can appropriately account for the various factors affecting a design and make appropriate decisions regarding test data interpretations.

The typical sequence of events related to direct shear testing includes the following:

1. An engineer requests a direct shear test series to obtain data to help solve a problem. The request should be very specific with regard to all the necessary details regarding

---

| Richard Thiel is a senior project manager at Vector Engineering Inc. in Grass Valley, Calif.

The Designer's Forum column is refereed by Greg Richardson, Ph.D., P.E., a principal at RSG & Associates, Raleigh, N.C., www.rsgengineers.com sampling, specimen preparation and setup in the testing device, and test execution in accordance with both project-specific conditions and industry standards.

2. A competent and certified laboratory performs the test series in accordance with the request and the industry standard test method (e.g., ASTM D5321 or D6243). The laboratory reports results to the engineer.

3. The engineer interprets and applies the results to the project design.

What we are measuring in the direct shear test is shear strength as a function of normal load. The test does not measure "friction" or "cohesion," as these are simply mathematical parameters derived from the laboratory test results.

Ideally the engineer who originally specified and required the shear test would be the same one who reviews and interprets the results. Sometimes, such as in a third-party construction quality assurance (CQA) project, an engineer other than the original designer will commission and review the testing. Interactions with test laboratories and other engineers over time have shown that there are often misconceptions and misunderstandings related to the interpretation of direct shear test data. Thus, this article is intended to serve the purpose of helping project participants avoid confusion. The key point of this article is that what we are measuring in the direct shear test is shear strength as a function of normal load. The test does not measure "friction" or "cohesion," as these are simply mathematical parameters derived from the laboratory test results.

Figure 1 presents shear test results of a 4-point test for an interface between a textured geomembrane and a reinforced GCL. Three shear points, each at a different normal stress, are the most common number of points used to run a test series, but the number of points could vary from as few as one, to perhaps as many as six points, depending on many factors beyond the scope of this article. The figure shows: (a) a table of the normal stresses vs. peak and large-displacement shear strengths measured at 2.5in. of displacement, (b) graphs of the shear stress vs. displacement measurements, and (c) notes describing test conditions and observations.

There is adequate information in this figure for a trained practitioner to evaluate and use the data. The laboratory has performed its duty, which is to measure and report the shear strength under specified normal stresses (we are simplifying the discussion here by not elaborating on other factors such as hydration, consolidation, etc.), showing how the shear strength changed with displacement of the two surfaces, and providing descriptive and observational notes.

Figure 2 shows additional information that can be provided by a laboratory in the form of a graph of the peak and large-displacement strengths plotted as a function of normal stress. Best-fit straight lines, called Mohr-Coulomb strength envelopes, named after the gentlemen who first publicized the relationship between shear strength and normal stress, have been drawn through the two sets (peak and large-displacement) of data points.

Equations can be written for these lines, as we learned in first-year algebra class, in the form of $y = mx + b$. In this case we define y as the shear strength (S); m as the slope of the line that we call the "coefficient of friction" and whose angle is *phi* (ϕ), which we call the "friction angle" (and thus $\tan[\phi]$ is the slope of the line); x is the normal stress (N); and b is the y-intercept of the line that we call either "adhesion" (a, usually used for geosynthetics-only tests) or "cohesion" (c, usually used for tests involving soils, which will be used for the remainder of this article).

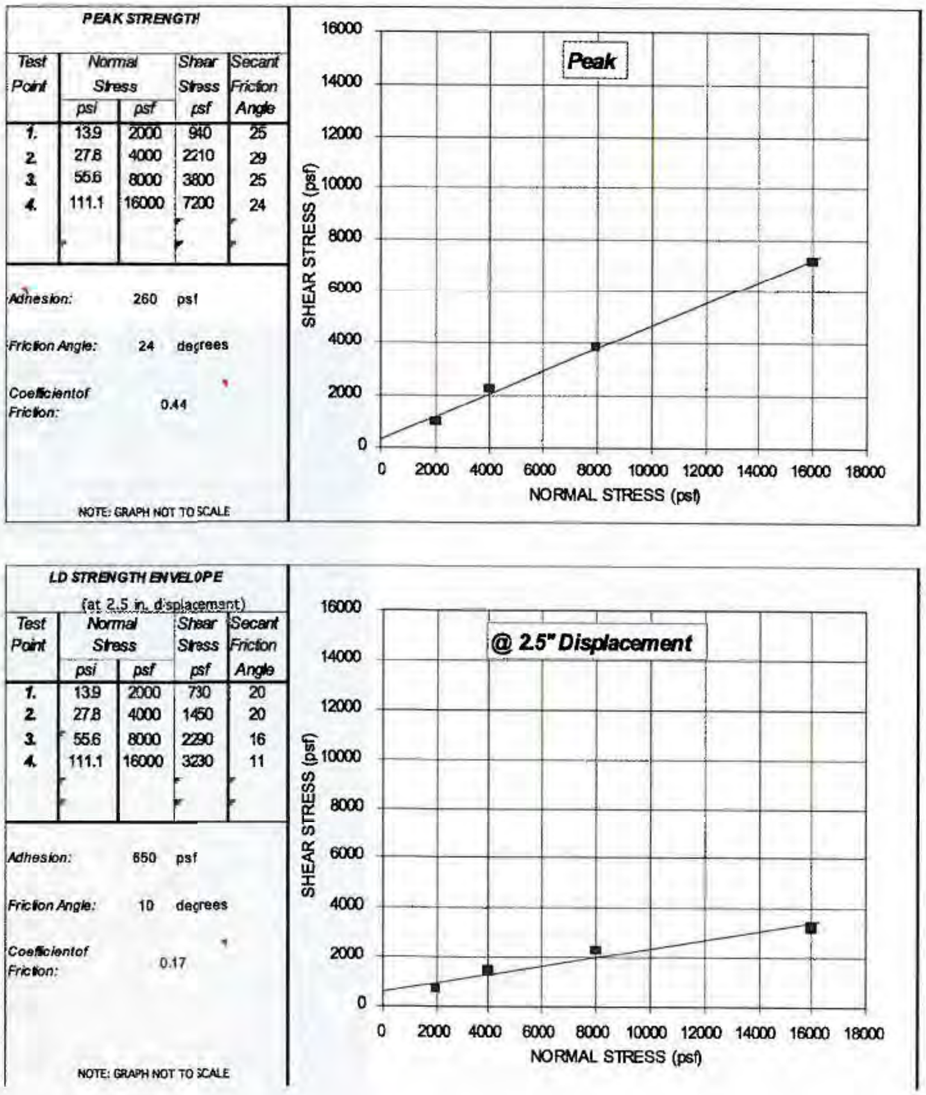

PEAK STRENGTH

Test Point	Normal Stress psi	Normal Stress psf	Shear Stress psf	Secant Friction Angle
1.	13.9	2000	940	25
2.	27.8	4000	2210	29
3.	55.6	8000	3800	25
4.	111.1	16000	7200	24

Adhesion: 260 psf

Friction Angle: 24 degrees

Coefficient of Friction: 0.44

NOTE: GRAPH NOT TO SCALE

LD STRENGTH ENVELOPE

(at 2.5 in. displacement)

Test Point	Normal Stress psi	Normal Stress psf	Shear Stress psf	Secant Friction Angle
1.	13.9	2000	730	20
2.	27.8	4000	1450	20
3.	55.6	8000	2290	16
4.	111.1	16000	3230	11

Adhesion: 650 psf

Friction Angle: 10 degrees

Coefficient of Friction: 0.17

NOTE: GRAPH NOT TO SCALE

Figure 2 | Example of supplemental data interpretation provided by the laboratory.

Mohr-Coulomb

In geotechnical engineering, we write the Mohr-Coulomb equation for these lines as:

$S = N \cdot \tan(\phi) + c$

This equation is written for peak, large-displacement, or residual shear strength conditions. The fundamental points in this article regarding the presentation of the data in **Figure 2** include the following:

1. The Mohr-Coulomb envelope should not be extrapolated beyond the limits of the normal stresses under which the testing was conducted. To do so would never be conservative and, in fact, may be significantly nonconservative. The reason that simple extension-extrapolations of the Mohr-Coulomb envelope are nonconservative is presented in **Figure 3.** Most shear strength envelopes are truly curved (nonlinear). This tendency for a curved failure envelope is exaggerated in **Figure 3**, but can clearly be identified for the real-life strength envelopes presented in **Figure 2**, in particular for large-displacement conditions.

The Mohr-Coulomb model is merely a linear simplification of a portion of the entire envelope over a limited range of normal stresses. If testing were performed over a large enough range of normal stresses the curvature would become more apparent. True shear strength envelopes are found to be most accurately described by hyperbolic functions. Giroud et al. (1993) provides a good method to describe hyperbolic strength envelopes.

2. The values of *phi* and *c* should be considered nothing more than mathematical parameters to describe the shear strength vs. normal stress *over the normal-load range the test was conducted.* It is perhaps better not to think of "friction" and "cohesion" as real material properties, but simply as mathematical parameters to describe the failure envelope.

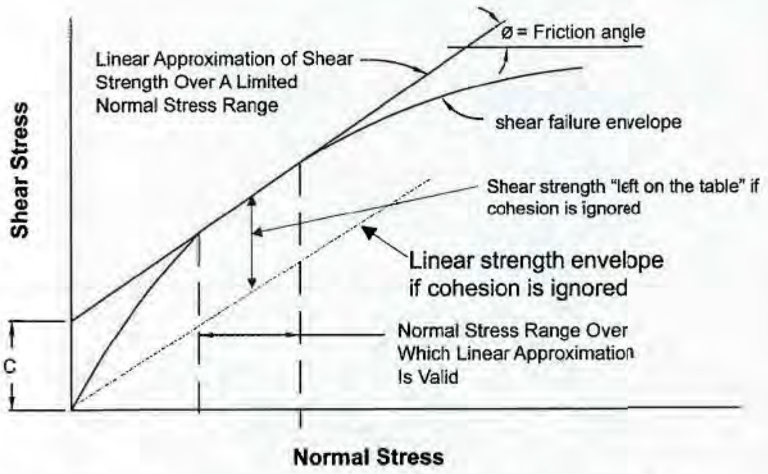

Figure 3 | Exaggerated schematic of true curvilinear shear strength envelope, linear interpretation over a selected normal stress range, and the penalty for ignoring cohesion.

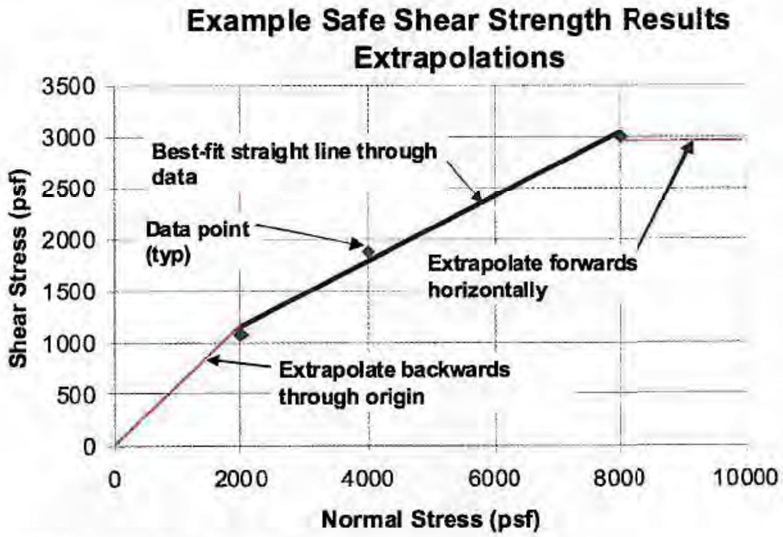

Figure 4 | Example of safe shear strength extrapolation.

In geotechnical practice with soils, there are situations and examples where the cohesion parameter is evaluated separately from the friction parameter, but these are sophisticated considerations that involve very project-specific materials and conditions and should only be done by experienced professionals.

For many geosynthetic interfaces and in the context of many types of projects, there is absolutely no reason to dissociate the slope of the line from its y-intercept, and the shear strength should be taken as a whole in those cases. Other situations may occur, however, where it is appropriate, but those considerations are beyond the scope of this article.

3. In many, if not most, cases with geosynthetics where there is no reason to ignore the cohesion value, it is important to re-emphasize that shear strength should only be defined within the range of normal stresses for which the Mohr-Coulomb envelope was derived. Ignoring the cohesion may be unjustifiably penalizing the shear strength values that were measured in the test, as illustrated in **Figure 3**.

Using the cohesion value at normal stresses extrapolated below the range of testing, however, could have dire consequences on the safety of a design project. This problem may occur when designers consider only the operational or final build-out of a facility and they ignore the construction condition. Several failures have occurred during construction because of this. For example, an embossed geomembrane against a geotextile may perform well under high normal loads by providing a good friction angle and a modest y-intercept for operating and final build-out conditions. However, under the low normal loads experienced during construction of a thin soil veneer on a steep sideslope, testing might reveal that the adhesion extrapolated from the high-normal load results do not exist at low normal loads. In this case, a more aggressive texturing that exhibits a "Velcro®-effect" type of adhesion, or a very high friction angle, at low normal loads may be needed and should be verified at the proper normal loads.

4. Figures 1 and **2** also report *secant* friction angles for each point. These are the angles of the straight lines from each point drawn back to the origin. A key concept regarding secant friction angles is that you should never extrapolate a secant angle line beyond the normal load for which it is measured. Secant values are conservative as long as the secant values are derived from a test whose normal stress was greater than the normal stresses of the design. They can quickly become nonconservative if the same friction angle is used for higher normal loads.

5. If users wish to extrapolate shear strength data, **Figure 4** illustrates the only "safe" way to accomplish this. Going from the low end of the Mohr-Coulomb envelope and extrapolating backward, the data can be extrapolated by drawing a straight line back to the origin. Going from the high end of the Mohr-Coulomb envelope and extrapolating forward, the data can be extrapolated by drawing a straight line

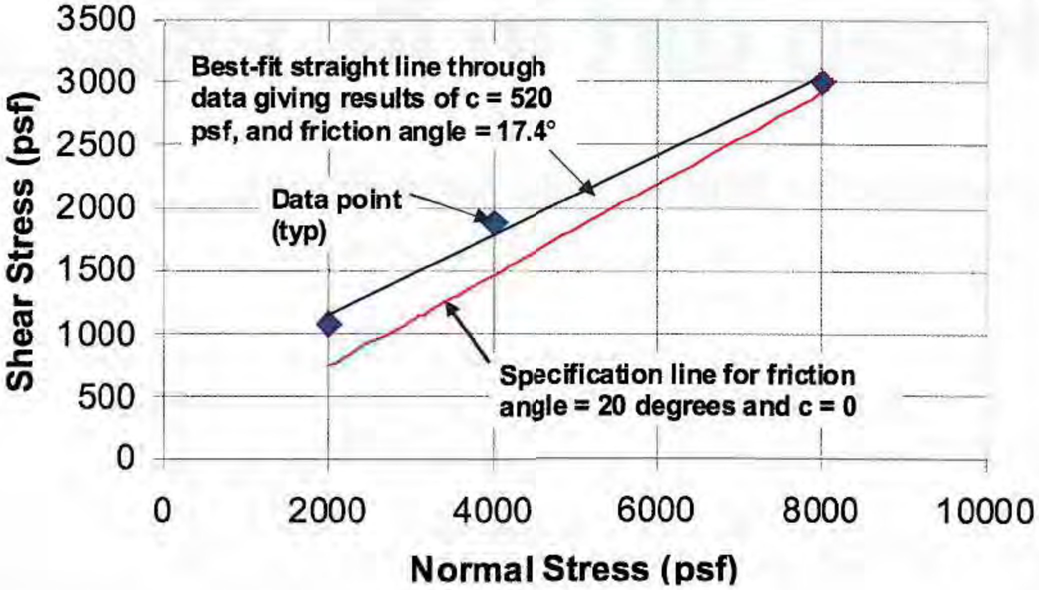

Figure 5 | Example project results where interpretation of test data results in lower friction angle than specified value, even though shear strength results are higher than the failure envelope implied by the specifications.

horizontally forward. This extrapolation rule is safe only when considering a single interface. When multiple interfaces are involved, it is not safe to extrapolate a multi-layered system on the high side of the Mohr-Coulomb envelope.

From the discussion above, we can now look at the ASTM standard D5321 with more understanding and critical thought. The first thing to note is that the title of that standard is poorly worded. The title is "*Determining the Coefficient of...Friction...*" This is somewhat misleading because it implies that the designer is simply after a coefficient of friction. In fact, what designers need is a relationship between shear strength and normal stress. Therefore, a more appropriate title for this method would be "*Determining the Relationship between Shear Strength and Normal Stress for Soil-to-Geosynthetic or Geosynthetic-to-Geosynthetic Interfaces Using the Direct Shear Method.*" Note that ASTM D6243 has already rectified this problem in its title.

Another misleading element in ASTM D5321 is the definition of *adhesion* (which applies equally to cohesion), which it states as: "The shearing resistance between two adjacent materials *under zero normal stress* (emphasis added). Practically, this is determined as the y-intercept to a straight line relating the limiting value of shear stress that resists slippage between two materials and the normal stress across the contact surface of the two materials."

This is actually *two separate definitions*, which are most likely not the intent of the standard. The first part of this definition, which defines the adhesion as the shear strength at zero normal stress, is not applicable relative to the test method. It *could be true* if we proposed to test the interface at zero normal load, but that is rarely done and generally of no use. The industry would be better served by deleting the first part of the definition. In reality, the second part of the definition is the controlling aspect of the definition, and the "y-intercept" concept is the true nature of the adhesion value which, as stated above, is simply a mathematical parameter.

Note that ASTM D6243 has a different set of definitions, and it is not clear if those definitions are unique to that standard, or are intended to be industry norms. ASTM D6243 suggests that adhesion is the true shear strength when there is truly zero normal load, and that cohesion is the mathematical parameter of the y-intercept obtained from the Mohr-Coulomb envelope. In the author's opinion these definitions are acceptable as stated, but the audience should know that the definition of *adhesion* may conflict with other definitions put forward in the industry. Also, other authors have introduced other terms for the measurable shear strength under zero normal load, such as Lambe and Whitman's (1969) "*true cohesion.*" Interested readers can research ASTM D6243 and the literature and judge for themselves.

Example problem 1

The following situation illustrates a common example of a problem that occurs with shear test data interpretation:

- A specification is written that requires a certain minimum interface friction angle to be achieved between a textured geomembrane and a GCL. For purposes of this example, the requirement is 20° peak shear strength for normal loads tested between 2,000 and 8,000 pounds per square foot (psf).
- The laboratory results, shown as an

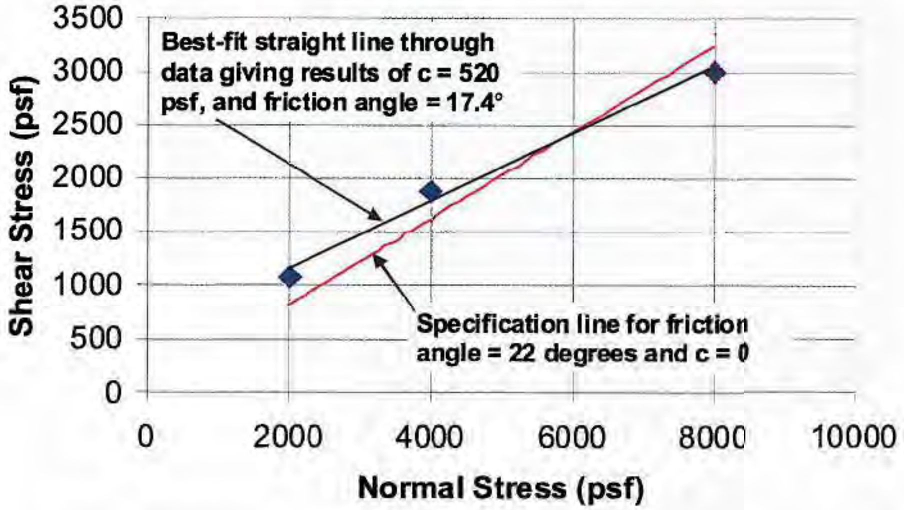

Figure 6 | Example project results where the two lower points are above the specification and the upper point is below the specification.

example in **Figure 5**, report a best-fit Mohr-Coulomb peak strength envelope with shear strength parameters of 500 psf cohesion and 15° friction. **Figure 5** also shows the line representing the minimum project specification.

Inspection of **Figure 5** shows that the shear strengths achieved in the direct shear test plot above the shear strength envelope required by the specification. Even though the plot appears to clearly indicate that the minimum required shear strength is achieved by the products tested, the author has experienced several projects where one of the project parties (e.g., the design engineer or perhaps a regulator) have declared the test a failure because the reported Mohr-Coulomb friction angle was less than the specified friction angle.

In the author's opinion, in many cases involving this particular interface, there is no reason to consider this a failing test.

This example illustrates the confusion that might arise when specification is written in terms of a shear-strength *parameter*, when the real objective is to achieve a certain value of absolute shear strength. Even though the materials provided the shear strength required by the specification, there is some confusion because one of the strength *parameters* did not meet the specified value for that parameter.

It is possible that the original specifier had taken into account the potential for cohesion, and had wished to discount cohesion, and really wanted a true minimum friction angle of 20°. If the specifier were truly that sophisticated and had such complex reasoning, then more than likely the specification would have also been more sophisticated in explaining these constraints on the test results.

In the author's experience it is rare that other designers and specifiers are discounting cohesion with geosynthetic interfaces, and usually it is simply a matter of proper interpretation and communication of the design intent compared to the actual test results. Nevertheless, as stated at the beginning of this article, it is not the intent of this article to provide guidance and suggestions on interpreting test results. Rather, the intent is to shed light on some common misunderstandings.

Example problem 2

The following problem has the same laboratory shear strength results as Problem 1, but the specification requirement is increased to 22° peak shear strength.

The relationship between the test results and the specification is shown in **Figure 6**. In this example, the two lower-normal load shear strength test results plot above the specification line, while the upper-normal load shear strength test result plots below the specification line. Based on the failing result of the upper-normal load test, most reviewers would initially say that this is a noncompliant test result and fails to meet the specification.

In the author's experience, curved failure envelopes are common, and the tendency for the highest normal-load result to fall beneath a straight-line friction-based specification is not unusual.

In this case, a more detailed review by the design engineer might reveal that the shear strength results provide an acceptable factor of safety for the intended purpose. It may be that the additional strength capacity provided in the lower normal load range that is above the specification more than offsets the reduced strength capacity in the upper normal load range that is below the specification. Clearly, the only person who can evaluate this issue, and who carries the requisite authority and responsibility, is the design engineer.

The following lessons can be gleaned from this example:

- Design engineers often attempt to specify a unique set of shear strength parameters as a minimum requirement for a given design. In reality, there may be an infinite combination of shear strength variations over the applicable range of normal loads that may satisfy the stability and shear resistance requirements, and many of these combinations may have a portion of their failure envelopes that fall below the specification.
- The tendency for natural and geosynthetic interfaces to yield curved failure envelopes can present a challenge to engineers, owners, and manufacturers who wish to optimize a design using simple straight-line shear strength specifications.
- A learned interpretation of direct shear testing data by an experienced practitioner may allow acceptance of apparently failing test results. This can occur because overly simplistic specification parameters may not ac-

count for other combinations of shear strength results that could provide acceptable overall shear resistance.

Summary

The direct shear test measures shear strengths as a function of normal stress. Period.

The test does not measure "friction angle" or "cohesion," as these values are parameters that are derived from the test results. Consideration of "friction angle" and "cohesion" simply as mathematical parameters used to describe shear strength data is of great benefit to practitioners for the following four reasons:

1. Interpretation of laboratory shear strength data should not be confused with the mathematical parameters used to describe it.

2. Proper data interpretation may avoid unnecessary penalization of the results by arbitrarily reducing the measured values.

3. This understanding can improve a designer's sensitivity to how important it is that shear strength is measured within the range of normal stresses that represent the design. Thus, the only defendable extrapolation of data should be: (a) back through the origin from the lowest normal stress, and (b) horizontally from the highest normal stress.

4. Laboratory shear strength data should be interpreted by a qualified practitioner experienced in the use and application of the results.

Often of much more importance than deciding whether to include or omit the cohesion (or adhesion) parameter is the decision of whether to use peak, post-peak, or residual shear strength. This discussion is beyond the scope of this technical note, and anyone commissioning and interpreting shear strength testing should be well versed in the issues surrounding this topic, as well.

Acknowledgements

The author would like to thank Richard Erickson and Chris Athanassopoulos for their review of this article.

References

Giroud, J.P., Darrasse, J., and Bachus, R.C., (1993). "Hyperbolic Expression for Soil-Geosynthetic or Geosynthetic-Geosynthetic Interface Shear Strength", *Geotextiles and Geomembranes*, Vol. 12, No.3, pp. 275–286.

Lambe, T.W. and Whitman, R.V., (1969). *Soil Mechanics*. John Wiley & Sons, New York, NY.

APPLICATION FOR PERMIT
SUNDANCE WEST

VOLUME III: LANDFILL ENGINEERING CALCULATIONS
SECTION 7: TENSILE STRESS ANALYSIS

ATTACHMENT III.7.G

THIEL, RICHARD. ***PEAK VS RESIDUAL SHEAR STRENGTH FOR BOTTOM LINER STABILITY ANALYSES.***

THIEL ENGINEERING. OREGON HOUSE, CALIFORNIA, USA

PEAK VS RESIDUAL SHEAR STRENGTH FOR LANDFILL BOTTOM LINER STABILITY ANALYSES

Richard Thiel
Thiel Engineering, Oregon House, CA, USA

ABSTRACT

The decision whether to use peak or residual shear strengths for a stability analysis must be made in the context of a specific design situation. Yet even when the specific situation is defined, the decision of whether to use peak or residual shear strength is often unclear. In general, if there are potential construction, operation, or design conditions that might cause relative displacement between layers, then a post-peak or residual shear strength for the layer having the lowest peak strength is appropriate. If seismic analyses predict deformation on a given interface, then the design should use the post-peak or residual shear strength for that interface. For bottom liner systems, where stress distribution along the liner system is very complex, it is advisable to verify that the slope stability has a factor of safety greater than unity for residual shear strength conditions along the critical interface.

INTRODUCTION

This paper is concerned with the forces that support a landfill on its liner system, and the shear strength of geosynthetic interfaces that keep the mass from sliding. Figure 1 schematically portrays the shear forces that work to keep the waste mass from sliding. If sliding occurs, the surface along which sliding would occur is called the critical surface, or potential slip plane. Bottom liner systems that use geosynthetics often have their critical surface along one of the geosynthetic interfaces. The shear strength of these interfaces can usually be measured by means of laboratory testing. These interfaces often realize their peak shear strength within a small amount of relative displacement (on the order of 25 mm), after which their shear strength decreases. Typically, after 50 to 300 mm of relative displacement, the shear strength is reduced to a steady minimum value, which is called the residual shear strength of that interface. Figure 2 shows a typical shear stress-displacement curve for a geosynthetic interface.

Over the life of a landfill the following activities occur: the liner system is built; waste is placed; settlement occurs; a final cover system is installed; and settlement and degradation of the waste continues. Each of these phases of the landfill's life produces different combinations of normal and shear stresses on the liner system. Landfill leachate and gas, which can create destabilizing pore pressures, are by-products of the landfill, and are removed with varying degrees of efficiency. The primary questions addressed in this paper are:

- Should a designer use peak or residual shear strengths, something in between, or a combination of peak and residual strengths, when evaluating a landfill design?
- What does the profession really know about the mobilized shear stresses? (This paper will focus on bottom liner systems.)
- Should the same choice whether to use peak or residual shear strengths be applied along the entire lining system, or should slopes and base liners be treated differently?
- Is there a preferred design approach?
- What factors of safety are appropriate for design?

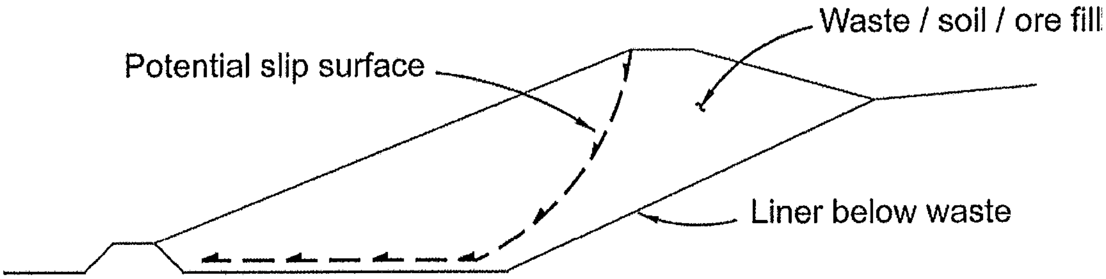

Figure 1 – Schematic of Shear Forces Along Critical Slip Plane

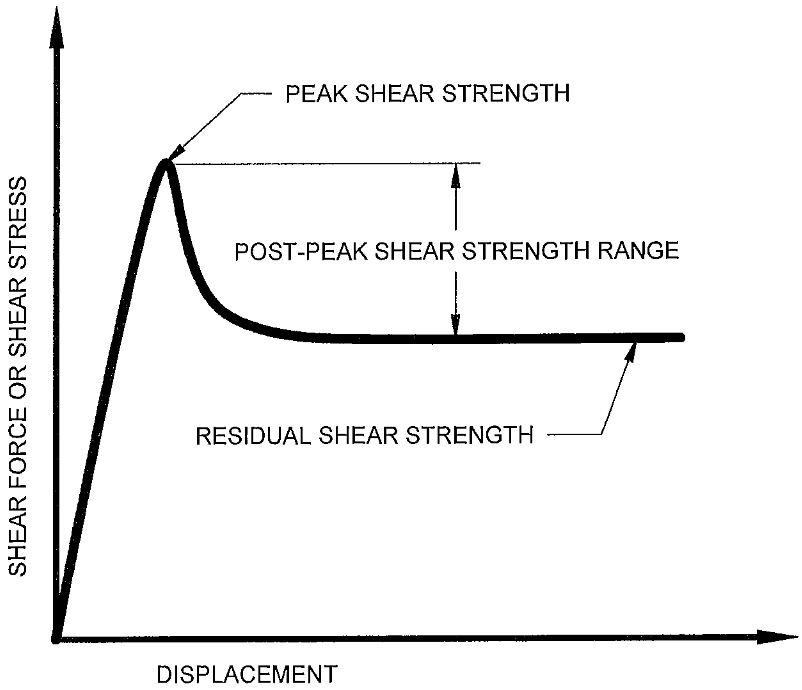

Figure 2 – Example Graph of Shear Force vs. Deformation for Geosynthetic Interface

ORGANIZATION OF THIS PAPER

Part 1 of the paper describes general considerations in performing slope stability analyses. It begins with a discussion of different types of slope stability analyses, including limit equilibrium, finite element, and 2-dimensional (2-D) vs. 3-dimensional (3-D) analyses. Understanding how the state-of-the-practice has developed, and the limitations of the analytical approach, both contribute strongly to making the right selection of appropriate shear strengths and factors of safety.

2-D limit-equilibrium analyses are by far the most common approach for evaluating slope stability. Part 1 discusses practical guidelines and common pitfalls that affect the results of these analyses, especially the selection of the critical shear plane on which the peak or residual shear strength will be modeled. Part 1 also discusses how pore pressures might cause a surface to exceed its peak shear strength and induce progressive failure. Selecting the appropriate shear strength requires an understanding of the effective normal stress range. Also, commissioning direct shear testing from a laboratory requires that one understand the proper testing parameters needed to obtain appropriate peak and/or residual shear strength values.

Part 2 of the paper directly addresses the question of peak vs. residual shear strength, and begins by discussing ductile vs. brittle behavior. Progressive failure, which occurs with brittle materials, then emerges as the chief concern of this paper. The discussion that follows considers conditions that could cause a brittle material to exceed its peak strength in the context of a landfill bottom liner, followed by a brief summary of field observations in this regard.

Part 3 discusses possible design approaches in terms of the selection of peak strength, residual strength, and hybrid approaches, and then considers the appropriate factors of safety for these different approaches.

Part 4 then presents conclusions reached from the preceding discussions. It also provides recommendations for practical design approaches based on the author's experience, as well as recommendations for further research.

This paper surveys the key considerations one employs when deciding whether to use peak or residual shear strength for bottom liner systems in landfills. It does not presume to make that decision, but rather seeks to outline and discuss all considerations that are necessary and pertinent to that process. Although many of the considerations this paper presents may be general enough to apply to cover (veneer) systems, it has been written solely with bottom liner systems in mind, and does not consider the long-term issues related to cover systems.

PART 1 – GENERAL CONSIDERATIONS

LIMIT-EQUILIBRIUM VS FINITE-ELEMENT ANALYSES

Limit-equilibrium analyses, whether 2-D or 3-D, are the most common methods of assessing slope stability. These methods can be performed by hand or, more commonly, by using a computer program. Such analyses evaluate the force and moment equilibrium of a slope on an assumed slip plane given assumed shear strength, unit weight, and pore pressure parameters. The result of these analyses is then presented as a factor of safety (*FS*) defined as:

$$FS = \frac{\text{Shear strength along the slip surface}}{\text{Shear stress along the slip surface}}$$

One defining characteristic of the limit-equilibrium approach is that it presumes that the factor of safety is the same everywhere along the slip plane. Therefore, the mobilized shear stress distribution along the slip plane is simplistically assumed to be a constant ratio of the shear strength along that plane. Such analyses also do not take into account elastic or plastic deformation. These are both significant considerations when deciding whether to use peak or residual shear strength.

Finite-element analyses attempt to calculate the stress distribution and deformations in a soil mass. In addition to considering force and moment equilibrium, these analyses also typically consider the materials' elastic modulus and Poisson's ratio, and some models can also calculate the change in shear strength with displacement for various materials. The result of these analyses is usually presented as a distribution of mobilized shear stress and displacements.

At first glance it would seem that finite-element analyses offer more of what we wish from a slope stability analysis as opposed to limit-equilibrium analyses. So much so, that we might even ask ourselves why we continue to bother with limit-equilibrium analyses. The fact remains, however, that the limit-equilibrium approach has been and will continue to be the basis of standard practice in the industry. The reasons for this, some of which also appear in the next section that considers 2-D vs. 3-D, are:

- Limit-equilibrium approaches have been performed and "calibrated" through industry experience for the past 80 years. Properly performed limit-equilibrium analyses have been proven to be adequate.
- Finite-element analyses are sophisticated and complicated to perform. The average design practitioner often is not adequately trained to perform such analyses, and the low frequency of projects that require their use do not justify the

resources needed to keep an engineer qualified to perform them on every landfill-design firm's staff.

- In the past few years the author has peer-reviewed a number of slope stability analyses. On four major landfill projects for which calculations had been prepared by separate reputable nationwide and local design firms, the author found fundamental errors in 2-D limit-equilibrium analyses. Some of these projects had already been built and were, in the author's opinion, at serious risk of large-scale failure. If such fundamental errors continue to be made with analyses as simple as 2-D limit-equilibrium, the prospects of universalizing a finite-element approach for the solid waste industry is not very promising. Finite-element analyses epitomize the expression "garbage-in garbage-out", so strict quality control and quality assurance is in order whenever they are employed.

2-D vs. 3-D ANALSYES

One issue that is periodically debated in the literature and at professional gatherings is the use of 2-D as opposed to 3-D analyses. Soong et al. (1998) question whether 2-D analyses are appropriate for landfills, and suggest it would be more appropriate to use 3-D analyses with residual strengths. From a pragmatic point of view, the everyday stability analysis has been, and will continue to be, 2-D in actual practice. There are three main reasons for this, clearly laid out by Duncan (1996):

- Inherent Conservatism. Properly performed 2-D analyses always give a factor of safety that is equal to or less than those given by 3-D analyses. 2-D analyses, therefore, are more conservative.

- Ease of Application. The average professional consulting engineer is interested in the amount of time it will take to arrive at an answer, the frequency of projects that will require special attention, and the effort it will take to organize the results in a final report. 3-D applications are simply not as easy to use as 2-D.

- Avoidance of Errors. As illustrated above, analyses are prone to errors, and 3-D analyses are more complicated than 2-D analyses. The author believes that the emphasis in the profession needs to be on performing solid, fundamental engineering, rather than on increased sophistication that invites more errors.

3-D analyses have mostly been used for forensic studies, and for those few complex situations that involve a very unusual geometry and/or distribution of shear strengths in the potential sliding mass. Examples of these can be found in Stark and Eid (1998). In the author's 16 years of experience performing stability analyses on dams, embankments, cut slopes, and landfills, there were only three situations where a 3-D analysis was warranted during design, and all three were satisfactorily accomplished using multiple 2-D sections. One of these projects was given as an example in the Stark and Eid (1998) paper. In that case Stark and Eid (1998) felt that a 2-D slope stability analysis could not anticipate the combined effects of the project's complicated geometry and shear strength zones. After discussion of the project's complexity, they reported a minimum 3-D factor of safety of 1.65 using a 3-D analysis program. In fact, the original design team, of which the author was a part, had two years earlier calculated a factor of safety of 1.60 using weighted averages of several 2-D cross-sections. Thus, even in this circumstance that had unusually complicated geometry and shear strength conditions, a modified-2-D approach gave results one would expect relative to the 3-D analysis results.

Notwithstanding the reservations given above, 3-D analyses will well serve those who have the time and budget to perform them.

To summarize, the refinements in accuracy offered by 3-D analyses are rarely matched by the average practitioner's understanding of basic slope stability mechanics, much less the level of confidence ordinarily offered by assumed shear-strength and pore-pressure parameters. Most often, the differences in shear strength and pore-pressure assumptions made by different engineers will substantially outweigh the refinements obtained by favoring 3-D over 2-D analyses. Compare, for example, the different conclusions reached by Schmucker and Hendron (1998) versus Stark et al. (2000) regarding the cause of a major landfill failure; or the difference in 2-D vs. 3-D comparisons for a landfill failure described by Soong et al. (1998), from those made by Stark et al. (1998). These case histories, recently published by experienced professionals, do not provide a compelling argument that 3-D analyses should be preferred. They do, however, reinforce the notion that the major factors contributing to uncertainty in a slope's performance are shear strengths and fluid pressures, and that this is where our attention should be focused. The purpose of this paper is to focus specifically on one of these issues, namely, when it is appropriate to use residual vs. peak shear strength for geosynthetic interfaces at the base of a waste containment facility.

GENERAL DISCUSSION OF 2-D ANALYSIS APPROACH

Method of Analysis

Slope stability analyses are most commonly assessed using computer programs that evaluate the limit equilibrium of a 2-D cross-section. Less sophisticated limit equilibrium analyses can be performed using hand-calculation methods or charts. Hand calculations are an effective analysis tool because they often provide a clearer understanding of the critical aspects of the problem, and mistakes in geometry and assumed failure planes are less likely. A common approach is to perform a hand check on the most critical surface that has been analyzed by a computer program. A good summary of slope stability approaches using hand calculations is provided by Abramson et al. (1996).

Limit-equilibrium analyses of varying complexity that have been developed are available to design practitioners. One of the first approaches was the Ordinary Method of Slices developed by Fellenius. Later refinements were presented by Bishop, Janbu, Morgenstern and Price, Spencer, and others. A review of these methods is beyond the scope of this paper, and the reader is referred to Abramson et al. (1996) and Duncan (1996) as a starting place for a comparison of the various limit-equilibrium methods. The author would, however, offer three points from his own practice as to which method to use for performing stability analyses of bottom liner systems:

- The Bishop method is generally not applicable when analyzing bottom liner system geometries because it was developed for circular failure surfaces. The critical slip plane for liner systems is often a translational block that is non-circular.
- Spencer's method, which is now commonly available in computer codes, is considered more rigorous and complete in its analysis than the simplified Janbu method, which is commonly used for block analyses. Spencer's method is computationally more intensive, however, and may be difficult to use for random searches for a critical failure surface, even with modern computers. It is also less stable and can yield incorrect results unless the line of thrust results are checked by the user. Therefore, a good practice is to search for the critical surface using Janbu's simplified approach, and then perform a final check on the stability using Spencer's method. Usually, but not always, Janbu's method will result in a slightly higher factor of safety.
- The approach developed by NAVFAC (1982) for translational block analyses is often a good and appropriate method for performing a hand-check on the computer results for a 2-D translational block failure along a bottom liner system.

Identification of Critical Slip Plane

The most typical requirement for static stability is to meet a specified factor of safety. Just what constitutes an appropriate factor of safety will be discussed later in this paper. The idea is that if the stability analysis is performed correctly with the proper input variables, the factor of safety should provide a level of confidence that the slope will in fact be stable.

The essential operative words in the above paragraph relating to stability analyses is that they are "*performed correctly*". The safety margin in a factor of safety exists to account for unknown or unpredicted deviations from the original design assumptions. It is not, however, supposed to account for errors in the analysis, or incorrect geometric and material property assumptions.

When performing a correct analysis the critical slip plane for analysis must be identified correctly. An experienced geotechnical engineer is usually required in order to select the critical cross-sections for analysis of a slope. Even for experienced practitioners, though, it is not always obvious which section is the most critical, and several trials generally need to be performed. For very complicated geometries, as described in the previous section, multiple 2-D sections may need to be weighted in order to simulate a 3-D analysis, or the more complex 3-D analysis can actually be performed.

In addition to selecting the proper cross-section, it is also important to search for and select the correct critical slip plane within that cross-section. In peer-reviewing slope stability analyses performed by others, the author has found errors in which the designer had correctly identified the critical cross-section, but incorrectly identified the critical slip plane within that cross-section. He found others, too, in which the designer had conceptually identified the correct slip plane, but failed to code the computer program to correctly place the slip plane at the correct interface within the liner system. The effects of such errors was to drop from an ignorantly-blissful factor of safety of 2 to 3, to an uncomfortable factor of safety of less than 1.1.

When the critical slip plane is along the liner system, the critical surface is always the one that has the lowest peak strength. If residual strengths are used in the analysis, they should reflect the surface that has the lowest peak shear strength, because that is the one that will govern deformations.

Pore Pressures

Next to gravity, pore pressures (most pervasively those caused by liquid as opposed to gas) are the single most prevalent factor contributing to slope stability failures. They are also among the most overlooked elements in slope stability analyses. Schmucker and Hendron (1998) illuminate this problem when they state that "Very little is known at this time regarding the generation and distribution of pore pressures in MSW landfills."

The one area where evaluating the influence of pore pressures on slope stability has been well focused has been in the design of dams. For this reason there have been few dam failures due to the neglect of pore pressures, with dam failures in the past century generally being caused by other factors (e.g. liquifaction or piping). Pore pressures are not commonly included in landfill analyses. Yet most (or at least many) of the dramatic landfill failures reported in the industry can be attributed to pore pressures that built up either in the foundation, due to waste loading, or in the waste itself, due to leachate buildup or leachate injection. Examples are the Rumpke landfill failure (see Schmucker and Hendron, 1998, who attributed the failure in part to leachate buildup caused by an ice dam at the toe), and the Dona Juana landfill failure (see Hendron et al., 1999, who attributed the failure to high-pressure leachate injection).

When performing slope stability analyses, designers should consider the potential for unanticipated pore pressures. Unanticipated conditions may occur in landfills due to clogging of the leachate collection systems, or aggressive leachate recirculation in the waste mass. Additional discussion of this issue is provided by Koerner and Soong (2000). Further discussion later in this paper describes how pore pressures could lead to a localized exceedence of peak strength, leading ultimately to a progressive failure.

Selecting and Measuring Material Shear Strengths

Shear Strength Definition. Figure 3 illustrates a non-linear shear strength envelope, which is typical for many soil and geosynthetic interfaces. Sometimes the non-linearity is slight, and a straight-line approximation over the entire load range under consideration can be valid. This is often true for very narrow load ranges such as those considered for cover veneer systems. At other times this non-linearity is quite significant, especially when shear strength characteristics are evaluated over the broad range of normal loads indicative of bottom lining systems.

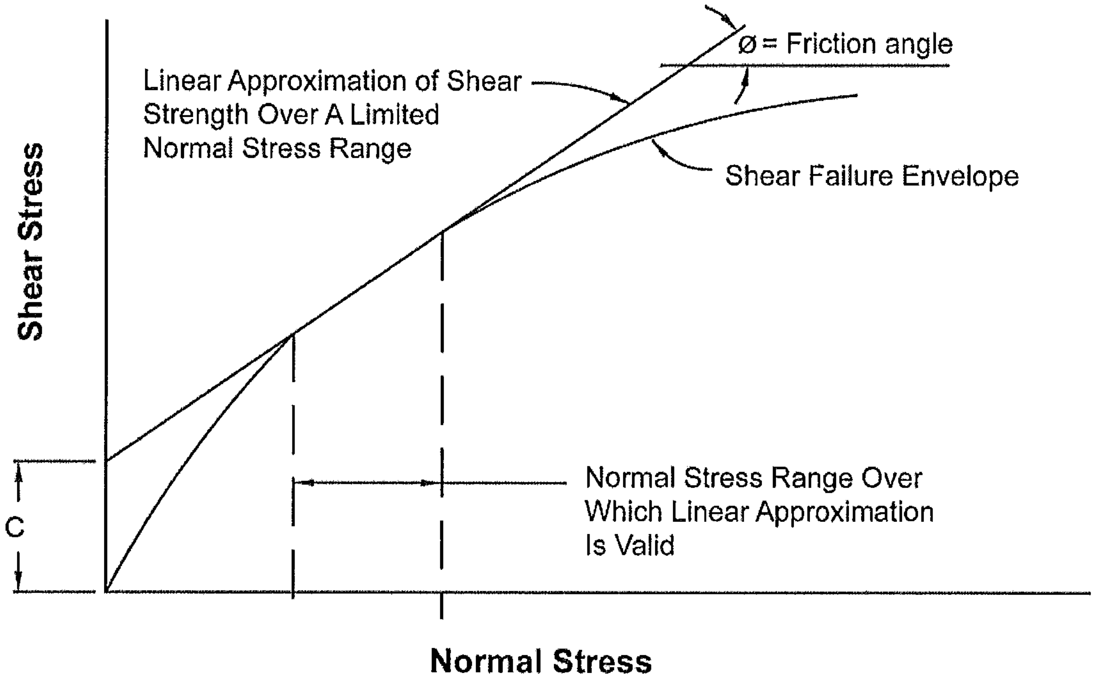

Figure 3 - Typical Shear Failure Envelope for Soil and Geosynthetic Materials.

If the shear strength curve of the evaluated materials is non-linear with respect to normal load, then special consideration should be given to defining the shear strength parameters within a specific normal load range. Many computer programs only allow the input of linear shear strength parameters. These parameters are normally identified as a friction parameter *(ϕ)* and a cohesion (or adhesion) parameter *(c)*. It is useful to recognize that these are often only mathematical parameters that describe the shear strength of a material or interface over a specific normal load range. The shear strength parameters are demonstrated in Figure 3.

Draft European Standards, and other publications (e.g. Koerner and Daniel, 1997) suggest that the apparent cohesion of a shear strength envelope can be ignored. As stated by Jones and Dixon (1998): "This assumption can have a significant effect in that the shear strength for any particular normal stress will be quoted as being lower than measured... It is possible that the failure envelope may curve to the origin at very low normal stresses, in which case ignoring the apparent cohesion will result in over conservative results." If we recognize that the values of the parameters ϕ and c are only mathematical tools used to describe the measured or estimated shear strength over a given normal load range, we can discount statements that advocate that cohesion can be ignored.

The friction parameter (ϕ) is related to the slope of the line (slope = $\tan\phi$), the cohesion parameter (c) is the y-intercept, and the normal load range is the abscissa range over which the straight-line approximation of the shear strength envelope is valid. Use of the shear strength parameters outside of the normal load range for which they were defined is generally non-conservative, as illustrated in Figure 3.

If the computer program only allows the consideration of linear shear strength envelopes, the shear strength envelope for non-linear materials should be discretized into a series of straight-line approximations for different normal load ranges. Furthermore, where the critical slip surface runs through a material or interface that exhibits a non-linear strength envelope, the designer should either use a computer code that allows input of a non-linear shear strength envelope, or assign different strength parameters to different zones of the material or interface according to the normal loading it theoretically experiences. For computer codes that do not allow non-linear shear strength envelopes, the delineation of different normal-load zones for non-linear materials is usually calculated by hand. This procedure is outlined in detail by Thiel et al. (2001).

Shear Strength Measurement. For geosynthetic lining systems, the internal and interface shear strength is normally determined by using the direct shear test in accordance with ASTM D 5321. For GCL internal and interface shear strength evaluation, direct shear testing is conducted in accordance with ASTM D 6243. In these direct shear tests, the geosynthetic material and one or more contact surfaces, such as soil or other geosynthetics, are placed within a direct shear box. The specimens are hydrated, consolidated, and placed under a constant normal load in accordance with the ASTM procedures, along with any project-specific testing clarifications/instructions from the design engineer. A tangential (shear) force is applied to the materials, causing one section of the box to move in relation to the other section. The shear force needed to cause movement is recorded as a function of horizontal displacement.

The test is normally performed for several different normal loads. Typically a series of at least three individual tests are performed at specified normal load conditions. The normal load and shear forces are converted to stresses by the given area over which shear occurred, typically a 12 in x 12 in (300 mm x 300 mm) sample. The peak and post-peak (or residual, if deformation is taken far enough) shear strengths are plotted on a graph, and a best-fit straight line or curve is fit through the data to represent the shear strength envelope. Several factors can influence the interface shear strength of geosynthetics. The most important of these are discussed below.

Valid Testing Technique. While not offering any endorsements, the author can state that he trusts very few laboratories in the nation to provide high quality direct shear test data. Initial ASTM round-robin testing of even the most simple interface (nonwoven geotextile against a smooth HDPE geomembrane) produced a shot-gun scatter of results with very poor correlation. Unless the initial test data has integrity, most of the further considerations offered in this paper become meaningless. It is imperative that the designer screen the testing laboratory in order to obtain test data of assured accuracy.

Rate of Shear Displacement. The typical default shear rate for direct shear testing with geosynthetics as presented in ASTM D 5321 is 0.04 in/min (1.0 mm/min). For testing hydrated GCLs, ASTM D 6243 provides guidance on attaining consolidated drained conditions that should preclude the build-up of excess pore pressures.

In general the rate of shear displacement affects peak strength more than residual strength. Depending on the interface being tested, the strain rate of the test should be slow enough to give results representative of long-term (slow) shear conditions.

Hydration. The moisture content, degree of saturation, and degree of consolidation of adjacent soils and geosynthetics can all exert an influence on the shear strength results. It is important to direct the testing laboratory as to the sequence of hydration and consolidation. With clay soils adjacent to geosynthetics, it is generally more conservative to hydrate under low normal loads before consolidating. Thus far, the type of hydrating fluid has not been reported in the literature as affecting shear strength results, especially in regard to typical landfill leachates.

Normal Stress. The most common strength-related errors in computer slope stability analyses stem from using strength parameters that do not correspond to the normal load conditions at the surface being analyzed (Lambe et al., 1989). It is generally unconservative to extrapolate linear strength envelopes beyond the limits for which they were defined. It is, therefore, important that shear test data be acquired under normal loading conditions that are representative of the conditions being analyzed. For base liners this is zero to full height of the waste mass.

Utilization of Representative Materials. Designers often tend to use either published literature values or previously obtained test results for shear strengths. In such cases, their experience and judgment may assist them in selecting shear strength parameters for the purposes of preliminary design. It is highly recommended, however, that material-specific testing be performed to assist in preparing the final construction specifications, and/or to verify the actual materials delivered as part of a CQA program. The reason for this is that the variation in geosynthetic manufacturing parameters from job to job can have a significant effect on shear strength. The most significant of these is the degree of texturing on coextruded geomembranes. Figure 4 presents a graph showing the difference in peak and post-peak shear strengths obtained with two different degrees of texturing. Designers can use this concept to their advantage, as will be discussed later. Designers unaware of this issue may test a manufacturer's sample and obtain passing results, and then use GRI-GM 13 as a texturing specification. This would provide an extremely low-level requirement for texturing that may not achieve the same interface shear strength as the nice sample provided for initial testing by the manufacturer. The same principle may hold for geotextile-based products, whose fiber denier size, fiber type, degree of needling, etc. can influence its interface shear strength properties. The only way to be sure is to test the actual materials provided for construction.

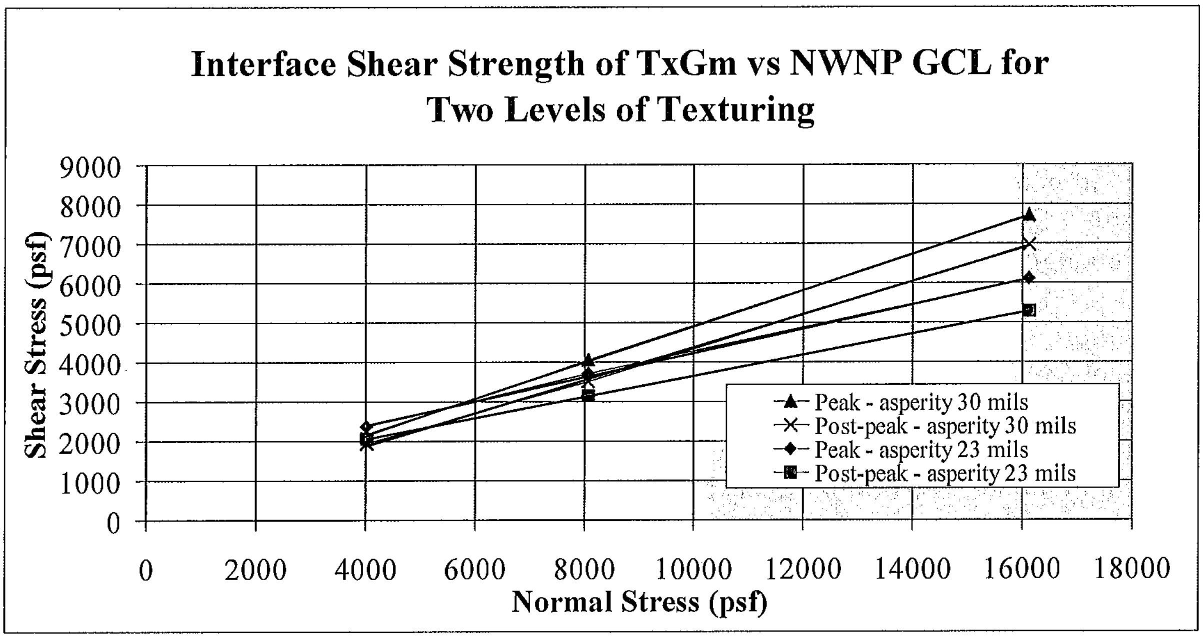

Figure 4 – Variation of Interface Shear Strength with Different Degrees of Geomembrane Texturing

Adjacent Materials and Consolidation Time. Using representative materials for direct shear testing refers not just to the materials for the interface being tested, but also to the adjacent materials. The use of realistic adjacent soil materials will typically provide slightly higher interface shear strengths than will, for example, the use of steel plates. In the same vein, Breitenbach and Swan (1999) show that longer load consolidation times result in a significant increase in interface shear strengths, apparently due to micro-scale load-induced deformation of the interface materials. Jones and Dixon (1998) question the used of the ring-shear apparatus for testing, because the narrow specimen of limited surface area on hard, smooth boundaries may not be representative of field conditions. These factors can affect both the peak and post-peak shear strength results.

Peak vs. Post-Peak vs. Residual Shear Strength. The highest level of shear strength measured in a direct shear test under a given normal load is defined as the peak strength. With continued shear displacement there is typically a loss of strength. The shear strength at any given displacement past the point of peak strength is referred to as "post-peak strength". The strength at which there is no further strength loss with continued displacement is called the "residual strength". Many of the most common direct shear devices do not allow enough displacement to occur that would enable true residual strength to be measured (e.g., see Stark et al., 1996). Therefore, in some cases it is not technically correct to refer to end-of-test conditions as representing the "residual" strength, but rather, to refer to "post-peak" strength while also specifying the amount of displacement. For the purposes of this paper, the lowest expected shear strength after significant deformation (typically more than 3-6 inches [70-150 mm]) is described as the residual shear strength. Shear strengths between the peak and residual shear strength are referred to as post-peak. This brings us then, to the main focus of this paper, which is whether it is appropriate to use peak or residual shear strengths (or something in between).

PART 2 – PEAK vs. RESIDUAL: THEORETICAL AND PRACTICAL CONSIDERATIONS

BACKGROUND DISCUSSION ON BRITTLE MATERIALS AND PROGRESSIVE FAILURE

Many, but not all, geosynthetic interfaces are strain softening. This highlights the essence of the peak vs. residual question. With a relatively short amount of deformation (typically less than 25 mm), the materials pass beyond peak strength into a lower post-peak shear strength, ultimately becoming what we call residual. In geotechnical engineering these shear strength characteristics are also sometimes called 'brittle' – brittle meaning that the material substantially decreases in strength after it is "broken", that is, has gone past peak strength. (Note that this has nothing to do with the tensile behavior of the material.) This behavior is in contrast to a ductile shear interface, which continues to deform after reaching its peak strength, but retains its strength close to the peak. An example of a brittle geosynthetic interface is an HDPE textured geomembrane against a geotextile, which produces a dramatic drop in strength after the peak strength is exceeded. An example of a ductile geosynthetic interface is a smooth PVC geomembrane against a geotextile (see data published by Hillman and Stark, 2001). Also, MSW waste is generally considered a ductile material in terms of shear strength (Kavazanjian, 2001).

As a progressive failure develops, the shear stresses are redistributed within the slope. This often involves the slow deformation of the failing mass over time, followed by an abrupt slide. If the critical plane supporting a slope is brittle, and for some reason part of it is stressed past its peak strength, then that part quickly becomes significantly weaker, which means it can carry less of the load. That in turn puts more of the load on other parts of the critical plane, which may in turn cause another part of that plane to become overstressed and exceed its peak strength. The continuation of this process is called progressive failure. At some point the entire system becomes overstressed and an abrupt failure occurs. This is the concern when there is a brittle interface.

Progressive failures have been characteristically noted for stiff clays, as described by LaRochelle (1989): "We have come to realize that we cannot count on the peak strength in this strain-softening material either for short- or long-term stability." Past landfill failures have been attributed to this same phenomenon (Schmucker and Hendron, 1998; Mazzucato et al., 1999; Stark et al., 2000), which holds significant potential for future failures (Gilbert and Byrne, 1996).

POTENTIAL CONDITIONS THAT MAY LEAD TO PROGRESSIVE FAILURE

Several reasons are provided below which explain why the peak strength of a bottom liner interface might unexpectedly be exceeded.

Non-Uniform Stress Distribution and Strain Incompatibility

Perhaps one of the most compelling reasons to be concerned about progressive failure in liner systems is that the stress distribution along the liner interface is not known. "It is impossible to obtain all of the necessary information in most cases" to perform a rigorous analysis of a progressive failure process (Tiande et al. 1999). "It is difficult to determine the available shear resistance along an interface exhibiting strain-softening behavior. It may be unsafe to assume that peak strength is available, while it may be excessively conservative and costly to assume that only the residual strength is available" (Gilbert and Byrne, 1996).

The complexities of stress distribution are affected by the type of loading and by pore pressures. According to Li and Lam (2001) ".. the development of progressive failure will also be different depending on whether failure is triggered by a rise in water table *[insert by author: namely, leachate]* or an increase in external loading *[insert by author: namely, continued waste stacking]*".

Reddy et al. (1996) present a most interesting finite-element modeling study that evaluates the stress distribution and deformations along a landfill liner system for an assumed landfill geometry. Their study compares smooth and textured interfaces for different stiffnesses of waste. Although their analysis did not model strain-softening behavior of the interfaces, the results provide valuable insight into stress and strain distribution. Some of the conclusions from their study are:

- The stiffness of the waste influences the distribution of interface stress and shear displacements. Stiffer waste puts more stress and strain on side slopes (especially the lower part of the slope). Softer (more compressible) waste puts more stress on the base liner below the highest part of the waste, and more strain accumulation towards the toe. The overall factor of safety, however, is not affected by the waste stiffness, assuming that no strain-softening of the interface shear strength occurs.

- The smooth interface with 11° friction reached its peak strength in a number of places along the interface in their example, even though the global factor of safety was 1.5. The textured interface did not approach its peak strength anywhere along the interface in their example, but had a factor of safety of over 4. This means that a typical stability evaluation that results in a factor of safety of 1.5 may actually result in areas of the critical interface achieving their peak strength and possibly going into a reduced post-peak strength.

A finite element study was performed by Filz et al. (2001) who reached conclusions similar to those obtained by Reddy et al. (1996). Filz et al. (2001) provided a compelling demonstration that a smooth clay-geomembrane interface exhibiting strain-softening characteristics might be inappropriate to analyze based on peak shear strengths. They showed that the distribution of mobilized shear stresses was not uniform along the base and side slope, and would result in progressive exceedence of peak strength. Their comparative analyses demonstrated that whereas a limit-equilibrium analysis based on peak strengths might result in FS = 1.6, the finite-element analysis would suggest impending failure (i.e. FS = 1.0). The same problems analyzed using residual shear strengths in limit-equilibrium analyses resulted in an average FS = 0.94. Furthermore, for a finite-element analysis to show FS = 1.5, the limit-equilibrium analysis based on peak strengths needed to show a FS of about 2.2, and the limit-equilibrium analyses using residual shear strength resulted in FS = 1.3.

Differences in the relative stiffnesses of the overlying waste as compared to that of the liner interface are also cited by Gilbert and Byrne (1996) as a significant potential cause of deformations along the liner interface that could lead to residual shear strengths.

Similar suppositions are made by Stark et al. (2000), who postulate that strain incompatibility between MSW and underlying interfaces can lead to progressive failure, as they believe was the underlying cause of the Rumpke landfill failure. The weaker lower interfaces may achieve post-peak strengths before the MSW ever achieves peak strength. After peak strength of the interfaces is achieved, the peak strength of the MSW may be mobilized at a time when the strength of the interfaces is reduced to the residual value. They state: "The greater the difference between the stress-strain characteristics of the MSW and the foundation soil or geosynthetic interfaces, the smaller the percentage of [peak] strength mobilized in the MSW and underlying materials." [1]

Unexpected Increases in Pore Pressure

The typical effect of pore pressures is to decrease the effective normal stress, which in turn decreases the effective shear strength, even as the shear stress that is driving instability remains unchanged. When pore pressures are introduced, the effective shear strength may be reduced to the point that the peak shear strength at that location is exceeded, at which point progressive failure can begin. This was what Schmucker and Hendron (1998) concluded was the triggering mechanism for the Rumpke landfill failure.

Seismic Loading

With seismic loading there is certainly the potential for deformation to occur along the critical failure plane, which can reduce the strength of the critical interface below its peak strength. In this regard the design practitioner needs to assess the potential for this type of deformation and, if the design earthquake is expected to produce deformation greater than about 20 mm, then the residual strength of that interface must be considered.

Construction Deformation

Construction conditions frequently result in temporary stability conditions with lower factors of safety than the completed fill scenario. To the author's knowledge, the effect of preliminary interface deformation at low normal loads on the subsequent shear strength at higher normal loads has only been documented in one recent study by Esterhuizen et al. (2001). They showed that for a smooth clay-geomembrane interface, deformations at low normal loads would partially, but not fully, reduce the peak strength of the interface at higher normal loads. They provide a very interesting "work-softening" model to describe this behavior in a manner that can be used in a finite-element analysis. Although their model fits the data very well, it is only applicable to the specific clay and geomembrane used for their study, and it is not know at this time how well their approach would work for other interfaces. This is an area for further research.

---

[1] For years now the author has heard the statement that the strain incompatibility between waste and liner systems could be a major consideration in selecting appropriate shear strengths. It is interesting, however, that some of the literature reports surprisingly low amounts of deformation required to reach the peak strength of the waste; on the order of only 40 mm for rigid-body deformation. See, for example, Eid et al. (2000), Stark et al. (1998), Mazzucato et al. (1999). Also Kavazanjian (2001) states his belief that strain compatibility with MSW is not nearly as significant an issue as has generally been supposed, based on direct- and simple-shear test results that show that the strains and deformations required to reach peak strength are comparable to those required for most soils.

Waste and Foundation Settlement

Over time there is substantial deformation and settlement of the waste that may cause unknown redistribution of stresses. The settlement of waste adjacent to a sideslope has often been noted as a source of downdrag forces, which may become great enough to exceed the peak strength of one of the slope liner interfaces. This phenomenon was cited by Stark and Poeppel (1994) as a mechanism contributing to the Kettleman Hills landfill failure, and is echoed in Gilbert and Byrne's (1996) theoretical study: "…it is more likely that the residual strength will be mobilized along the side slope rather than the buttress [bottom liner]", and they even go so far as to say "…it is unlikely that an average stress greater than the residual value could be mobilized along a typical side slope in a containment system." Likewise, foundation settlement has the potential to cause differential movements of the liner system.

Aging and Creep

Geosynthetic durability has been the subject of many papers and studies which address the ability of geosynthetics to maintain their physical properties as containment barriers, and to some extent as tensile reinforcement. Little has been published, however, regarding the long-term durability of shear interfaces such as, for example, the long-term dependence on the strength of geotextile fibers at interfaces with textured geomembranes, or within reinforced GCLs. Quantitative predictions regarding the long-term aging and creep potential of geosynthetic interfaces are certainly beyond the author's capacity, but are noted as an additional potential mechanism whereby the assumed peak strength of an interface might be reduced.

FIELD OBSERVATIONS

From the author's experience and his informal polling of industry representatives, two general field observations that have been made regarding deformations along geosynthetic interfaces on slopes:

- Slopes that were designed with robust interfaces using textured geomembrane or granular materials against geosynthetics, have not been observed to undergo tension or deformation.

- Slopes that had less brittle, but also less strong interfaces, such as a geotextile over a smooth geomembrane, have been observed to result in tension in the upper geosynthetic, presumably due to slippage along the interface which occurred as a result of downdrag forces.

It is worthwhile to note in the Gilbert and Byrne (1996) model that strain softening on the slope would generally only occur if the slope angle was greater than the peak friction angle of the lining material. Although unverified by the author, this may be a general guideline for estimating whether or not peak or residual shear strength would occur on a slope (excluding seismic forces). For example, on a 3(H):1(V) slope, perhaps a peak interface strength of 18° or more would maintain its peak strength, and an interface strength of less than that would have a higher potential for going into residual.

Given the large number of landfills constructed with geosynthetic bottom liner systems, it is quite surprising how few failures have actually been reported. Furthermore, none of the reported failures, to the author's knowledge, involved the progressive failure of a substantially brittle geosynthetic interface. Most of those failures have involved soil (including bentonite failures associated with unreinforced GCLs, which are ductile relative to shear strength). The best example of a pure geosynthetic failure that involved some degree of strain softening is the notorious Kettleman Hills failure, but the interfaces in that failure were fairly weak to begin with (all against smooth HDPE), and the initial factor of safety, even assuming peak strengths of the interfaces as they existed, was low, and below standard industry guidelines.

The conclusion of industry observations is that actual industry experience has not shown degradation of peak strength (i.e. progressive failure) to be a pervasive problem. Nonetheless, it definitely presents a potential problem that has on occasion bloomed into an unfortunate reality. It is, therefore, worth taking it into account by means of design and analysis considerations, which are discussed in the next section.

PART 3 - DESIGN APPROACHES

THE PEAK vs. RESIDUAL ISSUE IN THE CONTEXT OF THE DESIGN PROCESS

Many elements of a landfill are not designed, per se, but are largely dictated either by the owner's desires or by regulatory constraints. For example, the geometry of a landfill (boundaries, slopes, height, etc.) is often governed by an attempt to maximize the resource (i.e. volume) while meeting the constraints presented by conditional use permits, property line setbacks, maximum slope regulations and the like. Furthermore, the liner system is usually prescribed by regulation, at least in its fundamental requirements, and oftentimes by a default regulatory configuration.

In many cases then, the two major elements that influence a stability analysis are largely predetermined. That is, both the preferred landfill geometry and the liner system are more or less given to the "designer", who is charged with producing the "final design". From the point of view of slope stability, what is there left to do? Obviously the slope stability should be checked and verified. What does this mean and how is it done?

The first step in performing a slope stability analysis is to define the basis of the analysis. This is often documented in the project files as a Design Basis Memorandum (DBM), in which the following kinds of determinations are made:

- Will the analysis look at only the final configuration, or at interim operational configurations as well? (The latter option is highly recommended for risk management.)
- What unit weight will be assumed for the waste?
- What material strength values will be assumed for the different materials, and how will they be determined?
- Which pore-pressure scenarios will be evaluated?
- What will be the minimum acceptable factors of safety?
- Are seismic analyses required? If so, what approach will be used? How is the design earthquake defined? If a deformation approach is used, what is the maximum allowable deformation?

The results of the slope stability analyses will be:

- A static factor of safety (for each configuration analyzed).
- If a seismic analysis is required, the results will present either a potential magnitude of deformation along the critical slip plane, or a factor of safety for a simplified pseudo-static analysis.
- A description of the minimum required interface shear strength properties for the liner system construction.

It is this last point that makes slope stability analyses a design function rather than a mere geotechnical engineering exercise. It is essential that a clear linkage be made between the slope stability calculations and the ultimate project specifications, to ensure that the proper materials are provided during construction to meet the slope stability requirements. If the analysis results do not meet expectations, iterations of laboratory testing and/or alterations in slope geometry and/or liner materials may be required in order to achieve an acceptable design that can be adequately specified.

The design aspect of slope stability analyses becomes even more interesting when an additional constraint is put on the design criteria, namely to position the critical slip surface above the primary geomembrane. This is a common practice in Germany that is also employed by several design practitioners in the United States (and likely in other places as well, given the author's limited knowledge of practices worldwide). This design approach helps to ensure that, if for any reason slippage does occur, the barrier liner system will remain intact. Ensuring that the slip plane is above the primary geomembrane is not necessarily a simple matter; laboratory shear testing programs and iterations of slope stability analyses are often required in order to achieve acceptable results.

Implicit in the slope stability design and analysis process is the need to decide whether peak or residual shear strengths should be used. Though this is not generally an issue for waste materials, which are usually considered ductile, it is often a significant issue for liner system interfaces. This decision will significantly influence the calculated factor of safety. For seismic analyses, the influence is often less significant, because if the seismic analysis indicates deformation will occur, a prudent designer will use a post-peak shear strength (even as the question remains whether to use a deformation-based post-peak strength, or a true residual strength).

WHAT IS AN APPROPRIATE FACTOR OF SAFETY?

The author previously co-authored a paper whose title posed this same question concerning cover systems (Liu et al., 1997). That paper discussed assessing the degree of confidence in each of the variables that went into assessing the factor of safety, and assessing the potential risk and cost of a failure. This approach is espoused by Gilbert (pers. comm.) who believes that the factor of safety should be based on "uncertainties, assumptions, and the consequences of failure."

It is common in the literature to see geotechnical references that reiterate the idea that the greatest degree of uncertainty in performing slope stability analyses is the shear strength of the materials (e.g. Liu et al, 1997; Stark and Poeppel, 1994; Duncan, 1996). Given that the factor of safety is a reflection of uncertainty, it should logically reflect the degree of uncertainty in the shear strength properties. This was clearly noted by Terzaghi and Peck (1948, pg. 106):

> "The practical consequences of the observed differences between real soils and their ideal substitutes must be compensated by adequate factors of safety."

A commonly accepted value for the factor of safety in geotechnical engineering slope stability analyses is FS ≥ 1.5. Many engineers blindly accept this value while remaining ignorant of its basis. The origin of this value was the empirical result of analyzing the relative success and failure of dams that have been constructed over the past century. Experience proved that when an analysis was performed correctly, assuming reasonable and prudent material properties, an earthen structure with a factor of safety of 1.5 can be expected to remain stable even when some of its structural geometry and material properties have varied from those assumed in the analysis. Similarly, other values for an acceptable factor of safety have been established as general industry practice for other types of problems, such as bearing capacity (required FS generally between 2 and 5) or drainage applications (FS generally ranging from 1 to 20 depending on the problem).

It is also fundamental to the establishment of generally accepted factors of safety that analyses are performed correctly, and are based on prudent assumptions regarding material properties, geometry, unit weights, and pore pressures. Factors of safety are not intended to compensate for engineering errors or omissions. Indeed, the author has evaluated failures where the design factor of safety exceeded 1.5, which means that the original design neglected to take into account one or more critical factors.

With containment lining systems we meet a unique opportunity. We have a greater ability to know where the potential critical slip plane is, and can measure its shear strength characteristics more accurately than we can in a number of traditional geotechnical problems. We have far more knowledge of the geometry and shear strengths than when we are confronted with a natural slope, for example. Knowing where slippage is most likely to occur, we have to assess the implications for deformation. As described previously in this paper, we often don't really know if some deformation will occur, but experience from many analogous failures, along with the process of deduction, tells us that it *could* occur. Knowing this, we should at least be prepared to use the post-peak shear strength of the surface having the lowest peak strength.

SPECIFIC APPROACHES

Some specific design approaches, which the author has himself employed, are summarized below. This does not imply that others approaches do not exist, but simply that this paper is based on the author's experience.

1. <u>The Most Conservative Approach – Force the Slip Plane Above the Geomembrane and Use Residual Shear Strengths Everywhere the Slip Plane Occurs in the Liner System</u>. A simple and common way of achieving this objective is to use single-side textured geomembrane for the primary liner, and then cover it with a geotextile or geonet product. In nearly every case the author has been involved with (save a few inevitable exceptions), single-sided textured geomembrane (textured side down, of course) always caused whatever slippage occurred to take place on the top surface of the geomembrane, if it was covered with another geosynthetic. Even when directly covered by a granular material, it was often possible to make the bottom (textured) interface stronger than the smooth geomembrane/granular soil interface. In our experience there is often not a large difference between the peak and residual shear strength on smooth geomembrane interfaces with either other geosynthetics or granular soils, and these interfaces would not be considered very brittle. There may be some exceptions, such as a smooth HDPE geomembrane against a wet clay as described by Filz et al. (2001) for the Kettleman Hills failure analysis.

Some designs may need greater shear strength for interim construction and operational conditions than can be provided by a smooth geomembrane surface, so a double-sided textured geomembrane may be required. In this case the design condition of having the weak interface above the primary geomembrane may still be achieved by specifying a more aggressive texturing on the lower side of the geomembrane (see shear data presented in Figure 4).

If a designer is able to use the residual shear strength of the upper geomembrane interface and achieve acceptable factors of safety, this design can be very safe from the point of view of both stability and environmental containment. This approach is favored by Hullings and Sansome (1997), who recommend: "If possible, provide a slip plane and a stress-free geomembrane."

If true residual shear strengths are used for the analysis, and those strengths are measured with a degree of confidence that they represent worst case for the liner system interfaces, it follows that a lower-than-typical factor of safety can be allowed. Gilbert and Byrne (1996) suggest that a factor of safety simply greater than unity may be an adequate design criterion for analyses that assume residual shear strengths are the only strengths mobilized along the entire slip surface. Part of Gilbert's rationale (personal communication, 2001) is that even if a failure were induced for a slope analyzed with this criterion, things could not degenerate quickly, presuming the analysis were properly performed. The slope could subsequently be monitored and measures taken to reduce the deformation rate, if deemed necessary.

A similar recommendation is given by Stark et al. (1998): "...strain incompatibility can facilitate the development of slope instability because the geosynthetic interface may mobilize a post-peak or residual strength while the waste is mobilizing a strength that is significantly below the peak strength. This can be incorporated into a design by assigning a residual strength to the critical interface or slip surface and requiring a factor of safety, FS>1...Because field interface displacements and *effect(s) of progressive failure are not known [emphasis by author]*, a factor of safety, FS>1 with a ring shear residual interface strength assigned to all potential slip surfaces should be satisfied in addition to meeting regulatory requirements."

Filz et al. (2001) suggest that if true residual shear strengths are used for the analysis, then whatever factor of safety would normally be deemed appropriate for a given project could be reduced by the following reduction factor (*RF*):

$$RF = \tau_r / [\tau_r + 0.1(\tau_p - \tau_r)]$$

Where τ_r = residual shear strength, and τ_p = peak shear strength. They imply that the normally appropriate factor of safety would be determined based on considerations of uncertainty and consequences as described by Duncan (2000). Also, it should be noted that their discussion and recommendations were restricted to smooth-geomembrane/clay interfaces.

2. Safe Approach – Use Residual Shear Strength of the Interface with the Lowest Peak Strength. This approach could be the same as the above approach if the interface having the lowest shear strength happens to be above the primary geomembrane. If, due to overall slope stability constraints, the interface with the lowest peak strength is below the primary geomembrane (e.g. weak subgrade interface), this approach will still result in a very safe design relative to slope stability. It could, however, be less conservative in terms of environmental containment should deformation occur, causing a tear in the primary geomembrane. This approach is recommended by Gilbert and Byrne (1996) who "strongly recommended that the potential for instability be explored in a limit equilibrium analysis using residual strengths along all interfaces….It is strongly recommended that a factor of safety greater than one be achieved in all containment system slope designs, assuming residual strengths are mobilized along the entire slip surface."

   The same degree of factor of safety for this approach would apply as for Approach # 1 above. Holley et al. (1997) reported using residual shear strengths for a critical surface below the primary geomembrane in a steep canyon landfill, and obtaining operating factors of safety of 1.2 and an ultimate factor of safety of 1.4 for the final build-out. It is not clear if these were their minimum design criteria, or simply the results that they accepted.

3. Brute Strength Approach – This approach would employ very aggressive texturing to achieve high interface strengths, although the assumed strengths may be prorated by some factor to account for variability. The need to occasionally use this approach is suggested by Hullings and Sansome (1997): "Overall slope stability conditions often do not allow low interface strengths, so the interface strengths above the geomembrane cannot be much lower than the interface strength on the underside of the geomembrane."

   If the approach of high interface strength is used everywhere, and seismic analysis shows no deformation, an acceptable design basis may be to use peak shear strength with an adequately high factor of safety. How high is adequate is difficult to say, because the theoretical possibility of progressive failure still exists. The finite-element study performed by Filz et al. (2001) indicates that FS > 2 should be required for analyses based on peak strength of smooth-geomembrane/clay interfaces.

We have only the record of successful designs that were constructed based on peak strength to testify that the brute strength approach may be valid, but this does not demonstrate that it is conservative. The analysis should account for potential leachate build-up under worst case assumptions, for example after a post-closure maintenance period with substantial leachate still being generated, and the operations or leachate-collection layer completely clogged. Check that a submerged condition at the toe does not result in a reduction in shear strength (due to reduction in effective normal stresses) to the point that it fails the peak strength at the toe, which could lead to progressive failure through the rest of the fill (such as that discussed by Schmucker and Hendron, 1998).

4. Hybrid Approaches

   a) *Use Residual on the Side Slope and Peak on the Base.* To the author's knowledge, this approach was first documented in the literature by Stark and Poeppel (1994) in their review of the notorious Kettleman Hills failure. As they so aptly stated: "...it appears that peak and residual interface strengths should be assigned to the base and sideslopes, respectively, for design purposes." This was later echoed by Jones and Dixon (1998) from the U.K., who stated: "In some instances residual values may be appropriate on the side slope where large displacements are anticipated, used together with peak values on the base." In the author's opinion, this approach is a strong qualifier for accepting a traditional factor of safety in the range of 1.5 for ultimate build-out conditions (assuming unexpected pore-pressure scenarios are included in the evaluation), and 1.3 for operations.

   b) *Use Post-Peak Strength Values that Anticipate a Limited Amount of Deformation.* Shear strength reductions may occur due to relative deformations during construction, landfill operations, and waste settlement, but these deformations may be less than those which would lead to the minimum residual shear strength conditions. Also, based on their observation of numerous apparently successful facilities, design practitioners may consider peak shear strengths with an adequate factor of safety to be valid designs, while still wishing to incorporate an additional degree of conservatism by reducing the measured peak strength of the geosynthetic interfaces. These strength reductions would be applied to the side slope as well as the base. Use of this approach is suggested by Filz et al. (2001), who suggest using a mobilized strength that is higher than the residual by about 10% of the increment from residual to peak strength, and applying an appropriate factor of safety to this based on reliability concepts as described by Duncan (2000).

c) *Use Lower Waste Shear Strengths.* From the observation of trends published in the literature, shear strengths of 30° or more are commonly used for municipal solid waste. This level of shear strength has been documented as being generally conservative (e.g. Kavazanjian, 2001), but may require some amount of strain to become fully mobilized. As an approach to stability analyses designers may wish to reduce the mobilized strength of the waste material to more closely match the strain compatibility of the liner system.

The author has used all the above approaches in his own practice, which over the years has been based on improved levels of understanding. Currently (subject to change!) the author employs a combination of Approach #1 and #4 as his standard practice. That is, he usually defines a "design condition" which he believes will be the actual long-term conditions that interface shear strengths will experience. The decision as to what long-term shear strengths he selects is project-specific (there are many variations), and a complete discussion of this is beyond the scope of this paper. Suffice it to say that the decision is usually related to the criteria described for Approach #4. Next, the author follows the advice of Gilbert and Byrne (1996) and checks that the stability under the worst-case shear strength conditions (e.g. hydrated residual shear strength) results in FS > 1.0. This latter test is often the more significant.

A good example of the above approach is for bottom liner designs that involve the encapsulation of unreinforced bentonite between two geomembranes. The design scenario argues that most of the bentonite will remain dry for at least several centuries, and the basic slope stability analysis is performed on this basis. A second analysis is performed, however, to verify that the stability factor of safety is greater than unity even when all of the bentonite is under fully hydrated residual shear strength conditions. This example is more fully described in Thiel et al. (2001).

PART 4 – CONCLUSIONS AND RECOMMENDATIONS

CONCLUSIONS

- Many geosynthetic interfaces are highly strain-softening (i.e. "brittle"). The most common example is a textured geomembrane against some form of geotextile (whether it be a cushion, part of a geonet composite, or a GCL).

- There are mechanisms that can lead to exceedence of peak strength even though a correctly-performed slope stability analysis predicts a factor of safety greater than one. Examples of these mechanisms include:

  - Non-uniform mobilized stress distribution.

  - Relative differences in stiffness between waste and liner materials.
  - Unexpected pore pressures.
  - Seismic loading.
  - Deformation during construction.
  - Waste settlement.
  - Foundation settlement.
  - Aging and creep of the geosynthetics.

- Exceedence of peak strength in a brittle interface can result in progressive failure.

- Based on field observation, most facilities designed with aggressive interface shear strengths are not experiencing post-peak shear strength, which means that the working shear stress is probably less than or equal to the peak strength. Only a few examples of progressive failure along geosynthetic interfaces have occurred in the industry, and these have not been along highly brittle interfaces, which means that the projects did not have high factors of safety to begin with, even assuming peak interface strengths.

- Several design approaches have been used over the years and the standard-of-practice is evolving. In the United States a preferred approach has not yet clearly emerged.

RECOMMENDATIONS FOR PRACTICE

- Designers and CQA firms should conduct material-specific testing of interfaces to verify that the materials specified and/or supplied for a project are realistic and meet the design requirements. Whoever commissions the testing should possess a skilled familiarity with the design objectives as well as the testing technique.

- Designers should attempt to position the critical slip plane above the primary geomembrane to the extent feasible for a given project. If a double-sided textured geomembrane is required for construction or operational stability, attempt to specify more aggressive texturing on the under side of the geomembrane.

- Using peak shear strengths on the landfill base, and residual shear strengths on the side slopes appears to be a successful state-of-the-practice in many situations.

- Designers should consider evaluating all facilities for stability using the residual shear strength along the geosynthetic interface that has the lowest peak strength. This would be an advisable risk-management practice for designers, even if the FS under these conditions is simply greater than unity.

- Regardless of the design assumptions, specify soil spreading by pushing up-slope only, and require close monitoring of LCRS and operations soil placement on slopes during construction to verify that relative shear displacement does not occur during construction. Exceptions to this practice should be allowed only with field tests and CQA verification.

- If LCRS or operations soils are placed as part of landfill operations, designers should assume the worst and automatically assume residual side-slope shear strength conditions will occur (and extra leakage rates as well). The reason for this is that construction by landfill operators is usually not controlled and monitored closely.

- Check stability for a potential leachate buildup, especially near the toe of the landfill.

RECOMMENDATIONS FOR FURTHER RESEARCH

- More finite element analyses at an academic level, such as those performed by Reddy et al. (1996) and Filz et al. (2001) would be warranted, to gain a better understanding of the threshold beyond which localized stress distributions might cause exceedence of peak shear resistance. Refinements in the analyses would include modeling the strain-softening behavior of the geosynthetic interfaces, and checking different types of interfaces and geometries. The results of these analyses might prove useful for establishing guidelines as to when peak strengths might be exceeded and when they might be maintained. Ultimately, the author envisions correlations between the FS determined by limit equilibrium analyses, ratios of peak interface strengths to waste fill strengths, and relative stiffnesses (somewhat as proposed by Gilbert and Byrne (1996), but more specific and less general), being used to estimate when and where peak vs. post-peak strengths would be reached at the interfaces.

- The monitoring of slope deformation on geosynthetic interfaces that are being buried by waste is recommended. One fairly easy way to do this would be to use the simple tell-tale technique employed for the Cincinnati cover demonstration project (Koerner et al., 1996), though this would require participation by landfill owners and operators. This avenue of research echoes that suggested by Gilbert and Byrne (1996), who state: "Future research should focus on measuring deformations and mobilized shear resistances in existing waste containment facilities."

- The monitoring of pore pressures in the LCRS above liner systems, with the reporting of the worst-case conditions, would provide valuable information regarding long term conditions in landfills. Unfortunately, any high pressures would likely result in a permit violation at many facilities, so it is improbable that an existing owner will voluntarily monitor high pressures, much less report them. We are therefore left with only orphan or Superfund sites as a possible basis for monitoring. Because of this limitation, participation in international waste conferences is increasingly valuable.

- Additional laboratory testing, conducted on various types of interfaces, would be useful to assess the impact of interface deformations at low normal loads on the peak strength reductions at higher normal loads.

REFERENCES

Abramson, L.W., Lee, T.S., Sharma, S., and Boyce, G.M. (1996). Slope Stability and Stabilization Methods. John Wiley & Sons, Inc. New York.

Breitenbach, A.J. (1997) "Overview Study of Several Geomembrane Liner Failures Under High Fill Load Conditions." Proc. of Geosynthetics '97, IFAI, Vol. 2, pp. 1045-1061.

Breitenbach, A.J. and Swan, R.H. (1999) "Influence of High Load Deformations on Geomembrane Liner Interface Strengths." Proc. of Geosynthetics '99, IFAI, Vol. 1, pp. 517-529.

Brink, D., Day, P.W. and DuPreez, L. (1999) "Failure and Remediation of Bulbul Drive Landfill: Kwazulu-Natal, South Africa." Proc. Sardinia '99 Seventh International Waste Management and Landfill Symposium, CISA, Vol. III, pp. 555-562.

Duncan, J.M. (1996) "State of the Art: Limit Equilibrium and Finite-Element Analyses of Slopes." J. of Geotechnical Engineering, ASCE, Vol. 122, No. 7, May, pp. 577-596.

Duncan, J.M. (2000) "Factors of Safety and Reliability in Geotechnical Engineering" J. of Geotechnical and Geoenvironmental Engineering, ASCE, Vol. 126, No. 4, Apr., pp. 307-316.

Eid, H.T., Stark, T.D., Evans, W.D. and Sherry, P.E. (2000) "Municipal Solid Waste Slope Failure. I: Waste and Foundation Soil Properties." J. of Geotechnical and Geoenvironmental Engineering, ASCE, Vol. 126, No. 5, May, pp. 397-407.

Esterhuizen, J.B., Filz, G.M., and Duncan, J.M. (2001) "Constitutive Behavior of Geosynthetic Interfaces" J. of Geotechnical and Geoenvironmental Engineering, ASCE, Vol. 127, No. 10, Oct., pp. 834-840.

Filz, G.M., Esterhuizen, J.B., and Duncan, J.M. (2001) "Progressive Failure of Lined Waste Impoundments" J. of Geotechnical and Geoenvironmental Engineering, ASCE, Vol. 127, No. 10, Oct., pp. 841-848.

Gilbert, R.B. and Byrne, R.J. (1996) "Strain-Softening Behavior of Waste Containment System Interfaces." Geosynthetics International, IFAI, Vol. 3, No. 2, pp. 181-203.

Gilbert, R.B. (2001) Personal communication with the author.

Hendron, D.M., Fernandez, G., Prommer, P.J., Giroud, J.P., and Orozco, L.F. (1999) "Investigation of the Cause of the 27 September 1997 Slope Failure at the Dona Juana Landfill" Proc. Sardinia '99 Seventh International Waste Management and Landfill Symposium, CISA, Vol. III, pp. 545-554.

Hillman, R.P. and Stark, T.D. (2001) "Shear Strength Characteristics of PVC Geomembrance-Geosynthetic Interfaces." Geosynthetics International, IFAI, Vol. 8, No. 2, pp. 135-162.

Holley, K., Richardson, J., and Sadlier, M. (1997) "Design and Construction to Optimise Landfill Stability at the Nent Landfill, Hong Kong." Proc. Sardinia '99 Seventh International Waste Management and Landfill Symposium, CISA, Vol. III, pp. 565-574.

Hullings, D.E. and Sanome, L.J. (1997) "Geomembrane Anchor Trenches." J. of Geotextiles and Geomembranes, Elsevier, Vol. 15, Nos. 4-6, pp. 403-417.

Jones, D.R.V. and Dixon, N. (1998) "Shear Strength Properties of Geomembrane/Geotextile Interfaces." J. of Geotextiles and Geomembranes, Elsevier, Vol. 16, Nos. 1, pp. 45-71.

Kavazanjian, E. (2001) "Mechanical Properties of Solid Waste." Proc. Sardinia '01 Eighth International Waste Management and Landfill Symposium, CISA, Vol. III, pp. .

Koerner, R.M., Carson, D.A., Daniel, D.E., and Bonaparte, R. (1996) "Current Status of the Cincinnati GCL Test Plots" Proceedings of the 10th GRI Conference, Field Performance of Geosynthetics and Geosynthetic Related Systems. Geosynthetic Research Institute, Drexel University, Philadelphia, PA, pp. 147-175.

Koerner, R.M. and Daniel, D.E. (1997) Final Covers for Solid Waste Landfill and Abandoned Dumps. ASCE Press, Reston, VA.

Koerner, R.M. and Soong, T.Y. (2000) "Leachate in Landfills: The Stability Question." Geotextiles and Geomembranes, Elsevier, Vol. 18, pp. 293-309.

LaRochelle, P. (1989) "Problems of Stability: Progress and Hopes." The Art and Science of Geotechnical Engineering. Ed. by Corning et al., Prentice Hall, N.J., pp. 269-290.

Li, K.S. and Lam, J. (2001) Discussion of "Evolution of Progressive Failure of Landslides." J. of Geotechnical and Geoenvironmental Engineering, ASCE, Vol. 127, No. 1, Jan., pg. 98.

Liu, C.N., Gilbert, R.B., Thiel, R.S., and Wright, S.G. (1997). "What is an Appropriate Factor of Safety for Landfill Cover Slopes?" Conference Proceedings from Geosynthetics '97. IFAI, Roseville, MN, pp. 481-496.

Mazzucato, A., Somonini, P. and Colombo, S. (1999) "Analysis of Block Slide in a MSW Landfill." Proc. Sardinia '99 Seventh International Waste Management and Landfill Symposium, CISA, Vol. III, pp. 537-544.

NAVFAC (1982) Soil Mechanics. Design Manual 7.1, Department of the Navy, Naval Facilities Engineering Command, Alexandria, VA.

Reddy, K.R., Kosgi, S. and Motan, S. (1996) "Interface Shear Behavior of Landfill Composite Liner Systems: A Finite Element Analysis." Geosynthetics International, IFAI, Vol. 3, No. 2, pp. 247-275.

Schmucker, B.O. and Hendron, D.M. (1998) "Forensic Analysis of the 9 March 1996 Landslide at the Rumpke Sanitary Landfill, Hamilton County, Ohio." Proc. of the 12th GRI Conference, Lessons Learned from Geosynthetic Case Histories, Geosynthetic Institute, Folsom, PA, pp. 269-295.

Soong, T.Y., Hungr, O., and Koerner, R.M. (1998) "Stability Analyses of Selected Landfill Failures by 2-D and 3-D Methods" Proc. of the 12th GRI Conference, Lessons Learned from Geosynthetic Case Histories, Geosynthetic Institute, Folsom, PA, pp. 296-329.

Stark, T.D. and Eid, H.T. (1998) "Performance of Three-Dimensional Slope Stability Methods in Practice" J. of Geotechnical and Geoenvironmental Engineering, ASCE, Vol. 124, No.11, Nov., pp. 1049-1060.

Stark, T.D., Arellano, D., Evans, W.D., Wilson, V.L., and Gonda, J.M. (1998) "Unreinforced Geosynthetic Clay Liner Case History." Geosynthetics International, IFAI, Vol. 5, No. 5, pp. 521-544.

Stark, T.D., Eid, H.T., Evans, W.D. and Sherry, P.E. (2000) "Municipal Solid Waste Slope Failure. II: Stability Analyses." J. of Geotechnical and Geoenvironmental Engineering, ASCE, Vol. 126, No. 5, May, pp. 408-419.

Stark, T.D., and Poeppel, A.R. (1994) "Landfill Liner Interface Strengths from Torsional Ring Shear Tests." J. of Geotechnical Engineering, ASCE, Vol. 120, No. 3, March, pp. 597-615.

Terzaghi, K. and Peck, R. (1948) Soil Mechanics in Engineering Practice. John Wiley & Sons, New York, NY.

Thiel, R., Daniel, D.E., Erickson, R., Kavazanjian, E., and Giroud, J.P. (2001) *GundSeal GCL Design Manual.* Published by GSE, Houston, TX.

Tiande, M., Chongwu, M, and Shengzhi, W. (1999) "Evolution Model of Progressive Failure of Landslides." J. of Geotechnical and Geoenvironmental Engineering, ASCE, Vol. 125, No. 10, Oct,, pp. 827-831.

APPLICATION FOR PERMIT
SUNDANCE WEST

VOLUME III: LANDFILL ENGINEERING CALCULATIONS
SECTION 7: TENSILE STRESS ANALYSIS

ATTACHMENT III.7.H

BOWLES, JOSEPH E. 1977. *FOUNDATION ENGINEERING ANALYSIS AND DESIGN, 2ND EDITION*. UNITED STATES: MCGRAW HILL BOOK COMPANY

FOUNDATION ANALYSIS AND DESIGN

Joseph E. Bowles

Table 3-2. Standard designation and sizes for drill rods and casing

Drill rod	OD, in	Casing and core barrel	Core-barrel-bit OD, in	Approx. diam of borehole,* in	Diam of core sample, in
E	$1\frac{5}{16}$	EX	$1\frac{7}{16}$	$1\frac{1}{2}$	$\frac{7}{8}$
A	$1\frac{5}{8}$	AX	$1\frac{7}{8}$	2	$1\frac{1}{8}$
B	$1\frac{7}{8}$	BX†	$2\frac{3}{8}$	$2\frac{1}{2}$	$1\frac{5}{8}$
N	$2\frac{3}{8}$	NX	$1\frac{15}{16}$	3	$2\frac{1}{8}$

* Diameter of borehole is very nearly the ID of the casing.

† In soft or fractured rock, BX or larger cores are preferred.

The SPT was originally developed for cohesionless soils so that samples would not have to be taken. The test has evolved to the current practice of routinely determining N for all soils. In the zones of particular interest from about 2.5 ft or 1 m below ground surface to considerable depth below the estimated base of the foundation the test is performed every 2.5 ft or 1 m depth increment. At considerable depths where the boring becomes more informational the depth increment for testing is often increased to 5 ft or 2 m.

Empirical correlations between N and various soil properties have been attempted for cohesionless soils (Table 3-3). Table 3-3 should be used cautiously; for example, a "loose" soil with a range of D_r between 15 and 35 percent places rather arbitrary numbers on a rather tenuous description of a soil.

Table 3-3. Empirical values for ϕ, D_r, and unit weight of granular soils based on the standard penetration number with corrections for depth and for fine saturated sands

Description		Very loose		Loose		Medium		Dense		Very dense	
Relative density D_r*	0		0.15		0.35		0.65		0.85		1.00
Standard penetration no. N			4		10		30		50		
Approx. angle of internal friction ϕ°†	25°–30°		27–32°		30–35°		35–40°		38–43°		
Approx. range of moist unit weight, (γ) pcf (kN/m^3)		70–100‡ (11–16)		90–115 (14–18)		110–130 (17–20)		110–140 (17–22)		130–150 (20–23)	

* USBR [Gibbs and Holtz (1957)].

† After Meyerhof (1956). $\phi = 25 + 25D_r$ with more than 5 percent fines and $\phi = 30 + 25D_r$ with less than 5 percent fines. Use larger values for granular material with 5 percent or less fine sand and silt.

‡ It should be noted that excavated material or material dumped from a truck will weigh 70 to 90 pcf. Material must be quite dense and hard to weigh much over 130 pcf. Values of 105 to 115 pcf for nonsaturated soils are common.

APPLICATION FOR PERMIT
SUNDANCE WEST

VOLUME III: LANDFILL ENGINEERING CALCULATIONS
SECTION 7: TENSILE STRESS ANALYSIS

ATTACHMENT III.7.I

RICHARDSON, CLINTON P., PHD., PE 2009.

MUNICIPAL LANDFILL DESIGN CALCULATIONS: AN ENTRY LEVEL MANUAL OF PRACTICE. **CALIFORNIA: UBUILDABOOK, LLC.**

Municipal Landfill Design Calculations

An Entry Level Manual of Practice

Clinton P. Richardson, PhD. PE.

Chapter 28 Side-slope Liner Stability

Problem Statement

Liner stability or side-slope slippage is complicated for multi-layered liner and collection system. A unit load of waste gravitationally induces shear stress and a portion of stress is transmitted by means of friction to the geosynthetics components beneath. The difference between frictional components must be carried by the particular component in the form of tensile stress and then compared to the component's yield stress for the resulting factor of safety. The portion transmitted to upper component is then propagated to the next component in the multilayered sequence. An unbalanced portion is eventually transmitted to the subgrade soil beneath the lower geosynthetic. If mass failure is going to occur, it will seek the interface with the lowest friction angle. The liner stability method is simply a resolution of shear stresses Koerner, 1994).

Design Objective

Calculate the tensile stresses and shear stresses carried by the upper and lower geosynthetic components and estimate the factor of safety.

Design Equations

Figure 1 shows a schematic of a multi-layered liner and resolution of forces assuming a single waste lift thickness.

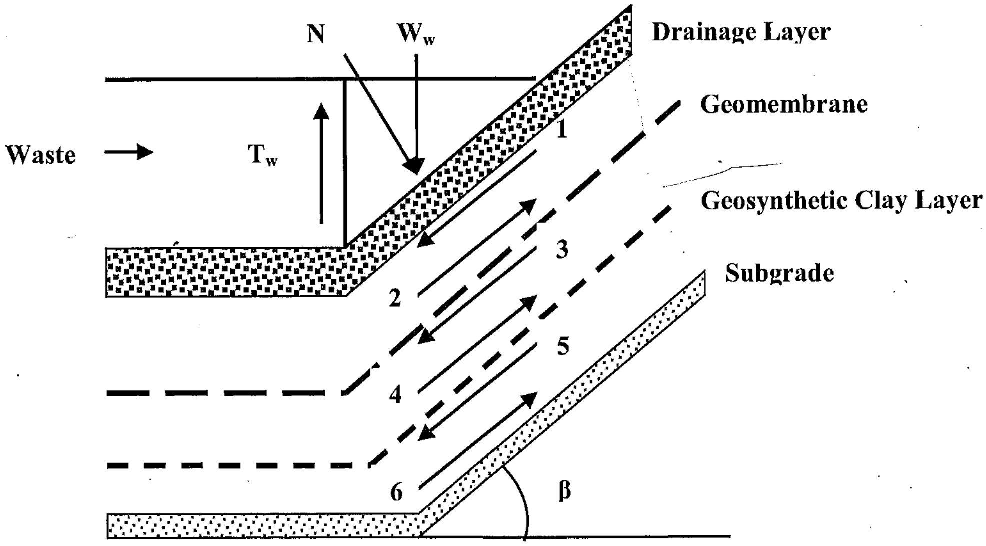

Figure 1: Resolution of Shear Forces in A Multi-layered Landfill Barrier Liner (adapted from Koerner, 1990).

The simple barrier system consists of a geomembrane underlain by a geosynthetic clay liner (GCL). The procedure may be extended to any number of interfaces, such a geotextile, geomembrane, clay liner, etc. Time is assumed to be sufficiently long between waste lifts that system readjustment will occur and either equilibrium or failure will exist. A unit width is assumed. The numbers 1 through 6 shown in the figure represent the forces that must be resolved sequentially.

The weight of a unit width of compacted waste is given by

$$W_w = \frac{1}{2}\gamma_w H \frac{H}{\tan\beta} \quad \text{Eq. 1}$$

where

W_W = weight of waste per unit width (lb_f/ft or kN/m)

H = lift height (ft or m)

β = slope angle (^{o})

γ_W = unit weight of waste (lb_f/ft^3 or kN/m^3)

The frictional resistance along the waste edge is given by

$$T_w = \sigma_h \tan\phi_w H = K_o \sigma_v \tan\phi_w H \quad \text{Eq. 2}$$

$$K_o = (1 - \sin\phi_w) \quad \text{Eq. 3}$$

$$\sigma_v = \frac{1}{2}\gamma_w H \quad \text{Eq. 4}$$

where

T_W = frictional resistance force per unit width (lb_f/ft or kN/m)

σ_h = horizontal stress of waste lift (lb_f/ft^2 or kN/m^2)

ϕ_W = waste fiction angle (^{o})

K_o = coefficient of earth pressure at rest (unitless)

σ_h = vertical stress of waste lift (lb_f/ft^2 or kN/m^2)

The net weight of the waste is the difference between the downward acting waste weight and the upward acting resistance force, or

$$W_{net} = W_w - T_w \quad \text{Eq. 5}$$

The net weight can now be resolved into its two components: a normal force component acting perpendicular to the slope and a parallel force component acting downslope, or

$$N = W_{net} \cos\beta \quad \text{Eq. 6}$$

$$P = W_{net} \sin \beta \qquad \text{Eq. 7}$$

where

N = normal force component of net weight (lb_f/ft or kN/m)

P = parallel force component of net weight (lb_f/ft or kN/m)

This latter force component is assumed to be dissipated through the drainage layer (Koerner, 1990). The forces that must be determined are a function of the normal force and the frictional resistance provided by the respective interface; for example, in the first force couple, the following relationships hold:

$$F_1 = N \tan \delta_1 = (W_{net} \cos \beta) \tan \delta_1 \qquad \text{Eq. 8}$$

$$F_2 = N \tan \delta_2 = (W_{net} \cos \beta) \tan \delta_2 \qquad \text{Eq. 9}$$

where

δ_1 = drainage layer friction angle with respect to the upper geomembrane surface (^{o})

δ_2 = lower geomembrane surface friction angle with respect to the upper GCL surface (^{o})

If F_1 exceeds F_2, then the geomembrane is in tension. The force difference must be carried by the geomembrane. The actual stress in the geomembrane is given by

$$\sigma_{\text{actual}_{\text{geomembrane}}} = \left(\frac{F_1 - F_2}{t_{geo}} \right) \qquad \text{Eq. 10}$$

where

$\sigma_{\text{actual geomembrane}}$ = actual stress in geomembrane (lb_f/ft^2 or kN/m^2)

t_{geo} = geomembrane thickness (ft or m)

The factor of safety for the geomembrane against failure in tension is

$$\text{FS}_{\text{geomembrane}} = \frac{\sigma_{\text{yield}}}{\sigma_{\text{actual}_{\text{geomembrane}}}} \qquad \text{Eq. 11}$$

where

σ_{yield} = allowable geomembrane stress at yield (lb_f/ft^2 or kN/m^2)

The allowable geomembrane stress at yield is usually given in terms of lb_f/in^2 or kN/m^2 or kPa based on a wide-width tensile test (ASTM D 4885-01 Determining Performance Strength of Geomembranes by the Wide Width Strip Tensile Method).

The frictional shear force acting on the lower geomembrane surface, or F_2, is equal and opposite to the frictional shear force above the GCL surface, or F_3; thus,

$$F_2 = N \tan\delta_2 = F_3 \qquad \text{Eq. 12}$$

The frictional shear force acting on the lower GCL is given by

$$F_4 = N \tan\delta_4 \qquad \text{Eq. 13}$$

where

δ_4 = friction angle between the lower GCL surface and the subgrade soil

The difference between F_3 and F_4 determines the tensile force carried by the GCL. If negative, the GCL is not in tension. If positive, then the GCL is in tension and a factor of safety must be evaluated based on the wide width strength test (ASTM D 6768-04 Standard Test Method for Tensile Strength of Geosynthetic Clay Liners). The force difference must be carried by the geomembrane. The actual stress in the GCL is given by

$$\sigma_{\text{actual}_{\text{GCL}}} = \left(\frac{F_3 - F_4}{t_{GCL}} \right) \qquad \text{Eq. 14}$$

where

$\sigma_{\text{actual GCL}}$ = actual stress in GCL (lb_f/ft^2 or kN/m^2)

t_{geo} = GCL thickness (ft or m)

The factor of safety for the GCL against failure is

$$\text{FS}_{\text{GCL}} = \frac{\sigma_{\text{yield}}}{\sigma_{\text{actual}_{\text{GCL}}}} \qquad \text{Eq. 15}$$

where

σ_{yield} = allowable GCL stress at yield (lb_f/ft^2 or kN/m^2)

If $\delta_2 = \delta_4$, then $F_4 = F_2 = F_3$. If the lower frictional shear force exceeds the upper frictional shear force for a given interface, then the factor of safety is infinite and only a value of the upper frictional shear force will be mobilized at the upper surface of the next interface below. This procedure is repeated for multiple interfaces until the lower most interface is encountered, i.e. a compacted subgrade or compacted clay. For compacted clay, special attention must be paid to its short-term friction angle *versus* its long-term friction angle with respect to the interface above. Compacted clay can consolidate with overburden stress and expel moisture, which can reduce the friction between it and the contact surface above, potentially placing the upper geosynthetic in tension.

Design Example #1

Evaluate the maximum stresses, if any, in the landfill liner system described in Figure 1 consisting of a textured 60 mil HDPE/non-woven, needle-punched Bentomat® GCL/USCS SP compacted subgrade sequence. The following data may be assumed:

$H = 10$ ft (3.0 m)

$\beta = 18.43\ ^{\circ}$ (3H:1V)

$\gamma_W = 60\ \text{lb}_f/\text{ft}^3$ or ($9.4\ \text{kN/m}^3$)

$\phi_W = 20\ ^{\circ}$

$\delta_1 = 18\ ^{\circ}$

$\delta_2 = 16\ ^{\circ}$

$\delta_4 = 30\ ^{\circ}$

$\sigma_{\text{allow geomembrane}} = 2100\ \text{lb}_f/\text{in}^2$ ($14{,}478\ \text{kN/m}^2$)

$T_{GCL} = 100\ \text{lb}_f/\text{in}$ (17.5 kN/m)

$t_{GCL} = 0.25$ in (6.4 mm)

Solution:

The critical interface lies between the HDPE geomembrane and the GCL based on the magnitude of the respective friction angles. The following parameters are calculated:

$W_w = 9.0 \times 10^3\ \text{lb}_f/\text{ft}$ (131 kN/m) Eq. 1

$K_o = 0.658$ Eq. 3

$\sigma_v = 300\ \text{lb}_f/\text{ft}^2$ ($14.4\ \text{kN/m}^2$) Eq. 4

$\sigma_h = 197\ \text{lb}_f/\text{ft}^2$ ($9.4\ \text{kN/m}^2$) Eq. 2

$T_w = 718\ \text{lb}_f/\text{ft}$ (10.5 kN/m) Eq. 2

$W_{net} = 8282\ \text{lb}_f/\text{ft}$ (120.9 kN/m) Eq. 5

$N = 7857\ \text{lb}_f/\text{ft}$ ($114.7\ \text{kN/m}^2$) Eq. 6

$F_1 = 2553\ \text{lb}_f/\text{ft}$ (37.3 kN/m) Eq. 8

APPLICATION FOR PERMIT
SUNDANCE WEST

VOLUME III: LANDFILL ENGINEERING CALCULATIONS
SECTION 7: TENSILE STRESS ANALYSIS

ATTACHMENT III.7.J

GSE LINING TECHNOLOGY, INC.,

GSE HD TEXTURED PRODUCT DATA SHEET

MINIMUM PROPERTIES FOR GSE HD TEXTURED

TESTED PROPERTY	TEST METHOD	FREQUENCY	MINIMUM VALUE				
Product Code			HDT 030G000	HDT 040G000	HDT 060G000	HDT 080G000	HDT 100G000
Thickness, (minimum average) mil (mm)	ASTM D 5994	every roll	29 (0.73)	38 (0.96)	57 (1.45)	76 (1.93)	95 (2.41)
Lowest individual for 8 out of 10 values			27 (0.69)	36 (0.91)	54 (1.40)	72 (1.80)	90 (2.30)
Lowest individual for any of the 10 values			26 (0.66)	34 (0.86)	51 (1.30)	68 (1.73)	85 (2.16)
Density, g/cm^3	ASTM D 1505	200,000 lb	0.94	0.94	0.94	0.94	0.94
Tensile Properties (each direction)(1)	ASTM D 6693, Type IV	20,000 lb					
Strength at Break, lb/in-width (N/mm)	Dumbell, 2 ipm		45 (8)	60 (11)	90 (16)	120(21)	150 (27)
Strength at Yield, lb/in-width (N/mm)			63 (11)	84 (15)	126 (22)	168 (29)	210 (37)
Elongation at Break, %	G.L. = 2.0 in (51 mm)		100	100	100	100	100
Elongation at Yield, %	G.L. = 1.3 in (33 mm)		12	12	12	12	12
Tear Resistance, lb (N)	ASTM D 1004	45,000 lb	21 (93)	28 (125)	42 (187)	56 (249)	70 (311)
Puncture Resistance, lb (N)	ASTM D 4833	45,000 lb	45 (200)	60 (267)	90 (400)	120 (534)	150 (667)
Carbon Black Content, %	ASTM D 1603*/4218	20,000 lb	2.0	2.0	2.0	2.0	2.0
Carbon Black Dispersion	ASTM D 5596	45,000 lb	+Note 1	+Note 1	+Note 1	+Note 1	+Note 1
Asperity Height	GRI GM 12	second roll	+Note 2	+Note 2	+Note 2	+Note 2	+Note 2
Notched Constant Tensile Load(2), hr	ASTM D 5397, Appendix	200,000 lb	300	300	300	300	300
REFERENCE PROPERTY	**TEST METHOD**	**FREQUENCY**	**NOMINAL VALUE**				
Oxidative Induction Time, min	ASTM D 3895, 200° C; O_2, 1 atm	200,000 lb	>100	>100	>100	>100	>100
Roll Length(3) (approximate), ft (m)	Standard Textured		830 (253)	700 (213)	520 (158)	400 (122)	330 (101)
Roll Width(3), ft (m)			22.5 (6.9)	22.5 (6.9)	22.5 (6.9)	22.5 (6.9)	22.5 (6.9)
Roll Area, ft^2 (m^2)			18,674 (1,735)	15,750 (1,463)	11,700 (1,087)	9,000 (836)	7,425 (690)

NOTES:

- +Note 1: Dispersion only applies to near spherical agglomerates. 9 of 10 views shall be Category 1 or 2. No more than 1 view from Category 3.
- +Note 2: 10 mil average. 8 of 10 readings ≥7 mils. Lowest individual ≥ 5 mils.
- GSE HD Standard Textured is available in rolls weighing about 4,000 lb (1,800 kg).
- (1)The combination of stress concentrations due to coextrusion texture geometry and the small specimen size results in large variation of test results. Therefore, these tensile properties are minimum average values.
- (2)NCTL for HD Textured is conducted on representative smooth membrane samples.
- All GSE geomembranes have dimensional stability of ±2% when tested with ASTM D 1204 and LTB of <-77° C when tested with ASTM D 746.
- (3)Roll lengths and widths have a tolerance of ± 1%.
- *Modified.

APPLICATION FOR PERMIT
SUNDANCE WEST

VOLUME III: LANDFILL ENGINEERING CALCULATIONS
SECTION 7: TENSILE STRESS ANALYSIS

ATTACHMENT III.7.K

GSE LINING TECHNOLOGY, INC.

WIDE WIDTH TENSILE STRENGTH TEST OF F42060060S GEOCOMPOSITE

From: Walter Steinbeck [wsteinbeck@gseworld.com]
Sent: Tuesday, January 05, 2010 4:03 PM
To: Mike Heinstein
Subject: RE: Question concerning wide width tensile strength of GSE FabriNet Geocomposite
Attachments: T5019-F4206-WW.XLS

Mike,

Unfortunately, we do not have the 10oz FabriNet geocomposite wide-width tensile information. However, we do have information for 6oz FabriNet geocomposite - which has the break strength of 270 lbs/inch and the break elongation of 80%. Again, while we do not have the 10oz FabriNet values available – this product should perform a little better than 6 oz. FabriNet. I hope these values help you.

The material price for the product is approximately $0.40/sf + scrap/lap of 8% + mark up of 15% = $0.50/sf + installation ($0.25/sf) ~ $0.75/sf - $0.80/sf should cover you.

I appreciate you contacting us and let me know if I can help you out any further.

Thanks,

Walt Steinbeck
GSE Lining Technology, Inc.
Phone: (951) 273-3474
Cell: (310) 617-2966

From: Mike Heinstein [mailto:MHeinstein@gordonenvironmental.com]
Sent: Tuesday, January 05, 2010 10:51 AM
To: Walter Steinbeck
Subject: Question concerning wide width tensile strength of GSE FabriNet Geocomposite

Walt

Can you please provide some information concerning the wide width tensile strength of GSE FabriNet Geocomposite with a 10 oz/sy non-woven geotextile bonded to it.

Thanks, Mike

Michael R. Heinstein, P.E.
Senior Project Engineer
Gordon Environmental, Inc.
213 S. Camino del Pueblo
Bernalillo, NM 87004
(505) 867-6990 (Office)
(505) 867-6991 (Fax)
mheinstein@gordonenvironmental.com

Wide Width Tensile Test of F42060060S Geocomposite
8" x8" Specimen, 4" gage Length, 0.4 in/min Test Speed, Tested in Machine Direction

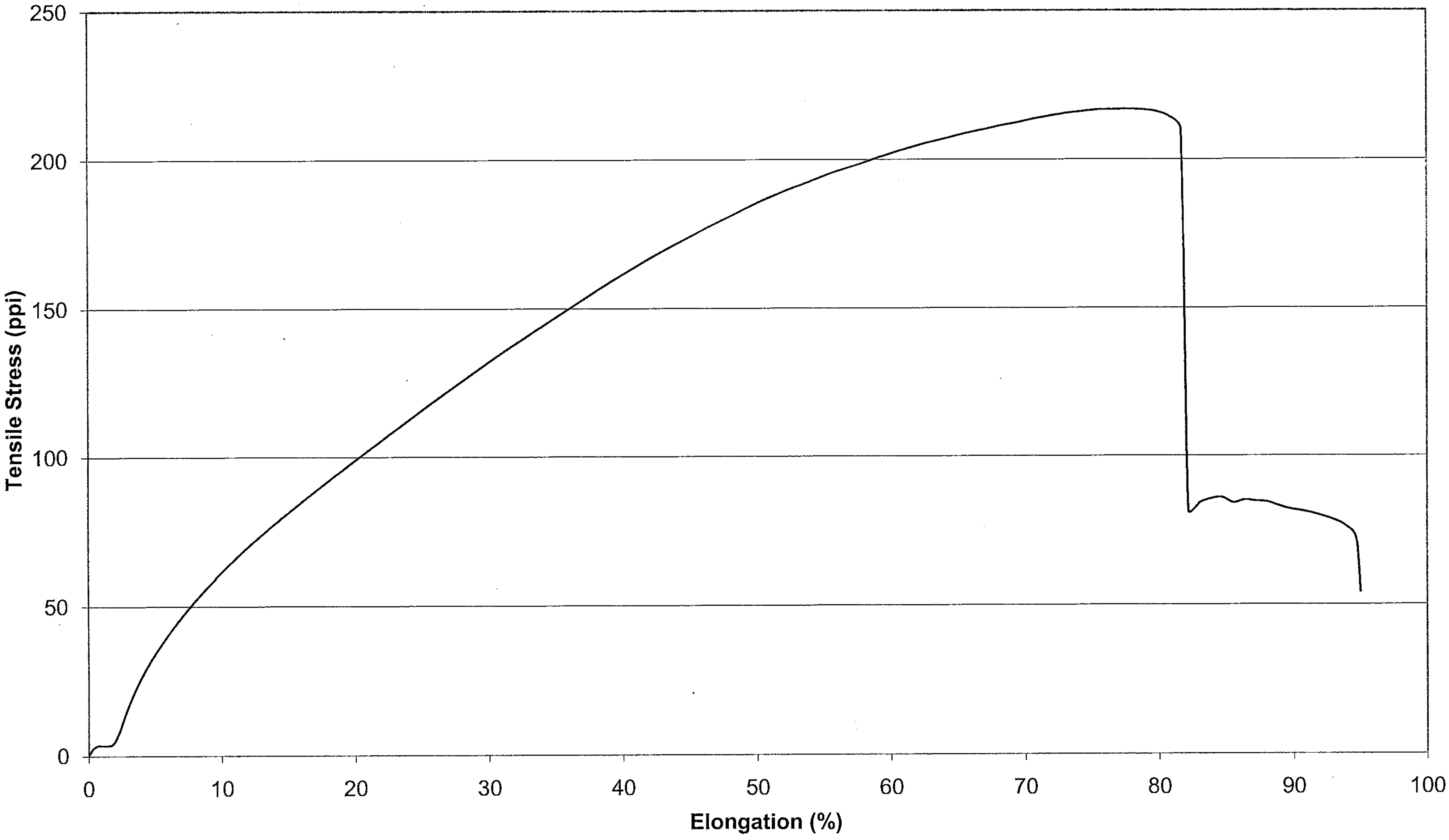

APPLICATION FOR PERMIT
SUNDANCE WEST

VOLUME III: LANDFILL ENGINEERING CALCULATIONS
SECTION 7: TENSILE STRESS ANALYSIS

ATTACHMENT III.7.L

CATERPILLAR, INC.,

CATERPILLAR PERFORMANCE HANDBOOK, EDITION 42

Caterpillar Performance Handbook

42

CAT®

Wheel Tractor-Scrapers

Specifications
- Twin Engine Open Bowl
- Optional Push-Pull

MODEL	627H		637G		657G	
Flywheel Power: Tractor	304 kW	**407 hp**	345/373 kW	**462/500 hp**	421/447 kW	**564/600 hp**
Scraper	216 kW	**290 hp**	198/211 kW	**266/283 hp**	306/337 kW	**410/451 hp**
Approx. Operating Weight (Empty)◀	40 913 kg	**90,213 lb**	51 963 kg	**114,559 lb**	68 384 kg	**150,760 lb**
Scraper Capacity: Struck	13 m³	**17.1 yd³**	18.3 m³	**24 yd³**	24.5 m³	**32 yd³**
Heaped	18.4 m³	**24 yd³**	26 m³	**34 yd³**	33.6 m³	**44 yd³**
Rated Load	26 127 kg	**57,610 lb**	37 013 kg	**81,600 lb**	47 174 kg	**104,000 lb**
Weight Distribution — Empty: Front	**59%**		**59%**		**58%**	
Rear	**41%**		**41%**		**42%**	
Weight Distribution — Loaded: Front	**50%**		**50%**		**50%**	
Rear	**50%**		**50%**		**50%**	
Engine Model: Tractor	**C13 ACERT**		**C18 ACERT**		**C18 ACERT**	
Scraper	**C9.3 ACERT**		**C9 ACERT**		**C15 ACERT**	
Rated Engine RPM: Tractor	**1700**		**1800**		**1800**	
Scraper	**1900**		**2000**		**1800**	
Displacement: Tractor	12.5 L	**763 in³**	18.1 L	**1105 in³**	18.1 L	**1105 in³**
Scraper	9.29 L	**567 in³**	8.8 L	**538 in³**	15.2 L	**928 in³**
Top Speed (Loaded)	53.9 km/h	**33.5 mph**	53 km/h	**33 mph**	53 km/h	**33 mph**
180° Curb-to-Curb Turning Width	11.8 m	**38'7"**	12.2 m	**40'1"**	14.2 m	**46'7"**
Tires — Tractor Drive	**33.25R29**E3**		**37.25R35★★E3**		**40.5/75R39★★E3**	
Scraper	**33.25R29**E3**		**37.25R35★★E3**		**40.5/75R39★★E3**	
Width of Cut	3.14 m	**10'4"**	3.51 m	**11'6"**	3.85 m	**12'8"**
Maximum Depth of Cut	315 mm	**12.4"**	437 mm	**17"**	440 mm	**17.3"**
Maximum Depth of Spread	540 mm	**21.3"**	480 mm	**18.9"**	660 mm	**26"**
Fuel Tank Refill Capacity: Tractor	—		—		—	
Scraper	1272 L	**336 U.S. gal**	1268 L	**335 U.S. gal**	1597 L	**424 U.S. gal**
GENERAL DIMENSIONS: Non Push-Pull						
Height — Overall Shipping	4.03 m	**13'2"**	4.18 m	**13'9"**	4.62 m	**15'2"**
Wheelbase	7.99 m	**26'2"**	8.77 m	**28'9"**	9.96 m	**32'8"**
Overall Length	14.02 m	**45'10"**	14.71 m	**48'3"**	16.2 m	**53'1"**
Overall Width	3.57 m	**11'7"**	3.94 m **	**12'11"**	4.35 m	**14'4"**
Shipping Width (Draft Arm on Inside of Bowl)	—		3.63 m *	**11'11"**	3.91 m **	**12'10"**
Center Line of Scraper Tread	2.29 m	**7'5"**	2.46 m	**8'1"**	2.81 m	**9'3"**
Center Line of Tractor Tread	2.28 m	**7'4"**	2.46 m	**8'1"**	2.63 m	**8'8"**
GENERAL DIMENSIONS: Push-Pull						
Operating Weight (Empty)◀	42 168 kg	**92,980 lb**	54 057 kg	**119,175 lb**	72 804 kg	**160,505 lb**
Overall Length	15.58 m	**51'1"**	16.64 m	**54'7"**	18.01 m	**59'1"**
Weight Distribution — Empty: Front	**59%**		**60%**		**58%**	
Rear	**41%**		**40%**		**42%**	
Weight Distribution — Loaded: Front	**50%**		**51%**		**51%**	
Rear	**50%**		**49%**		**49%**	

*Optional Shipping Configuration.

**Standard Shipping Configuration.

◀Operating weight includes standard machine, coolant, lubricants, full fuel tank, and operator. Operating weights for the 627H are based on Tier 4 Interim/Stage IIIB platforms machines. Deduct 413 kg (910 lb) for the operating weight for the 627H Tier 3/Stage IIIA equivilent.

APPLICATION FOR PERMIT
SUNDANCE WEST

VOLUME III: LANDFILL ENGINEERING CALCULATIONS
SECTION 8: SETTLEMENT CALCULATIONS

TABLE OF CONTENTS

LIST OF FIGURES

LIST OF TABLES

LIST OF ATTACHMENTS

APPLICATION FOR PERMIT
SUNDANCE WEST

VOLUME III: LANDFILL ENGINEERING CALCULATIONS
SECTION 8: SETTLEMENT CALCULATIONS

1.0 INTRODUCTION

Sundance West (Sundance West Facility) is a proposed Surface Waste Management Facility for oil field waste processing and disposal services. The proposed Sundance West Facility is subject to regulation under the New Mexico Oil and Gas Rules, specifically 19.15.36 NMAC, administered by the Oil Conservation Division (OCD). The Facility has been designed in compliance with 19.15.36 NMAC, and will be constructed and operated in compliance with a Surface Waste Management Facility Permit issued by the OCD. The Facility is owned by, and will be constructed and operated by, Sundance West, Inc.

1.1 Description

The Sundance West site is comprised of a 320-acre ± tract of land located approximately 3 miles east of Eunice, 18 miles south of Hobbs, and approximately 1.5 miles west of the Texas/New Mexico state line in the South ½ of Section 30, Township 21 South, Range 38 East Lea County, New Mexico (NM). Site access will be provided via NM 18 and Wallach Lane. The Sundance West Facility will include two main components; a liquid oil field waste Processing Area (80 acres ±), and an oil field waste Landfill (180 acres ±). Oil field wastes are anticipated to be delivered to the Sundance West Facility from oil and gas exploration and production operations in southeastern NM and west Texas. The Site Development Plan provided in the **Permit Plans, Volume III.1**, identifies the locations of the Processing Area and Landfill facilities.

2.0 DESIGN CRITERIA

The slope of the final cover, liner and leachate collection piping after settlement must be consistent with the performance specifications for leachate collection and stormwater control.

3.0 FOUNDATION SOILS SETTLEMENT

The methodology for estimating potential settlement involves selecting points on the landfill floor surface, computing the settlement at each point, and evaluating the resultant change in surface elevation. The foundation soils at the Sundance West site are predominately silty sands and a mixture of silty sands and clayey sands (i.e., USCS Classifications, SM, SC-SM, SC). The Chinle Formation is present sloping from east to west at depths approximated at 32 feet (ft) to 42 ft below existing grade. The west third of the proposed landfill base grades will encounter the Chinle Formation and settlement will be negligible since the Standard Penetration Test blow counts for the Chinle Formation are in excess of 50, which indicates an incompressible soil. **Attachment III.8.A** provides a summary of the laboratory testing results compiled from samples at various depths from two geotechnical borings installed on-site. In the calculations for foundation settlement, data from Measurement of Collapse Potential of Soils (ASTM D5333) Lab sample #9-1213-07 from GB-2 in **Attachment III.8.A** was used to calculate percentage the of settlement at various applied loads on the compressible soils below the landfill base grades. As the applied load increases, the consolidation (% of initial height) also increases.

Settlement was estimated at the locations (Points A13 through A34, B6, B7, B10 through B17,and C1 through C23) shown on the landfill cross sections (**Figure III.8.1**). Points A1 through A12, B1 through B5, and B8 & B9 were excluded based on the incompressible Chinle Formation. An example calculation is demonstrated at point C8 in Unit 2 on Cross Section C-C', where waste depth is approximately 139.30 ft.

Foundation settlement will increase towards the east end of the landfill since the depth of compressible soil between the base grades and the Chinle Formation increases as shown in **Figure III.8.1**.

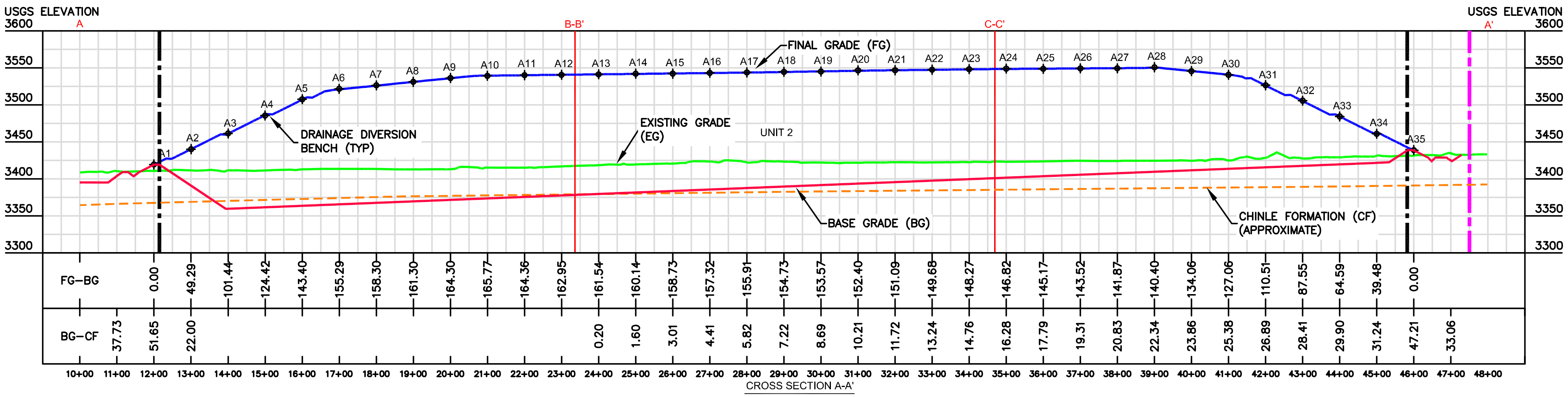

CROSS SECTION A-A'

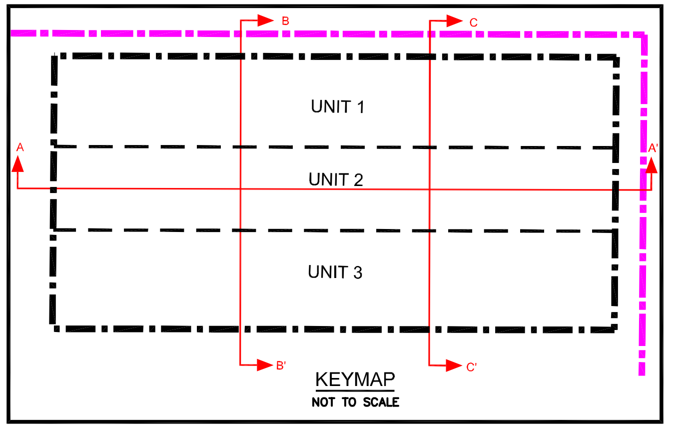

KEYMAP

NOT TO SCALE

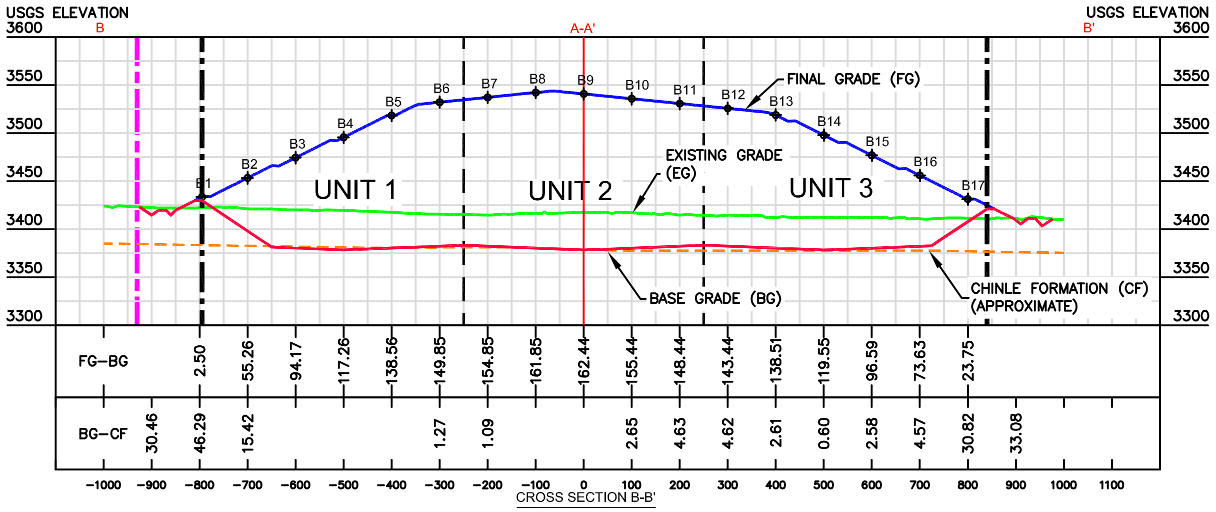

CROSS SECTION B-B'

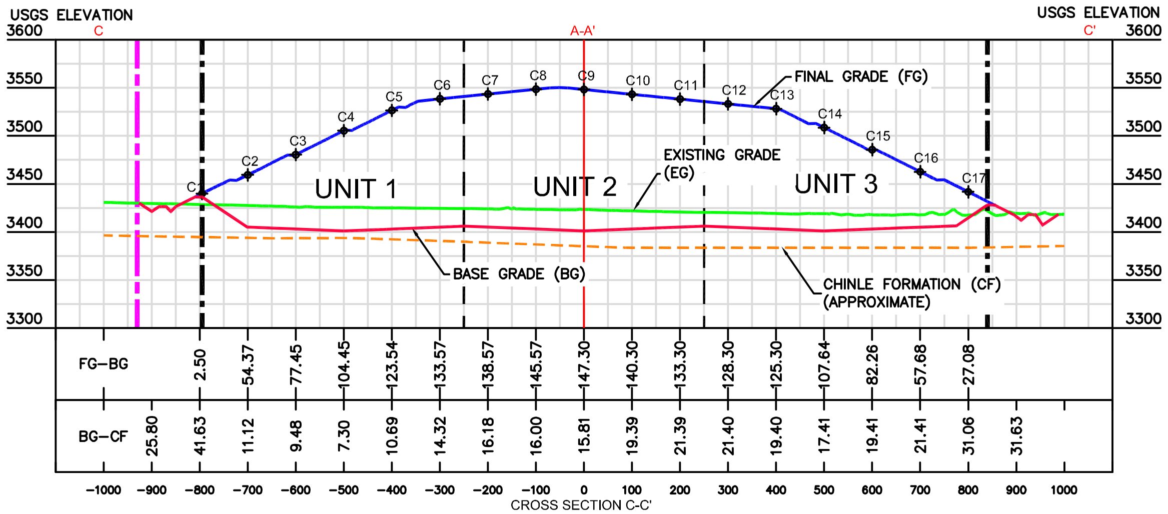

CROSS SECTION C-C'

DEPTH OF LANDFILL BETWEEN FINAL GRADES AND BASE GRADES

PT	FINALGRADE (FT)	BASEGRADE (FT)	DEPTH (FT)	PT	FINALGRADE (FT)	BASEGRADE (FT)	DEPTH (FT)	PT	FINALGRADE (FT)	BASEGRADE (FT)	DEPTH (FT)
A1	3419.09	3419.09	0.00	**B1**	3432.28	3429.78	2.50	**C1**	3438.78	3436.28	2.50
A2	3440.05	3390.76	49.29	**B2**	3453.38	3398.12	55.26	**C2**	3459.34	3404.97	54.37
A3	3461.02	3359.58	101.44	**B3**	3474.47	3380.31	94.16	**C3**	3480.42	3402.97	77.45
A4	3486.00	3361.58	124.42	**B4**	3495.57	3378.31	117.26	**C4**	3505.42	3400.97	104.45
A5	3506.98	3363.58	143.40	**B5**	3518.87	3380.31	138.56	**C5**	3526.52	3402.97	123.55
A6	3520.87	3365.58	155.29	**B6**	3532.16	3382.31	149.85	**C6**	3538.54	3404.97	133.57
A7	3525.87	3367.58	158.29	**B7**	3537.16	3382.31	154.85	**C7**	3543.54	3404.97	138.57
A8	3530.88	3369.58	161.30	**B8**	3542.16	3380.31	161.85	**C8**	3548.27	3402.97	145.30
A9	3535.88	3371.58	164.30	**B9**	3540.75	3378.31	162.44	**C9**	3548.27	3400.97	147.30
A10	3539.35	3373.58	165.77	**B10**	3535.75	3380.31	155.44	**C10**	3543.27	3402.97	140.30
A11	3539.94	3375.58	164.36	**B11**	3530.75	3382.31	148.44	**C11**	3538.27	3404.97	133.30
A12	3540.53	3377.58	162.95	**B12**	3525.75	3382.31	143.44	**C12**	3533.27	3404.97	128.30
A13	3541.12	3379.58	161.54	**B13**	3518.82	3380.31	138.51	**C13**	3528.27	3402.97	125.30
A14	3541.72	3381.58	160.14	**B14**	3497.86	3378.31	119.55	**C14**	3508.62	3400.97	107.65
A15	3542.31	3383.58	158.73	**B15**	3476.90	3380.31	96.59	**C15**	3485.23	3402.97	82.26
A16	3542.90	3385.58	157.32	**B16**	3455.94	3382.31	73.63	**C16**	3462.65	3404.97	57.68
A17	3543.49	3387.58	155.91	**B17**	3431.65	3407.9	23.75	**C17**	3441.69	3414.61	27.08
A18	3544.31	3389.58	154.73								
A19	3545.15	3391.58	153.57								
A20	3545.98	3393.58	152.40								
A21	3546.67	3395.58	151.09								
A22	3547.26	3397.58	149.68								
A23	3547.85	3399.58	148.27								
A24	3548.40	3401.58	146.82								
A25	3548.75	3403.58	145.17								
A26	3549.10	3405.58	143.52								
A27	3549.45	3407.58	141.87								
A28	3549.98	3409.58	140.40								
A29	3545.64	3411.58	134.06								
A30	3540.64	3413.58	127.06								
A31	3526.09	3415.58	110.51								
A32	3505.13	3417.58	87.55								
A33	3484.17	3419.58	64.59								
A34	3461.06	3421.58	39.48								

DEPTH OF FOUNDATION SOILS BETWEEN BASE GRADES AND CHINLE FORMATION

PT	BASEGRADE (FT)	CHINLE FORMATION (FT)	DEPTH (FT)	PT	BASEGRADE (FT)	CHINLE FORMATION (FT)	DEPTH (FT)	PT	BASEGRADE (FT)	CHINLE FORMATION (FT)	DEPTH (FT)
A1	3419.09	3419.09	0.00	**B1**	3429.78	3476.07	46.29	**C1**	3436.28	3477.91	41.63
A2	3390.76	3390.76	0.00	**B2**	3398.12	3413.54	15.42	**C2**	3404.97	3416.09	11.12
A3	3359.58	3359.58	0.00	**B3**	3380.31	3380.31	0.00	**C3**	3402.97	3412.45	9.48
A4	3361.58	3361.58	0.00	**B4**	3378.31	3378.31	0.00	**C4**	3400.97	3408.27	7.30
A5	3363.58	3363.58	0.00	**B5**	3380.31	3380.31	0.00	**C5**	3402.97	3413.66	10.69
A6	3365.58	3365.58	0.00	**B6**	3382.31	3383.58	1.27	**C6**	3404.97	3419.29	14.32
A7	3367.58	3367.58	0.00	**B7**	3382.31	3383.40	1.09	**C7**	3404.97	3421.15	16.18
A8	3369.58	3369.58	0.00	**B8**	3380.31	3380.31	0.00	**C8**	3402.97	3418.97	16.00
A9	3371.58	3371.58	0.00	**B9**	3378.31	3378.31	0.00	**C9**	3400.97	3416.78	15.81
A10	3373.58	3373.58	0.00	**B10**	3380.31	3382.96	2.65	**C10**	3402.97	3422.36	19.39
A11	3375.58	3375.58	0.00	**B11**	3382.31	3386.94	4.63	**C11**	3404.97	3426.36	21.39
A12	3377.58	3377.58	0.00	**B12**	3382.31	3386.93	4.62	**C12**	3404.97	3426.37	21.40
A13	3379.58	3379.78	0.20	**B13**	3380.31	3382.92	2.61	**C13**	3402.97	3422.37	19.40
A14	3381.58	3383.18	1.60	**B14**	3378.31	3378.91	0.60	**C14**	3400.97	3418.38	17.41
A15	3383.58	3386.59	3.01	**B15**	3380.31	3382.89	2.58	**C15**	3402.97	3422.38	19.41
A16	3385.58	3389.99	4.41	**B16**	3382.31	3386.88	4.57	**C16**	3404.97	3426.38	21.41
A17	3387.58	3393.40	5.82	**B17**	3407.9	3438.72	30.82	**C17**	3414.61	3445.67	31.06
A18	3389.58	3396.80	7.22								
A19	3391.58	3400.27	8.69								
A20	3393.58	3403.79	10.21								
A21	3395.58	3407.30	11.72								
A22	3397.58	3410.82	13.24								
A23	3399.58	3414.34	14.76								
A24	3401.58	3417.86	16.28								
A25	3403.58	3421.37	17.79								
A26	3405.58	3424.89	19.31								
A27	3407.58	3428.41	20.83								
A28	3409.58	3431.92	22.34								
A29	3411.58	3435.44	23.86								
A30	3413.58	3438.96	25.38								
A31	3415.58	3442.47	26.89								
A32	3417.58	3445.99	28.41								
A33	3419.58	3449.48	29.90								
A34	3421.58	3452.82	31.24								

PROTECT SOIL LAYER THICKNESS (PSL) = 2 FT.
INTERMEDIATE COVER LAYER THICKNESS = 1 FT.
FINAL COVER LAYER THICKNESS = 3 FT.
UNIT WEIGHT OF PSL AND COVER SOILS = 105 lb/ft^2.
UNIT WEIGHT OF WASTE = 74 lb/ft^2.

LEGEND

‒ · ‒ ·	FACILITY BOUNDARY
━ · ━ ·	LIMIT OF WASTE
‒ ‒ ‒	UNIT BOUNDARY
━━━	EXISTING GRADE
- - - -	CHINLE FORMATION (APPROXIMATE)
━━━	BASE GRADE
━━━	FINAL GRADE
A ▲ ▲ A'	CROSS SECTION LOCATION

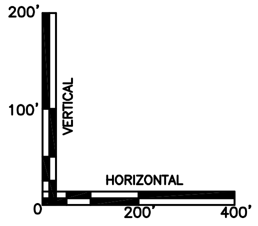

CROSS SECTION SCALE

Drawing:P:\acad 2003\530.06.01\REVISED FIGURES(RAI 1)\X SEC SETTLEMENT.dwg
Date/Time:Jul. 22, 2016-12:34:01

LANDFILL SETTLEMENT POINTS
CROSS–SECTIONS A, B & C

SUNDANCE WEST
SURFACE WASTE MANAGEMENT FACILITY
LEA COUNTY, NEW MEXICO

Gordon Environmental, Inc.
Consulting Engineers
213 S. Camino del Pueblo
Bernalillo, New Mexico, USA
Phone: 505-867-6990
Fax: 505-867-6991

DATE: 07/22/2016	CAD: XSEC SETTLEMENT.dwg	PROJECT #: 530.06.01
DRAWN BY: DMI	REVIEWED BY: CWF	FIGURE III.8.1
APPROVED BY: IKG	gei@gordonenvironmental.com	

Point C8

Foundation Soil Settlement

Thickness of Waste = 139.30 *ft*

Unit Weight of Soil = 105 lb/ft^3

Unit Weight of Waste = 74 lb/ft^3

$\Delta\sigma$=[(139.30')(74 lb/ft^3)+(2')(105 lb/ft^3)+(1')(105 lb/ft^3)+(3')(105 lb/ft^3)]/2000 *lbs/ton* = 5.47$tons/ft^2$; thus, approximate consolidation is 4.8%.

H_o= 16.00 ft, this is the depth of soil between the landfill base grade and the Chinle Formation.

Foundation Settlement = (.048)(16 ft) = 0.768 ft

The angular distortion between points C7 and C8 is determined as follows:

$$Distortion = \frac{(Settlement_{C8} - Settlement_{C7})}{distance = 100'} * 100 = \%$$

$$Distortion = \frac{(0.768\,ft - 0.764\,ft)}{100 - \ ft} * 100 = 0.004\%$$

A summary of potential foundation soils settlement is provided in **Tables III.8.1 – III.8.3.** The angular distortion between each point is calculated as above. The maximum angular distortion of the foundation soils on the floor of the landfill is 0.182% between points C5 and C6 on cross section C-C'. Therefore, after settlement, the slope of the liner on the landfill floor will be 2.8% - 0.182% = 2.62%. The slope of the leachate collection pipe will be the settlement that occurs on cross section A-A', and the maximum angular distortion occurs between points A19 and A20 on the floor of the landfill, which is 0.074%. Therefore after settlement, the slope of the leachate collection pipe will be 2.0% - 0.074% = 1.93%. These slopes will ensure that the design and performance standards for the leachate collection system will be met.

TABLE III.8.1
Sundance West
Settlement and Angular Distortion of Foundation Soils Between Points Cross Section A-A’

Point Location	Total Settlement (feet)	Distance between points (feet)	Angular Distortion (%)	Distortion Direction
A13	0.010			
		100	0.070	▼
A14	0.080			
		100	0.071	▼
A15	0.151			
		100	0.070	▼
A16	0.221			
		100	0.068	▼
A17	0.289			
		100	0.069	▼
A18	0.358			
		100	0.070	▼
A19	0.428			
		100	0.074	▼
A20	0.502			
		100	0.070	▼
A21	0.572			
		100	0.074	▼
A22	0.646			
		100	0.068	▼
A23	0.714			
		100	0.074	▼
A24	0.788			
		100	0.066	▼
A25	0.854			
		100	0.073	▼
A26	0.927			
		100	0.065	▼
A27	0.992			
		100	0.062	▼
A28	1.054			
		100	0.053	▼
A29	1.107			
		100	0.053	▼
A30	1.160			
		100	0.012	▼
A31	1.172			
		100	-0.019	▲
A32	1.153			
		100	-0.107	▲
A33	1.047			
		100	-0.154	▲
A34	0.894			

Notes:

Points Correspond to **Figure III.8.1**
▲ = potential upward distortion
▼ = potential downward distortion

TABLE III.8.2
Sundance West
Settlement and Angular Distortion of Foundation Soils Between Points Cross Section B-B'

Point Location	Total Settlement (feet)	Distance between points (feet)	Angular Distortion (%)	Distortion Direction
B1	0.000			
		100	0.614	▼
B2	0.503			
		100	-0.614	▲
B3	0.000			
		100	0.000	▲
B4	0.000			
		100	0.000	▲
B5	0.000			
		100	0.062	▼
B6	0.062			
		100	-0.008	▲
B7	0.054			
		100	-0.054	▲
B8	0.000			
		100	0.000	▲
B9	0.000			
		100	0.131	▼
B10	0.131			
		100	0.093	▼
B11	0.224			
		100	-0.004	▲
B12	0.222			
		100	-0.098	▲
B13	0.123			
		100	-0.095	▲
B14	0.027			
		100	0.081	▼
B15	0.108			
		100	0.063	▼
B16	0.175			
		100	0.600	▼
B17	0.771			

Notes:

Points Correspond to **Figure III.8.1**
▲ = potential upward distortion
▼ = potential downward distortion

TABLE III.8.3
Sundance West
Settlement and Angular Distortion of Foundation Soils Between Points Cross Section C-C’

Point Location	Total Settlement (feet)	Distance between points (feet)	Angular Distortion (%)	Distortion Direction
C1	0.000			
		100	0.363	▼
C2	0.363			
		100	0.007	▼
C3	0.370			
		100	-0.056	▲
C4	0.314			
		100	0.168	▼
C5	0.482			
		100	0.182	▼
C6	0.664			
		100	0.100	▼
C7	0.764			
		100	0.004	▼
C8	0.768			
		100	-0.003	▲
C9	0.765			
		100	0.150	▼
C10	0.915			
		100	0.078	▼
C11	0.993			
		100	-0.015	▲
C12	0.978			
		100	-0.097	▲
C13	0.881			
		100	-0.127	▲
C14	0.754			
		100	0.019	▼
C15	0.773			
		100	-0.058	▲
C16	0.715			
		100	0.099	▼
C17	0.814			

Notes:

Points Correspond to **Figure III.8.1**
▲ = potential upward distortion
▼ = potential downward distortion

4.0 WASTE SETTLEMENT CALCULATIONS

The methodology to estimate cover surface settlement involves selecting points on the cover surface, computing the settlement at each point, and evaluating the resulting change in surface elevation. Points were selected from a cross sections A-A’, B-B’, and C-C’ (**Figure III.8.1**). Qian, et al., (**Attachment III.8.B**) present a method developed by Sowers (1973) for determining settlement in landfills. This method is based on general soils consolidation theory, which relates settlement to layer thickness and changes in void ratio.

The primary settlement is estimated using equation 12.8 (**Attachment III.8.B, p. 451**):

$$\delta_C = \mathrm{H_o}\frac{\mathrm{C_c}}{1+\mathrm{e_o}}\log\frac{\sigma_o+\Delta\sigma}{\sigma_o}$$

Where: δ_C= Primary settlement

$\frac{C_c}{1+e_o}$ = 0 .006 (**Attachment III.8.C, p. 393,** D_r=80%)

H_o = Initial thickness of the waste layer before settlement (**Figure III.8.1**)

e_o = Waste void ratio before settlement= 0.4 **(Attachment III.8.C, p. 105)**

σ_o = Total overburden pressure applied at the mid level of the waste layer

$\Delta\sigma$= increment of overburden pressure due to vertical expansion or other extra load.

Long-term secondary settlement is estimated by equation 12.10 (**Attachment III.8.B, p.451**):

$$\delta_S = \mathrm{H_s}\frac{\mathrm{C_r}}{1+\mathrm{e_s}}\log\frac{\mathrm{t_2}}{\mathrm{t_1}}$$

Where: δ_S= secondary settlement = Ho - δ_C

$\frac{C_r}{1+e_s}$ = Secondary compression index = $\frac{1}{3}(\frac{C_c}{1+e_o})$ then (.333)(.006) = 0.002 (**Attachment III.8.C, p. 393**)

H_s = Waste thickness at start of secondary settlement = H_o- δ_C (**Figure III.8.1)**

e_s = Waste void ratio = 0.4 **(Attachment III.8.C, p. 105)**

t_1= starting time of secondary settlement (year 1)

t_2= ending time of secondary settlement = Assume 30 years

Settlement is estimated at the locations (Points A1 through A34, Points B1 through B17, and C1 through C17) shown on the landfill cross sections (**Figure III.8.1**). An example calculation is demonstrated at point C8.

Point C8

Primary Waste Settlement

$$\delta_C = \mathrm{H_o} \frac{\mathrm{C_c}}{1+\mathrm{e_o}} \log \frac{\sigma_o + \Delta\sigma}{\sigma_o}$$

Thickness of Waste = 139.30 *ft*

Thickness of Intermediate and Final Cover = 1 ft + 3 ft= 4 ft

Unit Weight of Soil = 105 lb/ft^3

Unit Weight of Waste = 74 lb/ft^3

$\Delta\sigma$= (3')(105 lb/ft^3)+(1')(105 lb/ft^3)= 420 lb/ft^2

$$\sigma_o = \frac{H_o}{2}\left(74\,lb/\,ft^2\right) = \frac{139.30\,ft}{2}\left(74\,lb/\,ft^2\right) = 5{,}154.10$$

$$\delta_c = 139.30(0.006)\log\left(\frac{5{,}154.10+420}{5{,}154.10}\right)$$

$$\delta_c = 0.0284\,ft$$

Secondary Waste Settlement

$$\delta_S = \mathrm{H_s} \frac{C_\mathrm{r}}{1+\mathrm{e_s}} \log \frac{\mathrm{t_2}}{\mathrm{t_1}}$$

$\mathrm{H_s}$= 139.30 ft – 0.028 ft = 139.272 ft

$\delta_s = 139.27(0.002) \log \frac{30}{1}$ =0.411 ft

Total waste settlement = 0.028 ft + .411 ft = 0.439 ft.

Primary Protective Soil Layer Settlement

$$\delta_C = \mathrm{H_o} \frac{\mathrm{C_c}}{1+\mathrm{e_o}} \log \frac{\sigma_o + \Delta\sigma}{\sigma_\mathrm{o}}$$

Thickness of Protective Soil Layer (PSL) = H_o = 2 *ft*;

Thickness of Intermediate and Final Cover = 4 *ft*;

Thickness of Waste = 139.30 *ft*;

Unit Weight of Soil = 105 lb/ft^3 Dry Density;

Unit Weight of Waste = 74 lb/ft^3 Dry Density;

$\Delta\ \sigma$ = (139.30 ft)(74 lb/ft^3) + (4 ft)(105 lb/ft^3)= 10,728.20 lb/ft^2;

$$\sigma_o = \frac{H_O}{2}(105) = \frac{2}{2}(105) = 105.00\, lb/ ft^2$$

$$\delta_c = (2\, ft)(0.006)\log\left(\frac{105.00 + 10{,}728.20}{105.00}\right)$$

$$= 0.0242\, ft$$

Secondary Protective Soil Layer Settlement

$$\delta_S = \mathrm{H_s} \frac{C_\mathrm{r}}{1+\mathrm{e_s}} \log \frac{\mathrm{t_2}}{\mathrm{t_1}}$$

H_o= 2’ – 0.024’ = 1.975’;

$$\delta_S = 1.975(0.002) \log\left(\frac{30}{1}\right) = 0.006\, ft$$

Total protective soil layer settlement = 0.024 ft + 0.006 ft = 0.029 ft.

The cover soil layer consisting of vegetative, barrier and intermediate cover layers will also experience nominal consolidation due to its own weight. The method for evaluating settlement of the soil cover and cushion layers is based on equation 12.10 (**Attachment III.8.B, p.451**).

Secondary Cover Soil Layer Settlement

$$\delta_S = H_s \frac{C_r}{1+e_s} \log \frac{t_2}{t_1}$$

H_s= 4 *ft*

$$\delta_S = (4\,ft)(0.002)\log\left(\frac{30}{1}\right) = 0.012\,ft$$

Total cover soil layer settlement = 0.012 ft.

The maximum settlement of waste is the sum of primary and secondary settlement at point C8. The waste settlement is equal to 0.439 ft. The soil cover layer settlement is equal to 0.012 ft. The protective soil layer settlement is equal to 0.029 ft. The foundation soil settlement is equal to 0.768 ft. The maximum total settlement that could occur at Point C8 on the final cover of the landfill is the sum of the waste settlement, protective soil layer settlement, cover settlement and foundation soil settlement, i.e.: 0.439 ft + 0.012 ft +0.029 ft+ 0.768 ft = 1.248 ft. The methodology used to determine settlement at point C8 was used to find the settlement of points for cross sections A-A’, B-B’ and C-C’. The total settlement of points for cross sections A-A’, B-B’ and C-C’ and the angular distortion between them is provided on **Table III.8.4** through **Table III.8.6**. The maximum angular distortion at the level of the top of final cover occurs between points C9 and C10 and equals 0.129%. Therefore, after conservative assumptions for settlement, the minimum slope of the final cover will be 5.00% - 0.129% = 4.87%.

5.0 CONCLUSION

Settlement projections have been calculated for the landfill foundation and for the landfill cover. Settlement estimates include elastic deformation and both primary and secondary consolidation in the foundations soils, in the waste, and in the cover materials. Settlement increases to the east since the elastic soil between the base grades and the Chinle Formation increase in depth.

The maximum height of the waste and cover occurs at Point A10 in Unit 2 on cross section A-A’ on **Figure III.8.1**. Total depth of waste and cover at this point is approximately 165.77 ft. Based on engineering analysis, the settlement under the weight of the waste and soils at Point A10 is expected to be 0.543 ft.

Final cover slope after hypothetical settlement is equal to the landfill design top of cover minus the maximum angular distortion between Points C9 and C10: 5.00% - 0.129%= 4.87%. Similarly, after settlement between Points C5 and C6, the slope of the liner on the landfill floor will be 2.8% - 0.182% = 2.62%, and between Points A19 and A20, the slope of the leachate collection pipe will be 2.0% - 0.074% = 1.93%.

The slope of the final cover and liner after settlement is consistent with the performance specifications for leachate collection system and stormwater controls.

TABLE III.8.4
Sundance West
Total Settlement and Angular Distoration Between Points Cross Section A-A'

Point Location	Total Settlement (feet)	Distance between points (feet)	Angular Distortion (%)	Distortion Direction
A1	0.026			
		100	0.165	▼
A2	0.191			
		100	0.159	▼
A3	0.350			
		100	0.069	▼
A4	0.419			
		100	0.057	▼
A5	0.476			
		100	0.036	▼
A6	0.512			
		100	0.009	▼
A7	0.521			
		100	0.009	▼
A8	0.530			
		100	0.009	▼
A9	0.539			
		100	0.004	▼
A10	0.543			
		100	-0.004	▲
A11	0.539			
		100	-0.004	▲
A12	0.535			
		100	0.006	▼
A13	0.541			
		100	0.065	▼
A14	0.606			
		100	0.067	▼
A15	0.673			
		100	0.065	▼
A16	0.738			
		100	0.064	▼
A17	0.802			
		100	0.066	▼
A18	0.868			
		100	0.066	▼
A19	0.934			
		100	0.071	▼
A20	1.005			
		100	0.066	▼
A21	1.071			
		100	0.07	▼
A22	1.141			
		100	0.064	▼
A23	1.205			
		100	0.069	▼
A24	1.274			
		100	0.061	▼
A25	1.335			
		100	0.068	▼
A26	1.403			
		100	0.060	▼
A27	1.463			
		100	0.059	▼
A28	1.522			
		100	0.033	▼
A29	1.555			
		100	0.032	▼
A30	1.587			
		100	-0.037	▲
A31	1.550			
		100	-0.089	▲
A32	1.461			
		100	-0.177	▲
A33	1.284			
		100	-0.231	▲
A34	1.053			

Notes:

Points Correspond to **Figure III.10.1**

▲ = potential upward distortion

▼ = potential downward distortion

TABLE III.8.5
Sundance West
Total Settlement and Angular Distortion Between Points Cross Section B-B'

Point Location	Total Settlement (feet)	Distance between points (feet)	Angular Distortion (%)	Distortion Direction
B1	0.026			
		100	0.685	▼
B2	0.711			
		100	-0.383	▲
B3	0.328			
		100	0.070	▼
B4	0.398			
		100	0.064	▼
B5	0.462			
		100	0.096	▼
B6	0.558			
		100	0.007	▼
B7	0.565			
		100	-0.034	▲
B8	0.531			
		100	0.002	▼
B9	0.533			
		100	0.111	▼
B10	0.644			
		100	0.072	▼
B11	0.716			
		100	-0.017	▲
B12	0.699			
		100	-0.113	▲
B13	0.586			
		100	-0.153	▲
B14	0.433			
		100	0.013	▼
B15	0.446			
		100	-0.002	▲
B16	0.444			
		100	0.444	▼
B17	0.888			

Notes:

Points Correspond to **Figure III.8.1**
▲ = potential upward distortion
▼ = potential downward distortion

TABLE III.8.6
Sundance West
Total Settlement and Angular Distortion Between Points Cross Section C-C'

Point Location	Total Settlement (feet)	Distance between points (feet)	Angular Distortion (%)	Distortion Direction
C1	0.016			
		100	0.551	▼
C2	0.567			
		100	0.078	▼
C3	0.645			
		100	0.026	▼
C4	0.671			
		100	0.226	▼
C5	0.897			
		100	0.212	▼
C6	1.109			
		100	0.115	▼
C7	1.224			
		100	0.024	▼
C8	1.248			
		100	0.003	▼
C9	1.251			
		100	0.129	▼
C10	1.380			
		100	0.057	▼
C11	1.437			
		100	-0.030	▲
C12	1.407			
		100	-0.106	▲
C13	1.301			
		100	-0.180	▲
C14	1.121			
		100	-0.058	▲
C15	1.063			
		100	-0.133	▲
C16	0.930			
		100	0.001	▼
C17	0.931			

Notes:

Points Correspond to **Figure III.8.1**
▲ = potential upward distortion
▼ = potential downward distortion

APPLICATION FOR PERMIT
SUNDANCE WEST

VOLUME III: LANDFILL ENGINEERING CALCULATIONS
SECTION 8: SETTLEMENT CALCULATIONS

ATTACHMENT III.8.A

SUMMARY OF GEOTECHNICAL LABORATORY TESTING RESULTS

AMEC Earth Environmental, Inc.

Client: Gordon Environmental, Inc.
213 Camino del Pueblo
Bernalillo, NM 87004-

Report Date: October 23, 2009

Project #: 8-519-005168
Work Order #: 2
Sampled By: Client
Date Sampled:

Attention: Larry Coons
Project Name: Gordon Environmental Inc. 2008 Misc. Testing

ABQ, NM

Project Manager: Herman Garcia

Sieve Analaysis (ASTM C117-04/C136-06)
Plasticity Index (ASTM D4318-05)
Soil Classification (ASTM D2487-06)

SOILS / AGGREGATES

Sample Location	Soil Class.	L.L.	P.I.	#200	#100	#50	#40	#30	#16	#10	#8	#4	1/4"	3/8"	1/2"	3/4'	1"	1 1/4"	1 1/2"	2"	2 1/2"	3"	6"	12"	Lab Number
GB-1 @ 15 - 20'	SC-SM	24	5	33	55	90	96	98	98	99	99	99		100											9-1213-01
GB-1 @ 20'	SC	42	18	29	47	70	74	76	78	79	80	83		87	88	93	100								9-1213-02
GB-1 @ 40 - 45'	CL	30	14	56	67	79	82	86	92	95	96	99		100											9-1213-03
GB-1 @ 45'	CL	46	28	80	92	97	98	98	99	99	99	100													9-1213-04
GB-2 @ 5'	SM	20	2	24	54	92	97	98	99	99	99	99		100											9-1213-05
GB-2 @ 10 - 20'	SM	NV	NP	27	46	80	85	88	91	93	94	97		100											9-1213-06
GB-2 @ 15'	SM	29	5	23	47	88	95	97	98	99	99	99		100											9-1213-07
CH-1 @ 154'	CL	38	16	65	77	96	99	100																	9-1213-08
CH-2 @ 149'	CL	30	11	73	78	91	97	99	100																9-1213-09
CH-3 @ 79'	ML	44	13	75	83	95	98	99	100																9-1213-10
CH-4 @ 64'	SM	24	3	30	53	67	73	81	94	96	97	99		100											9-1213-11

Reviewed By:

Distribution: Client: ✓ File: ✓ Supplier: ✓ Other: Addressee (2)
Email:

amec

Client: Gordon Environmental, Inc.
213 Camino del Pueblo
Bernalillo, NM 87004-

Attn: Larry Coons

Project Name: Gordon Environmental Inc. 2008 Misc Testing

ABQ, NM

Report Date: November 04, 2009

Project #: 8-519-005168
Report #: 1003
Work Order #: 2
Sampled By: Client
Date Sampled:

Project Manager: Herman Garcia

SOILS / AGGREGATES

MOISTURE CONTENT OF SOIL (ASTM D2216-05) AND IN-SITU DENSITY

Lab #	Color & Type of Material	Sample Source	Test Method	Oven Temp. (C)	Mass less than Min Req.	Material Type *	Moisture (%)	Dry Density (pcf)
9-1213-01		GB-1 @ 15 - 20'	A	110			10	
9-1213-02		GB-1 @ 20'	A	110			12	
9-1213-03		GB-1 @ 40 - 45'	A	110			9	
9-1213-04		GB-1 @ 45'	A	110			12	
9-1213-05		GB-2 @ 5'	A	110			5	
9-1213-06		GB-2 @ 10 - 20'	A	110			3	
9-1213-07		GB-2 @ 15'	A	110			8	
9-1213-08		CH-1 @ 154'	A	110			13	
9-1213-09		CH-2 @ 149'	A	110			8	
9-1213-10		CH-3 @ 79'	A	110			20	
9-1213-11		CH-4 @ 64'	A	110			5	

***Sample contains more than one type of material.**

Reviewed By:

Distribution: Client ✓ File: ✓ Supplier: ✓ Other: Addressee (2)
Email:

AMEC Earth Environmental, Inc.
8519 Jefferson NE
Albuquerque, NM 87113
Tel 5058211801
Fax 5058217371

www.amec.com

Client: Gordon Environmental, Inc.
213 Camino del Pueblo
Bernalillo, NM 87004-

Report Date: October 23, 2009

Project #: 8-519-005168
Work Order #: 2
Lab #: 9-1213-01
Sampled By: Client
Date Sampled:
Visual Description of Material:
Sample Source: GB-1 @ 15 - 20'

Attn: Larry Coons

Project Name: Gordon Environmental Inc. 2008 Misc. Testing

ABQ, NM

Project Manager: Herman Garcia

SOILS / AGGREGATES

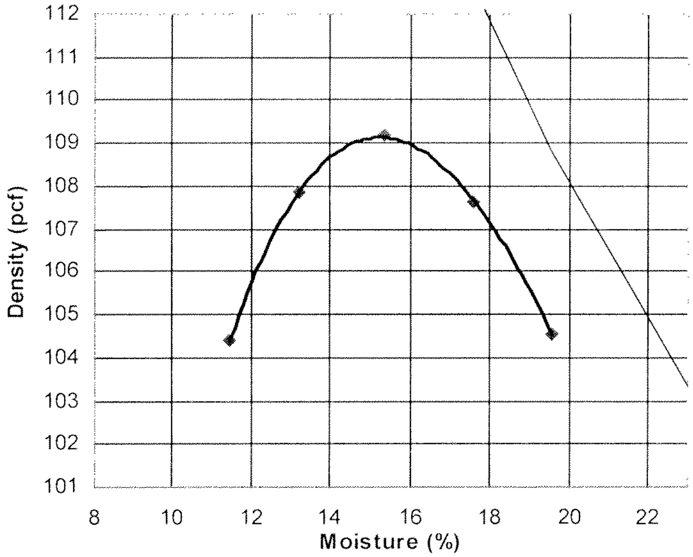

Sieve Analysis (ASTM C117-04/C136-06)

200 Wash Procedure: A

Sieve Size	Passing
3/8in.	100%
#4	99%
#8	99%
#10	99%
#16	98%
#30	98%
#40	96%
#50	90%
#100	55%
#200	33%

Moisture Density Relationship: (ASTM D698-07) Method: A

Preparation Method: Dry Rammer Type: Mechanical

Specific Gravity: 2.651 Assumed

Maximum Density: 109.1

Optimum Moisture: 15.2

Plasticity Index (ASTM D4318-05)

Liquid Limit: 24
Plastic Limit: 19
Plasticity Index: 5

Preperation Method: Dry Liquid Limit Method: A

PI Air Dried.

Soil Classification (ASTM D2487-06) SC-SM

Reviewed By:

Jan

Distribution: Client ✓ File: ✓ Supplier: ✓ Other: Addressee (2)
Email:

Client: Gordon Environmental, Inc.
213 Camino Del Pueblo
Bernalillo, NM 87004-

Attn: Larry Coons
Project Name: Gordon Environmental, Inc. 2008 Misc. Testing

ABQ, NM

Report Date: November 10, 2009

Project #: 8-519-005168
Work Order #: 2
Lab #: 9-1213-02
Sampled By: Client
Date Sampled: Unknown
Material: Silty Clayey Sand
Sample Source: GB-1 at 20 ft

Project Manager: Herman Garcia **SOILS/AGGREGATES**

Measurement of Collapse Potential of Soils (ASTM D5333)

Sample Preparation: In Situ

Initial Volume (in^3):	4.60	**Final Volume (in^3):**	4.39
Initial Moisture (%):	17.7%	**Final Moisture (%)**	15.5%
Initial Dry Density (lb/ft^3):	80.3	**Initial Dry Density (lb/ft^3):**	83.9
Initial Degree of Saturation:	45%	**Final Degree of Saturation:**	42%
Initial Void Ratio:	1.0	**Final Void Ratio:**	0.9
Estimated Specific Gravity:	2.600	**Saturated At:**	Not Saturated

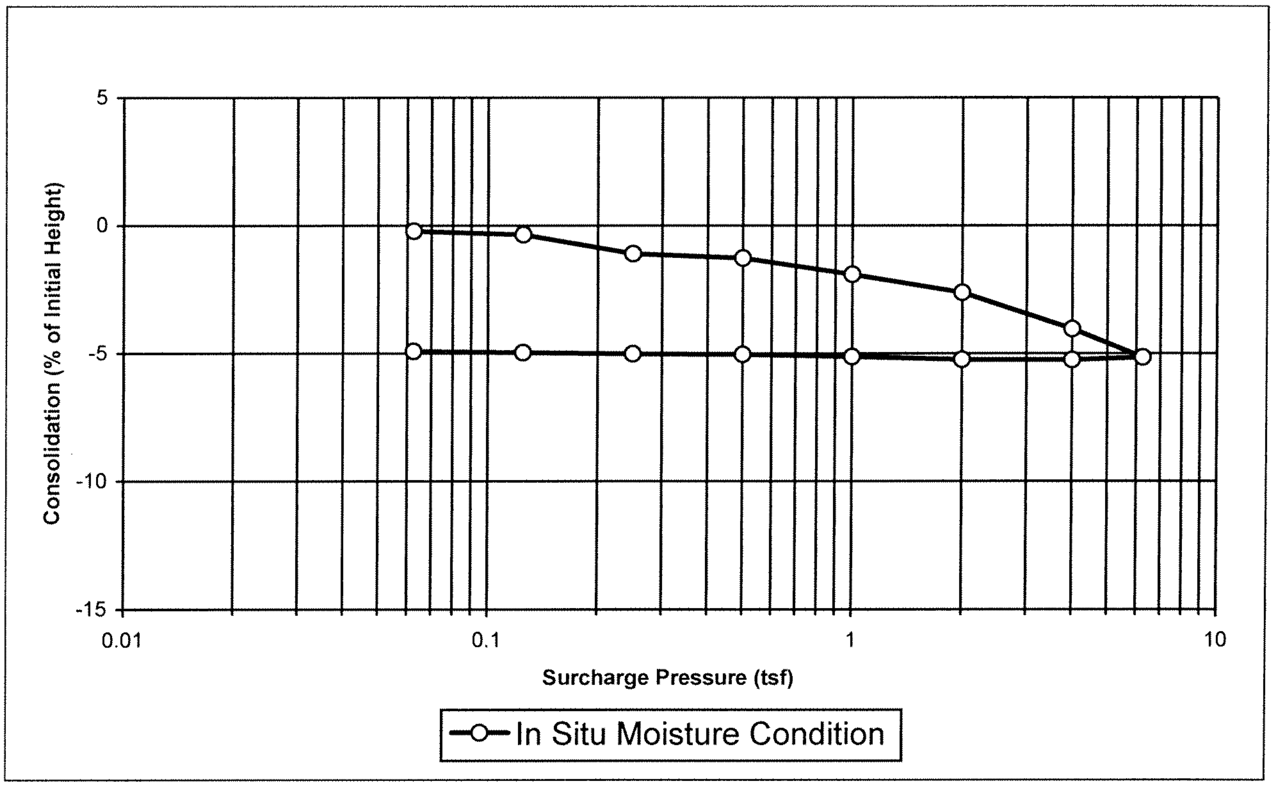

Reviewed By:
Jan

Distribution: **Client** ☑ **File** ☑ **Supplier:** ☑ **Other:** Addressee (2)
Email: ☐

amec

PROJECT: Gordon Environmental Inc. 2008 Misc Testing
CLIENT: Smith Engineering Co.
MATERIAL: Silty Clayey Sand
SAMPLE SOURCE: GB-1 at 20 ft
PREPARATION: In Situ

JOB NO: 8-519-005168
LAB NO: 9-1213-02
DATE SAMPLED: Unknown
SAMPLED BY: Client

REVIEWED BY:

Measurement of Hydraulic Conductivity (Applicable Portions of ASTM D5856-95)

Lab Number	Sample Source	Method	K_{sat} (cm/s)*	K_{sat} (ft/day)*	Initial Moisture Content ** (%)	Saturated Moisture Content ** (%)	Dry Bulk Density (lb/ft^3)	Calculated Porosity (%)
9-1213-02	GB-1 at 20 ft	Constant Head	9.36E-05	2.65E-01	17.6%	42.3%	80.2	50.6%

*Corrected to 20 °C
**Gravimetric Moisture (percent by mass)

AMEC Earth Environmental, Inc.
8519 Jefferson NW
Albuquerque, NM 87113
Phone: (505) 821-1801
Fax: (505) 821-7371
www.amec.com

amec

Client: Gordon Environmental, Inc.
213 Camino del Pueblo
Bernalillo, NM 87004-

Attn: Larry Coons

Project Name: Gordon Environmental Inc. 2008 Misc. Testing

ABQ, NM

Project Manager: Herman Garcia

Report Date: October 26, 2009

Project #: 8-519-005168
Work Order #: 2
Lab #: 9-1213-03
Sampled By: Client
Date Sampled:
Visual Description of Material:
Sample Source: GB-1 @ 40 - 45'

SOILS / AGGREGATES

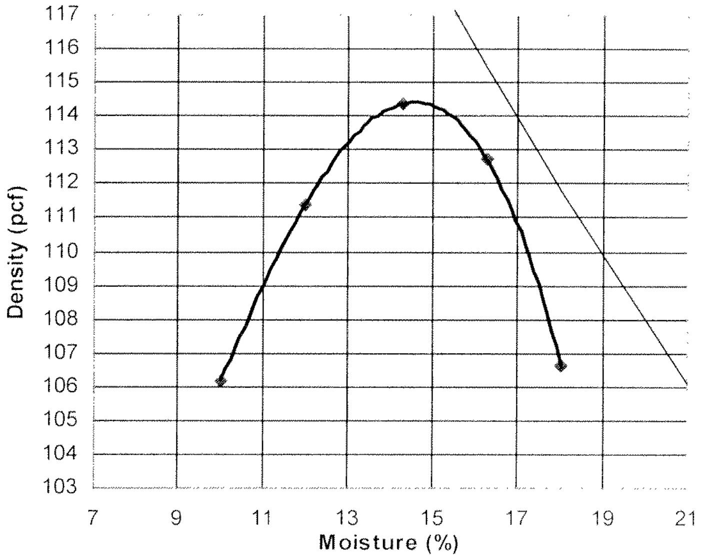

<u>Sieve Analysis</u> (ASTM C117-04/C136-06)
200 Wash Procedure: A

Sieve Size	Passing
3/8in.	100%
#4	99%
#8	96%
#10	95%
#16	92%
#30	86%
#40	82%
#50	79%
#100	67%
#200	56%

<u>Moisture Density Relationship:</u> <u>(ASTM D698-07)</u> **Method:** B
Preparation Method: Dry **Rammer Type:** Mechanical
Specific Gravity: 2.651 **Assumed**
Maximum Density: 114.4
Optimum Moisture: 14.6

<u>Plasticity Index</u> <u>(ASTM D4318-05)</u>

Liquid Limit: 30
Plastic Limit: 16
Plasticity Index: 14

Preperation Method: Dry **Liquid Limit Method:** A
PI Air Dried.

<u>Soil Classification (ASTM D2487-06)</u> CL

Reviewed By:
Jan

Distribution: **Client** ✓ **File:** ✓ **Supplier:** ✓ **Other:** Addressee (2)
Email:

AMEC Earth Environmental, Inc.
8519 Jefferson NE
Albuquerque, NM 87113
Tel 5058211801
Fax 5058217371

www.amec.com

Client:	Gordon Environmental, Inc. 213 Camino del Pueblo Bernalillo, NM 87004
Attn:	Larry Coons
Project Name:	Gordon Environmental Inc. 2008 Misc. Testing

Report Date: 11/11/2009

Project #: 8-519-005168
Work Order #: 2
Lab #: 9-1213-04
Sampled By: Client
Date Sampled: Unknown
Visual Description of Material: Sandy Clay
Sample Source: GB-1 at 45 ft

Measurement of Hydraulic Conductivity of Saturated Porous Materials Using a Flexible Wall Permeameter (ASTM D5084-03)

SAMPLE PREPARATION: In Situ

METHOD OF COMPACTION: NA

PERMEANT LIQUID: Tap Water
TESTING METHOD: Method F: Constant Volume Falling Head (by Mercury) Rising Tailwater

FIELD MOISTURE:	NA	LAB MOISTURE:	NA
INITIAL DIAMETER (cm):	6.04	FINAL DIAMETER	6.17
INITIAL LENGTH (cm):	7.62	FINAL LENGTH	7.72
INITIAL MOISTURE CONTENT (%):	12.7	FINAL MOISTURE CONTENT (%):	20.7
CONSOLIDATED? (Y/N):	N		
CELL PRESSURE (psi):	NA	POST CONSOLIDATION DIAMETER (cm):	NA
BACKPRESSURE (psi):	NA	POST CONSOLIDATION LENGTH (cm):	NA

EFFECTIVE STRESS (psi):	4.0	SPECIFIC GRAVITY:	2.651
INITIAL DRY BULK DENSITY (lb/ft^3):	114.6	SPECIFIC GRAVITY ASSUMED? (Y/N):	Y
		PERCENT SATURATION:	100%
FINAL DRY BULK DENSITY (lb/ft^3):	108.5		
FINAL B PARAMETER READING:	1.00	FINAL BACKPRESSURE (psi):	70
AVERAGE K_{sat}* (cm/s):	**2.32E-06**	**AVERAGE K_{sat}* (ft/day):**	**6.58E-03**

MAXIMUM GRADIENT USED: 4.29
MINIMUM GRADIENT USED: 2.91

*Corrected to 20 °C
**N.B.: All final sample dimensions are subject to sample deformation caused by exsolution of air in pore water and handling during removal from cell.

Reviewed By:

amec

Client:	Gordon Environmental, Inc. 213 Camino del Pueblo Bernalillo, NM 87004-	**Report Date:**	November 05, 2009
		Project #:	8-519-005168
		Work Order #:	2
		Lab #:	9-1213-04
Attn:	Larry Coons	**Sampled By:**	Client
Project Name:	Gordon Environmental Inc. 2008 Misc. Testing ABQ, NM	**Date Sampled:**	
		Visual Description of Material:	
		Sample Source:	GB-1 @ 45'
Project Manager:	Herman Garcia		

SOILS / AGGREGATES

One-Dimensional Swell or Settlement Potential of Cohesive Soils (ASTM D4546-08)

Initial Volume (cu.in.):	4.58	Final Volume (cu.in.):	4.58
Initial Moisture (%):	9.6%	Final Moisture (%):	17.3%
Initial Dry Density (pcf):	104.7	Final Dry Density (pcf):	104.7
Final Degree Saturation:	79%	Initial Degree of Saturation:	44%
Initial Void Ratio:	0.6	Final Void Ratio:	0.6
Moisture pick-up (% Dry weight.):	7.7%	Moisture pick-up (% in volume):	12.9%
Estimated Specific Gravity:	2.651	Load:	1 tsf
Type of Water Used:	Distilled Water	Swell (% of Initial Height):	0.0%

Expansion - Log Time Curve

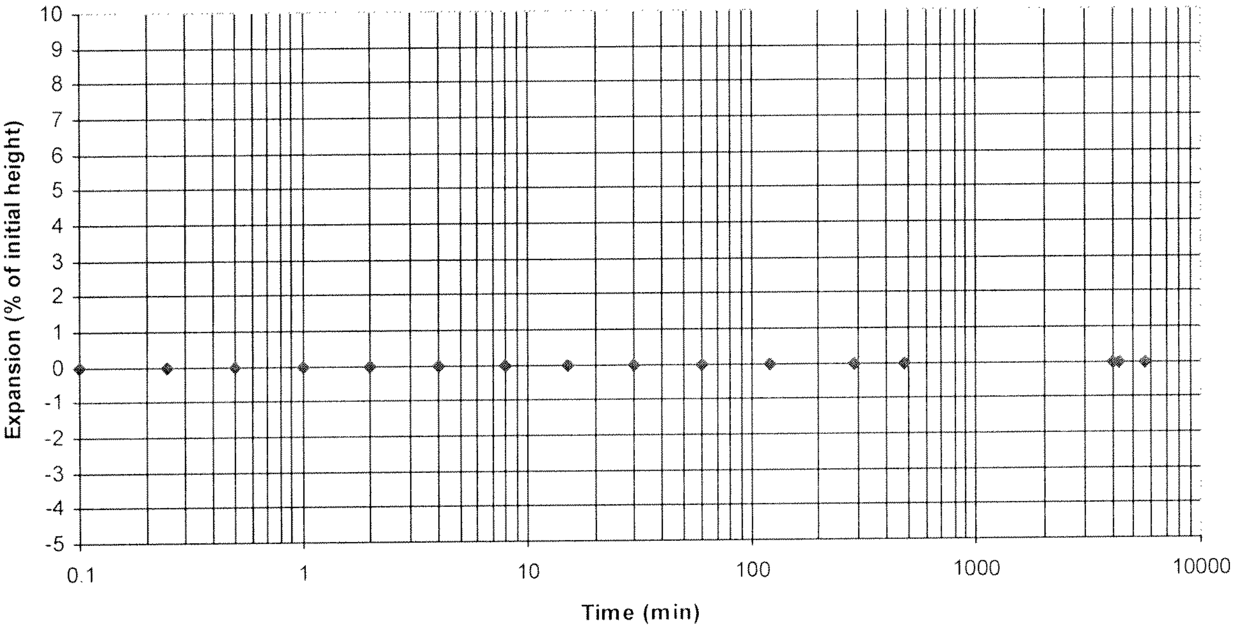

Reviewed By:
fs

Distribution: Client ✓ File: ✓ Supplier: ✓ Other: Addressee (2)
Email:

AMEC Earth Environmental, Inc.
8519 Jefferson NE
Albuquerque, NM 87113
Tel 5058211801
Fax 5058217371

www.amec.com

amec

Client: Gordon Environmental, Inc.
213 Camino del Pueblo
Bernalillo, NM 87004-

Attn: Larry Coons

Project Name: Gordon Environmental Inc. 2008 Misc. Testing

ABQ, NM

Project Manager: Herman Garcia

Report Date: October 26, 2009

Project #: 8-519-005168
Work Order #: 2
Lab #: 9-1213-06
Sampled By: Client
Date Sampled:
Visual Description of Material:
Sample Source: GB-2 @ 10 - 20'

SOILS / AGGREGATES

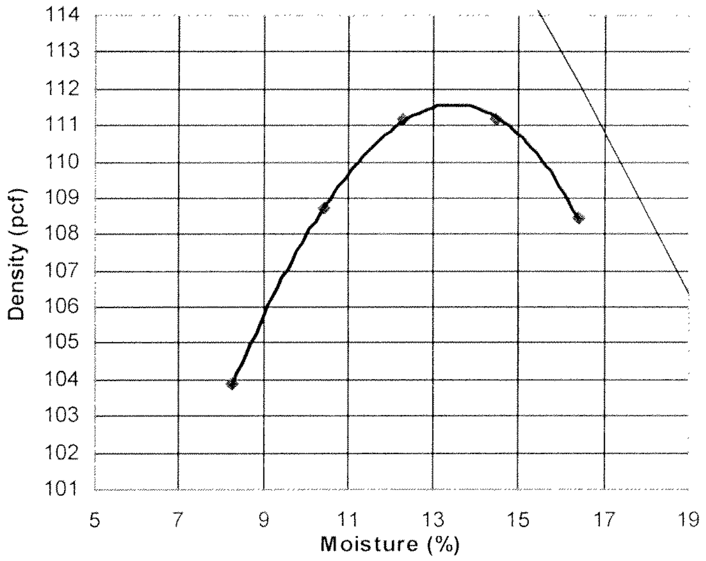

Sieve Analysis (ASTM C117-04/C136-06)

200 Wash Procedure: A

Sieve Size	Passing
3/8in.	100%
#4	97%
#8	94%
#10	93%
#16	91%
#30	88%
#40	85%
#50	80%
#100	46%
#200	27%

Moisture Density Relationship: (ASTM D698-07) **Method:** B
Preparation Method: Dry **Rammer Type:** Mechanical
Specific Gravity: 2.551 **Assumed**
Maximum Density: 111.6
Optimum Moisture: 13.5

Plasticity Index (ASTM D4318-05)

Liquid Limit: NV
Plastic Limit: NV
Plasticity Index: NP

Preperation Method: Dry **Liquid Limit Method:** A
PI Air Dried.

Soil Classification (ASTM D2487-06) SM

Reviewed By:
fs

Distribution: Client ✓ File: ✓ Supplier: ✓ Other: Addressee (2)
Email:

AMEC Earth Environmental, Inc.
8519 Jefferson NE
Albuquerque, NM 87113
Tel 5058211801
Fax 5058217371

www.amec.com

PROJECT: Gordon Environmental Inc. 2008 Misc Testing
CLIENT: Gordon Environmental, Inc.
MATERIAL: Silty Clayey Sand
SAMPLE SOURCE: GB-2 at 15 ft
PREPARATION: In Situ

JOB NO: 8-519-005168
LAB NO: 9-1213-07
DATE SAMPLED: Unknown
SAMPLED BY: Client

REVIEWED BY:

Measurement of Hydraulic Conductivity (Applicable Portions of ASTM D5856-95)

Lab Number	Sample Source	Method	K_{sat} (cm/s)*	K_{sat} (ft/day)*	Initial Moisture Content ** (%)	Saturated Moisture Content ** (%)	Dry Bulk Density (lb/ft^3)	Calculated Porosity (%)
9-1213-07	GB-2 at 15 ft	Constant Head	2.90E-04	8.22E-01	11.2%	24.5%	94.8	41.6%

*Corrected to 20 °C
**Gravimetric Moisture (percent by mass)

Client: Gordon Environmental, Inc.
213 Camino Del Pueblo
Bernalillo, NM 87004-

Attn: Larry Coons
Project Name: Gordon Environmental, Inc. 2008 Misc. Testing

ABQ, NM

Project Manager: Herman Garcia

Report Date: November 10, 2009

Project #: 8-519-005168
Work Order #: 2
Lab #: 9-1213-07
Sampled By: Client
Date Sampled: Unknown
Material: Silty Clayey Sand
Sample Source: GB-2 at 15 ft

SOILS/AGGREGATES

Measurement of Collapse Potential of Soils (ASTM D5333)

Sample Preparation: In Situ

Initial Volume (in^3):	4.60	**Final Volume (in^3):**	4.40
Initial Moisture (%):	17.7%	**Final Moisture (%)**	15.5%
Initial Dry Density (lb/ft^3):	80.3	**Initial Dry Density (lb/ft^3):**	83.7
Initial Degree of Saturation:	45%	**Final Degree of Saturation:**	42%
Initial Void Ratio:	1.0	**Final Void Ratio:**	0.9
Estimated Specific Gravity:	2.600	**Saturated At:**	Not Saturated

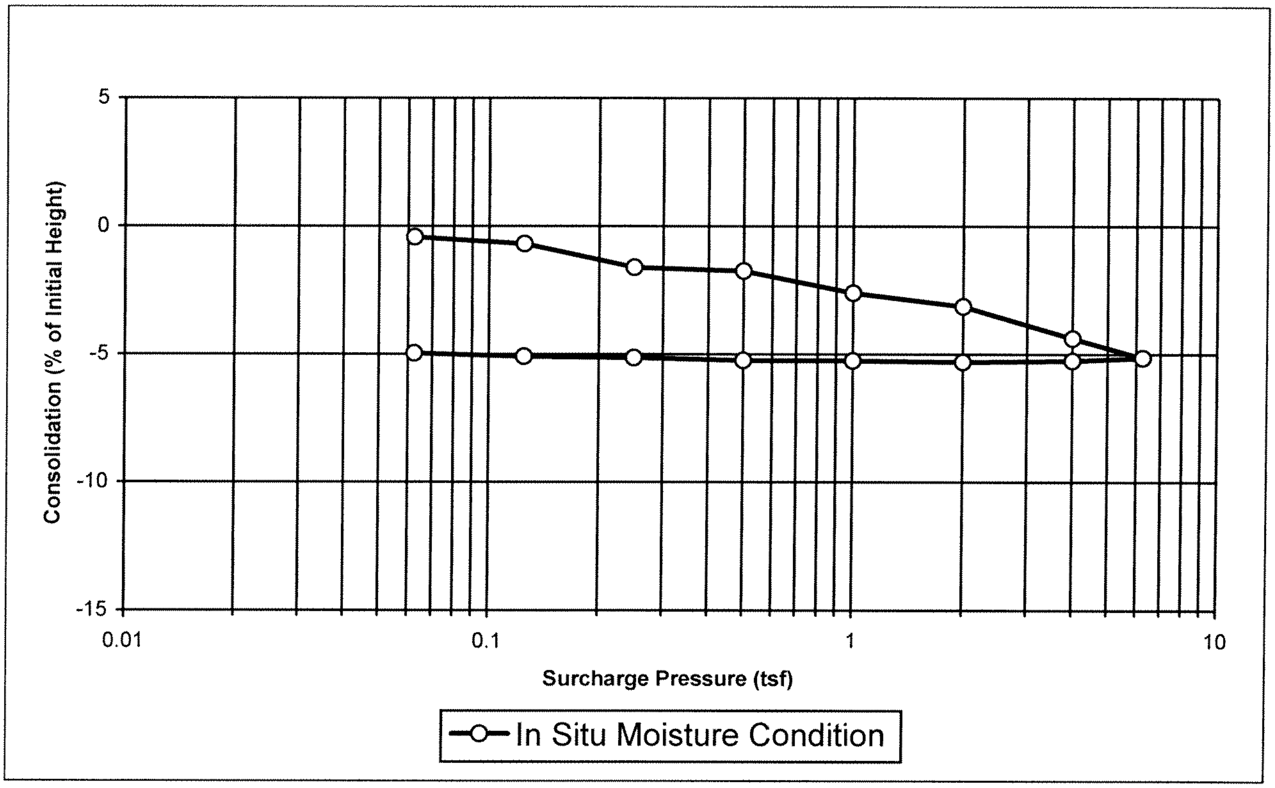

Reviewed By:
Jan

Distribution: **Client** ☑ **File** ☑ **Supplier:** ☑ **Other:** Addressee (2)
Email: ☐

Calculated Porosities

Lab #	**Test Sample**	%
9-1213-02	K_{sat}	50.6
9-1213-02	Settlement	50.5
9-1213-04	K_{sat}	29.4
9-1213-04	Swell	39.9
9-1213-07	K_{sat}	41.6
9-1213-07	Settlement	29.9

Based on a specific gravity of 2.6 g/cm^3. Note that the Ksat and settlement for lab number 9-1213-04 were taken from different ring samples

GORDON ENVIRONMENTAL INC. *Soil/Rock Coring Log* *Page* 1 *of* 2

Depth (ft)	Boring Operation	% Core Recovery	Drill Time: Clock Time	Drill Time: Elapsed Time per 5 feet (min)	Sample Interval	Rig Blow Counts (per foot)	Lab Dry Density (lb/cf)	Lab Moisture (% Dry Wt)	Lab Unified Soil Classification	Graphical Log	Comments	Visual Field Classification
0	A/C	25 ↓	10/3/09 0957								HSA continuous core w/ 6.5” OD HSA and 3.5” OD (2.5” ID) 5’ continous sampler	**SAND; fine; reddish tan; slightly moist to 4’**
	↓	100 ↓										**SAND; silty v. fine to fine; reddish brown; slightly moist; thin brown clay lenses @ 4’; caliche @ 5’**
10	↓	↓	1005									
	↓	↓									Variable caliche/ caliche cementation	
20	↓	↓	1024									
	↓	↓									Gravel to ½” @ 27’	
30	↓	↓	1035									
	↓	↓									Caliche stringers/ lenses	
40	↓	↓	1047								Gravel to 1” @ 43’ to 44’	**SAND; v. fine to fine; pinkish tan; dry to slightly moist**
	↓	↓										**CLAYSTONE [CHINLE FM]; variable silt; reddish brown; dry to slightly moist**
50	↓	↓	1104									
	↓	↓									Grey clay lenses/ inclusions; dry	
60	↓	↓	1315									**CLAYSTONE; red to purple; dry**
70	↓	↓	1359									
80	↓	↓	1450								Grey clay lenses/ inclusions; dry	
90	↓	↓	1536									
	↓	↓	10/3/09 0750									
100	↓	↓	0818									

SAMPLE TYPE

A - Auger cuttings: NR = No recovery
R - Rotary cuttings
C - Continuous core (as specified)

GROUNDWATER

DEPTH	HOUR	DATE
NONE		

CORING LOG

CH-1

(1 of 2)

F:\GEI\Templates\Soil-Rock Coring Log

LOGGED BY **L Coons**
DRILLER **Rodgers - John Aguirre**
DATE COMPLETED **10/9/09**
RIG/BORING TYPE **CME 75 HSA/Core**
SURFACE ELEVATION **3410.89**
PROJECT **SSI - West**
PROJECT NUMBER **530.01.01/02**
LOCATION **N528975.8 E921004.5 (NAD83)**

GORDON ENVIRONMENTAL INC. *Soil/Rock Coring Log* Page 2 of 2

Depth (ft)	Boring Operation	% Core Recovery	Drill Time: Clock Time	Drill Time: Elapsed Time per 5 feet (min)	Sample Interval	Rig Blow Counts (per foot)	Lab Dry Density (lb/cf)	Lab Moisture (% Dry Wt)	Lab Unified Soil Classification	Graphical Log	Comments	Visual Field Classification
100	A/C		10/4/09								very dense; slow drilling	**CLAYSTONE; reddish brown; dry**
		75	0857									
110		50	0944									
		50	1019								Grey clay lenses/ inclusions; dry	
120		100	1103									
			1215	33								
			1248									
			1259	60								
130			1359									
			1413	45								
			1458									
			1510	45							Tripped out augers on 10/5/09 @ 0850	
140			1555 10/9/09									
			1409	85							Driller added ~ 1.5 gal each of Quick Foam and Con Det to facilitate drilling on 10/9/09	
		75	1534									
			1544	9								
150		100	1553								Thin (6") layers of moderately indurated siltsone; reddish brown; dry @ 148'	
			1605									
		100	1628	23				13	CL			**TD = 154'@ 1628 on 10/9/09** **Plugged boring to surface on 10/9/09 w/ 5% bentonite grout mixture**
160												
170												
180												
190												
200												

SAMPLE TYPE

A - Auger cuttings: NR = No recovery
R - Rotary cuttings
C - Continuous core (as specified)

GROUNDWATER

DEPTH	*HOUR*	*DATE*
NONE		

LOGGED BY **L Coons**
DRILLER **Rodgers - John Aguirre**
DATE COMPLETED **10/9/09**
RIG/BORING TYPE **CME 75 HSA/Core**
SURFACE ELEVATION **3410.89**
PROJECT **SSI - West**
PROJECT NUMBER **530.01.01/02**
LOCATION **N528975.8 E921004.5 (NAD83)**

CORING LOG

CH-1

(2 of 2)

F:\GEI\Templates\Soil-Rock Coring Log

GORDON ENVIRONMENTAL INC. *Soil/Rock Coring Log* Page 1 of 2

Depth (ft)	Boring Operation	% Core Recovery	Drill Time		Sample Interval	Rig Blow Counts (per foot)	Lab Dry Density (lb/cf)	Lab Moisture (% Dry Wt)	Lab Unified Soil Classification	Graphical Log	Comments	Visual Field Classification
			Clock Time	Elapsed Time per 5 feet (min)								
0	A/C	0	10/5/09 1328 1330	2							HSA continuous core w/ 6.5" OD HSA and 3.5" OD (2.5" ID) 5' continous sampler	**SAND; v. fine to fine; rust tan; slightly moist to moist; soft**
			1456 1502								Soft to medium hardness	**SAND; silty v. fine to fine; rust tan; dry to slightly moist; minor caliche**
10		25	1508 1515	6								
		25	1519 1522	7							Moderately indurated; grey-rust to tan	
20		50	1528 1532	3							Soft	**CALICHE; silty v. fine to fine; pinkish white to white; dry to slightly moist**
			1537 1539	4								
30			1546 1548	2							Minor gravel to 1" dia; lt tan	
			1553 1555	2								
40			1600	2							Friable	SILT/SILTSTONE; gravelly; reddish brown; dry
			1606 10/6/09 0745	6							Gravel to 1"; minor black mafic(?) inclusions	**CLAYSTONE [CHINLE FM]; silty w/ gravel; reddish brown w/ grey clay inclusions; dry**
			0752									
50		75	0757 0804	7								
			0757 0804	7							Moderatley dense; plastic	**CLAYSTONE; reddish brown; dry**
60			0810 0826	16								
			0833 0844	11								
70			0849 0902	13							Grey clay inclusions w/ mafic dentrites	
			0910 0920	10								
80			0927 0938	11							[change to combination bit]	
			10/7/09 1240 1250	10								
90			1257 1321	24								
			1332 1350	18							Grey clay lenses/ inclusions; dry	
100			1404 1422	18								

SAMPLE TYPE

A - Auger cuttings: NR = No recovery
R - Rotary cuttings
C - Continuous core (as specified)

GROUNDWATER

DEPTH	*HOUR*	*DATE*
NONE		

LOGGED BY **L Coons**
DRILLER **Rodgers - John Aguirre**
DATE COMPLETED **10/8/09**
RIG/BORING TYPE **CME 75 HSA/Core**
SURFACE ELEVATION **3403.4**
PROJECT **SSI - West**
PROJECT NUMBER **530.01.01/02**
LOCATION **N527727.1 E921002.4 (NAD83)**

CORING LOG

CH-2

(1 of 2)

F:\GEI\Templates\Soil-Rock Coring Log

GORDON ENVIRONMENTAL INC. *Soil/Rock Coring Log* *Page* 2 *of* 2

Depth (ft)	*Boring Operation*	*% Core Recovery*	*Drill Time*: *Clock Time*	*Drill Time*: *Elapsed Time per 5 feet (min)*	*Sample Interval*	*Rig Blow Counts (per foot)*	*Lab Dry Density (lb/cf)*	*Lab Moisture (% Dry Wt)*	*Lab Unified Soil Classification*	*Graphical Log*	*Comments*	*Visual Field Classification*
100	A/C		1431 1452								Very dense; slow drilling	**CLAYSTONE; reddish brown; dry**
		100	1502 1528	19								
110		100	1539 1558	26								
		100	10/8/09 0756 0839	19								
120		75	0854 0933	42							Very dense; plastic`	
		75	0947 1030	39								
130		50	1047 1100	43								
		75	1228 1306	13							Driller added ~ 1.5 gal of Quick Foam to facilitate drilling on 10/8/09	
140			1353 1405	22								
			1419 1425	12							Thin (6”) layers of moderately indurated siltsone; reddish brown; dry @ 145’	
				6 (4’)				8	CL			
150												**TD = 149’@ 1425 on 10/8/09** **Plugged boring to surface on 10/8/09 w/ 5% bentonite grout mixture**
160												
170												
180												
190												
200												

SAMPLE TYPE

A - Auger cuttings: NR = No recovery
R - Rotary cuttings
C - Continuous core (as specified)

GROUNDWATER

DEPTH	*HOUR*	*DATE*
NONE		

LOGGED BY **L Coons**
DRILLER **Rodgers - John Aguirre**
DATE COMPLETED **10/8/09**
RIG/BORING TYPE **CME 75 HSA/Core**
SURFACE ELEVATION **3403.40**
PROJECT **SSI - West**
PROJECT NUMBER **530.01.01/02**
LOCATION **N527727.1 E921002.4 (NAD83)**

CORING LOG

CH-2

(2 of 2)

F:\GEI\Templates\Soil-Rock Coring Log

GORDON ENVIRONMENTAL INC. *Soil/Rock Coring Log* Page 1 of 1

Depth (ft)	Boring Operation	% Core Recovery	Drill Time: Clock Time	Drill Time: Elapsed Time per 5 feet (min)	Sample Interval	Rig Blow Counts (per foot)	Lab Dry Density (lb/cf)	Lab Moisture (% Dry Wt)	Lab Unified Soil Classification	Graphical Log	Comments	Visual Field Classification
0	A/C		10/10/09 0837 0838								HSA continuous core w/ 6.5" OD HSA and 3.5" OD (2.5" ID) 5' continous sampler	**SAND; v. fine to fine; yellow tan to rust tan; slightly moist; soft**
		30	0843 0845	1							Lighlty indurated @ 4'	**SAND; silty v. fine to fine; red to pinkish tan; slightly moist**
10		100	0848 0850	2							Root fibers	**CALICHE; silty v. fine to fine; pinkish white to light tan; dry to slightly moist**
		100	0853 0855	2								
20		100	0858 0859	2							Variable induration	
		60	0903 0904	1								
30		50	0908 0909	1								
		30	0913 0914	1							Minor gravel to 1/4" to ½" dia @ 35'; soft	
40		30	0917 0918	1							Gravel 1/4" to ½"	**SAND; gravelly fine to v. coarse; minor silt; reddish brown; slightly moist**
		100	0923 0924	1							Gravel to 1"; minor black mafic(?) inclusions	**SILT/SILTSTONE [CHINLE FM]; gravelly; reddish brown; dry to slightly moist**
50			0928 0930	1							Fine to medium sandy; s. moist	
			0936 0938	2							Clay and gravel @ 54'; dry	
60			0943 0949	2							Mod. dense; plastic	**CLAYSTONE; reddish brown; dry**
											Mod. soft; fissle; micaceous	**SILTSTONE; v. fine sandy; reddish brown; dry to slightly moist**
			0953 1002	9							Dense; plastic	**CLAYSTONE; silty w/ gravel; reddish brown w/ grey clay inclusions; dry**
70			1009 1014	6								
			1019 1030	9								
				5 (4')				20	ML			
80												**TD = 79'@ 1030 on 10/10/09** **Plugged boring to surface on 10/10/09 w/ 5% bentonite grout mixture**
90												
100												

SAMPLE TYPE

A - Auger cuttings: NR = No recovery
R - Rotary cuttings
C - Continuous core (as specified)

GROUNDWATER

DEPTH	HOUR	DATE
NONE		

CORING LOG

CH-3

LOGGED BY **L Coons**
DRILLER **Rodgers - John Aguirre**
DATE COMPLETED **10/10/09**
RIG/BORING TYPE **CME 75 HSA/Core**
SURFACE ELEVATION **3401.30**
PROJECT **SSI - West**
PROJECT NUMBER **530.01.01/02**
LOCATION **N527335.9 E921307.5 (NAD83)**

APPLICATION FOR PERMIT
SUNDANCE WEST

VOLUME III: LANDFILL ENGINEERING CALCULATIONS
SECTION 8: SETTLEMENT CALCULATIONS

ATTACHMENT III.8.B

GEOTECHNICAL ASPECTS OF LANDFILL DESIGN AND CONSTRUCTION

QAIN, KOERNER, AND GRAY, 2002

GEOTECHNICAL ASPECTS OF LANDFILL DESIGN AND CONSTRUCTION

Xuede Qian
Geotechnical Engineering Specialist
Michigan Department of Environmental Quality

Robert M. Koerner
H. L. Bowman Professor of Civil Engineering, Drexel University
Director, Geosynthetic Research Institute

Donald H. Gray
Professor of Civil and Environmental Engineering
The University of Michigan

Prentice Hall

PRENTICE HALL
Upper Saddle River, New Jersey 07458

TABLE 6.5 Index Properties of Solid Waste

Source	Unit Weight		Volumetric Moisture Content	Porosity	Void Ratio
	lb/ft^3	kN/m^3			
Rovers and Farquhar (1973)	59	9.3	0.16	–	–
Fungaroli (1979)	63	9.9	0.05	–	–
Wigh (1979)	73	11.5	0.08	–	–
Walsh and Kinman (1979)	90	14.1	0.17	–	–
Walsh and Kinman (1981)	89	14.0	0.17	–	–
Schroeder et al. (1984a, b)	–	–	0.28	0.52	1.08
Oweis et al. (1990)	40 to 90	6.3 to 14.1	0.10 to 0.20	0.40 to 0.50	0.67 to 1.0
Schroeder et al. (1994a, b)	–	–	0.29	0.67	2.03
Zornberg et al. (1999)	64 to 95	10 to 15	0.30	0.49 to 0.62	1.02 to 1.65

Based on its constituent composition the average moisture content of the solid waste shown in Table 6.4 can be calculated as follows:

$$\begin{aligned} w_d &= [(60.0)(10.4) + (50.0)(19.1) + (20.0)(34.6) + (10.0)(6.0) + (15.0)(5.0) \\ &\quad + (15.0)(9.5) + (2.0)(4.0) + (2.0)(7.2) + (8.0)(2.8) + (3.0)(1.4)]/100 \\ &= (624 + 955 + 692 + 60 + 75 + 142.5 + 8 + 14.4 + 22.4 + 4.2)/100 \\ &= 2597.5/100 \\ &= \underline{26.0\,\%} \end{aligned}$$

Thus, the average dry gravimetric moisture content of the solid waste shown in Table 6.4 is 26.0%.

More information about the moisture content of solid waste can be found in Table 6.5. It should be noted that the values of moisture content listed in Table 6.5 are calculated on a volume basis and differ from those calculated on a weight basis, which is more common to geotechnical analyses.

6.4 POROSITY OF MUNICIPAL SOLID WASTE

Porosity is defined as the ratio of the volume of voids to the total volume occupied by a solid waste or soil. Void ratio is defined as the ratio of the volume of voids to the volume of solids. Porosity can be related to the void ratio by using the relationships

$$n = \frac{e}{1 + e} \tag{6.7}$$

and

$$e = \frac{n}{1 - n} \tag{6.8}$$

where n = porosity of solid waste; and
e = void ratio of solid waste.

The porosity of MSW varies typically from 0.40 to 0.67 depending on the compaction and composition of the waste. For comparison, a typical compacted clay liner material will have a porosity of about 0.40. Table 6.5 shows a summary of the index properties of municipal solid waste, which includes initial volumetric moisture content, initial porosity, initial void ratio and unit weight data.

6.5 HYDRAULIC CONDUCTIVITY OF MUNICIPAL SOLID WASTE

Proper assessment of the hydraulic conductivity of municipal solid waste is important in the design of leachate collection systems and in leachate recirculation planning particularly for bioreactor landfills (see Chapter 15). The hydraulic conductivity can be measured using a field leachate pumping test and a large-scale percolation test in test pits or by using large-diameter permeameters in the laboratory.

Hydraulic conductivity measured in test pits at several landfills in Canada by Landva and Clark (1990) is plotted against unit weight in Figure 6.3. The values shown are based on an intermediate stage of water level recession, after the flow had stabilized and before any debris could clog the voids. The measured coefficients of hydraulic conductivity (1.0×10^{-3} to 4.0×10^{-2} cm/sec) correspond to those associated with clean sand and gravel. Qian (1994) used three-year field data from an active landfill in the state of Michigan to develop a relationship between precipitation and leachate volume from a primary leachate collection system with time. With this information, the hydraulic conductivity of the waste can be calculated based on the water travel time, hydraulic gradient, and waste thickness. The hydraulic conductivity calculated in this way was estimated to be about 9.2×10^{-4} to 1.1×10^{-3} cm/sec. Table 6.6 summarizes the hydraulic conductivity of different types of MSW taken from the

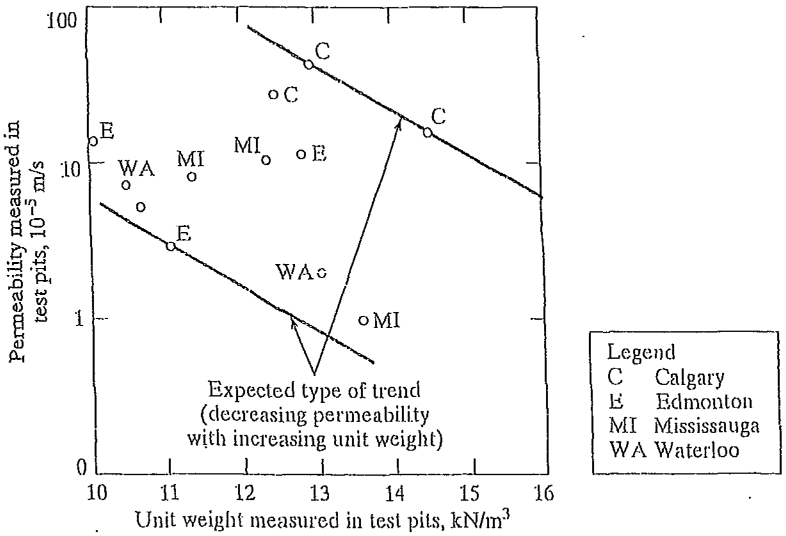

FIGURE 6.3 Unit Weight and Permeability (from Percolation) as Measured in Landfill Test Pits (Landva and Clark, 1990)

FIGURE 6.9 Compressive Strain versus Log Pressure for Various Landfills in Canada (Landva and Clark, 1990)

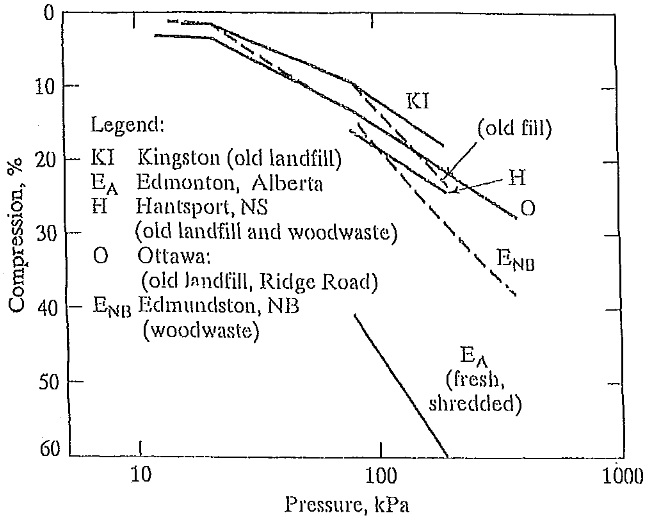

KI: $C_C' = 0.17$ ($p = 20 - 200$ kPa)
O: $C_C' = 0.21$ ($p = 100 - 400$ kPa)
E_A: $C_C' = 0.35$ ($p = 80 - 200$ kPa)
E_{NB}: $C_C' = 0.36$ ($p = 100 - 400$ kPa)
H: $C_C' = 0.22$ ($p = 80 - 200$ kPa)

cans; the lower values are for the less resilient materials. The maximum C_c for peat is about one-third greater than the maximum observed for waste fills.

Landva and Clark (1990) found that the coefficient of secondary consolidation, C_α, (the gradient of the compression versus log time relationship) was in the range 0.2 to 3.0 percent per log cycle time, depending on the type of waste involved. Field testing results using a settlement platform (Keene, 1977) showed that the coefficient of secondary consolidation, C_α, varies between 0.014 and 0.034. Too few tests have been carried out for any firm relationship to be established between the value of C_α and the type of waste, but it does appear that C_α increases with increasing organic content. Sowers (1973) pointed that the coefficient of secondary consolidation, C_α, is also a

FIGURE 6.10 Compressibility of MSW Landfills (Sowers, 1973)

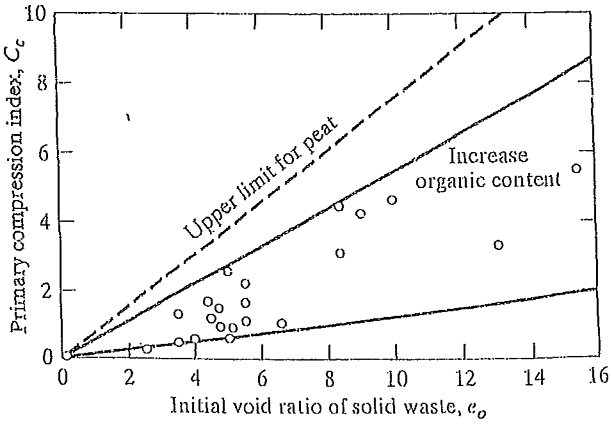

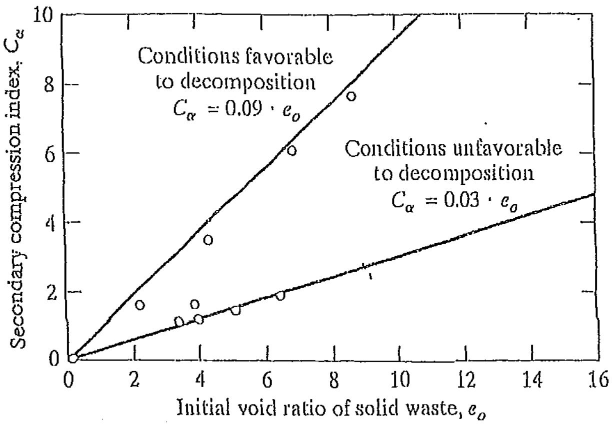

FIGURE 6.11 Secondary Compression of MSW Landfills (Sowers, 1973)

function of the void ratio, as shown in Figure 6.11. For any given void ratio, there is a large range in C_α, related to the potential for physico-chemical and bio-chemical decay. The value is high if the organic content subject to decay is large and the environment is favorable: namely, warm, moist, with fluctuating water table that pumps fresh air into the fill. The value is low for more inert materials and an unfavorable environment. More research and data are necessary before this relationship can be defined more closely.

The most widely reported compressibility parameter is the modified secondary compression index (C'_α). The reported values of C'_α range from 0.001 to 0.59. The lowest value represents the compressibility of a landfill that had been subjected to dynamic compaction. For typical landfills the lower limit of C'_α is generally around 0.01 to 0.03. This compares to 0.005 to 0.02 for common clays (Holtz and Kovacs, 1981). Fasset et al. (1994) observed that the typical upper limit of C'_α appears to be approximately 0.1.

According to Yen and Scanlon (1975), the settlement rate of waste increases with depth, hence larger values of C'_α should be associated with thicker fills. They observed that this effect leveled off at about 90 ft. and suggested that conditions within the landfill at great depths limit the biological activity to anaerobic decomposition, which is much slower than the aerobic decomposition believed to occur in shallower fills.

The values of C_α and C'_α, like C_c and C'_c, are dependent on the values used for e_0 or H_0. The value of C'_α is also dependent on stress level, time, and on how the origin of time is selected. The waste placement or filling period for landfills is often long and should be taken into consideration for settlement rate analyses (Yen and Scanlon, 1975). The zero time selection has a large impact on C'_α particularly during earlier phases of a landfill (Fassett et al., 1994)

An additional problem with determining C'_α is the fact that this parameter is generally not constant. Edgers (1992) presents settlement log-time data from 22 case histories (shown in Figure 6.12). The majority of the curves show a relatively flat slope (i.e. low C'_α values) at small times, but at larger times the slope greatly increases (Figure 6.13). They attributed the higher slopes in the later stages of compression to increasing decomposition, but it may simply be an artifact of the log-time scale. It is

d = diameter of perforated hole or width of perforated slot on the pipe, in or m; and

n = number of perforated holes or slots per row per foot of pipe.

Pipe stiffness is measured according to ASTM D2412 (Standard Test Method for External Loading Properties of Plastic Pipe by Parallel-Plate Loading). The elastic modulus of the pipe material depends on the type of resin and formulation being used. Three formulas that can be used to calculate pipe stiffness are

$$PS = \frac{E \cdot I}{0.149 \cdot r^3} \tag{9.24}$$

$$PS = 0.559 \cdot E \cdot (t/r)^3 \tag{9.25}$$

and

$$PS = 4.47 \cdot \frac{E}{(SDR - 1)^3} \tag{9.26}$$

where PS = pipe stiffness, lb/in^2 or kN/m^2;

E = elastic modulus of the pipe material, lb/in^2 or kN/m^2;

I = moment of inertia of the pipe wall per unit length, $I = t^3/12$, in^4/in = in^3 or m^4/m = m^3;

r = mean radius of pipe, in or m;

t = wall thickness of pipe, in or m; and

SDR = standard dimension ratio, the same as the dimension ratio.

The allowable deflection ratios for a typical commercial polyethylene pipe are listed in Table 9.4.

Deflections of buried flexible pipe are commonly calculated using Equation 9.16 or 9.21. These equations use the soil reaction modulus, E', as a surrogate parameter for soil stiffness. It should be noted that the values of E' in Table 9.3 only apply for soil fills of less than 50 ft (15 m). However, megafills built over leachate collection pipes often exceed 150 ft (46 m) in height. The soil reaction modulus is not a directly measurable soil parameter; instead it must be determined by back-calculation using observed pipe deflections. Research by Selig (1990) showed that E' is a function of the bedding condition and overburden pressure. Selig's studies were carried out to seek a correlation between the soil reaction modulus and soil stiffness parameters such as

TABLE 9.4 Allowable Deflection Ratio of Polyethylene Pipe

SDR	Allowable Deflection Ratio
11	2.7%
13.5	3.4%
15.5	3.9%
17	4.2%
19	4.7%
21	5.2%
26	6.5%
32.5	8.1%

Young's modulus of soil, E_s, and the constrained modulus of soil, M_s, where E_s and D_s are related through Poisson's ratio of soil, v_s, by

$$M_s = \frac{E_s \cdot (1 - \nu_s)}{(1 + \nu_s)(1 - 2 \cdot \nu_s)} \tag{9.27}$$

where M_s = constrained modulus of soil, lb/ft^2 or kN/m^2;
E_s = elastic modulus of soil, lb/ft^2 or kN/m^2; and
ν_s = Poisson's ratio of soil.

The studies and analyses by Neilson (1967), Allgood and Takahashi (1972), and Hartely and Duncan (1987) indicated that for

$$E' = k \cdot M_s \tag{9.28}$$

the value of k may vary from 0.7 to 2.3. Using $k = 1.5$ as a representative value and $\nu_s = 0.3$, in addition to combining Equations 9.27 and 9.28 yields the following relationship between the elastic modulus of the pipe and soil (Selig, 1990):

$$E' = 2 \cdot E_s \tag{9.29}$$

The values of elastic parameters, E_s and ν_s, can be found in Table 9.5 according to different percents of density from a standard Proctor compaction test (ASTM D698).

TABLE 9.5 Elastic Soil Parameters (Selig, 1990)

Soil Type	Stress Level		85% Standard Density			95% Standard Density		
			E_s			E_s		
	psi	kPa	psi	MPa	ν_s	psi	MPa	ν_s
SW, SP, GW, GP	1	7	1,300	9	0.26	1,600	11	0.40
	5	35	2,100	14	0.21	4,100	28	0.29
	10	70	2,600	18	0.19	6,000	41	0.24
	20	140	3,300	23	0.19	8,600	59	0.23
	40	280	4,100	28	0.23	13,000	90	0.25
	60	420	4,700	32	0.28	16,000	110	0.29
GM, SM, ML, and GC, SC with < 20% fines	1	7	600	4	0.25	1,800	12	0.34
	5	35	700	5	0.24	2,500	17	0.29
	10	70	800	6	0.23	2,900	20	0.27
	20	140	850	6	0.30	3,200	22	0.29
	40	280	900	6	0.38	3,700	25	0.32
	60	420	1,000	7	0.41	4,100	28	0.35
CL, MH, GC, SC	1	7	100	1	0.33	400	3	0.42
	5	35	250	2	0.29	800	6	0.35
	10	70	400	3	0.28	1,100	8	0.32
	20	140	600	4	0.25	1,300	9	0.30
	40	280	700	5	0.35	1,400	10	0.35
	60	420	800	6	0.40	1,500	10	0.38

Table 12.2 Comparison of Settlement and Construction Period (Yen and Scanlon, 1975)

Range of Fill Depth H_f, feet, (meter)	Average Construction Period, t_c (month)	Total Time Required for Construction and Settlement (months)	Approximate Time Required for Settlement to Complete (month)
40 to 80 (12 to 24)	12	113	101
40 to 80 (12 to 24)	72	324	252
80 to 100 (24 to 30)	12	245	233
80 to 100 (24 to 30)	72	310	238

Used with permission of ASCE.

12.4 ESTIMATION OF LANDFILL SETTLEMENT

The usual laboratory tests for soil consolidation testing are not well suited for obtaining accurate consolidation parameters for solid waste that has a heterogeneous composition and extremely large particle sizes. By analyzing the field settlement data from some large-scale pilot landfill cells, Sowers (1973) proposed an alternative method to estimate the amount of the landfill settlement. In recent years, this method has been revised and refined several times by other investigators.

The settlement of solid waste includes primary settlement and long-term secondary compression. The total amount of settlement is given by the expression

$$\Delta H = \Delta H_c + \Delta H_\alpha \tag{12.3}$$

where ΔH = total settlement of solid waste;
ΔH_c = primary settlement of solid waste;
ΔH_α = long-term secondary settlement of solid waste.

12.4.1 Settlement of New Solid Waste

Based on the procedure proposed by Sowers (1973), the equations that follow can be used to calculate the settlement for new landfilled solid waste. The *Initial primary settlement* is given by

$$\Delta H_c = C_c \cdot \frac{H_0}{1 + e_0} \cdot \log \frac{\sigma_i}{\sigma_0} \tag{12.4}$$

or

$$\Delta H_c = C_c' \cdot H_0 \cdot \log \frac{\sigma_i}{\sigma_0} \tag{12.5}$$

where ΔH_c = primary settlement;
e_0 = initial void ratio of the waste layer before settlement;
H_0 = initial thickness of the waste layer before settlement;
C_c = primary compression index (recall Figure 6.10);
C_c' = modified primary compression index, $C_c' = 0.17 \sim 0.36$;
σ_0 = previously applied pressure in the waste layer (assumed equal to the compaction pressure, $\sigma_0 = 1{,}000$ lb/ft^2 or 48 kN/m^2);
σ_i = total overburden pressure applied at the mid level of the waste layer.

The previous compaction pressure applied on the solid waste layer during placement with compaction equipment is assumed to be 1,000 lb/ft^2 (48 kN/m^2) based on 1973 compaction efforts for municipal solid waste landfills. In other words, the waste that has been placed in the landfill is essentially incompressible at normal pressure below 1,000 lb/ft^2 (48 kN/m^2) due to the preconsolidation effect caused by previous compaction of the material. The value of the previously applied pressure, σ_o, should be changed during estimation of settlement if the compaction effort is much lower or higher than 1,000 lb/ft^2 (48 kN/m^2) for a specific landfill project. Indeed, current practices of using waste compactors in the 100 to 150 U.S. tons (900 to 1,300 kN) range will significantly increase the value of σ_o.

The *long-term secondary settlement* can be obtained from

$$\Delta H_\alpha = C_\alpha \cdot \frac{H_0}{1 + e_0} \cdot \log \frac{t_2}{t_1} \tag{12.6}$$

or

$$\Delta H_\alpha = C'_\alpha \cdot H_0 \cdot \log \frac{t_2}{t_1} \tag{12.7}$$

where ΔH_α = long-term secondary settlement;
e_0 = initial void ratio of the waste layer before settlement;
H_0 = initial thickness of the waste layer before settlement;
C_α = secondary compression index (recall Figure 6.11);
C'_α = modified secondary compression index, $C'_\alpha = 0.03 \sim 0.1$;
t_1 = starting time of the time period for which long-term settlement of the layer is desired, $t_1 = 1$ month;
t_2 = ending time of the time period for which long-term settlement of the layer is desired.

Because a standard consolidation test method for solid waste has not yet been developed, the selection of waste compression indices are mainly based on experience and limited field data. The value of the primary compression index C_c can be selected from Figure 6.10 based on the initial void ratio and organic content of the solid waste. The value of the secondary compression index C_α can be selected from Figure 6.11 based on the initial void ratio of the waste and the decomposition conditions.

Generally, the initial void ratio of municipal solid waste placed in a landfill after compaction is quite difficult to determine, and hence the values of the primary compression index C_c and the secondary compression index C_α cannot be estimated readily for settlement analysis. Accordingly, an alternative approach has been used in engineering practice—namely, the use of a "modified" primary compression index C'_c and a "modified" secondary compression index C'_α. Based on experience, the value of the modified primary compression index C'_c varies from 0.17 to 0.36, and the value of the modified secondary compression index C'_α varies from 0.03 to 0.1 for municipal solid waste (depending on the initial compaction effort and composition of the solid waste). The value of the modified secondary compression index C'_α for common clay ranges from 0.005 to 0.02. Therefore, the secondary settlement for municipal solid waste is approximately five to six times that of common clay.

12.4.2 Settlement of Existing Solid Waste

The following equations can be used to calculate the settlement of an existing solid waste landfill caused by vertical expansion (Chapter 14) or other additional extra loading, such as a light structure on a raft foundation.

The *primary settlement* is obtained by

$$\Delta H_c = C_c \cdot \frac{H_0}{1 + e_0} \cdot \log \frac{\sigma_0 + \Delta\sigma}{\sigma_0} \tag{12.8}$$

or

$$\Delta H_c = C_c' \cdot H_0 \cdot \log \frac{\sigma_0 + \Delta\sigma}{\sigma_0} \tag{12.9}$$

where ΔH_c = primary settlement;
e_0 = initial void ratio of the waste layer before settlement;
H_0 = initial thickness of the waste layer of the existing landfill;
C_c = primary compression index;
C_c' = modified primary compression index, $C_c' = 0.17 \sim 0.36$;
σ_0 = existing overburden pressure acting at the mid level of the waste layer;
$\Delta\sigma$ = increment of overburden pressure due to vertical expansion or other extra load.

The *long-term secondary settlement* is given by

$$\Delta H_\alpha = C_\alpha \cdot \frac{H_0}{1 + e_0} \cdot \log \frac{t_2}{t_1} \tag{12.10}$$

or

$$\Delta H_\alpha = C_\alpha' \cdot H_0 \cdot \log \frac{t_2}{t_1} \tag{12.11}$$

where ΔH_α = secondary settlement;
e_0 = initial void ratio of the waste layer before starting secondary settlement;
H_0 = initial thickness of the waste layer before starting secondary settlement;
C_α = secondary compression index;
C_α' = modified secondary compression index, $C_\alpha' = 0.03 \sim 0.1$;
t_1 = starting time of the secondary settlement. It is assumed to be equal to the age of the existing landfill for vertical expansion project;
t_2 = ending time of the secondary settlement.

(e.g., temperature within landfill and oxygen reaching the waste) still is not entirely clear. These functions should be used with caution in engineering practice and should be supported by additional testing data and research.

12.7 ESTIMATION OF LANDFILL FOUNDATION SETTLEMENT

If the landfill is underlain by a soil layer, particularly a thick layer of soft, fine-grained soil, consolidation settlements may be large. In these cases, design analyses should consider settlement of the foundation clay layer. Both primary consolidation and long-term secondary settlement should be considered. Calculations are performed using conventional equations from soil mechanics theory and a time frame at least equal to the active life and postclosure care period of the landfill.

Excessive settlement of an underlying foundation clay layer will affect the performance of a landfill liner and leachate collection system. The purposes of analyzing the settlement of a foundation clay layer and overlying landfill liner and leachate collection/removal system are as follows:

(i) Tensile strain induced in the liner system and leachate collection and removal system must be limited to a minimum allowable tensile strain for the components of these two systems. The compacted clay liner usually has the smallest allowable tensile strain value between 0.1% and 1.0% and an average allowable tensile strain of 0.5%.

(ii) Post-settlement grades of the landfill cell subbase and the leachate collection pipes must be sufficient to maintain leachate performance to prevent grade reversal and leachate ponding in accordance with the rule requirements.

12.7.1 Total Settlement of Landfill Foundation

The total settlement of landfill foundation soil can be divided into three portions: elastic settlement, primary consolidation settlement, and secondary consolidation settlement. The settlement of sandy soils includes only elastic settlement. The settlement of clayey soils includes all three types of settlements. The total settlement of clayey soil is equal to the sum of the elastic settlement and the primary and secondary settlements. Because the permeability of clay is quite low, it takes a long time to complete the whole process of consolidation settlement. The settlement of clayey soil is usually much larger than the settlement of sandy soils.

Because the settlement of sandy soils includes only elastic settlement, the settlement of sand layer can be calculated from the Elastic Settlement equation, which is

$$Z_e = (\Delta\sigma/M_s)H_o \tag{12.20}$$

where Z_e = elastic settlement of soil layer, ft or m;
H_o = initial thickness of soil layer, ft or m;
$\Delta\sigma$ = increment of vertical effective stress, lb/ft^2 or kN/m^2;
M_s = constrained modulus of soil, lb/ft^2 or kN/m^2.

The constrained modulus is given by

$$M_s = \frac{E_s \cdot (1 - v_s)}{(1 + v_s)(1 - 2 \cdot v_s)} \tag{12.21}$$

where M_s = constrained modulus of soil, lb/ft^2 or kN/m^2;
E_s = elastic modulus of soil, see Table 9.5, lb/ft^2 or kN/m^2;
v_s = Poisson's ratio of soil, see Table 9.5.

The *primary consolidation settlement* is given by

$$Z_c = C_r \cdot \frac{H_{oi}}{1 + e_{oi}} \cdot \log \frac{p_c}{\sigma_o} + C_c \cdot \frac{H_o}{1 + e_{oi}} \cdot \log \frac{\sigma_o + \Delta\sigma}{p_c} \tag{12.22}$$

where Z_c = primary consolidation settlement of clay layer, ft or m;
H_o = initial thickness of clay layer, ft or m;
e_{oi} = initial void ratio of clay layer;
C_r = recompression index;
C_c = primary compression index.
σ_o = initial vertical effective stress, lb/ft^2 or kN/m^2;
p_c = preconsolidation pressure, lb/ft^2 or kN/m^2;
$\Delta\sigma$ = increment of vertical effective stress, lb/ft^2 or kN/m^2.

The *secondary compression settlement* is given by

$$Z_\alpha = C_\alpha \cdot \frac{H_{os}}{1 + e_{os}} \cdot \log \frac{t_2}{t_1} \tag{12.23}$$

where Z_α = long-term secondary compression settlement, ft or m;
e_{os} = initial void ratio of clay layer before starting secondary consolidation settlement;
C_α = secondary consolidation compression index;
H_{os} = initial thickness of clay layer before starting secondary consolidation settlement, ft or m;
t_1 = starting time of the time period for which long-term settlement of the layer is desired;
t_2 = ending time of the time period for which long-term settlement of the layer is desired.

The total settlement of clay layer includes three portions: elastic settlement, primary consolidation settlement, and secondary consolidation settlement. These three types of settlement for clayey soil layers can be calculated from Equations 12.20, 12.22, and 12.23, respectively. The total settlement of clayey soil at point *i* can be determined from the equation

$$Z_i = (Z_e)_i + (Z_c)_i + (Z_\alpha)_i \tag{12.24}$$

where Z_i = total settlement of points *i*;
$(Z_e)_i$ = elastic settlement of point *i*;
$(Z_c)_i$ = primary consolidation settlement of point *i*;
$(Z_\alpha)_i$ = secondary consolidation settlement of point *i*.

APPLICATION FOR PERMIT
SUNDANCE WEST

VOLUME III: LANDFILL ENGINEERING CALCULATIONS
SECTION 8: SETTLEMENT CALCULATIONS

ATTACHMENT III.8.C

GEOTECHNICAL ENGINEERING: PRINCIPLES AND PRACTICES

CODUTO, DONALD P., 2002

Geotechnical Engineering

Principles and Practices

Donald P. Coduto

Professor of Civil Engineering
California State Polytechnic University, Pomona

PRENTICE HALL, Upper Saddle River, NJ 07458

where:

$(N_1)_{60}$ = corrected SPT N-value, as defined in Chapter 3

C_P = grain size correction factor

C_A = aging correction factor

C_{OCR} = overconsolidation correction factor

D_{50} = grain size at which 50 percent of the soil is finer (mm) as defined in Section 4.4

t = age of soil (time since deposition in years). If no age information data is available, use t = 100 yr.

OCR = overconsolidation ratio, as defined in Chapter 11. If no information is available to assess the OCR, use a value of 2.

q_c = cone resistance (kg/cm^2 or ton/ft^2), as defined in Chapter 3

Q_c = compressibility factor

= 0.91 for highly compressible sands

= 1.00 for moderately compressible sands

= 1.09 for slightly compressible sands

For purposes of solving this formula, a sand with a high fines content or a high mica content is "highly compressible," whereas a pure quartz sand is "slightly compressible."

σ_z' = vertical effective stress (lb/ft^2; kPa), as defined in Chapter 10

Many people confuse relative density with relative compaction. The latter is defined in Chapter 6. Although the names are similar, and they measure similar properties, these two parameters are numerically different. In addition, some people in other professions use the term "relative density" to describe what we call specific gravity! Geotechnical engineers should never use the term in this way.

Table 4.5 presents typical values of e_{min} and e_{max} for various sandy soils. These are not intended to be used in lieu of laboratory or in-situ tests, but could be used to check test results or for preliminary analyses.

TABLE 4.5 TYPICAL VALUES OF e_{min} AND e_{max} (Hough, 1969; Adapted by permission of John Wiley and Sons, Inc.)

Soil Description	e_{min} (dense)	e_{max} (loose)
Equal spheres (theoretical values)	0.35	0.92
Clean, poorly graded medium sand (Ottawa, Illinois)	0.50	0.80
Clean, fine-to-medium sand	0.40	1.0
Uniform inorganic silt	0.40	1.1
Silty sand	0.30	0.90
Clean fine-to-coarse sand	0.20	0.95
Micaceous sand	0.40	1.2
Silty sand and gravel	0.14	0.85

TABLE 11.3 TYPICAL CONSOLIDATION PROPERTIES OF SATURATED NORMALLY CONSOLIDATED SANDY SOILS AT VARIOUS RELATIVE DENSITIES (Adapted from Burmister, 1962)

Soil Type	$C_c/(1+e_0)$					
	$D_r = 0\%$	$D_r = 20\%$	$D_r = 40\%$	$D_r = 60\%$	$D_r = 80\%$	$D_r = 100\%$
Medium to coarse sand, some fine gravel (SW)	-	-	0.005	-	-	-
Medium to coarse sand (SW/SP)	0.010	0.008	0.006	0.005	0.003	0.002
Fine to coarse sand (SW)	0.011	0.009	0.007	0.005	0.003	0.002
Fine to medium sand (SW/SP)	0.013	0.010	0.008	0.006	0.004	0.003
Fine sand (SP)	0.015	0.013	0.010	0.008	0.005	0.003
Fine sand with trace fine to coarse silt (SP-SM)	-	-	0.011	-	-	-
Find sand with little fine to coarse silt (SM)	0.017	0.014	0.012	0.009	0.006	0.003
Fine sand with some fine to coarse silt (SM)	-	-	0.014	-	-	-

For saturated overconsolidated sands, $C_r/(1+e_0)$ is typically about one-third of the values listed in Table 11.3, which makes such soils nearly incompressible. Compacted fills can be considered to be overconsolidated, as can soils that have clear geologic evidence of preloading, such as glacial tills. Therefore, many settlement analyses simply consider the compressibility of such soils to be zero. If it is unclear whether a soil is normally consolidated or overconsolidated, it is conservative to assume it is normally consolidated.

Very few consolidation tests have been performed on gravelly soils, but the compressibility of these soils is probably equal to or less than those for sand, as listed in Table 11.3.

Another characteristic of sands and gravels is their high hydraulic conductivity, which means any excess pore water drains very quickly. Thus, the rate of consolidation is very fast, and typically occurs nearly as fast as the load is applied. Thus, if the load is due to a fill, the consolidation of these soils may have little practical significance.

However, there are at least two cases where consolidation of coarse-grained soils can be very important and needs more careful consideration:

1. **Loose sandy soils subjected to dynamic loads, such as those from an earthquake.** They can experience very large and irregular settlements that can cause serious damage. Kramer (1996) discusses methods of evaluating this problem.

APPLICATION FOR PERMIT
SUNDANCE WEST, INC.

VOLUME III: ENGINEERING DESIGN AND CALCULATIONS
SECTION 9: EVAPORATION CALCULATIONS

TABLE OF CONTENTS

LIST OF FIGURES

LIST OF TABLES

LIST OF ATTACHMENTS

APPLICATION FOR PERMIT
SUNDANCE WEST, INC.

VOLUME III: ENGINEERING DESIGN AND CALCULATIONS
SECTION 9: EVAPORATION CALCULATIONS

1.0 INTRODUCTION

Sundance West (Sundance West Facility) is a proposed Surface Waste Management Facility for oil field waste processing and disposal services. The proposed Sundance West Facility is subject to regulation under the New Mexico Oil and Gas Rules, specifically 19.15.36 NMAC, administered by the Oil Conservation Division (OCD). The Facility has been designed in compliance with 19.15.36 NMAC, and will be constructed and operated in compliance with a Surface Waste Management Facility Permit issued by the OCD. The Facility is owned by, and will be constructed and operated by, Sundance West, Inc.

1.1 Description

The Sundance West site is comprised of a 320-acre ± tract of land located approximately 3 miles east of Eunice, 18 miles south of Hobbs, and approximately 1.5 miles west of the Texas/New Mexico state line in the South ½ of Section 30, Township 21 South, Range 38 East Lea County, New Mexico (NM). Site access will be provided via NM 18 and Wallach Lane. The Sundance West Facility will include two main components; a liquid oil field waste Processing Area (80 acres ±), and an oil field waste Landfill (180 acres ±). Oil field wastes are anticipated to be delivered to the Sundance West Facility from oil and gas exploration and production operations in southeastern NM and west Texas. The Site Development Plan provided in the **Permit Plans, Volume III.1**, identifies the locations of the Processing Area and Landfill facilities.

2.0 DESIGN CRITERIA

The Processing Area will include evaporation ponds for the disposal of Produced Water. The area and volume of the lined portion of each evaporation pond is 1.88 acres of water surface with a capacity of 9.5 acre-feet (ft). Sundance West will include a total of ten ponds which will provide a total of 18.80 surface acres for evaporation of 95 total acre-ft of pond capacity.

2.1 General Site Conditions

The site terrain is gently sloping toward the west with sparse vegetation. The macro-climate of the Sundance West area is classified by the Koppen Climate Classification System as a “BSk”, which indicates a semi-arid steppe with much of the characteristics of a desert. Meteorological climatic data was obtained from the Western Regional Climate Center for pan evaporation at Lake Avalon and precipitation at the Hobbs FAA Airport weather stations which are the closest reporting points for these two data sets.

The evaluation of climate data for these nearby weather stations indicates that they are relatively similar and will likely provide reasonable precipitation estimates for the site (**Table III.9.1**). Climatic data available for the Lake Avalon weather station includes pan evaporation for the years of record from 1914 through 1979. The Hobbs FAA Airport weather station includes precipitation for the years of record from 1942 through 2006. The Lake Avalon pan evaporation data was used to estimate monthly evaporation values at the Sundance West site. The observed pan evaporation values were scaled by a factor of 0.7 to represent actual pond evaporation. The average monthly evaporation and precipitation data used for design of the Sundance West evaporation ponds is summarized in **Table III.9.1**. Considering this climatic data, the annual evaporation exceeds annual precipitation on average by over six times.

The predominant wind directions for the site are from the south and southeast, with an average annual wind speed of 11 miles per hour (mph). The maximum sustained wind speed conservatively used for facility design is 14 mph.

3.0 EVAPORATION POND DESIGN

This section provides the engineering analyses and technical details to support design of the evaporation ponds for the Sundance West Facility with an average evaporation rate of 1,000 bbl per pond per day. While maintaining potential drift within the pond boundary.

TABLE III.9.1
Sundance West
Produced Water Evaporation Ponds - Evaporator Water Balance

	January	February	March	April	May	June	July	August	September	October	November	December	**Total**
Rainfall	0.42	0.37	0.29	0.78	2.06	0.87	1.56	1.76	2.09	1.61	0.22	0.11	**12.14**
Pan Evaporation	4.49	5.33	9.42	12.36	14.31	15.16	14.14	12.33	9.25	7.26	4.68	4.2	**112.93**
Actual Evaporation	3.14	3.73	6.59	8.65	10.02	10.61	9.90	8.63	6.48	5.08	3.28	2.94	**79.05**
NET	-2.72	-3.36	-6.30	-7.87	-7.96	-9.74	-8.34	-6.87	-4.39	-3.47	-3.06	-2.83	**-66.91**
Net Evaporation (bbl/pond)	3314	4090	7672	9580	9684	11856	10147	8362	5336	4225	3719	3444	81430

Mechanical Evaporation Analysis													
% Mech Evap Potential	30%	32%	44%	50%	50%	50%	50%	50%	44%	40%	35%	34%	
BBL/D@75GPM	386	411	566	643	643	643	643	643	566	514	450	437	
Assume 25% Mech Evap	25%	25%	25%	25%	25%	25%	25%	25%	25%	25%	25%	25%	
BBL/D@75GPM	321	321	321	321	321	321	321	321	321	321	321	321	
Evap Units Req													
1000 bbl/Pond	3	3	3	3	3	3	3	3	3	3	3	3	
Phase I @3000 bbl	9	9	9	9	9	9	9	9	9	9	9	9	
Phase II @7000 bbl	22	22	22	22	22	22	22	22	22	22	22	22	
Phase VI @9000 bbl	28	28	28	28	28	28	28	28	28	28	28	28	
Cushion bbl/day	64	90	244	321	321	321	321	321	244	193	129	116	**224**
% Cushion	6%	9%	24%	32%	32%	32%	32%	32%	24%	19%	13%	12%	22%

Notes:

1. Rainfall obtained from Hobbs FAA Airport and is average monthly rainfall from 1942-2006.
2. Input is the maximum Monthly Produced water that can be introduces to Evaporation Ponds based on Water Balance.
3. Evaporation rates obtained from Lake Avalon, New Mexico from 1914 -1979.
4. Actual Evaporation rates represent 70% of reported Pan Evaporation rate.
5. % Mech Evap Potential is the expected mechanical evaporation rate (%) for the pan Evaporation Rate per TurboMist calculation criteria
6. Assume 25% Mech Evap is the mechanical evaporation rate (%) minimum expected from SMI Evaporator 420F
7. BBL/D@75GPM is the flow rate for the SMI Evaporator Model 420F (assumes 12HRS of operation/Day)

3.1 Design Criteria

3.1.1 Design Regulations

Regulations relevant to the design of the evaporation ponds presented here in Section 3.0 are summarized below.

Key Regulatory Agencies and Documents:

New Mexico Oil Conservation Division (OCD): Title 19 Natural Resources and Wildlife, Chapter 15 Oil and Gas, Part 36 Surface Waste Management Facilities, Section 17 Specific Requirements Applicable to Evaporation, Storage, Treatment and Skimmer Ponds, specifically B(12) which indicates that "*The maximum size of an evaporation or storage pond shall not exceed 10 acre-feet*".

New Mexico Office of the State Engineer (NMOSE): Title 19 Natural Resources and Wildlife, Chapter 25 Administration and Use of Water – General Provisions, Part 12 Dam Design, Construction and Dam Safety, Section 7 Definitions, D. (1) Dams, (a) Jurisdictional Dam which indicates that "*A dam 25 feet or greater in height, which impounds more than 15 acre-feet of water or a dam that impounds 50 acre-feet or more of water and is 6 feet or greater in height.*" (b) Non-jurisdictional dam which indicates that "*Any dam not meeting the height and storage requirements of a jurisdictional dam.*" exempting this facility's structures from this rule.

3.1.2 Project Design Criteria

Design criteria relevant to the analyses presented here in Section 3.0 are summarized below.

Geometry:

Process Operations: Design evaporation capacity of 1,000 barrels per day (bbl/d) of produced water per pond, with potential expansion capacity to 9,000 bbl/d.

Evaporation Pond Storage Capacity: Less than 10 acre-ft per pond, with potential expansion to 10 ponds. Developing an ultimate pond design configuration resulted in a 9.5 acre-foot pond capacity with a surface water area of 82,000 square feet (ft) and measuring 410 ft x 200 ft.

Maximum Evaporative Surface Area: for ten ponds would be 820,000 square ft or 18.8 acres.

Process Design Life: 50 years.

Produced Water Properties:

Design Volumetric Flow Rate: 9,000 bbl/d or 263 gallons per minute (gpm).

System Requirements:

> **Evaporation Pond Liner System:** Double layer liner system as follows (top to bottom): (1) upper (secondary) 60 mil HDPE geomembrane liner; (2) leak detection system consisting of a 200 mil HDPE geonet; (3) lower (primary) 60 mil HDPE geomembrane liner; underlain by (4) a density controlled compacted subgrade.
>
> **Leak Detection System:** The leak detection system will meet the following requirements:(1) constructed with a bottom slope of at least two percent; (2) constructed with a 200 mil HDPE geonet with a transmissivity of $1x10^{-3}$ m^2/sec or greater; (3) constructed of materials that are chemically resistant to the waste and leachate; (4) designed and operated to minimize clogging during the active life; and (5) constructed with sumps and liquid removal methods (i.e., pumps).

3.2 Design Concepts

This section presents the general evaporation pond design concepts with the technical aspects of these concepts discussed in detail in the following sections.

The Sundance West Facility is designed for start-up operations at 3,000 bbl/d routinely, with a potential to expand to 9,000 bbl/d on average. The design produced water flows from the Produced Water Tanks will be discharged to the evaporation ponds. The average design flow rates associated with the start-up and ultimate production rates are 88 and 263 gallons per minute (gpm), respectively.

The evaporation pond system is designed for construction in phases. Phase I includes 4 ponds, each with a surface dimension of 410 ft by 200 ft (i.e. 1.88 acres), designed to evaporate the inflows associated with the average receipt of 3,000 bbl/d. Similarly, Future Phases will include an additional 6 ponds with the same dimensions designed to evaporate the flows associated with an additional 6,000 bbl/d of produced water received daily. All ponds are designed and constructed to provide contingency storage with an additional 3 ft of freeboard (above the required design capacities). Pond berms with a minimum crest width of 15 ft are designed between ponds to allow access to all sides of the ponds, as well as operation and maintenance of the evaporation equipment. Two leak detection system (LDS) sumps have been included in the design of each evaporation pond. Liquids collected in the LDS sumps will be pumped using a mobile pump, and returned to the evaporation ponds.

In order to improve performance of the evaporation pond system (i.e., enhance the evaporative capabilities), the design includes implementation of a mechanical evaporation system. The evaporators will be placed and sized to maximize evaporation and minimize the potential for wind-drift beyond the extents of the lined evaporation pond area. A continuous liner is designed over the entire evaporation pond area, including over the separation berms. A textured geomembrane will be extrusion welded on top of the berms between pond cells to facilitate access (i.e., pedestrian or ATV).

3.3 Water Balance Modeling

A probabilistic water balance model was developed to assist in determining the evaporation potential of the pond system (i.e., required evaporative surface area). Water balance calculations were performed (See **Table III.9.1**).

The following water balance components were considered: (1) the amount of Produced Water entering the pond system from the Produced Water Tanks, (2) water entering the pond system through meteoric precipitation, and (3) the amount of water released to the atmosphere through evaporation.

Precipitation values are likely to exhibit largest variations, and were therefore treated as stochastic inputs (i.e., probabilistic), while the other parameters were treated as deterministic variables. **Figure III.9.1** presents the process flow diagram for the evaporation pond water balance.

Preliminary analyses revealed a prohibitively large evaporation area for extreme precipitation events when considering evaporation losses solely from the pond surface. To reduce the required evaporative area, subsequent analyses included a mechanical evaporation system resulting in enhanced evaporation losses. All evaporators will be located at points within the ponds (as depicted in **Figure III.9.2**) to minimize the probability of wind-drift blowing the produced water beyond the lined evaporation pond area.

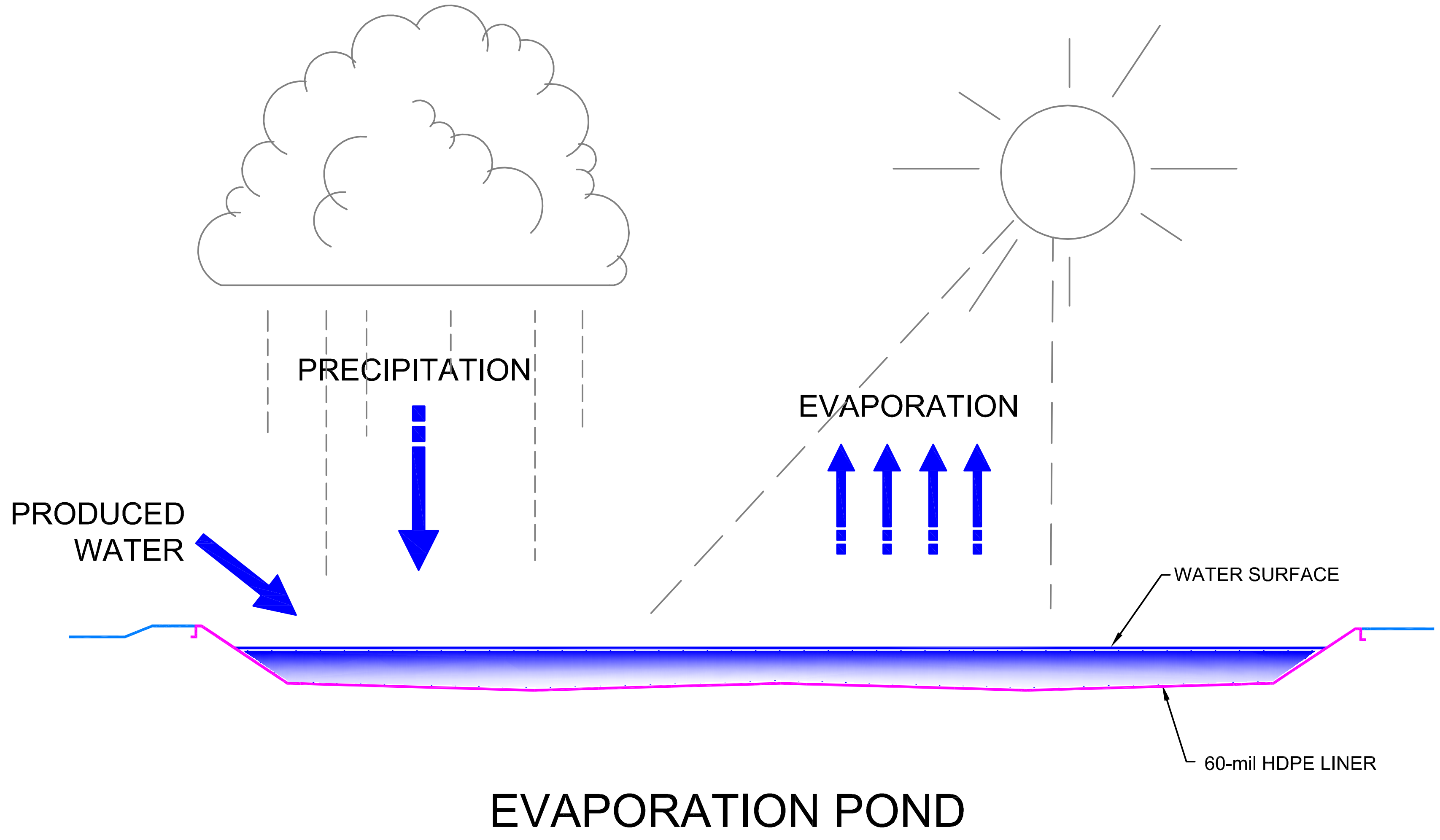

Drawing:P:\acad 2003\530.06.01\REVISED FIGURES(RAI 1)\EVAPORATION FIGURE III.9.1.dwg
Date/Time:Jul. 25, 2016-07:17:09 ;   LAYOUT: A (LS)

EVAPORATION POND WATER BALANCE FLOW DIAGRAM

SUNDANCE WEST
SURFACE MANAGEMENT FACILITY
LEA COUNTY, NEW MEXICO

Gordon Environmental, Inc.
Consulting Engineers

213 S. Camino del Pueblo
Bernalillo, New Mexico, USA
Phone: 505-867-6990
Fax: 505-867-6991

DATE: 02/22/2016	CAD: EVAPORATION.dwg	PROJECT #: 542.06.01
DRAWN BY: DMI	REVIEWED BY: CWF	FIGURE III.9.1
APPROVED BY: IKG	gei@gordonenvironmental.com	

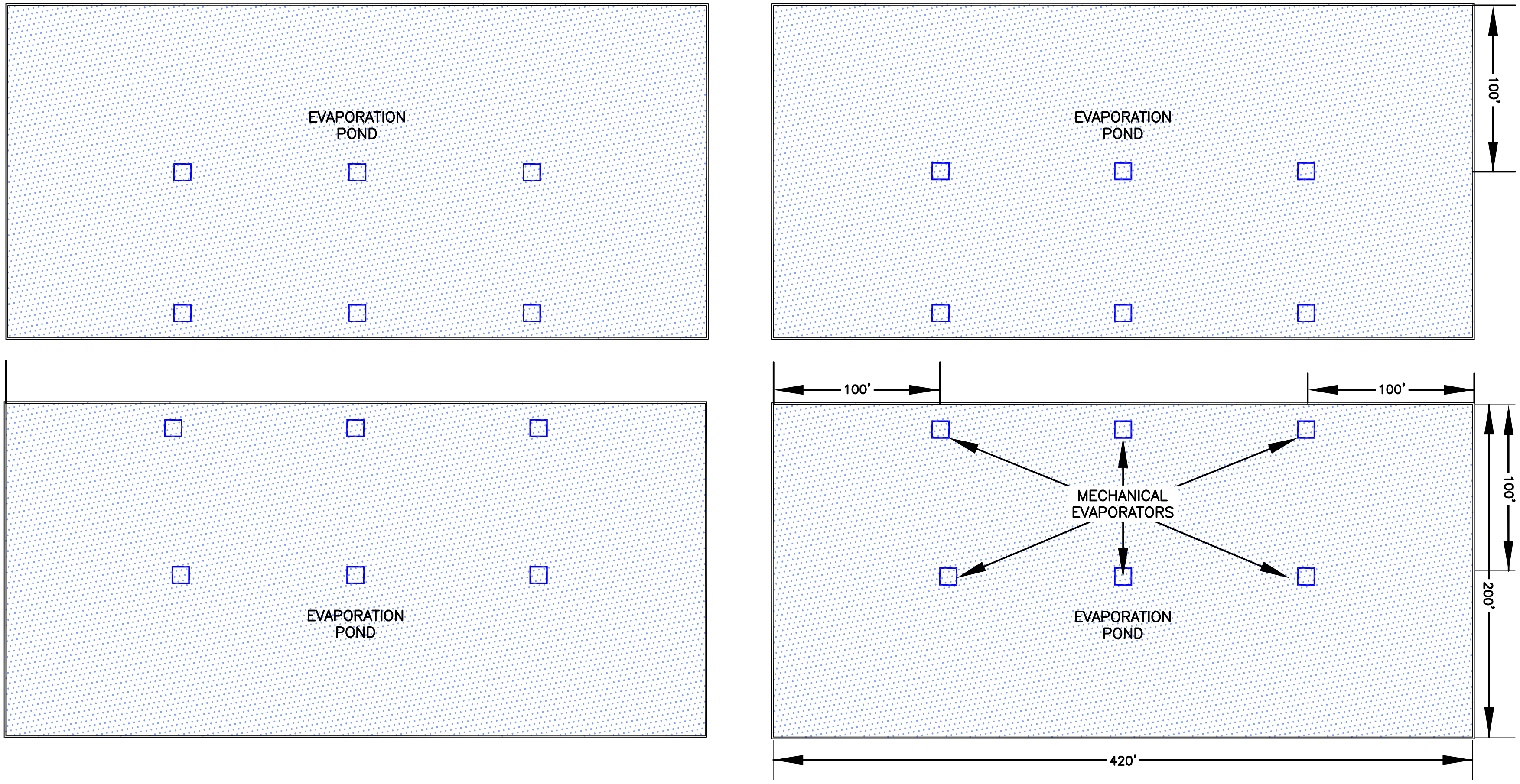

Drawing:P:\acad 2003\530.06.01\REVISED FIGURES(RAI 1)\REVISED MECH EVAPORATORS.dwg
Date/Time:Jul. 22, 2016-12:26:24

TYPICAL MECHANICAL EVAPORATOR LOCATION–PHASE I

SUNDANCE WEST
SURFACE WASTE MANAGEMENT FACILITY.
LEA COUNTY, NEW MEXICO

Gordon Environmental, Inc.
Consulting Engineers

213 S. Camino del Pueblo
Bernalillo, New Mexico, USA
Phone: 505-867-6990
Fax: 505-867-6991

DATE: 07/22/2016	CAD: MECH EVAPORATORS.dwg	PROJECT #: 530.06.01
DRAWN BY: DMI	REVIEWED BY: CWF	FIGURE III.9.2
APPROVED BY: IKG	gei@gordonenvironmental.com	

The results of the water balance for each pond were calculated assuming the average annual rainfall; the percentage of the an average day when the wind speed is under 12 mph when the mechanical evaporators will be running; limiting the mechanical evaporators to no more than 10 gpm flow rate through the evaporators (even though extensive experience with this equipment indicated a greater evaporative expectation); and an input of 1,000 bbl/d of Produced Water. Based on these assumptions, the required number of mechanical evaporators per pond to evaporate 1,000 bbl/d was estimated to be three. The conservative assumption was made to discount the surface evaporation potential from the pond due to the micro-climate created by the mechanical evaporators. **Table III.9.1** details the evaporation potential per pond and identifies the additional evaporation potential that may be available based on extensive industry experience with the mechanical evaporators.

The influence of dissolved solids in the process water flow to the evaporation ponds may affect pond evaporation. It will be important to collect field evaporation measurements during the early years of pond operations to confirm the adequacy of this initial design. These field measurements will assist in refining expansion design of the evaporation ponds for an increase to 9,000 bbl/d average evaporation potential.

3.4 Mechanical Evaporator Lateral Drift Analysis

The proposed mechanical evaporators were analyzed for drift potential to ensure that all of the mist generated in the evaporation process would remain within the area of the lined pond. The objective of this analysis was to determine at what distance the suspended solids would fall out with a given wind speed, droplet diameter and known level of Total Suspended Solids (TDS).

The higher the TDS the less lateral distance traveled and time the water droplet spends suspended in the air. For this analysis an 8% total TDS saturation was assumed. The proposed mechanical evaporator makes 150 micron water droplet particle sizes. This analysis will assume a droplet particle size of 150 microns for the drift calculations. Based on **Table III.9.2** the distance required for a 150 micron particle size to fall 10 ft is 10 seconds in a 3 mph wind is 39 feet.

TABLE III.9.2
Influence of Droplet Size on Potential Drift Distance
Sundance West

Droplet Diameter (Microns)	**Type of droplets**	**Time required to fall 10 feet**	**Lateral distance Droplets travel in falling 10 feet in a 3 mph wind**
5	Fog	66 minutes	3 miles
20	Very fine spray	4.2 minutes	1,100 feet
100	**Fine spray**	**10 seconds**	**44 feet**
150	Evaporator Standard	9 seconds	39 feet
240	Medium spray	6 seconds	28 feet
400	Course spray	2 seconds	8.5 feet
1,000	Fine rain	1 second	4.7 feet

The proposed mechanical evaporator propels the water droplets 15 ft in the air resulting in a 15 ft anticipated fall height for the water droplet particles generated. In this 3 mph wind the water droplet could drift 59 ft before falling back into the pond.

An analysis was performed with DRIFTSIM a computer modeling program (**Attachment III.9.B**) that predicts the drift distance of spray droplets. This program was developed by Ohio State University, Food Agriculture, and Biological Engineering Department in coordination with the United States Department of Agriculture, Agricultural Research Service. The results from this model, utilizing a low TDS liquid (assuming greater drift), a 12 mph maximum wind speed (maximum average sustained wind speed onsite) and variable humidity's at various temperatures confirmed that based on the anticipated 150 micron droplet size, all lateral drift will fall back into the lined pond area. **Table III.9.3** and **Figure III.9.3** provide a summary of the output from this analysis.

TABLE III.9.3
DRIFTSIM Analysis Results
(12 MPH Wind)
Sundance West, Inc.

Temp	Drop Diameter	Humidity	Drift
50	150	10	85
50	150	20	79
50	150	30	79
50	150	40	78
50	150	50	77
50	150	60	77
50	150	70	77
50	150	80	75
50	150	90	75
50	150	100	74
60	150	10	84
60	150	20	82
60	150	30	82
60	150	40	81
60	150	50	80
60	150	60	79
60	150	70	79
60	150	80	77
60	150	90	76
60	150	100	75
70	150	10	86
70	150	20	84
70	150	30	84
70	150	40	83
70	150	50	82
70	150	60	80
70	150	70	80
70	150	80	78
70	150	90	76
70	150	100	74
80	150	10	94
80	150	20	92
80	150	30	92
80	150	40	90
80	150	50	88
80	150	60	86
80	150	70	84
80	150	80	82
80	150	90	79
80	150	100	76

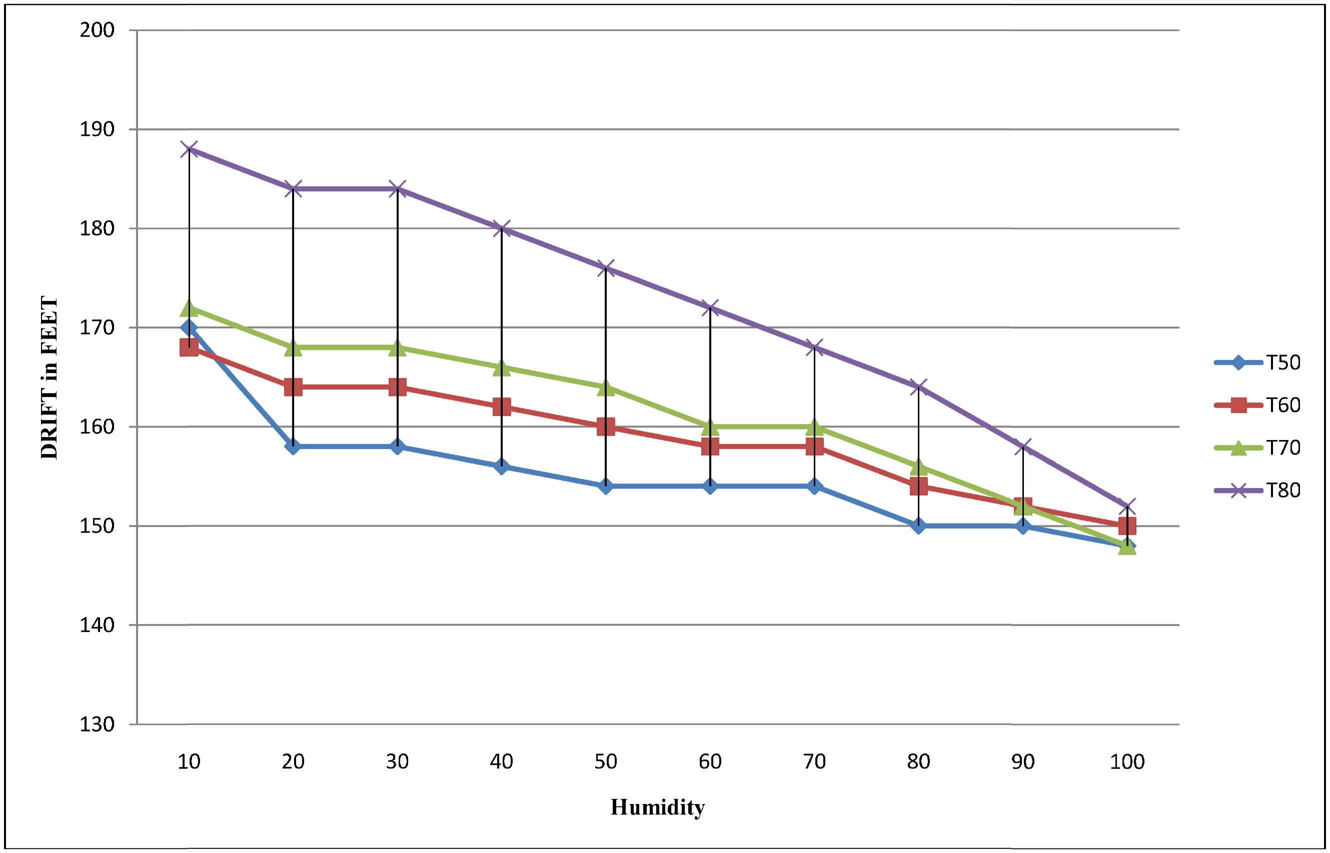

EFFECT OF HUMIDITY AND TEMPERATURE ON DRIFT

SUNDANCE WEST
SURFACE WASTE MANAGEMENT FACILITY.
LEA COUNTY, NEW MEXICO

Gordon Environmental, Inc.
Consulting Engineers

213 S. Camino del Pueblo
Bernalillo, New Mexico, USA
Phone: 505-867-6990
Fax: 505-867-6991

DATE: 07/22/2016	CAD: DRIFT GRAPH.dwg	PROJECT #: 530.06.01
DRAWN BY: DMI	REVIEWED BY: MRH	FIGURE III.9.3
APPROVED BY: IKG	gei@gordonenvironmental.com	

Drawing:P:\acad 2003\530.06.01\REVISED FIGURES(RAI 1)\DRIFT GRAPH.dwg
Date/Time:Jul. 22, 2016-12:22:32

The majority of the strong winds at this location come from the southeast direction. Given the layout of the evaporation ponds, the proposed mechanical evaporators could operate in up to 14 mph wind before the automation would need to shut the machines down relative to concerns that drift might escape the lined ponds.

The mechanical evaporators will be controlled by a weather station with software designed to monitor wind speed and control (start and stop) the equipment to optimize evaporation hours and minimize the potential for freezing during cold periods. This weather station will also control for wind speed and direction to minimize any potential for over spray and drift situations on windy days.

4.0 SUMMARY

The proposed evaporation ponds with mechanical evaporators will be able to evaporate the proposed volumes of Produced Waters that are anticipated for receipt in the various phases of this facility's development. The potential for drift can be managed to ensure that all materials remain within the lined area of the evaporation ponds. **Figure III.9.4** provide a Wind Rose for this location.

STATION: HOBBS, NEW MEXICO
LATITUDE: 32° 41' 15" N
LONGITUDE: -103° 13' 01" W
ELEVATION: 3661 FT
ELEMENT: WIND SPEED

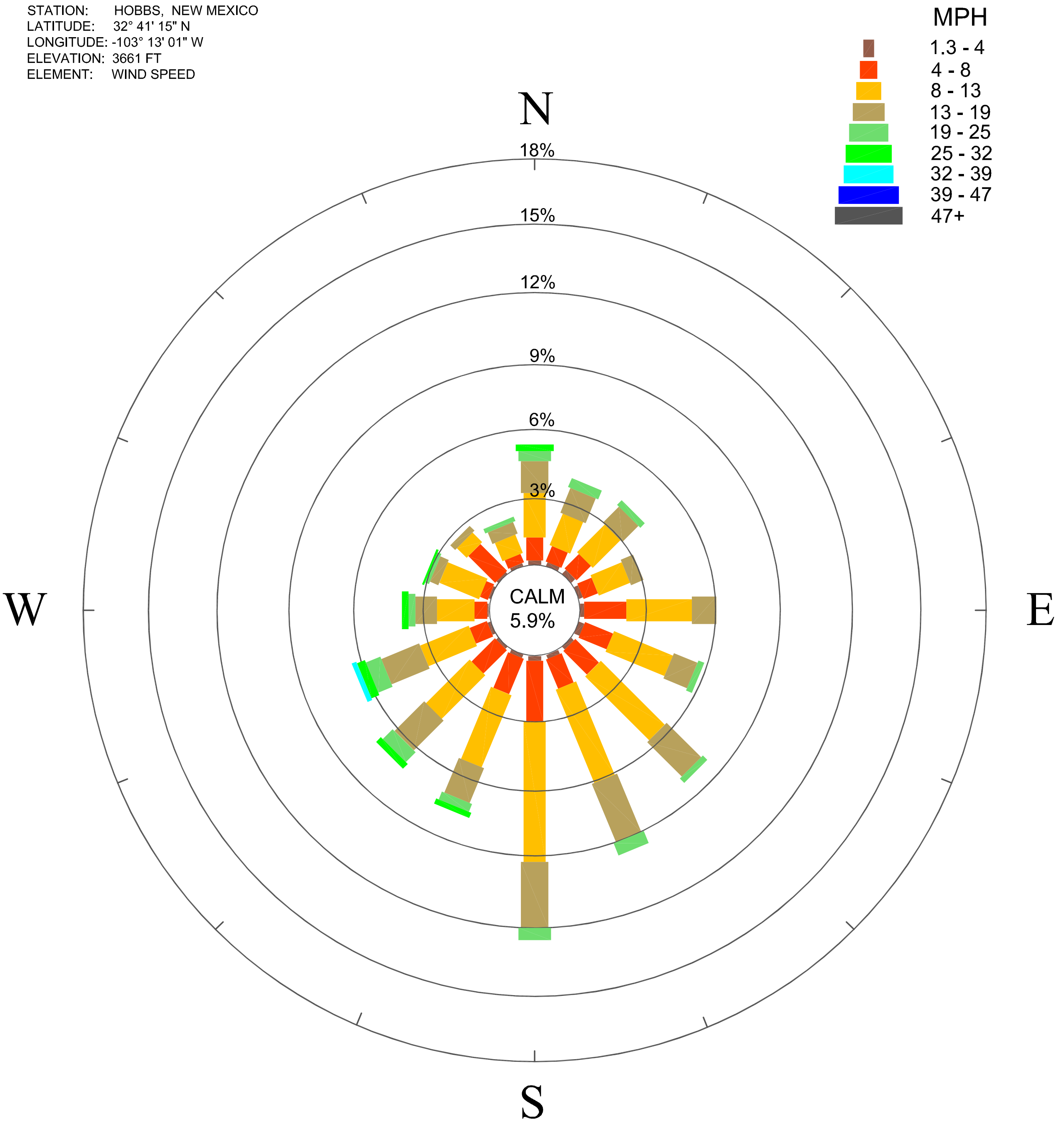

START DATE: JULY 1, 1948
END DATE: DEC. 31, 2014
OF DAYS: 24,290 of 24,290
OBS: Poss: 86,251 of 582,960
WESTERN REGIONAL CLIMATE CENTER

Drawing:P:\acad 2003\530.06.01\REVISED FIGURES(RAI 1)\REVISED WINDROSE 6-22-2016.dwg
Date/Time:Aug. 09, 2016-12:12:03 ; LAYOUT: A (P)

WIND ROSE

SUNDANCE WEST
SURFACE WASTE MANAGEMENT FACILITY
LEA COUNTY, NEW MEXICO

Gordon Environmental, Inc.
Consulting Engineers

213 S. Camino del Pueblo
Bernalillo, New Mexico, USA
Phone: 505-867-6990
Fax: 505-867-6991

DATE: 07/22/2016	CAD: WIND ROSE.dwg	PROJECT #: 560.01.02
DRAWN BY: DMI	REVIEWED BY: CWF	FIGURE III.9.4
APPROVED BY: IKG	gei@gordonenvironmental.com	

APPLICATION FOR PERMIT
SUNDANCE WEST

VOLUME III: ENGINEERING DESIGN AND CALCULATIONS
SECTION 9: EVAPORATION CALCULATIONS

ATTACHMENT III.9.A

EFFECTS OF MAJOR VARIABLES ON DRIFT DISTANCES OF SPRAY DROPLETS

ohioline.ag.ohio-state.edu -- your Link to Information, News, and Education

THE OHIO STATE UNIVERSITY FactSheet Extension

Ohio State University Extension Fact Sheet

Food, Agricultural, and Biological Engineering

590 Woody Hayes Drive, Columbus, Ohio 43210

Effect of Major Variables on Drift Distances of Spray Droplets

AEX-525-98

Author

H. Erdal Ozkan
Professor
The Ohio State University
Food, Agricultural and Biological Engineering Department
590 Woody Hayes Drive
Columbus, OH 43210

Pesticide applications are required to ensure an adequate and high quality supply of many agricultural crops. Due to concerns for production costs, safety, and the environment, it is important to maximize the pesticide deposit on the target. One of the major problems challenging pesticide applicators is spray drift, which is defined as movement of pesticides by wind from the application site to an off-target site.

Spray drift occurs wherever liquid sprays are applied. Although complete elimination of spray drift is impossible, problems can be reduced significantly if the pesticide applicator is aware of major factors which influence drift, and takes precautions to minimize their influence on off-target movement of droplets.

Drift is influenced by many factors that usually may be grouped into one of the following categories: 1) Spray characteristics, 2) Equipment and application techniques used, 3) Weather, and 4) Operator care and skill. A general discussion of these factors can be found in another publication by Ozkan (1991). In this publication, you will find specific information on how much influence some of these major factors have on the drift distances of spray droplets.

The factors that significantly influence off-target movement of droplets are wind velocity and direction, droplet size and density, and distance from the atomizer to the target. Other factors that influence drift include droplet velocity and direction of discharge from the atomizer, volatility of the spray fluid, relative humidity, ambient temperature, and atmospheric turbulence intensity. Many scientists have conducted field tests to study influence of these variables on spray drift. Unfortunately, field tests have the limitation that weather conditions cannot be controlled and the variables that influence spray drift may interact and vary during a test. Computer simulations can allow determination of the effects of different values of variables such as droplet size and velocity, relative humidity, and wind velocity on spray drift. One such computer model was developed by Reichard et al.(1992a) in Ohio for modeling the effects of several variables on spray drift. Using the computer program, individual or mean droplet trajectories were determined for different values of several variables listed above. Experiments were also conducted to verify the accuracy of the computer model in predicting drift distances of water droplets in a wind tunnel. These tests revealed that the computer model can be used to accurately calculate spray drift distances for a wide range of spray droplet sizes and wind velocities (Reichard et. al., 1992b).

The major drift factors included in this publication are droplet size, wind velocity, relative humidity, ambient temperature, droplet discharge height, and initial droplet velocity. Although turbulence intensity is a major factor which influence drift, data related to this variable was not included in this publication because it is not something pesticide applicators can assess easily, and its magnitude can vary rapidly unlike the changes in other atmospheric conditions such as relative humidity and temperature. The affect of turbulence intensity on drift distances of droplets is discussed in the publication by Reichard et. al. (1992a). A turbulence intensity of 20% was assumed for all the computer simulation results reported in this publication,.

Although the accuracy of the drift data produced by computer simulation has been validated, one has to be cautious when drawing conclusions from the data presented in this publication. Due to the many variables that influence spray drift, it is extremely difficult to precisely predict drift distances of droplets for field conditions. Some of the variables that affect drift distances, such as wind turbulence, velocity and direction can vary considerably while a droplet is drifting. It is common for terrain and vegetation (size and density) to vary over the path of a drifting droplet and these influence local wind velocity and direction. The drift distance data presented in this publication are only valid for the constant conditions specified. The data presented are useful in comparing the relative effects of several factors on drift distances, but are not intended to precisely model variable field conditions.

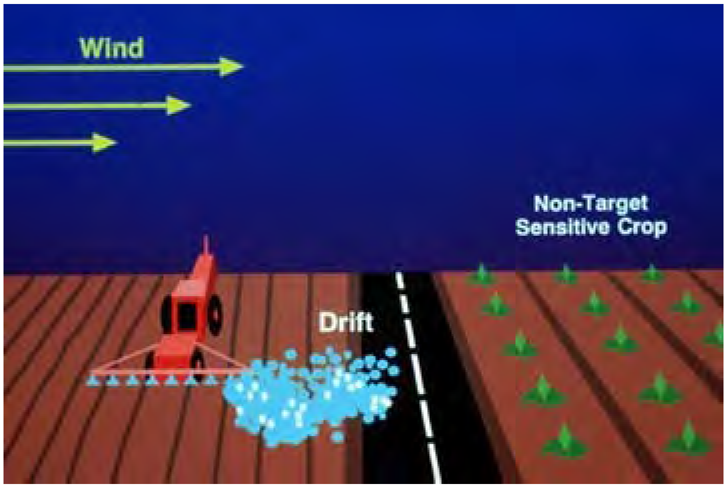

Spray drift is the reason for the discoloration of part of the wheat crop shown in this photograph. The size of the area affected by drift and its severity depend on how adverse the weather conditions are and poor decisions made by the operator of the sprayer.

Droplet Size, Wind Velocity and Relative Humidity

Droplet size and wind velocity are the two most influential factors affecting drift. Relative humidity influences the evaporation rate of a droplet and hence its size, flight time, velocity and drift distance. Table 1 and Figure 1 show the simulated mean drift distances for various sizes of water droplets (50-200 micron diameter), wind velocities (2-8 mph), relative humidities (20-80%), and 75 degrees F ambient temperature. (Additional data are included in Tables in the publication by Zhu et al., 1994). Unless otherwise indicated, all simulated drift distances discussed in this publication are for droplets discharged downward with 65 ft/second (45 mph) velocity toward a target 18 inches below the point of discharge.

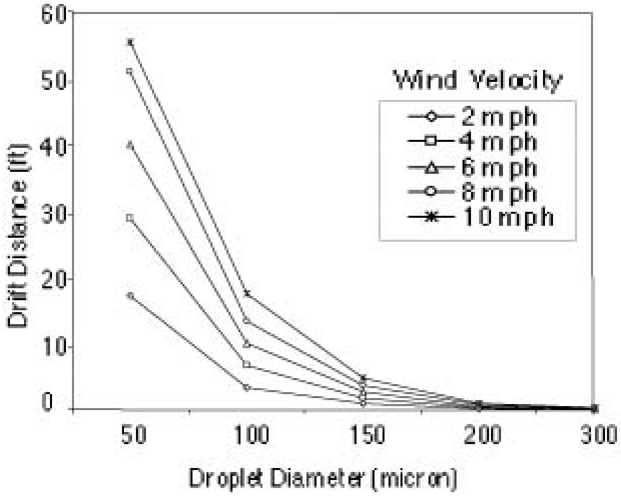

Figure 1. Effect of droplet diameter and wind velocity on drift distances of water droplets directed downward at 65 ft/second toward a target 18 inches below disharge point (Temperature = 75 degrees F; Relative Humidity = 60%).

Table 1. Effect of wind velocity and relative humidity on drift distances of droplets directed downward with initial velocity of 65 ft/second toward target 18 inches below discharge point. (Temperature = 75 degrees F; turbulence intensity = 20%)

Initial droplet size (microns)	Wind velocity (mph)	20	40	60	80
20	2	3.03*	3.72*	6.41*	15.29*
20	4	6.00*	6.47*	10.24*	21.45*
20	6	6.57*	7.66*	11.87*	23.23*
20	8	7.96*	8.97*	13.29*	26.42*
20	10	8.99*	10.58*	15.06*	30.10*
50	2	10.70*	12.10	17.20*	25.30*
50	4	18.70*	21.00*	28.80*	41.70*
50	6	26.50*	30.00*	40.00*	55.60*
50	8	34.30*	38.20*	50.90*	69.00*
50	10	37.60*	42.00*	55.32*	87.24*
100	2	3.44	3.41	3.37	3.30
100	4	6.87	6.81	6.71	6.58
100	6	10.30	10.20	10.05	9.85
100	8	13.72	13.61	13.39	13.14
100	10	17.94	17.77	17.48	17.05
150	2	0.92	0.92	0.92	0.91

150	4	1.83	1.82	1.82	1.82
150	6	2.74	2.74	2.73	2.71
150	8	3.67	3.66	3.62	3.60
150	10	4.78	4.78	4.75	4.77
200	2	0.20	0.20	0.20	0.20
200	4	0.38	0.38	0.38	0.38
200	6	0.55	0.55	0.55	0.55
200	8	0.75	0.75	0.75	0.75
200	10	0.96	0.96	0.96	0.96
300	2	0.05	0.05	0.05	0.05
300	4	0.10	0.10	0.10	0.10
300	6	0.15	0.15	0.15	0.15
300	8	0.21	0.21	0.21	0.21
300	10	0.26	0.26	0.26	0.26
* Droplet completely evaporated before deposition.					

Water droplets with 50 micron diameter and smaller are highly susceptible to drift. All droplets 50 micron diameter and smaller completely evaporated before they reached 18 inches below point of discharge for wind velocities between 2.0 and 10.0 mph and relative humidities (RH) between 20 and 80% (Table 1). The mean drift distances of small droplets increased rapidly with increased wind velocity. For example, with 60% RH, 50 micron diameter droplets were displaced 17.2, 28.8, 40.0, 50.9, and 55.3 ft before they completely evaporated when wind velocities were 2, 4, 6, 8, and 10 mph, respectively.

The mean drift distances of 50 micron diameter water droplets and smaller increased with increased relative humidity because high relative humidity increased the lifetimes of the volatile droplets. Although both evaporated completely before deposition, the mean drift distances of 50 micron diameter droplets were greater than for 20 micron diameter droplets with the same relative humidity and wind velocity. This occurs because 50 micron diameter droplets have 15.6 times more volume and hence longer life than 20 micron diameter droplets. With 10 mph wind velocity and 60% RH, 20 and 50 micron diameter droplets drifted 15.1 and 55.3 ft downwind from the discharge point, respectively.

Most nozzles used for applying pesticides produce a large portion of the spray volume in 100 micron diameter droplets and larger. For example, our measurements of spray droplets from an XR 8002 VS nozzle (Spraying Systems Co., Wheaton, IL 60189) with 0.2 gpm flow rate when operated at 40 psi indicated that about 75% of the total spray volume was in droplets 100 micron diameter and larger. Computer simulation results indicate that all 100 micron and larger diameter water droplets reached 18 in below point of discharge at wind velocities up to 10 mph regardless of the relative humidity. However, due to affecting the evaporation rate, and hence droplet size, relative humidity significantly influenced the drift distances of 50 micron diameter droplets before they evaporated. With wind velocity of 10 mph, the mean drift distances of 50 micron diameter water droplets increased from 37.6 to 87.2 ft as relative humidity increased from 20% to 80%.

Data in Table 1 indicate that drift distances of droplets 200 micron diameter and larger are much less than for 100 micron diameter. For example, with 10 mph wind velocity and 60% RH, the mean drift distance of 100 micron diameter droplets was about 18 times that of 200 micron diameter droplets (0.96 ft versus 17.48 ft). The mean drift distances of 200 micron diameter droplets were 0.20, 0.38, 0.55, 0.75, and 0.96 ft for wind velocities of 2, 4, 6, 8, and 10 mph, respectively. Relative humidity over a range of 20-80% had very little influence on the drift distances of 200 micron diameter droplets. The mean drift distances of all droplets 200 micron diameter and larger did not exceed 0.96 ft with wind velocities up to 10.0 mph.

Figure 1 illustrates the effect of water droplet size (50-300 micron diameter) on mean drift distance for wind velocities of 2.0, 4.0, 6.0, 8.0, and 10.0 mph, and 60% RH at 75 degrees F. All droplets 100 micron diameter or larger reached 18 in below point of discharge and deposited. The mean drift distances of the droplets increased with increased wind velocity but decreased as initial droplet size increased. The amount of droplet displacement that can be tolerated depends on several factors including the crop and surrounding area, and the pest control agent. If the target is a row crop that is sprayed from a nozzle centered over each row, then small amounts of droplet displacement by wind can result in large portions of the spray missing the target. It is also common for gusts with velocities two or more times the mean wind velocity to occur while spraying. Figure 1 indicates that drift is far less likely to be a problem when spraying with 200 micron diameter and larger droplets.

Figure 2 illustrates the simulated effect of wind velocities up to 10.0 mph on the mean drift distances for 100, 150, 200, and 300 micron diameter water droplets at 60% RH. Figure 2 and Table 1 both indicate that the influence of wind velocity on drift distance increases as droplet size decreases. Figure 2 shows that there is a nearly linear relationship between mean drift distance and wind velocity for each droplet size. The rate of change in drift distance with change in wind velocity was much greater for 100 than 200 micron diameter droplets. For example, over a range of 2 to 10 mph wind velocity the drift distances of 100 and 200 micron diameter droplets increased 1.8 and 0.01 ft per mph increase in wind velocity respectively.

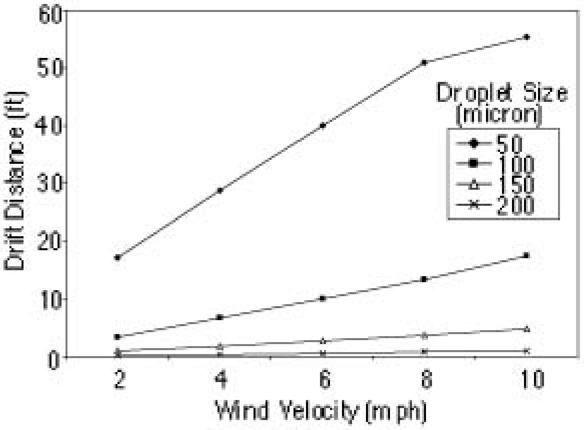

Figure 2. Effect of wind velocity and droplet diameter on drift distances of water droplets directed downward at 65ft/second toward a target 18 inches below discharge point (temperature = 75 degrees F; Relative Humidity = 60%).

Some spray carriers are oil or nonvolatile liquids. If the nonvolatile droplet density is close to the density of water, drift distances would be similar to drift distances in Table 1 for water droplets with 80% RH. Droplets 50 micron diameter or smaller can have very long drift distances with 100% RH. For example, the mean drift distances of 10 micron diameter droplets are beyond 650 ft with wind velocities of 5.5 mph and higher. For many pesticide applications, a small portion of the mixture is nonvolatile.

For small droplets that are still airborne when all of the water evaporates, there is potential for the small nonvolatile portion remaining to drift very long distances.

Temperature and Relative Humidity

Pesticides are applied over wide ranges of temperatures and relative humidities which influence the evaporation rates of droplets. Since evaporation of liquid from a droplet decreases its mass, it also influences the drift distance of the droplet. Table 2 shows the effects of temperatures (50, 68, and 86 degrees F) on droplet diameters at the end of droplet flights, and mean drift distances for water droplets with initial diameters ranging from 50 to 300 micron, wind velocities of 1 to 22 mph and 50% RH.

Table 2. Effect of temperature and wind velocity on droplet size at the end of flight of various size water droplets discharged downward at 65 ft/second toward a target 18 inches below point of discharge. (Relative humidity = 50%)

Initial Droplet size (micron)	Wind Velocity (mph)	Final Droplet Size (micron) and Drift Distance (ft)					
		Temperature (degrees F)					
		50		68		86	
		DS#	DD##	DS#	DD##	DS#	DD##
50	1.1	0.0	11.58*	0.0	9.84*	0.0	9.74*
50	5.6	0.0	53.14*	0.0	32.8*	0.0	23.52*
50	11.1	0.0	105.94*	0.0	61.34*	0.0	41.32*
50	22.4	0.0	208.61*	0.0	117.75*	0.0	75.76*
70	1.1	59.4	5.18	43.6	6.30	0.0	12.50*
70	5.6	59.2	26.14	42.7	32.14	0.0	38.70*
70	11.1	59.0	52.48	41.9	64.61	0.0	70.19*
70	22.4	58.8	105.94	40.4	132.18	0.0	132.51*
100	1.1	96.7	2.13	93.7	2.13	88.7	2.36
100	5.6	96.7	10.53	93.7	10.73	88.7	11.64
100	11.1	96.7	19.48	93.7	21.48	88.6	23.39
100	22.4	96.6	42.97	93.5	43.62	88.3	47.56
150	1.1	149	0.59	148	0.59	147	0.59
150	5.6	149	2.72	148	2.85	147	2.98
150	11.1	149	5.58	148	5.74	147	6.04
150	22.4	149	11.97	148	12.27	147	12.82
200	1.1	200	0.13	199	0.13	199	0.13
200	5.6	200	0.56	199	0.56	199	0.56
200	11.1	200	1.18	199	1.18	199	1.18
200	22.4	200	2.69	199	2.69	199	2.69
300	1.1	300	0.03	300	0.03	299	0.03
300	11.1	300	0.33	300	0.33	299	0.33

300	22.4	300	0.69	300	0.69	299	0.69

* Droplet completely evaporated before deposition.
# DS - Droplet diameter (micron) at end of flight.
DD - drift distance (ft).

Table 2 indicates that ambient temperature had more influence on droplet sizes at end of flights for smaller droplets than larger droplets. For 70 micron diameter droplets, 5.6 mph wind velocity, and 50% RH, the mean droplet sizes at end of flights were 59.2, 42.7, and zero micron for ambient temperatures of 50, 68, and 86 degrees F, respectively. For 200 micron diameter droplets and the same conditions, the mean droplet sizes at times of deposition were 200, 199, and 199 micron. Over a temperature range of 50-86 degrees F, the volumes of 100 and 200 micron diameter water droplets changed about 20.9 and 1.5% respectively during flights when wind velocity was 1.1 m/s.

Table 2 also shows that wind velocities up to 22.4 mph had greater influence on droplet size change during flight on smaller than on larger droplets. For 70 micron diameter droplets at 68 degrees F and 50% RH, the droplet diameters at deposition were 43.6 and 40.4 micron with wind velocities of 1.1 and 22.4 mph, respectively. The 70 micron diameter water droplets lost 76 and 81% of their volume during flights with wind velocities of 1.1 and 22.4 mph, respectively. For 200 micron diameter droplets with the same conditions, the final droplet sizes at time of deposition were 199 micron for all wind velocities over a range of 1.1 to 22.4 mph.

Temperature can affect evaporation rate during flight and hence droplet size and drift distance. Because smaller droplets have greater surface area to volume ratios and longer flight times than larger droplets, temperature has greater influence on the drift distances of smaller droplets. With wind velocity of 5.6 mph and relative humidity of 50%, 50 micron diameter water droplets drifted 53.1 and 23.5 ft before completely evaporating at temperatures of 50 and 86 degrees F, respectively. With the same conditions, 100 micron diameter droplets drifted 10.5 and 11.6 ft before deposition at temperatures of 50 and 86 degrees F, respectively. Ambient temperatures within the range of 50 and 86 degrees F had very little influence on drift distances of 200 micron diameter and larger water droplets when wind velocity varied from 1.1 to 22.4 mph.

Figure 4 illustrates the simulated mean drift distances for 50, 100 and 200 micron diameter water droplets with 10 mph wind velocity, 50% RH and ambient temperatures of 55, 65, 75 , and 85 degrees F. The curve for 50 micron droplets shows that drift distance decreased as temperature increased. The 50 micron diameter droplets completely evaporated before deposition. Small droplets tend to travel at speed close to wind velocity. When temperature, and hence evaporation rate increases, their travel distance over their lifetime tends to decrease. The curve for 100 micron diameter droplets shows that drift distance before deposition increased with increased temperature. The drift distance tended to increase with increased temperature because increased temperature resulted in faster evaporation rate, smaller droplet size and increased travel distance before deposition. Temperature over the range of 50 to 86 degrees F had little influence on drift distances of 200 micron diameter droplets. The data used to produce the curves on Figure 3 are presented in Table 3.

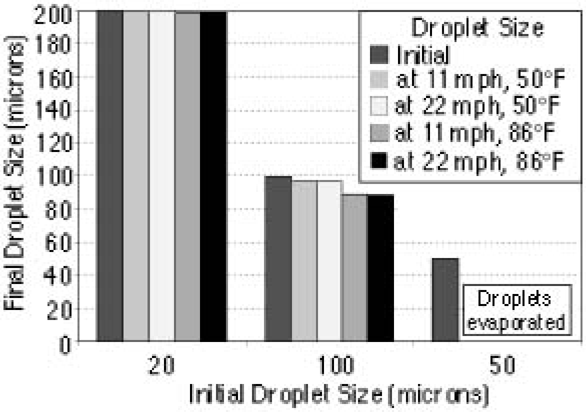

Figure 3. Effect of temperature and wind velocity on droplet sizes at the end of flight of 50, 100 and 200 micron diameter water droplets discharged down at 65 ft/second toward a target 18 inches below nozzle (RH=50%).

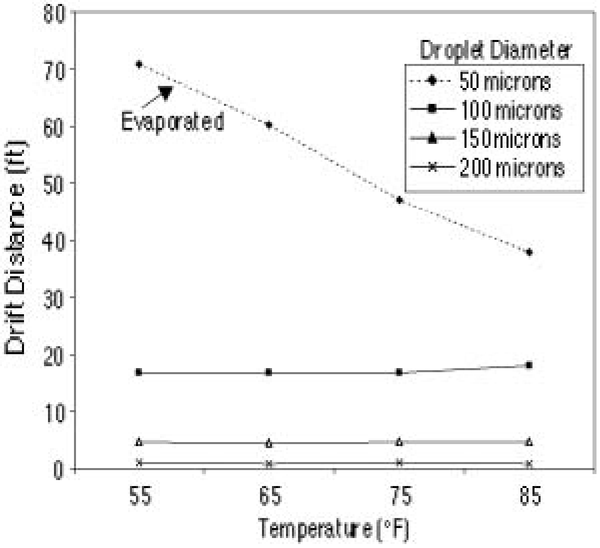

Figure 4. Mean drift distances for 50, 100 and 200 micron diameter water droplets with 10 mph wind velocity, 50% RH and ambient temperatures of 55, 65, 75 , and 85 degrees F.

Table 3. Effect of wind velocity and temperature on drift distances of droplets directed downward with initial velocity of 65 ft/second toward target 18 inches below discharge point. (Relative humidity = 50%; Turbulence intensity = 20%)

Initial Droplet size (micron)	Wind velocity (mph)	Drift Distance (ft)			
		Temperature (degrees F)			
		55	65	75	85
20	2	4.24*	4.47	4.64	4.79*
20	4	7.23*	7.33*	7.71*	7.79*

20	6	10.07*	9.20*	9.22*	9.07
20	8	12.82*	11.33*	10.42*	10.38*
20	10	15.55*	13.27*	11.92*	11.44
50	2	15.73*	14.97*	13.51*	12.60*
50	4	29.55*	26.39*	22.00*	18.82*
50	6	43.28*	37.87*	30.19*	25.18*
50	8	56.91*	49.21*	38.73*	31.79*
50	10	70.92*	60.31*	46.97*	37.90*
100	2	3.35	3.34	3.53	3.63
100	4	6.69	6.71	7.03	7.23
100	6	10.03	10.05	10.58	10.82
100	8	13.37	13.40	14.08	14.44
100	10	16.74	16.76	16.73	18.10
150	2	0.94	0.92	0.96	0.94
150	4	1.85	1.82	1.91	1.88
150	6	2.77	2.73	2.85	2.81
150	8	3.69	3.64	3.78	3.76
150	10	4.64	4.56	4.75	4.70
200	2	0.21	0.20	0.21	0.20
200	4	0.39	0.39	0.39	0.38
200	6	0.57	0.54	0.58	0.54
200	8	0.74	0.76	0.78	0.74
200	10	0.98	0.95	0.96	0.93

* Droplet completely evaporated before deposition.

Table 4 shows the mean drift distances for water droplets with initial diameters (25-300 micron), ambient temperatures (55-85 degrees F), relative humidities (20-100%), and 10 mph wind velocity. At low temperature (55 degrees F) and high relative humidity (80%), 50 micron diameter droplets were able to reach 18 in below their discharge point but traveled about 120 ft downwind before depositing. Table 4 indicates that relative humidity has little influence on drift distances of 150 micron diameter and larger droplets. This is because the flight times of these droplets are short. With wind velocity of 10 mph, 200 micron diameter droplets were only displaced over a range of less than 1 foot (0.93 to 0.98 ft) for the ranges of relative humidity and ambient temperature.

Table 4. Effect of relative humidity and ambient temperature on mean drift distances of various size water droplets directed downward at 65 ft/second toward a target 18 inches below point of discharge. (Wind velocity = 10 mph)

Droplet size (micron)	**Ambient temp. (degrees F)**	**Drift distances (ft)**				
		Relative humidity (%)				
		20	**40**	**60**	**80**	**100**

25	55	17.93*	20.37*	29.76*	56.43*	381.60
25	65	14.67*	16.63*	23.53*	43.18*	377.97
25	75	12.58*	14.41*	19.94*	37.95*	391.31
25	85	11.41*	12.77*	17.81*	33.25*	400.12
50	55	63.32*	60.87*	60.87*	119.73	76.78
50	65	48.21*	53.93*	63.82*	93.51*	76.05
50	75	37.58*	42.00*	55.32*	87.24*	78.82
50	85	30.81*	34.40*	44.81*	73.93*	80.34
100	55	16.90	16.82	16.63	16.43	16.20
100	65	16.97	16.88	16.64	16.36	15.99
100	75	17.94	17.77	17.48	17.05	16.46
100	85	18.55	18.28	17.88	17.34	16.55
150	55	4.65	4.64	4.62	4.62	4.59
150	65	4.58	4.57	4.56	4.54	4.50
150	75	4.78	4.78	4.72	4.72	4.66
150	85	4.76	4.73	4.70	4.64	4.58
200	55	0.98	0.98	0.95	0.95	0.95
200	65	0.95	0.95	0.94	0.94	0.94
200	75	0.96	0.96	0.96	0.96	0.96
200	85	0.93	0.93	0.93	0.93	0.93
300	55	0.98	0.98	0.95	0.95	0.95
300	65	0.95	0.95	0.94	0.94	0.94
300	75	0.96	0.96	0.96	0.96	0.96
300	85	0.93	0.93	0.93	0.93	0.93
* Droplet completely evaporated before deposition.						

Figure 5 illustrates the effect of relative humidity on mean drift distances of 25, 50, 100 and 200 micron size water droplets for 10 mph wind velocity. The ambient temperature was 65 degrees F for the simulations. The mean drift distances of 25 and 50 micron diameter water droplets, before complete evaporation, increased with increased relative humidity over the range of 20 to 80%. For the same conditions, but with 100% RH, 50 micron diameter droplets deposited 18 in below and 76 ft downwind from the point of discharge while 25 micron diameter droplets drifted beyond 378 ft. There was no change in drift distance of 200 micron diameter water droplets over the 10 to 80% range of relative humidity.

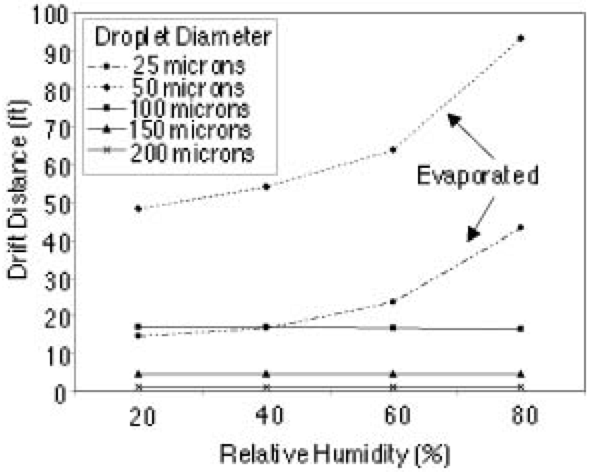

Figure 5. The effect of relative humidity on mean drift distances of 25, 50, 100 and 200 micron size water droplets for 10 mph wind velocity. (The ambient temperature= 65 degrees F).

Droplet Discharge Height

Agricultural pesticides are applied with a very wide range of nozzle heights above targets. Nozzle height depends on several factors including the sprayer setup, target and operating conditions. Table 5 shows the effects of discharge height (0.5-3.0 ft), droplet diameter (50-300 micron) and wind velocity (2.0-10.0 mph) on mean drift distances of water droplets directed downward with initial velocity of 65 ft/seconds. Relative humidity and ambient temperature were 50% and 70 degrees F, for all simulations. The mean drift distances of 50 micron diameter and smaller droplets were nearly constant with each wind velocity for the discharge height range of 0.5 to 3.0 ft. This occurs because these droplets have short life times and do not travel downward far enough to deposit before completely evaporating.

Table 5. Effect of droplet discharge height and wind velocity on drift distances of various size droplets discharged downward at 65 ft/second toward a target. (Temperature: 70 degrees F; Relative Humidity = 50%)

Initial Droplet size (micron)	Wind velocity (mph)	Drift distances (ft)					
		Nozzle height (ft)					
		0.5	1	1.5	2	2.5	3.0
50	2	0.43*	13.87*	14.02*	14.14*	14.22*	13.97*
50	4	14.28*	23.51*	23.72*	23.80*	23.83*	23.98*
50	6	19.96*	32.92*	33.41*	33.65*	33.78*	33.76*
50	8	25.61*	42.32*	43.18*	43.40*	43.39*	43.73*
50	10	31.20*	51.48*	52.29*	52.89*	53.37*	53.43*
100	2	0.50	1.50	3.37	5.40	7.51	9.85
100	4	0.99	2.99	6.76	10.82	15.02	19.72
100	6	1.48	4.47	10.15	16.23	22.54	29.62
100	8	1.98	5.97	13.51	21.63	30.05	39.51

100	10	2.49	7.47	16.91	27.06	37.59	49.40
150	2	0.04	0.29	0.92	1.80	2.77	3.76
150	4	0.07	0.57	1.82	3.57	5.50	7.49
150	6	0.11	0.86	2.73	5.34	8.25	11.23
150	8	0.16	1.15	3.63	7.12	11.01	14.99
150	10	0.19	1.43	4.55	8.92	13.78	18.75
200	2	0.02	0.07	0.20	0.61	1.13	1.76
200	4	0.03	0.14	0.38	1.19	2.24	3.51
200	6	0.05	0.20	0.55	1.76	3.34	5.23
200	8	0.06	0.27	0.75	2.37	4.48	7.01
200	10	0.08	0.34	0.93	2.98	5.63	8.79
300	2	0.00	0.01	0.05	0.11	0.20	0.38
300	4	0.02	0.05	0.10	0.24	0.41	0.79
300	6	0.02	0.07	0.15	0.35	0.62	1.17
300	8	0.02	0.08	0.21	0.46	0.80	1.56
300	10	0.04	0.12	0.26	1.04	1.04	1.97
* Droplet completely evaporated before deposition.							

Increased discharge height resulted in increased drift distances for 100 micron diameter and larger water droplets (Table 5). For example, with 10 mph wind velocity and 65 ft/second initial droplet velocity, when discharge height increased from 0.5 to 3.0 ft, the mean drift distance of 200 and 300 micron diameter droplets increased from 2.49 to 49.40 ft and 0.08 to 8.79 ft, respectively. When the discharge height increased from 0.5 to 3.0 ft, the mean drift distance of 100 micron diameter droplets increased from 1.98 to 39.51 ft and kept increasing until the discharge height of 10 ft is reached. When the discharge height is increased beyond 10 ft, the drift distance remained constant (217 ft) because the 100 micron diameter water droplets completely evaporated before deposition.

When simulations for large size droplets were performed, results indicated that if the discharge height becomes too large, even the large droplets have tendency to drift under high wind velocity conditions. For example, the mean drift distance of 1000 micron diameter droplets was 5 ft for wind velocity and discharge height of 22 mph and 10 ft, respectively. Computer simulation also indicated that the mean drift distances of 1000 and 2000 micron diameter droplets were 57 and 19 ft, respectively, before impaction 13 ft below the point of discharge for 22 mph wind velocity, 50% relative humidity, and zero mph initial droplet velocity.

Figure 6 illustrates the effect of discharge height of droplets on the mean drift distances of 50, 100, 200, and 300 micron diameter water droplets for 10 mph wind velocity, 50% RH and 65 degrees F. The graph shows that increasing discharge height above 0.5 ft had no affect on the mean drift distance of 50 micron diameter droplets because they completely evaporated before depositing. However, increasing discharge height of 100 micron diameter and larger droplets affects their mean drift distances. Changes in discharge heights have less effect on mean drift distances as droplet size increases above 200 micron diameter.

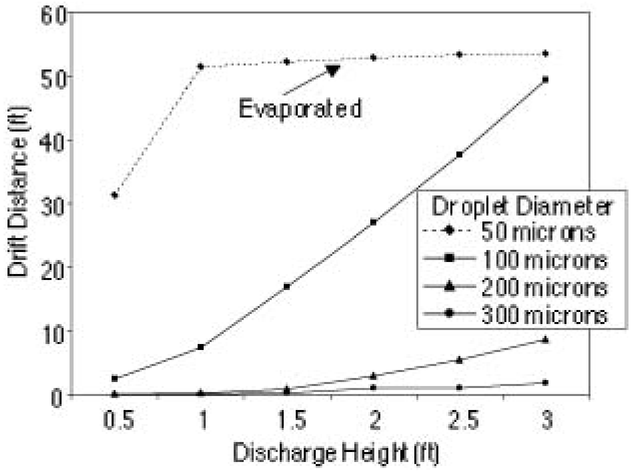

Figure 6. The effect of discharge height of droplets on drift distances of 50, 100, 200, and 300 micron diameter water droplets at 10 mph wind velocity (RH= 50%, T= 65 degrees F.)

Initial Droplet Velocity

Pesticides are applied with many different types of nozzles. The velocity of droplets delivered by nozzles depends on the configuration of the nozzle, and operating pressure. Table 6 shows the effects of initial droplet velocity (0-120 ft/second) and wind velocity (2.5-10.0 mph) on the mean drift distances of various size water droplets directed downward toward a target 1.5 ft below the point of discharge. Relative humidity and ambient temperature were 50% and 70 degrees F, for all simulations. The data indicate that increasing the initial downward droplet velocity can decrease the mean drift distances before deposition of 75 micron diameter and larger droplets. When spray is directed downward from a nozzle centered over a row of plants, for example, it is important to maximize spray deposition on the target. Even for 30 ft/second initial droplet velocities, the drift distances of 100 micron diameter and smaller water droplets would be excessive when spraying row crops if the droplets were exposed to crosswinds with velocities of only 1 mph. Also, for many applications where the spray is exposed to crosswinds, the drift distances of 200 micron diameter droplets would be excessive for droplets directed downward with slow velocities. For example, the mean drift distances of 200 micron diameter droplets in 2.5 mph crosswinds are 2.4 and 0.9 ft for droplets directed downward with 0 and 30 ft/sec velocities, respectively. When wind velocity was 10 mph, the mean drift distance of 200 micron diameter droplets decreased from 9.88 to 0.28 ft as the initial downward droplet velocity increased from 0 to 120 ft/s. Some applicators use large droplets to reduce spray drift potential. With no initial downward droplet velocity (zero ft/second) and 18 in discharge height, the mean drift distances of 1000 micron diameter droplets were 0.24, 0.63, 1.08, and 1.62 ft when wind velocities were 2.5, 5.0, 7.5, and 10.0 mph, respectively. With 60 ft/sec instead of 0 m/s initial velocity, the mean drift distance of the 1000 micron diameter drops was only 0.04 ft when wind velocity was 10 mph. Table 6 also illustrates that initial droplet velocities had no effect on drift distances of 50 micron diameter water droplets. None of the 50micron diameter and smaller droplets reached 18 in below the point of discharge before complete evaporation for a range of initial droplet velocities from zero to 120 ft/second and wind velocities from 2.5 to 10.0 mph.

Table 6. Effect of initial droplet velocity and wind velocity on drift distances of various size water droplets directed downward toward a target 18 inches below point of droplet discharge. (Temperature: 70 degrees F;

Relative Humidity = 50%)

Droplet size (micron)	Wind velocity (mph)	Drift Distances (ft)				
		Initial Droplet Velocity (ft/second)				
		0	**30**	**60**	**90**	**120**
50	2.5	16.50*	16.42*	16.40*	16.53*	16.50*
50	5.0	28.80*	28.74*	28.62*	28.67*	28.67
50	7.5	40.76*	40.73	40.74	40.70	40.54*
50	10.0	52.98*	52.70*	52.43*	52.48*	52.67*
75	2.5	17.86	13.05	11.35	10.29	9.09
75	5.0	33.83	25.82	22.19	20.03	18.31
75	7.5	49.58	38.64	33.03	29.74	27.17
75	10.0	65.28	52.26	44.00	39.49	36.01
100	2.5	5.39	5.39	4.37	3.64	3.06
100	5.0	14.51	10.79	8.75	7.26	6.10
100	7.5	21.84	16.25	13.11	10.88	9.12
100	10.0	29.25	21.75	17.51	14.48	12.15
150	2.5	3.64	2.05	1.26	0.73	0.39
150	5.0	7.34	4.10	2.49	1.45	0.76
150	7.5	11.07	6.19	3.73	2.15	1.12
150	10.0	14.83	8.34	5.00	2.87	1.49
200	2.5	2.36	0.89	0.31	0.13	0.07
200	5.0	4.82	1.79	0.58	0.25	0.15
200	7.5	7.34	2.72	0.89	0.82	0.20
200	10.0	9.88	3.72	1.20	0.52	0.28
300	2.5	1.39	0.24	0.08	0.04	0.03
300	5.0	2.91	0.49	0.15	0.08	0.5
300	7.5	4.56	0.76	0.22	0.12	0.07
300	10.0	6.23	1.06	0.31	0.17	0.11
500	2.5	0.67	0.08	0.03	0.01	0.00
500	5.0	1.52	0.16	0.05	0.03	0.03
500	7.5	2.49	0.25	0.09	0.05	0.03
500	10.0	3.58	0.34	0.11	0.06	0.04
1000	2.5	0.24	0.03	0.00	0.00	0.00
1000	5.0	0.63	0.05	0.03	0.01	0.00
1000	7.5	1.08	0.08	0.03	0.03	0.01
1000	10.0	1.62	0.11	0.04	0.03	0.03

* Droplet completely evaporated before deposition.

Figure 7 illustrates the influence of droplet size and initial downward velocity on drift distances of 50 to 300 micron diameter water droplets for 10 mph wind velocity. The relative humidity and ambient temperature were 50% and 70 degrees F for all simulations. As evident from the data presented on Figure 7, for 10 mph wind velocity, drift distances are greatly influenced by both droplet size and the initial downward velocity of the droplet. The drift distances of 100 micron diameter and larger droplets decreased with increased initial droplet velocity. Figure 7 also illustrates the large difference in drift distances between 100 and 200 micron diameter water droplets.

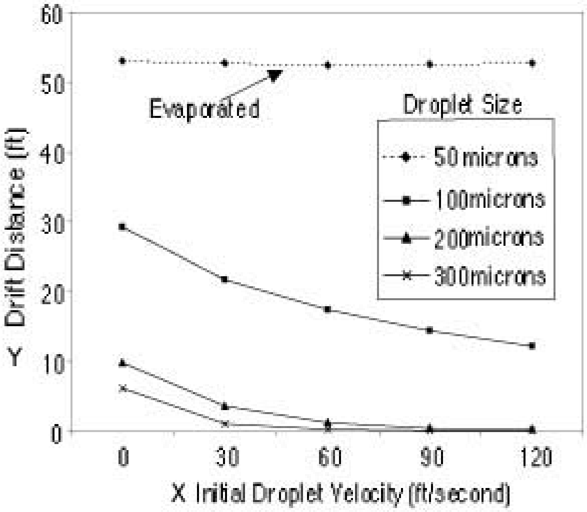

Figure 7. The influence of droplet size and initial downward velocity on drift distances of 50 to 300 micron diameter water droplets for 10 mph wind velocity (RH= 50%, T=70 degrees F).

Conclusions

The following conclusions are based on the computer simulations of mean drift distances of water droplets within the range of variables discussed in this publication.

1. 1. Changes in wind velocity, discharge height, ambient temperature and relative humidity had much greater influence on the drift distances of droplets 100 micron diameter or less than on 200 micron diameter and larger droplets. For droplets that did not evaporate before deposition, there was a nearly linear relationship between wind velocity and drift distance.

2. 2. With 100% RH, 10 micron diameter droplets drifted beyond 650 ft when wind velocity exceeded 5.5 mph.

3. 3. Droplets 50 micron diameter and smaller completely evaporated before reaching 18 inches below the discharge point, regardless of initial velocity, for relative humidities 60% and lower and temperatures between 55 and 85 degrees F. Also, the mean drift distances of these droplets increased with increased droplet size.

4. 4. Mean drift distances of 100 micron diameter and larger droplets increased with increased wind velocity and discharge height, but decreased with increased droplet size and discharge velocity.

5. 5. Drift distances of water droplets as large as 200 micron diameter were influenced by initial

droplet velocity and height of discharge.

6. 6. For 10 mph wind velocity, 20% turbulence intensity, 50% RH, 70 degrees F ambient temperature, 60 ft/second initial downward droplet velocity and 18 inches discharge height, the mean drift distances of 100, 200, and 500 micron diameter droplets were 17.5, 1.2, and 0.11 ft, respectively.

7. 7. The drift potential of 200 micron diameter droplets is considerably less than for 100 micron diameter droplets. Unless some means such as shields or air jets are used, drift reduction techniques should be directed toward reducing the portion of spray volume contained in droplets less than 200 micron diameter for applications where minimizing drift is important. For some applications, such as with high nozzles and slow initial downward velocity and high wind velocity, droplets larger than 200 micron diameter may be needed to satisfactorily reduce drift.

Acknowledgment

Most of the information presented in this publication was adapted from the following publication.

Zhu, H., D.L. Reichard, R.D. Fox, R.D. Brazee and H.E. Ozkan. 1994. Simulation of drift of discrete sizes of water droplets from field sprayers. Transactions of the ASAE 37(5):1401-1407.

References

Ozkan, H.E. 1991. Reducing spray drift. OSU Extension Bulletin 816. Ohio State University Extension, Columbus, Ohio.

Reichard, D.L., H. Zhu, R.D. Fox and R.D. Brazee. 1992a. Computer simulation of spray drift that influence spray drift. Transactions of the ASAE 35(5):1401-1407.

Reichard, D.L., H. Zhu, R.D. Fox and R.D. Brazee. 1992b. Wind tunnel evaluation of a computer program to model spray drift. Transactions of the ASAE 35(3):755-758.

Keith L. Smith, Associate Vice President for Ag. Adm. and Director, OSU Extension.

TDD No. 800-589-8292 (Ohio only) or 614-292-1868

APPLICATION FOR PERMIT
SUNDANCE WEST

VOLUME III: ENGINEERING DESIGN AND CALCULATIONS
SECTION 9: EVAPORATION CALCULATIONS

ATTACHMENT III.9.B

DRIFTSIM: PREDICTING DRIFT DISTANCE OF SPRAY DROPLETS AND RESULTING EVAPORATION

Bulletin 923

DRIFTSIM—Predicting Drift Distances of Spray Droplets

Heping Zhu and Robert D. Fox
Agricultural Engineers
USDA-ARS
Application Technology Research Unit
Wooster, OH 44691

H. Erdal Ozkan
Professor and Extension Agricultural Engineer
Food, Agricultural, and Biological
Engineering Department
The Ohio State University
Columbus, OH 43210

Introduction

Spray drift, movement of pesticide droplets through air during or after application to a site other than the intended targets of application, is one of the most critical problems pesticide applicators have to deal with. For example, three-fourths of agriculture-related complaints investigated by the Ohio Department of Agriculture involved drift issues; two-thirds of the total complaints in a five-year period brought to the attention of Iowa Department of Agriculture were related to drift problems; about one-third of court cases due to spray misapplications reported by a major insurance company involved drift damages. Drift problems will become even more critical in the future when farmers use more genetically modified crops which restrict use of non-selective herbicides because even a small amount of these herbicides can cause serious damage to neighboring crops.

Although complete elimination of spray drift is impossible, problems can be minimized if chemicals are applied with the proper equipment and methods under favorable weather conditions. Increased awareness of environmental quality and better understanding of the causes of spray drift can help operators make reasonable judgments for safer, more efficient applications.

Factors that significantly influence off-target movement of droplets are wind velocity and direction, droplet size and density, and distance from the atomizer to the target. Other factors that influence drift include droplet velocity, and direction of discharge from the atomizer, volatility of the spray fluid, relative humidity, ambient temperature, and atmospheric turbulence intensity. Many scientists have conducted field tests to study influence of these variables on spray drift. Unfortunately, field tests have the limitation that weather conditions cannot be controlled and the variables that influence spray drift may interact and vary during a test.

Computer simulations can allow determination of effects of different variables such as droplet size and velocity, relative humidity, and wind velocity on spray drift. One such computer model or commercially available computational fluid dynamics (CFD) program was evaluated by Reichard et al. (1992) in Ohio for modeling the effects of several variables on spray drift. Experiments were conducted to verify the accuracy of the computer model in predicting drift distances of water droplets in a wind tunnel with a single size droplet generator. These tests revealed that the computer model could be used to accurately calculate spray drift distances for a wide range of spray droplet sizes and wind velocities. With the computer model, individual or mean droplet trajectories were determined for different values of several variables listed above (Zhu et al., 1994). However, the model is very expensive and requires special operator skills and a high-speed computer with a large memory space to operate. It also takes long time to calculate a drift distance even for a single simulation condition.

DRIFTSIM is a simplified and user-friendly version of a computer model developed with a visual BASIC language program to interpolate values from a large database of drift distances originally calculated from the CFD model evaluated by Reichard et al. (1992). Detailed information on DRIFTSIM is given in a publication by Zhu et al. (1995). DRIFTSIM can be used to determine effects of major drift-causing factors on the mean drift distances up to 656 feet from the release point for individual water droplets or classes of droplets. These factors or variables used in DRIFTSIM are listed in Table 1, with the limiting values acceptable to DRIFTSIM.

Table 1. Variables and their ranges used in DRIFTSIM program

Variable	Range			
	American Unit		Metric Unit	
Wind velocity	0-22	mph	0-10	m/s
Droplet size	10-2000	Micron (µm)	10-2000	µm
Droplet velocity	0-110	mph	0-50	m/s
Discharge height	0-6.5	ft	0-2.0	m
Temperature	50-86	°F	10-30	°C
Relative humidity	10-100	%	10-100	%

Turbulence intensity is another important factor indicating how much the wind velocity varies about the mean. It can vary considerably in field conditions, but based on the frequency of nearly 20% turbulence intensity observed in many of the field measurements conducted in Ohio, a constant value of 20% turbulence intensity was used in DRIFTSIM for all calculations.

For classes of droplets in this version of DRIFTSIM, the upper-limit log normal (ULLN) method (Goering and Smith, 1978) was used to calculate the drop-size distribution produced by a nozzle. The ULLN method used three size measurements, $D_{V.1}$, $D_{V.5}$, and $D_{V.9}$ to estimate the volume of spray in droplets less than a selected droplet size. The $D_{V.1}$, $D_{V.5}$, and $D_{V.9}$ for the droplet size spectra produced by a specific nozzle can be measured with most modern droplet sizing instruments. DRIFTSIM computes the drift distance for the average of lower and upper droplet size for each size class. It also computes the portion of spray in each size class.

Terms used in DRIFTSIM program

Single size droplets: For the program to calculate a mean drift distance of a given size droplets with other variables

Array of droplets (DVs): For the program to calculate drift distances with the portion of volume for many size classes of droplets by entering $D_{v.1}$, $D_{v.5}$ and $D_{v.9}$

$D_{v.1}$: Droplet diameter such that 10% of total liquid volume that is in droplets smaller than $D_{v.1}$ (micron or μm)

$D_{v.5}$: Droplet diameter such that 50% of total liquid volume that is in droplets smaller than $D_{v.5}$ (micron or μm)

$D_{v.9}$: Droplet diameter such that 90% of total liquid volume that is in droplets smaller than $D_{v.9}$ (micron or μm)

Array of droplets (nozzle): For the program to calculate drift distances with the portion of volume for many size classes of droplets by selecting nozzle type [**Note:** In DRIFTSIM, data is available for only a limited number of nozzles]

Temperature: Ambient air temperature during spray operation (°F in American unit or °C in Metric unit)

Relative humidity: Relative humidity of ambient air (%)

Wind velocity: Wind speed at nozzle level during the spray application (mph in American unit or m/s in Metric unit)

Discharge height: Nozzle orifice height above the ground (ft in American unit or m in Metric unit)

Droplet velocity: Velocity of droplets near the outlet of the nozzle orifice (mph in American unit or m/s in Metric unit)

Droplet diameter: Droplet diameter near the outlet of the nozzle orifice (micron or μm)

Operating pressure: Liquid pressure acting on the nozzle orifice (psi or kPa)

Operating DRIFTSIM

To operate DRIFTSIM, minimum requirements for a computer are Pentium PC with a CD drive, MS-Windows version 3.1 or later, 8 MB of memory, 30 MB free hard drive space, and a mouse.

DRIFTSIM is compact enough to fit on a CD. It can be operated from either a CD or a computer hard drive. DRIFTSIM automatically starts running when the CD containing DRIFTSIM is inserted in the CD drive of the computer. To operate the program from the computer hard drive, DRIFTSIM files and program should be first copied onto the hard drive, and then the user should execute DRIFTSIM.exe file to start the program. The program may run somewhat faster from a hard drive than a CD.

After the program starts, it gives three on-screen boxes for choosing units and droplet size types and entering values of simulation variables. A selection of units or droplet size types can be changed at any time during the operation without needing to exit the program. To change the value of any variable, simply click on the input area next to the variable, and enter a value that is within the acceptable range defined in Table 1. Only two screens appear during the whole calculation process: input and result screens.

Steps to run DRIFTSIM from a CD

(1) Insert CD in the computer.

(2) Introductory information for DRIFTSIM as shown in Figure 1 appears on the screen.

Figure 1

DRIFTSIM

Version 1.12.04

Created by

Dr. Heping Zhu and Dr. Robert D. Fox

Application Technology Research Unit
USDA-ARS

and Dr. H. Erdal Ozkan

Professor and Extension Agricultural Engineer

Food, Agriculture, and Biological Engineering Department
The Ohio State University

(3) Click on the *"Start Driftsim"* box. Three on-screen boxes for choosing and entering simulation conditions appear on the screen as shown in Figure 2. [**Note:** initial values for drift variables shown on the screen are built into DRIFTSIM. These values are only examples, not recommended values.]

Figure 2

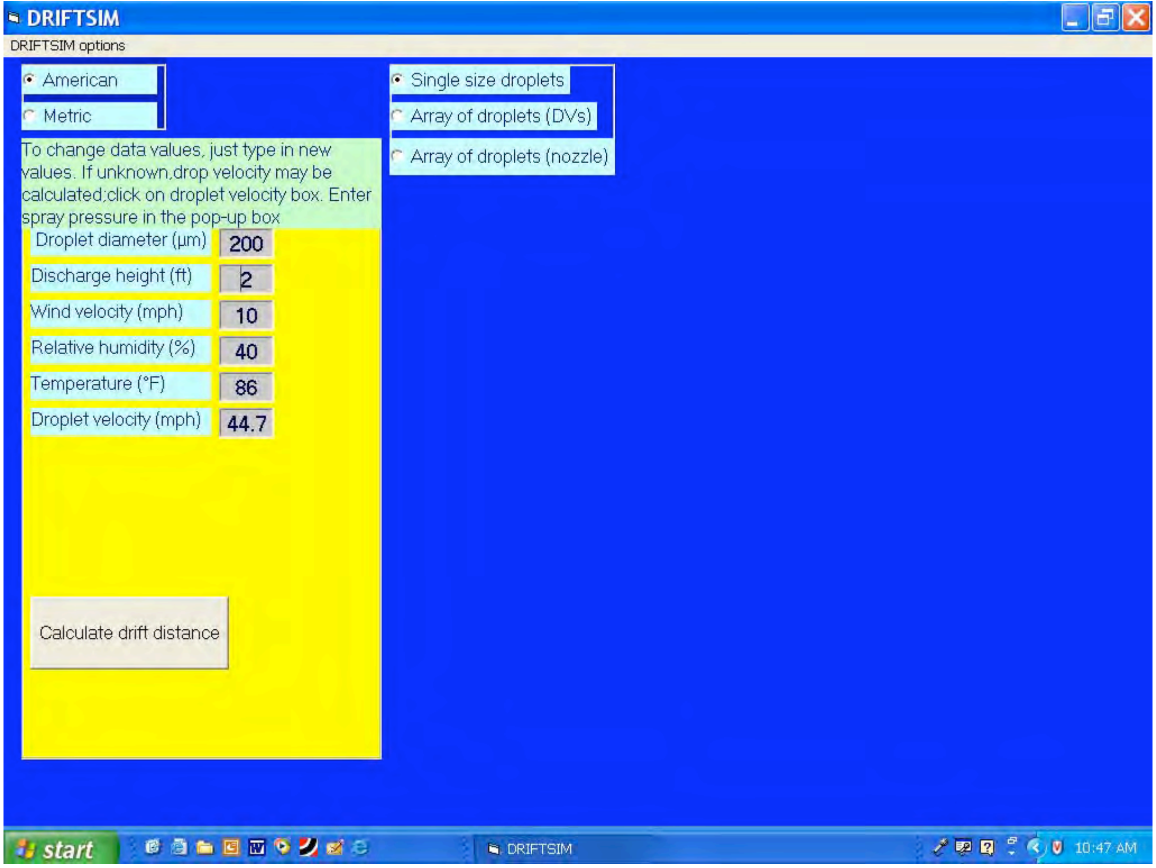

● American
○ Metric

● Single size droplets
○ Array of droplets (DVs)
○ Array of droplets (nozzle)

To change data values, just type in new values. If unknown,drop velocity may be calculated;click on droplet velocity box. Enter spray pressure in the pop-up box

Droplet diameter (µm)	200
Discharge height (ft)	2
Wind velocity (mph)	10
Relative humidity (%)	40
Temperature (°F)	86
Droplet velocity (mph)	44.7

(4) Select either *"American"* or *"Metric"* unit for calculation.

(5) Select one of the three choices as a type of input for the droplet size: "*Single size droplets", "Array of droplets (DVs)",* or *"Array of droplets (nozzle)".*

(6) For "*Single size droplets*", follow steps (7) to (11); for "*Array of droplets (DVs)*", follow steps (12) to (17); for "*Array of droplets (nozzle)*", follow steps (19) to (23).

[**Note:** Steps (7) to (11) are for *"Single size droplets"* only]

(7) Enter or change values for *"Droplet diameter", "Wind velocity", "Discharge height", "Droplet velocity", "Temperature", "Relative humidity"* for inputs of variables. The value of *"Droplet velocity"* can be entered either by the user, or automatically by the program once the user enters a value for the operating pressure on the box which pops up on the screen as shown in Figure 3 after the user empties the "*Droplet velocity*" box. A red error message appears in the box under the variables if the value of an individual variable is outside the range defined in Table 1.

Figure 3

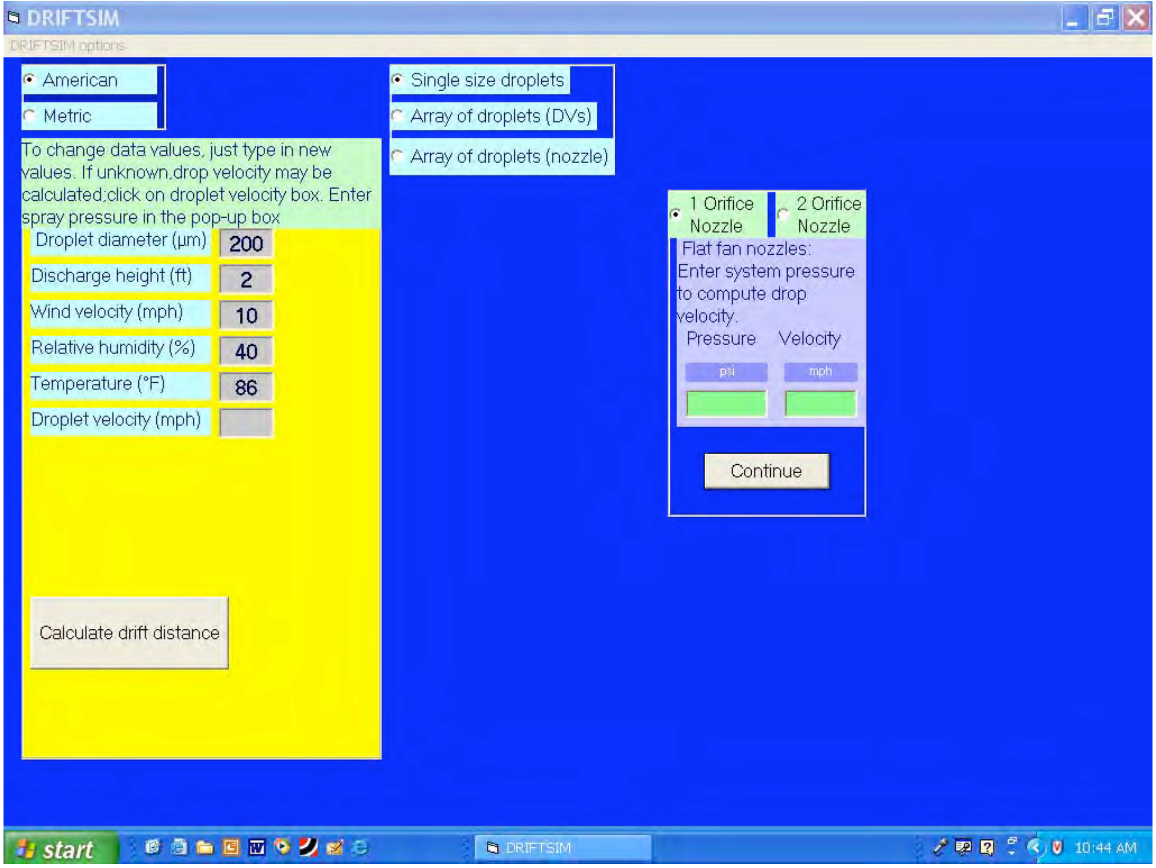

● American
○ Metric

To change data values, just type in new values. If unknown,drop velocity may be calculated;click on droplet velocity box. Enter spray pressure in the pop-up box

Droplet diameter (µm) 200
Discharge height (ft) 2
Wind velocity (mph) 10
Relative humidity (%) 40
Temperature (°F) 86
Droplet velocity (mph)

● Single size droplets
○ Array of droplets (DVs)
○ Array of droplets (nozzle)

● 1 Orifice Nozzle
○ 2 Orifice Nozzle

Flat fan nozzles: Enter system pressure to compute drop velocity.

Pressure
Velocity

(8) Click on *"Compute drift distance"* to obtain the results on the screen as shown in Figure 4.

Figure 4

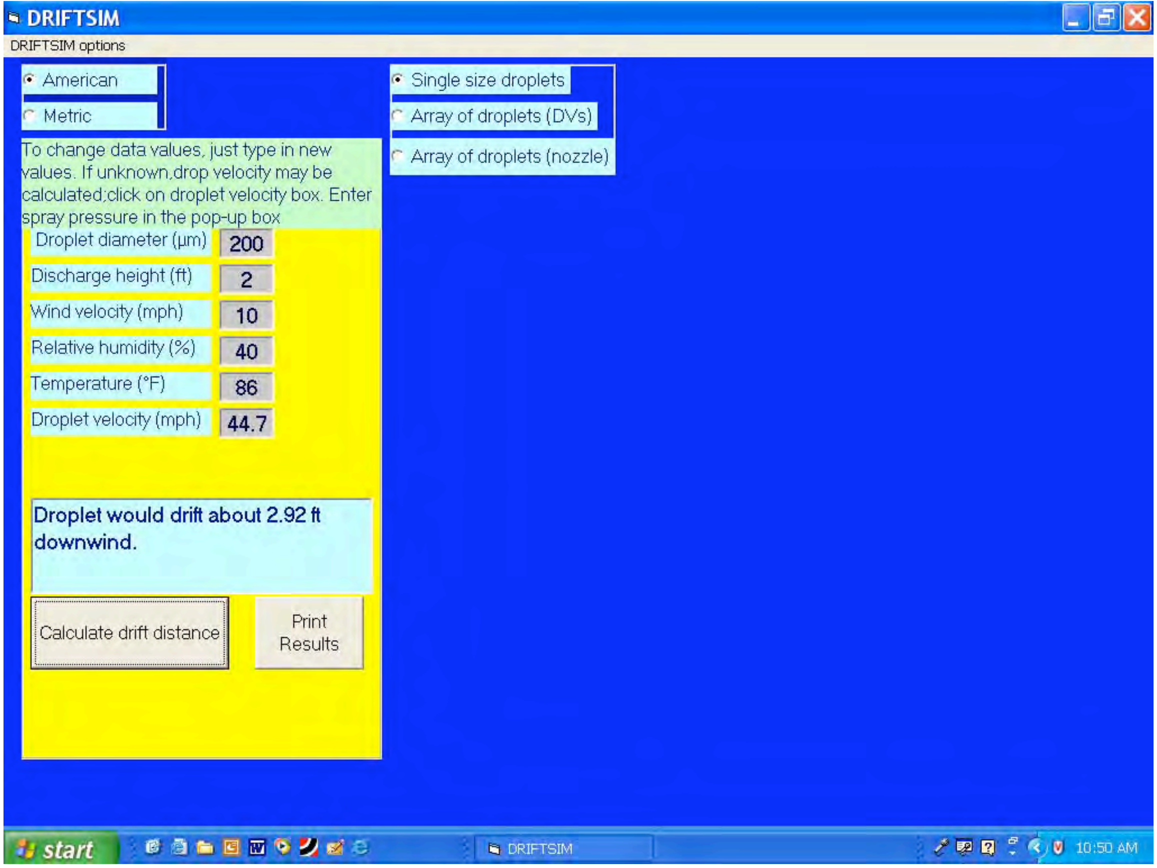

● American
○ Metric

● Single size droplets
○ Array of droplets (DVs)
○ Array of droplets (nozzle)

To change data values, just type in new values. If unknown,drop velocity may be calculated;click on droplet velocity box. Enter spray pressure in the pop-up box

Droplet diameter (μm)	200
Discharge height (ft)	2
Wind velocity (mph)	10
Relative humidity (%)	40
Temperature (°F)	86
Droplet velocity (mph)	44.7

Droplet would drift about 2.92 ft downwind.

(9) Click on *"Print results"* if you want to get a printout of input variables and the result.

(10) To continue running DRIFTSIM with a new or revised set of inputs for the "*single size droplet*", repeat steps (7) to (10).

(11) When you are done with all the simulations, exit DRIFTSIM by clicking on the **X** at the upper right corner of the window on the screen.

[**Note:** Steps (12) to (17) are for "*Array of droplets (DVs)*" only]

(12) After choosing "*Array of droplets (DVs)*", a new box for droplet size distribution appears on the screen as shown in Figure 5.

Figure 5

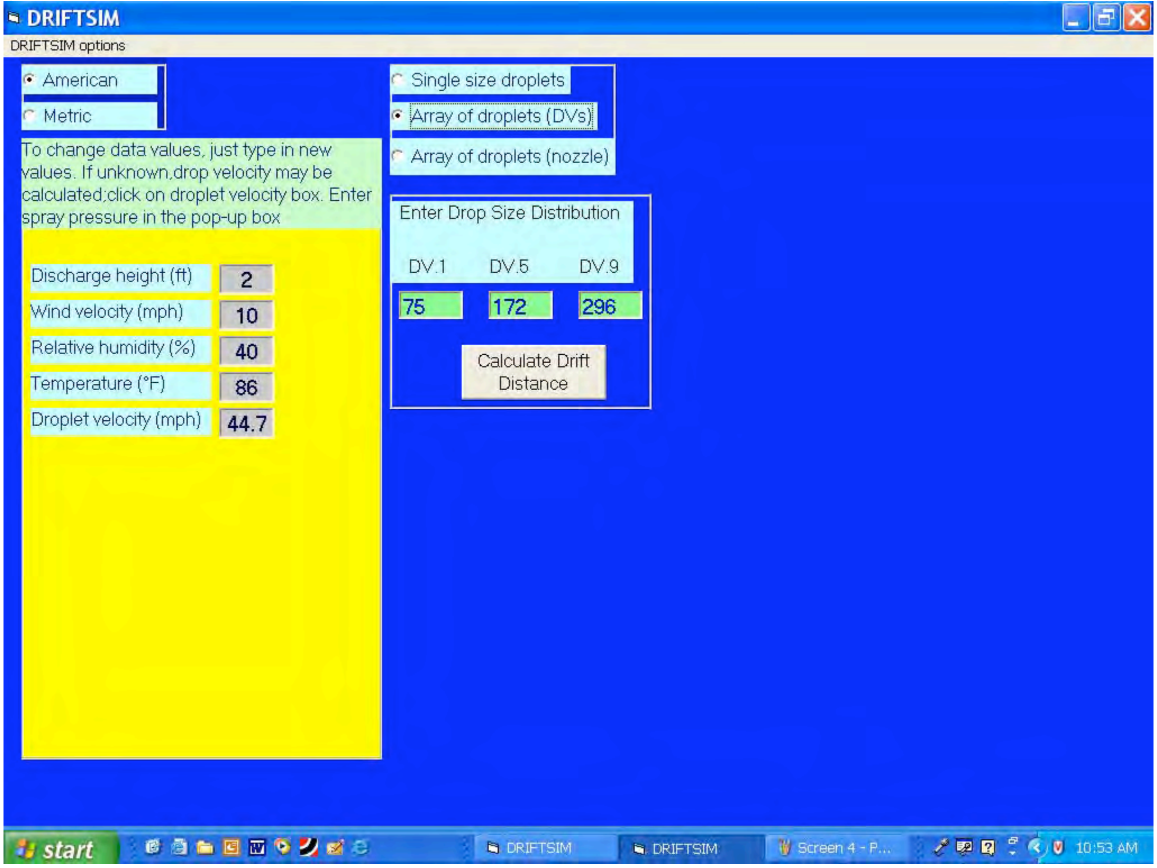

● American
○ Metric

○ Single size droplets
● Array of droplets (DVs)
○ Array of droplets (nozzle)

To change data values, just type in new values. If unknown,drop velocity may be calculated;click on droplet velocity box. Enter spray pressure in the pop-up box

Discharge height (ft) 2
Wind velocity (mph) 10
Relative humidity (%) 40
Temperature (°F) 86
Droplet velocity (mph) 44.7

Enter Drop Size Distribution

DV.1	DV.5	DV.9
75	172	296

Calculate Drift Distance

(13) Enter “$D_{v.1}$”, “$D_{v.5}$“ and “$D_{v.9}$“ values in boxes.

(14) Enter or change values for “*Wind velocity*”, “*Discharge height*”, “*Droplet velocity*”, “*Temperature*” and “*Relative humidity*”.

(15) Click on “*Calculate Drift Distance*”. Drift distances of 9 size classes of droplets along with the portion of the spray volume corresponding to each size class appear on the screen as shown in Figure 6. Error message appears on this screen if “$D_{v.1}$”, “$D_{v.5}$“ and “$D_{v.9}$“ values are not reasonable.

Figure 6

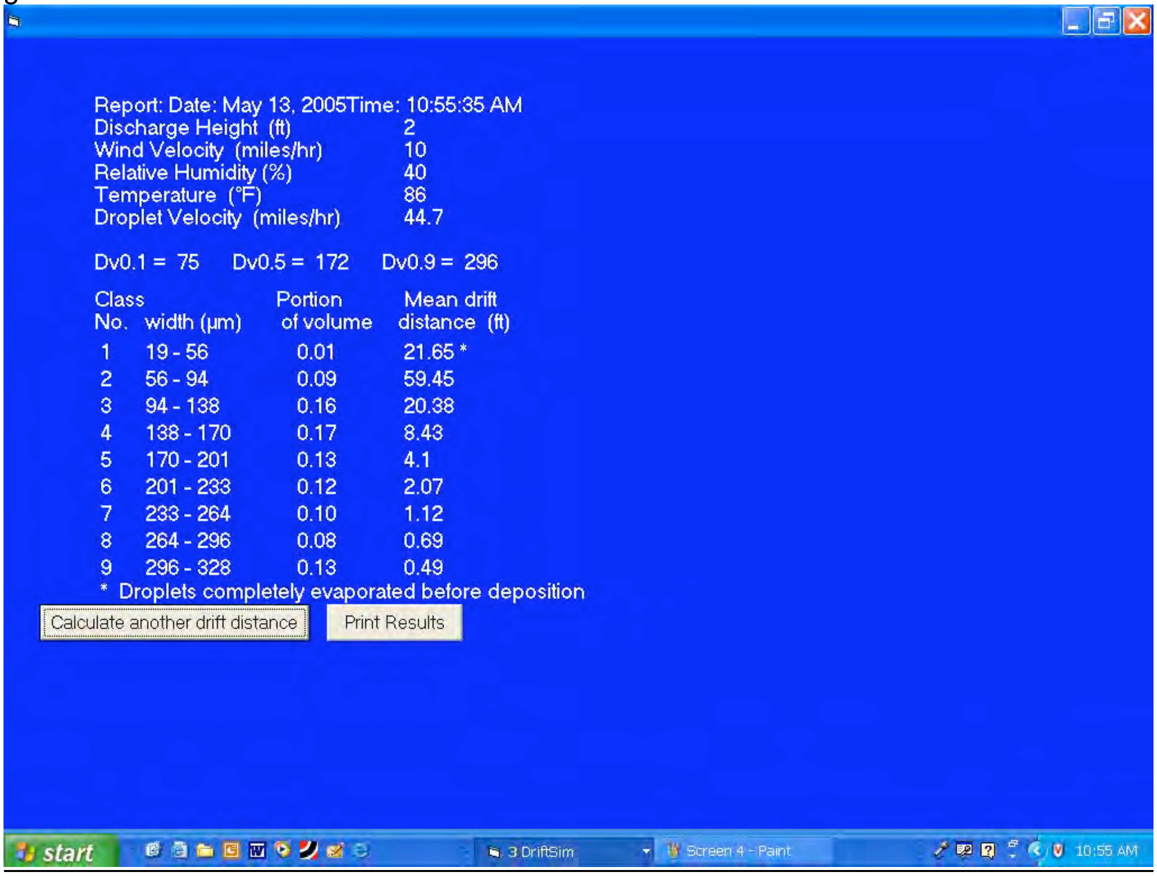

```
Report: Date: May 13, 2005Time: 10:55:35 AM
Discharge Height  (ft)                2
Wind Velocity  (miles/hr)             10
Relative Humidity (%)                 40
Temperature  (°F)                     86
Droplet Velocity  (miles/hr)          44.7

Dv0.1 =  75     Dv0.5 =  172     Dv0.9 =  296

Class                  Portion      Mean drift
No.   width (µm)       of volume    distance  (ft)
 1    19 - 56           0.01        21.65 *
 2    56 - 94           0.09        59.45
 3    94 - 138          0.16        20.38
 4    138 - 170         0.17        8.43
 5    170 - 201         0.13        4.1
 6    201 - 233         0.12        2.07
 7    233 - 264         0.10        1.12
 8    264 - 296         0.08        0.69
 9    296 - 328         0.13        0.49
 *  Droplets completely evaporated before deposition
```

(16) Click on either "*Print Results*" to get a printout of the results, or "*Calculate another drift distance*" to repeat steps (13) to (16) for a revised or new set of inputs.

(17) When you are done with all the simulations, exit DRIFTSIM by clicking on the **X** at the upper right corner of the window on the screen.

[**Note:** Steps (18) to (23) are for *"Array of droplets (nozzle)"* only]

(18) After choosing "*Array of droplets (nozzle)*", a new box with a list of several nozzles appears on the screen as shown in Figure 7.

Figure 7

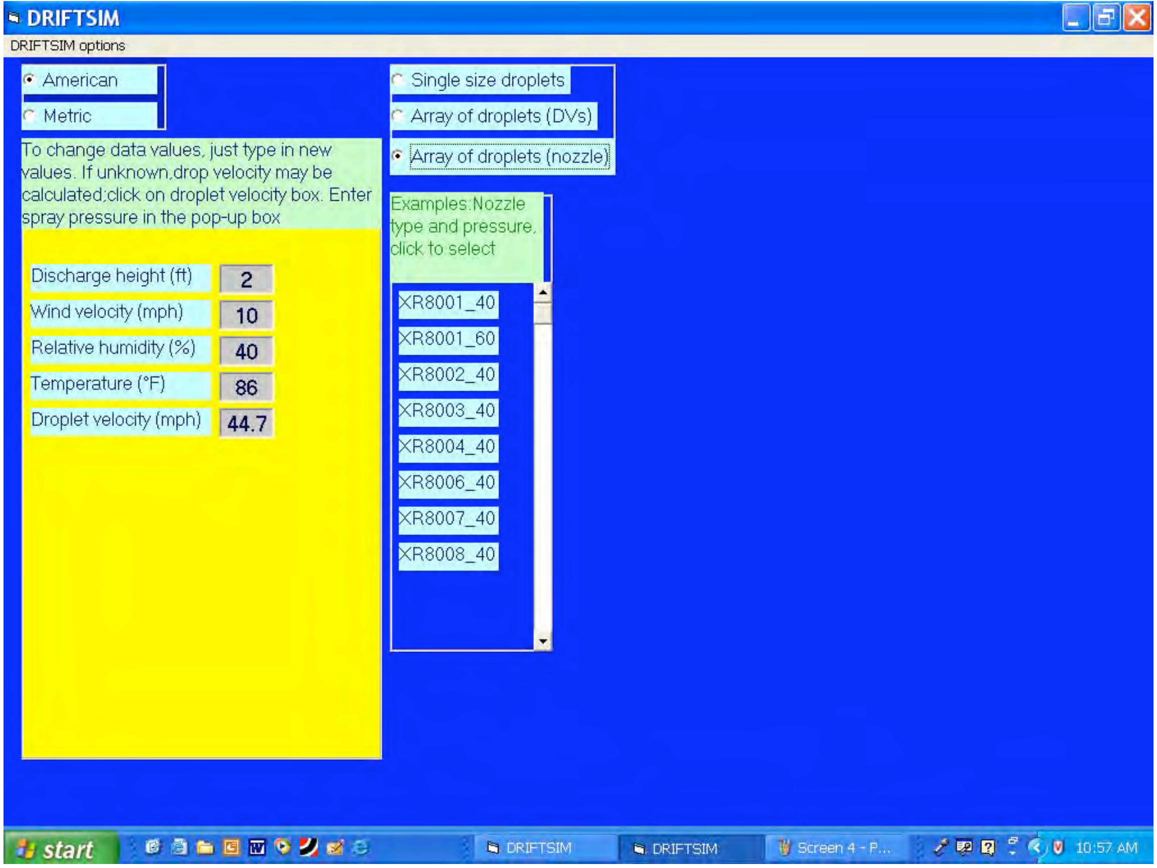

● American
○ Metric

To change data values, just type in new values. If unknown,drop velocity may be calculated;click on droplet velocity box. Enter spray pressure in the pop-up box

Discharge height (ft) 2
Wind velocity (mph) 10
Relative humidity (%) 40
Temperature (°F) 86
Droplet velocity (mph) 44.7

○ Single size droplets
○ Array of droplets (DVs)
● Array of droplets (nozzle)

Examples:Nozzle type and pressure, click to select

XR8001_40
XR8001_60
XR8002_40
XR8003_40
XR8004_40
XR8006_40
XR8007_40
XR8008_40

(19) Click on one of nozzle choices, then “$D_{v.1}$”, “$D_{v.5}$“ and “$D_{v.9}$“ values automatically appear in boxes for the nozzle chosen, as shown in Figure 8.

Figure 8

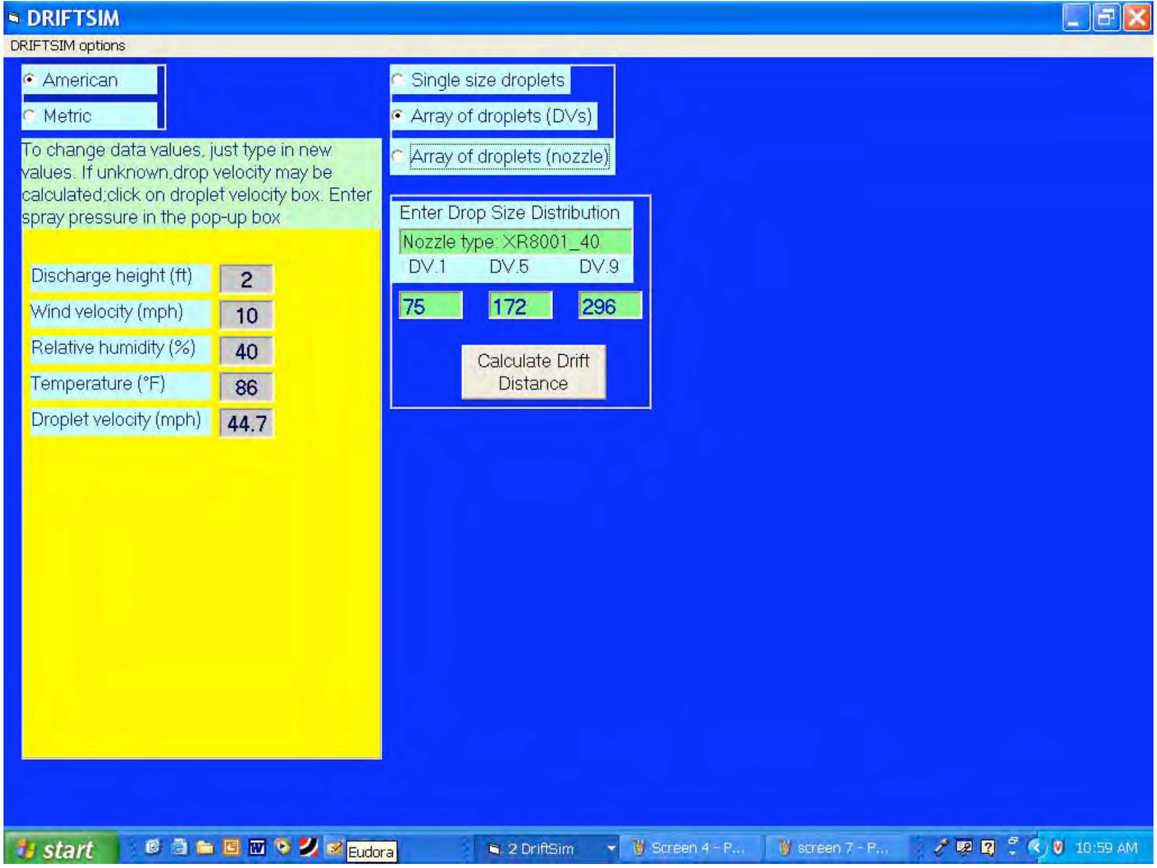

● American
○ Metric

○ Single size droplets
● Array of droplets (DVs)
○ Array of droplets (nozzle)

To change data values, just type in new values. If unknown,drop velocity may be calculated;click on droplet velocity box. Enter spray pressure in the pop-up box

Discharge height (ft)	2
Wind velocity (mph)	10
Relative humidity (%)	40
Temperature (°F)	86
Droplet velocity (mph)	44.7

Enter Drop Size Distribution

Nozzle type: XR8001_40

DV.1	DV.5	DV.9
75	172	296

(20) Enter or change values for "*Wind velocity*", "*Discharge height*", "*Droplet velocity*", "*Temperature*", and "*Relative humidity*".

(21) Click on "*Calculate Drift Distance*". Drift distances of 9 size classes of droplets along with the portion of the spray volume corresponding to each size class appear on the screen as the same as step (15). Error message appears on this screen if "$D_{v.1}$", "$D_{v.5}$" and "$D_{v.9}$" values are not reasonable.

(22) Click on either "*Print Results*" to get a printout of the results, or "*Calculate another drift distance*" to repeat steps (18) to (22) for a revised or new set of inputs.

(23) When you are done with all the simulations, exit DRIFTSIM by clicking on the **X** at the upper right corner of the window on the screen.

Steps to run DRIFTSIM from a computer hard drive

To operate DRIFTSIM from a hard drive, the user should copy both DRIFTSIM subdirectory and all contents in the subdirectory, except AUTORUN.INF and Browsercall.exe, from the CD to the hard drive [**Note:** the subdirectory name must be DRIFTSIM; otherwise, the program will not work]. After the copying process is completed, go to DRIFTSIM subdirectory in the hard drive and click on DriftSim.exe file. DRIFTSIM introductory page should appear on the screen. Then follow steps (3) to (23) above to run the program.

References

Goering, C.E. and D.B. Smith. 1978. Equations for droplet size distributions in sprays. Transactions of ASAE 21(2): 209-216.

Reichard, D.L., H. Zhu, R.D. Fox and R.D. Brazee. 1992. Wind tunnel evaluation of a computer program to model spray drift. Transactions of the ASAE 35(3):755-758.

Zhu, H., D.L. Reichard, R.D. Fox, R.D. Brazee and H.E. Ozkan. 1994. Simulation of drift of discrete sizes of water droplets from field sprayers. Transactions of the ASAE 37(5):1401-1407.

Zhu, H., D.L. Reichard, R.D. Fox, H.E. Ozkan and R.D. Brazee. 1995. DRIFTSIM, a program to estimate drift distances of spray droplets. Applied Engineering in Agriculture 11 (3): 365-369.

This manual, as well as other information on spray drift, is available at Ohio State University Extension's web site "Ohioline" (**http://ohioline.osu.edu**) by clicking on "Search" and entering "DRIFTSIM" or "spray drift" in the search box.

Keith L. Smith, Associate Vice President for Agricultural Administration and Director, OSU Extension

TDD No. 800-589-8292 (Ohio only) or 614-292-1868

APPLICATION FOR PERMIT
SUNDANCE WEST

VOLUME III: ENGINEERING DESIGN AND CALCULATIONS
SECTION 10: WAVE ACTION CALCULATIONS

TABLE OF CONTENTS

LIST OF ATTACHMENTS

APPLICATION FOR PERMIT
SUNDANCE WEST

VOLUME III: ENGINEERING DESIGN AND CALCULATIONS
SECTION 10: WAVE ACTION CALCULATIONS

1.0 INTRODUCTION

Sundance West (Sundance West Facility) is a proposed Surface Waste Management Facility for oil field waste processing and disposal services. The proposed Sundance West Facility is subject to regulation under the New Mexico Oil and Gas Rules, specifically 19.15.36 NMAC, administered by the Oil Conservation Division (OCD). The Facility has been designed in compliance with 19.15.36 NMAC, and will be constructed and operated in compliance with a Surface Waste Management Facility Permit issued by the OCD. The Facility is owned by, and will be constructed and operated by, Sundance West, Inc.

1.1 Description

The Sundance West site is comprised of a 320-acre ± tract of land located approximately 3 miles east of Eunice, 18 miles south of Hobbs, and approximately 1.5 miles west of the Texas/New Mexico state line in the South ½ of Section 30, Township 21 South, Range 38 East Lea County, New Mexico (NM). Site access will be provided via NM 18 and Wallach Lane. The Sundance West Facility will include two main components; a liquid oil field waste Processing Area (80 acres ±), and an oil field waste Landfill (180 acres ±). Oil field wastes are anticipated to be delivered to the Sundance West Facility from oil and gas exploration and production operations in southeastern NM and west Texas. The Site Development Plan provided in the **Permit Plans, Volume III.1**, identifies the locations of the Processing Area and Landfill facilities.

2.0 DESIGN CRITERIA

The purpose of the Wave Action Calculations presented herein is to provide the wave height and run-up for the evaporation ponds proposed for the Sundance West Processing Area. The Sundance West Processing Area is planned to include 10 evaporation ponds, approximately 420 feet (ft) in length and 200 ft in width, each with a capacity of approximately 9.5 acre-ft.

These calculations assume a pond length of 420 ft and a conservative wind speed of 75 miles per hour (mph). Wave height and run-up must be less than the 3 ft of freeboard provided in the pond design. The methodology applied for determining wave height and run-up in reservoirs for the Wave Action Calculations is provided in two documents, *Low Cost Shore Protection: A Guide for Engineers and Contractors* (U.S. Army Corps of Engineers 2004; (**Attachment III.10.A**); and *Water-Resources Engineering* (Linsley & Franzini 1979; **Attachment III.10.B**).

3.0 CALCULATION

The fastest mile wind speed for a 25-year return period was obtained from Figure 16, **Attachment III.10.A**. The fastest mile wind speed is approximately 75 mph for the Sundance West site vicinity.

Wave height in a pond is estimated using the following equation (i.e., page 166, Equation 7-4, **Attachment III.10.B)**:

$$Z_w = 0.034\ (V_w)^{1.06}\ F^{0.47}$$

Where: Z_w = height of wave (feet)
V_w = wind speed (mph) = 75 mph
F = fetch length (miles) = 420 feet/5,280 feet/mile = 0.080 miles

Therefore: $Z_w = 0.034\ (75\text{ mph})^{1.06}\ (0.080\text{ miles})^{0.47}$

$$Z_w = 0.034\ (97.2)\ (0.30)$$

Z_w = 0.99 feet = height of wave in pond due to a 75 mph wind

The height of wave runup for a smooth (i.e., HDPE liner) surface can be obtained from Table 11, **Attachment III.10.A**. On Table 11, R = 1.75H for a 2.5H:1V smooth slope and R = 1.50H for a 4.0H:1V smooth slope. Interpolating between these two values a value of R = 1.68H is obtained for a 3.0H:1V smooth slope. Therefore:

Wave Runup = 1.68H = 1.68 (0.99 feet) = 1.66 feet for a 3H:1V smooth sideslope.

Total: Wave height + Wave run-up = 0.99 feet + 1.66 feet = 2.65 feet

4.0 SUMMARY

When considering a 75 mph wind across the length of the pond, a wave height of 0.99 ft is obtained. This wave will run-up approximately 1.66 ft up the sideslope of the pond. The ponds have been design with a minimum freeboard of 3 ft which will provide adequate protection against the combined potential impact of waves, wave run-up, and simultaneous rainfall event (i.e., 25 year, 24 hour rainfall = 4.9”).

APPLICATION FOR PERMIT
SUNDANCE WEST

VOLUME III: ENGINEERING DESIGN AND CALCULATIONS
SECTION 10: WAVE ACTION CALCULATIONS

ATTACHMENT III.10.A

LOW COST SHORE PROTECTION: A GUIDE FOR ENGINEERS AND CONTRACTORS **(U.S. ARMY CORPS OF ENGINEERS 2004)**

LOW COST SHORE PROTECTION

... a Guide for Engineers and Contractors

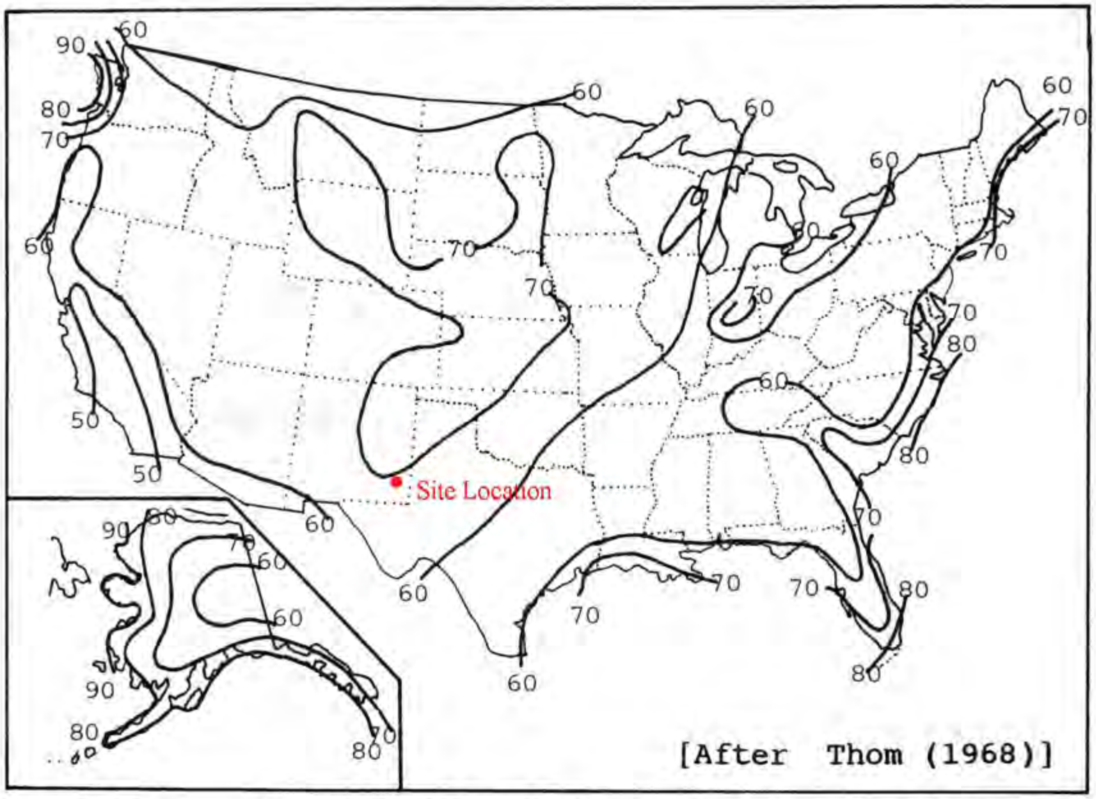

[After Thom (1968)]

Figure 15 Fastest-Mile Wind Speeds: 10-year Return Period

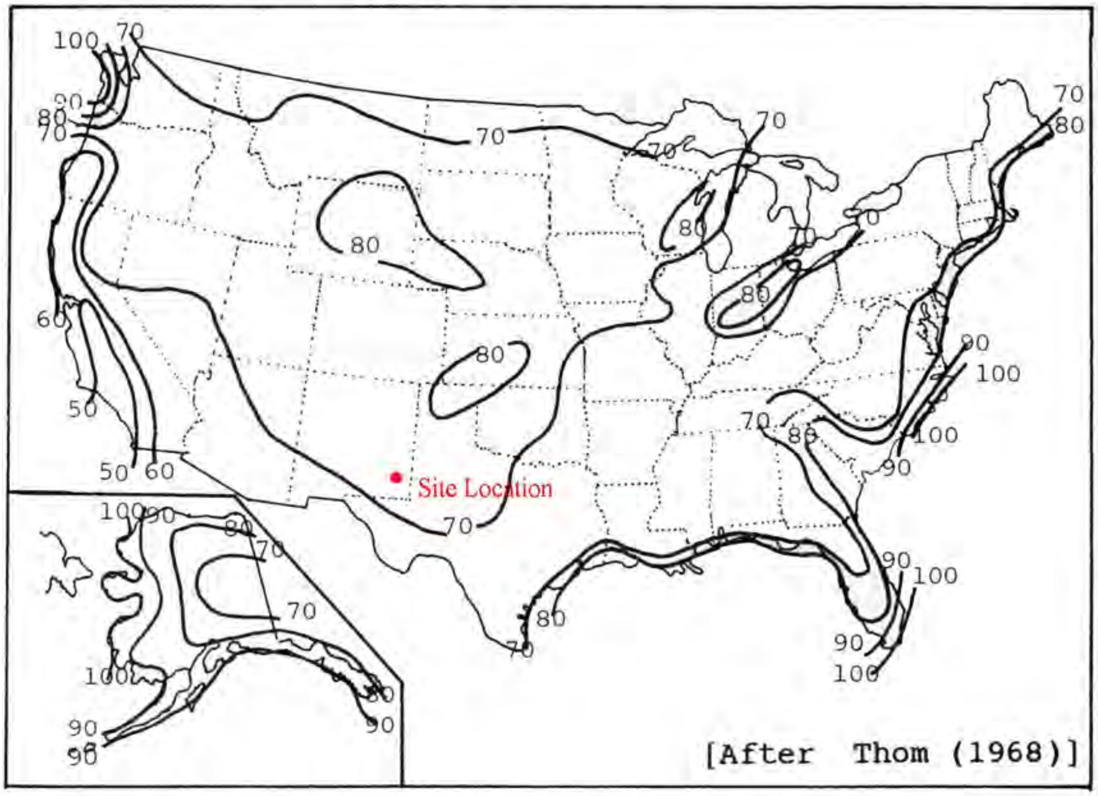

[After Thom (1968)]

Figure 16 Fastest-Mile Wind Speeds: 25-year Return Period

Structure Height

Waves breaking against an inclined structure will run up to an elevation higher than the Stillwater level depending on the roughness of the structure. Smooth concrete surfaces experience higher runup than rough stone slopes. Vertical structures also cause splashing and can experience overtopping. If possible, the structure should be built high enough to preclude severe overtopping. White spray does little damage, but solid jets of "green" water should be avoided. The required height of the structure will depend on the computed runup height based on the wave and structure characteristics. Detailed guidance is presented in Stoa (1978) and (1979). The runup height, R, can be found by a more approximate method as given below.

First, find the wavelength at the structure by using either Figure 26 or Equation (3) with the known depth at the structure and the design wave period. The definition sketch for runup is shown on Figure 27. For SMOOTH impermeable slopes, the runup, R, is given in Seelig (1980) by,

$$R=HC_1\,(0.12L/H){}^\wedge(C_2\,(H/d_s)^{0.5} + C_3)$$

where: L = the local wavelength from Figure 26 or Eq. (3),
d_s = the depth at the structure (feet),
the approaching wave height (feet), and
C_1, C_2, C_3 = coefficients given below.

Structure Slope *	C_1	C_2	C_3
Vertical	0.96	0.23	+0.06
1 on 1.0	1.47	0.35	-0.11
1 on 1.5	1.99	0.50	-0.19
1 on 2.25	1.81	0.47	-0.08
1 on 3.0	1.37	0.51	+0.04

*Interpolate linearly between these values for other slopes.

For ROUGH slopes, Seelig (1980) gives the runup as,

$$R = (0.69\xi/1+0.5\xi)H \qquad (14)$$

$$\xi = \tan\theta/(H/L_o)^{0.5} \qquad (15)$$

$$L_o = 5.12\ T^2 \qquad (16)$$

θ = structure of the slope (e. g., $\tan\theta = 0.25$ for a slope of 1V on 4H

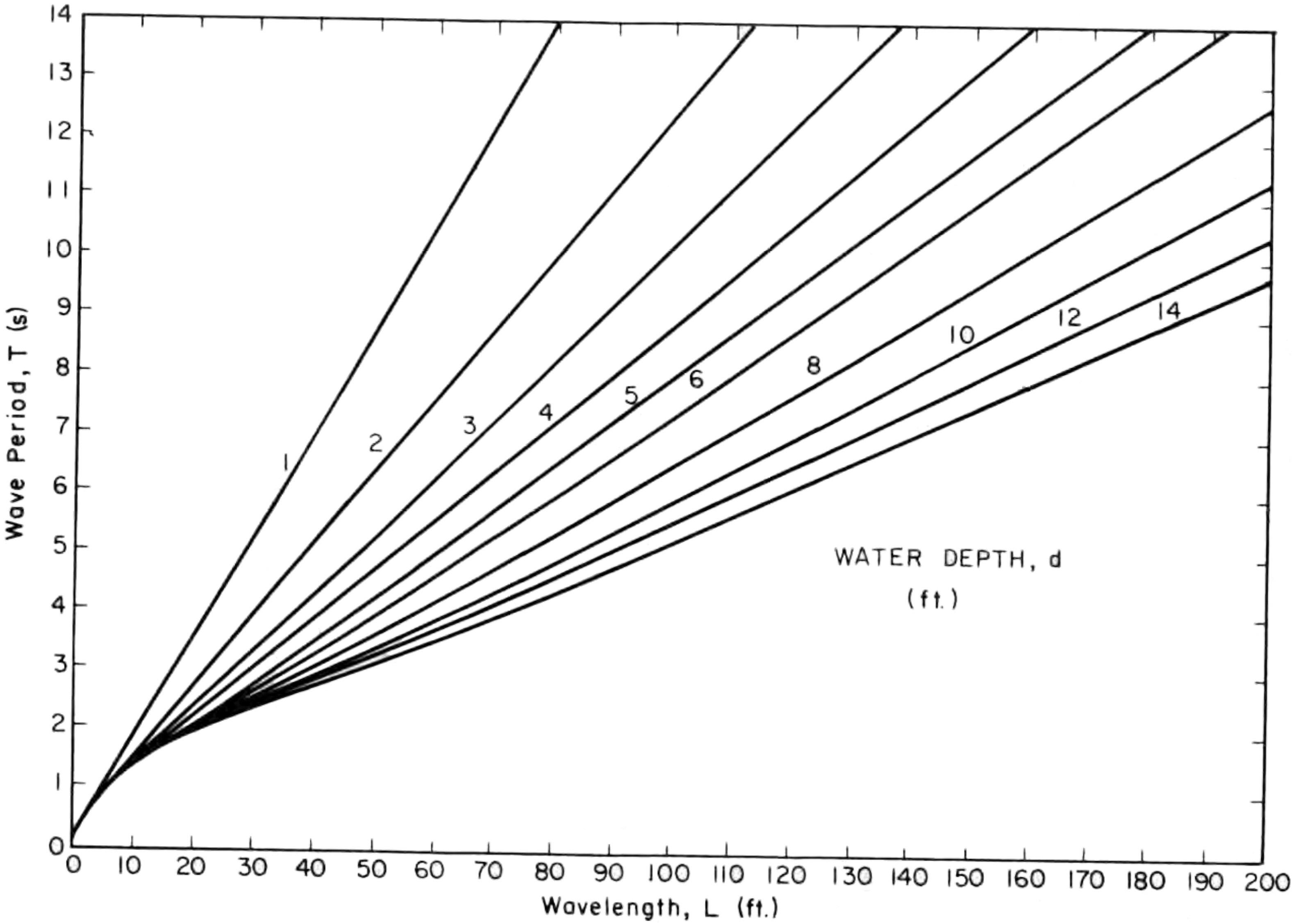

Figure 26 Local Wavelength Given Depth and Period [After Giles and Eckert (1979)]

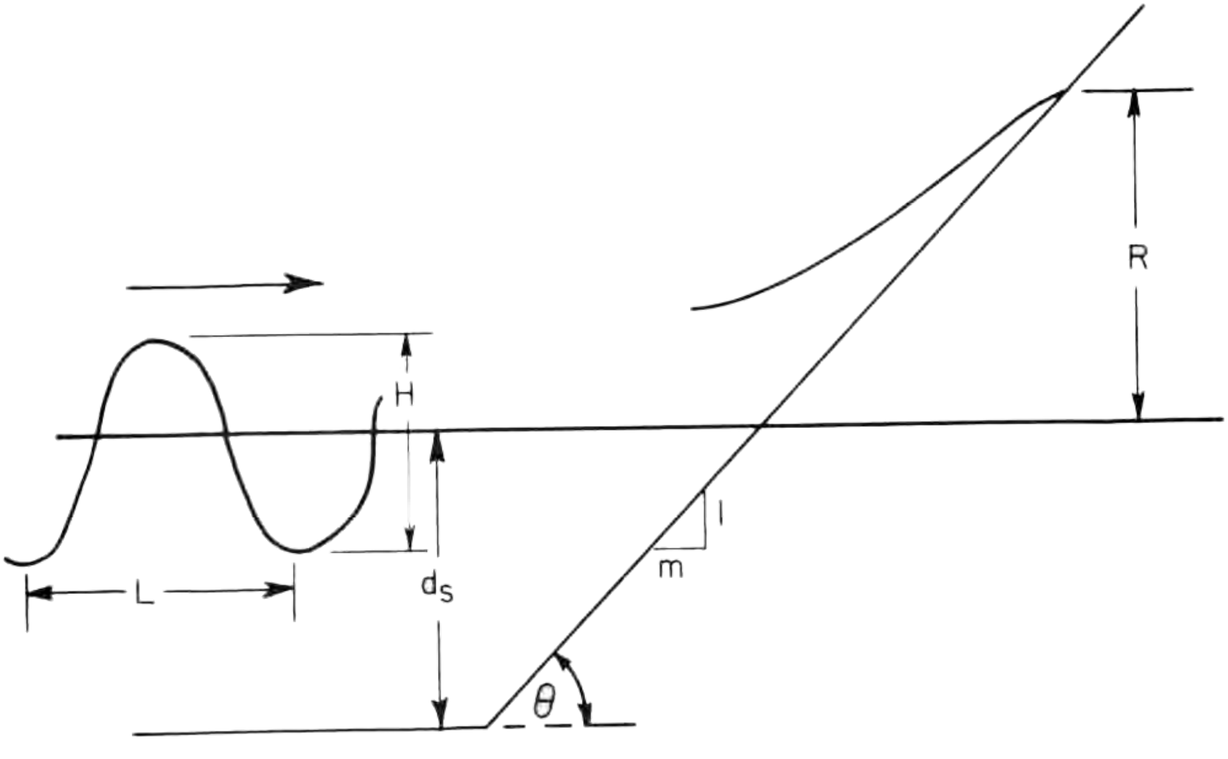

Figure 27 Wave Runup Definition Sketch

For STEPPED slopes, Stoa (1979) recommends using 70 to 75 percent of the smooth slope runup if the risers are vertical, and 86 percent if the edges are rounded.

A rough approximation of the runup height can be obtained from Table 11. However, the values in the table tend to represent the upper bound of the available data and may result in over design. Equations (13) and (14) or the methods given in Stoa (1978) and (1979) are recommended.

If it is impossible or undesirable to build a structure to the recommended height, a splash apron should be provided at the top of the structure. These are generally constructed of rock and they prevent the ground at the top from being eroded and undermining that portion of the structure.

Environmental Factors

Many different materials can be used to construct shore protection structures, including rock, concrete, timber, metal and plastics. The choice often depends on the desired permanence of the protection. Durable materials usually cost considerably more than shorter-lived materials used for temporary protection. The choice of materials is important because the coastal environment is a harsh testing ground for all man-made structures. Aside from wave forces, which are formidable in and of themselves, a host of chemical, biological and other factors can degrade structural materials. A brief review of these follows.

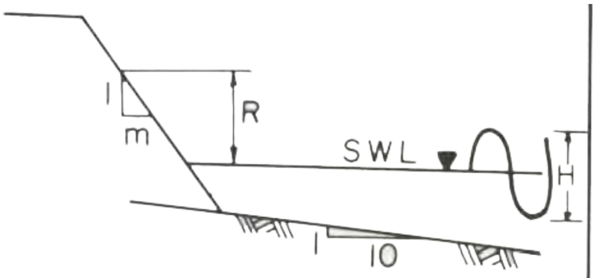 *SMOOTH FACE*	m 1.5 2.5 4.0	R 2.25H 1.75H 1.50H
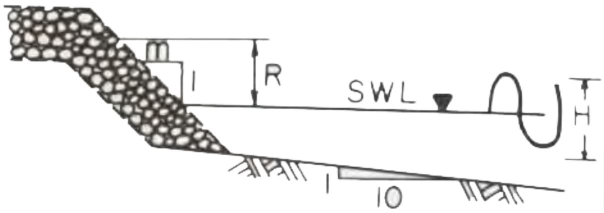 *ROUGH FACE*	m 1.5 2.5 4.0	R 1.25H 1.00H 0.75H
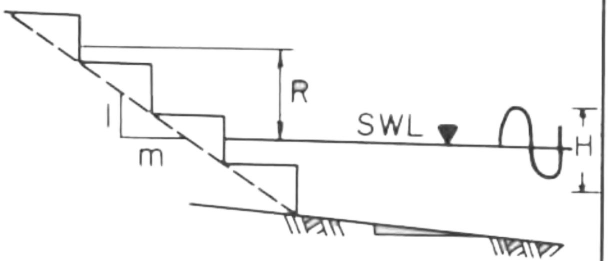 *STEPPED FACE*	m 1.5	R 2.00H
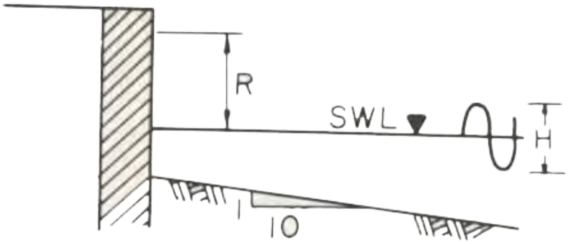 *VERTICAL FACE*	m —	R 2.00H

Table 11 Wave Runup Heights

APPLICATION FOR PERMIT

SUNDANCE WEST

VOLUME III: ENGINEERING DESIGN AND CALCULATIONS
SECTION 10: WAVE ACTION CALCULATIONS

ATTACHMENT III.10.B

WATER-RESOURCES ENGINEERING

(LINSLEY & FRANZINI 1979)

WATER-RESOURCES ENGINEERING

THIRD EDITION

Ray K. Linsley
Professor Emeritus of Hydraulic Engineering
Stanford University
Partner, Linsley, Kraeger Associates

Joseph B. Franzini
Professor of Civil Engineering
Associate Chairman, Department of Civil Engineering
Stanford University

McGraw-Hill Book Company

New York St. Louis San Francisco Auckland Bogotá Düsseldorf
Johannesburg London Madrid Mexico Montreal New Delhi Panama
Paris São Paulo Singapore Sydney Tokyo Toronto

by ordinary earth-moving methods would be expensive unless the excavated sediment has some sales value.

7-9 Wind setup and waves in reservoirs Earth dams must have sufficient freeboard above maximum pool level so that waves cannot wash over the top of the dam. Waves in reservoirs may also damage shoreline structures and embankments adjacent to the water and interfere with navigation. Part of the design of any reservoir is an estimate of wind setup and wave height.

Wind setup is the tilting of the reservoir water surface caused by the movement of the surface water toward the leeward shore under the action of the wind. This current of surface water is a result of tangential stresses between the wind and the water and of differences in atmospheric pressure over the reservoir. The latter, however, is, typically, a smaller effect. As a consequence of wind setup, the reservoir water surface is above normal still-water level on the leeward side and below the still-water level on the windward side. This results in hydrostatic unbalance, and a return flow at some depth must occur. The water-surface slope which results is that necessary to sustain the return flow under conditions of bottom roughness and cross-sectional area of flow which exist. Wind setup is generally larger in shallow reservoirs with rough bottoms.

Wind setup may be estimated from

$$Z_s = \frac{V_w^2 F}{1400d} \tag{7-3}$$

where Z_s is the rise in feet (meters) above still-water level, V_w is the wind speed in miles (kilometers) per hour, F is the *fetch* or length of water surface over which the wind blows in miles (kilometers), and d is the average depth of the lake along the fetch in feet (meters). In SI metric units, the constant in the denominator becomes 63,200.

Equation (7-3) is modified[1] from the original equation developed by Dutch engineers on the Zuider Zee. Additional information and techniques are given in other references.[2] Wind-setup effects may be transferred around bends in a reservoir and the value of F used may be somewhat longer than the straight-line fetch.

When wind begins to blow over a smooth surface, small waves, called capillary waves, appear in response to the turbulent eddies in the wind stream. These waves grow in size and length as a result of the continuing push of the wind on the back of the waves and of the shearing or tangential force between the wind and the water. As the waves grow in size and length, their speed increases until they move at speeds approaching the speed of the wind. Because growth of a wave depends in part upon the difference between wind speed and wave speed, the growth rate approaches zero as the wave speed approaches the wind speed.

[1] T. Saville, Jr., E. W. McClendon, and A. L. Cochran, Freeboard Allowances for Waves in Inland Reservoirs, *J. Waterways and Harbors Div., ASCE*, pp. 93–124, May, 1962.

[2] Shore Protection, Planning and Design, *Tech. Rept.* 3, 3d ed., U.S. Army Coastal Engineering Research Center, June, 1966.

The duration of the wind and the time and direction from which it blows are important factors in the ultimate height of a wave. The variability of the wind and the amazingly complex and yet to be fully understood response of the water surface to the wind lead to a wave pattern that is a superposition of many waves. The pattern is often described by its energy distribution or spectrum. The growth of wind waves as a function of fetch, wind speed, and duration can be calculated from knowledge of the mechanism of wave generation and use of collected empirical results.[1] The duration of the wind and the fetch play an important role because a wave may not reach its ultimate height if the wave passes out of the region of high wind or strikes a shore during the growth process. The depth of water also plays a key role, tending to yield smaller and shorter waves in deep water.

Wave-height data gathered at two major reservoirs[2] confirm the theoretical and experimental data for ocean waves if a modified value of fetch is used. The derived equation is

$$z_w = 0.034V_w^{1.06}F^{0.47} \tag{7-4}$$

---

[1] W. J. Pierson, Jr., and R. W. James, Practical Methods for Observing and Forecasting Ocean Waves, *U.S. Navy Hydrographic Office Pub.* 603, 1955 (reprinted 1960).

[2] T. Saville, Jr., E. W. McClendon, and A. L. Cochran, Freeboard Allowances for Waves in Inland Reservoirs, *J. Waterways and Harbors Div., ASCE*, pp. 93–124, May, 1962.

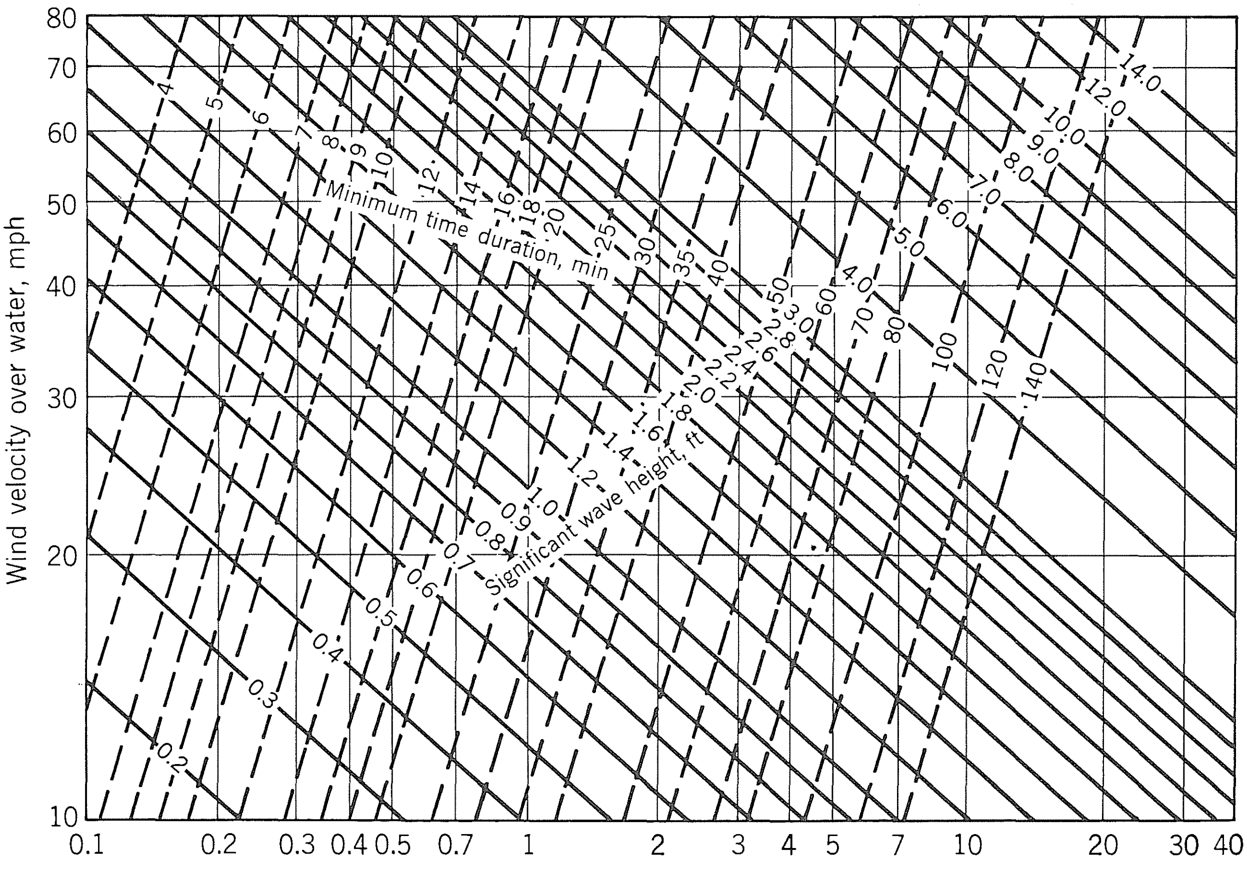

Figure 7-14 Significant wave heights and minimum wind durations (*from Saville, McClendon, and Cochran*). For metric version see Appendix B.

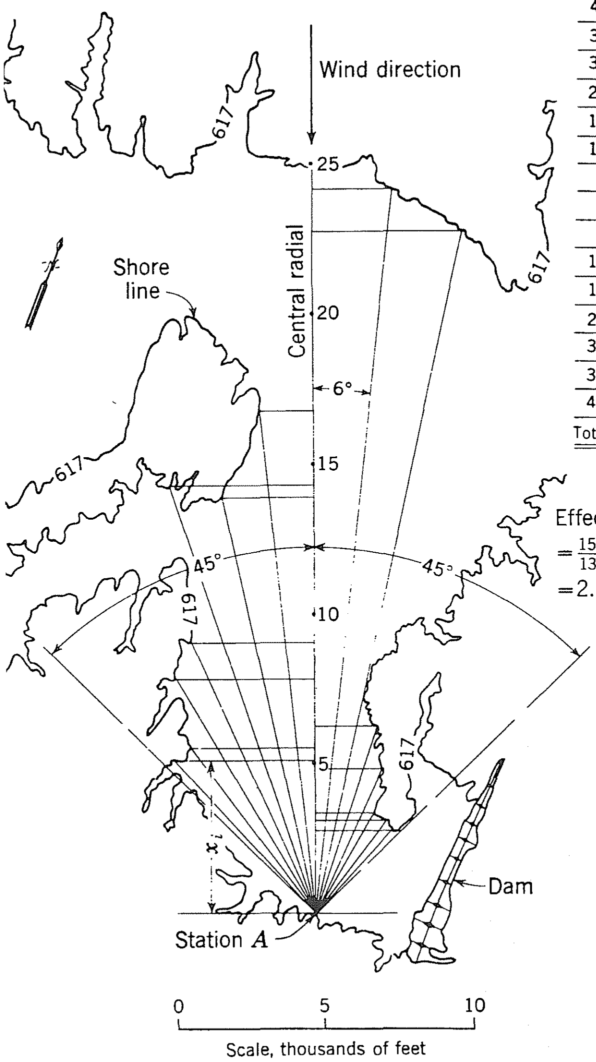

θ	cos θ	x_i	x_i cos θ
42	0.743	5.1	3.79
36	0.809	5.5	4.45
30	0.866	7.8	6.75
24	0.914	9.0	8.23
18	0.951	14.2	13.50
12	0.978	13.8	13.50
6	0.995	16.7	16.62
0	1.000	24.7	24.70
6	0.995	24.1	23.98
12	0.978	22.7	22.20
18	0.951	6.2	5.90
24	0.914	4.8	4.39
30	0.866	3.3	2.86
36	0.809	3.1	2.51
42	0.743	2.8	2.08
Total	13.512		155.46

Effective fetch

$= \frac{155.46}{13.512} \times 10^3 = 11{,}510$ ft

$= 2.18$ mi

igure 7-15 Computation of effective fetch. (*Modified from Saville, McClendon, and Cochran*)

vhere z_w is the average height in feet (meters) of the highest one-third of the waves nd is called the *significant wave height*, V_w is the wind velocity in miles (kil-meters) per hour about 25 ft (7.6 m) above the water surface, and F is the fetch in niles (kilometers). In SI metric units the coefficient becomes 0.005. The equation s shown graphically in Fig. 7-14[1] together with lines showing the minimum dura-ion of wind required to develop the indicated wave height. Figure 7-15 shows the nethod of computing the effective fetch for a narrow reservoir.

Since the design must be made before the reservoir is complete, wind data ver land must generally be used. Table 7-2 gives ratios of wind speed over land to hose over water and may be used to correct observed wind to reservoir condi-ions. Waves are critical only when the reservoir is near maximum levels. Thus in electing the critical wind speed for reservoirs subject to seasonal fluctuations,

---

[1] A graph for the solution of Eq. (7-4) in SI metric units is given in Appendix B-1.

Table 7-2 Relationship between wind over land and that over water. (After Saville, McClendon, and Cochran)

Fetch, mi (km)	0.5 (0.8)	1 (1.6)	2 (3.2)	4 (6.5)	6 (9.7)	8 (12.9)
$V_{\text{water}}/V_{\text{land}}$	1.08	1.13	1.21	1.28	1.31	1.31

only winds which can occur during the season of maximum pool levels should be considered. The direction of the wind and the adopted fetch must also be the same.

The height of the significant wave is exceeded about 13 percent of the time. If a more conservative design is indicated, a higher wave height may be chosen. Table 7-3 gives ratios of z'/z_w for waves of lower exceedance.

When a wave strikes a land slope, it will *run up* the slope to a height above its open-water height. The amount of run-up depends on the surface. Figure 7-16 shows the results of small-scale experiments[1] on smooth slopes and rubble mounds. Height of run-up z_r is shown as a ratio z_r/z_w and is dependent on the ratio of wave height to wavelength (wave steepness). Wavelength λ for deep-water waves may be computed from

$$\lambda = 5.12t_w^2 \text{ ft} \qquad \text{or} \qquad \lambda = 1.56t_w^2 \text{ m} \tag{7-5}$$

where the wave period t_w is given by

$$t_w = 0.46V_w^{0.44}F^{0.28} \tag{7-6}$$

For shallow-water waves other length relations are appropriate.[2] In metric units the coefficient of Eq. (7-6) becomes 0.32. The curves for rubble mounds represent extremely permeable construction, and for more typical riprap on earth embankments the run-up may be somewhat higher, depending on both the permeability and the relative smoothness of the surface.

---

[1] T. Saville, Jr., Wave Run-up on Shore Structures, *Trans., ASCE*, Vol. 123, pp. 139–158, 1958; R. Y. Hudson, Laboratory Investigation of Rubble-mound Breakwaters, *Trans. ASCE*, Vol. 126, Part IV, pp. 492–541, 1962.

[2] Shore Protection, Planning and Design, *Tech. Rept.* 3, 3d ed., U.S. Army Coastal Engineering Research Center, June, 1966.

Table 7-3 Percentage of waves exceeding various wave heights greater than z_w. (After Saville, McClendon, and Cochran)

z'/z_w	1.67	1.40	1.27	1.12	1.07	1.02	1.00
Percentage of waves > z'	0.4	2	4	8	10	12	13

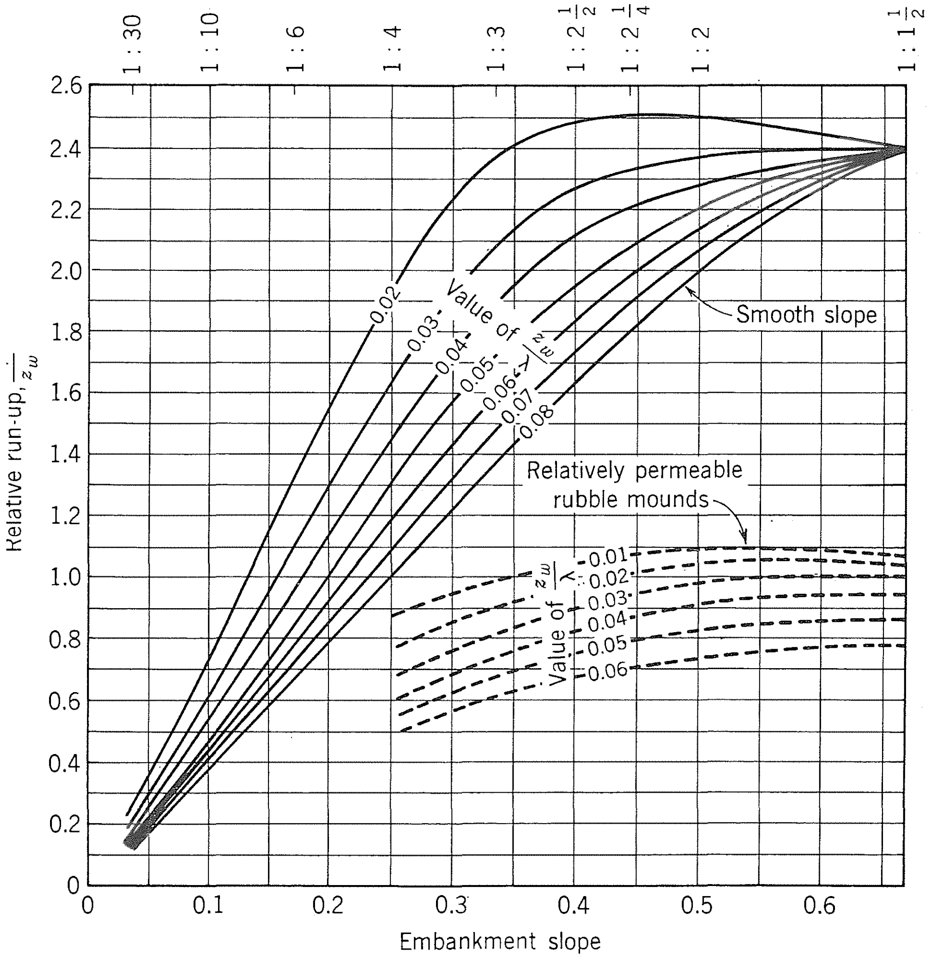

Figure 7-16 Wave run-up ratios versus wave steepness and embankment slopes. (*From Saville, McClendon, and Cochran*)